Teza de abilitare: *Dinamica amplificatoarelor de turație planetare cu intrări și ieșiri multiple pentru sisteme eoliene contrarotative*

Autor: *Prof. dr. ing. Mircea Neagoe*

Domeniul de doctorat: *Inginerie mecanică*

PORTOFOLIU DE LUCRĂRI RELEVANTE DIN DOMENIUL DE DOCTORAT VIZAT

Inginerie Mecanică

1. **Neagoe, M.**, Saulescu, R., Jaliu, C., Neagoe, I. Dynamic Analysis of a Single-Rotor Wind Turbine with Counter-Rotating Electric Generator under Variable Wind Speed, Applied Sciences 2021, 11(19):8834, p. 1-21, ISSN: 2076-3417, DOI: 10.3390/app11198834, WOS: 000650300900001 (**IF = 2,838**).
2. **Neagoe, M.**, Jaliu, C., Saulescu, R. Dynamic Modeling and Simulation of a Counter-Rotating Wind System with 1-DOF Planetary Speed Increaser, Mechanisms and Machine Science 149, Vol. 3, p. 742–752, 2024, ISSN: 2211-0992, DOI: 10.1007/978-3-031-45709-8_72.
3. Saulescu, R., **Neagoe, M.** Dynamic Response of a Single-Rotor Wind Turbine with Planetary Speed Increaser and Counter-Rotating Electric Generator in Starting Transient State, Applied Sciences 2025, 15, 191, ISSN: 2076-3417, DOI:10.3390/app15010191, WOS: 001393444500001 (**IF = 2,500**).
4. **Neagoe, M.**, Saulescu, R. Comparative Energy Performance Analysis of Four Wind Turbines with Counter-Rotating Rotors in Steady-State Regime, Energy Reports 2022, 8, p. 1154-1169, ISSN: 2352-4847, DOI: 10.1016/j.egyr.2022.07.092, WOS: 000841651400062 (**IF = 5,200**).
5. **Neagoe, M.**, Saulescu, R., Jaliu, C. Design and Simulation of a 1 DOF Planetary Speed Increaser for Counter-Rotating Wind Turbines with Counter-Rotating Electric Generators, Energies 2019, 12(9), 1754, p. 1-19, ISSN: 1996-1073, DOI: 10.3390/en12091754, WOS: 000469761700170 (**IF = 2,702**).
6. **Neagoe, M.**, Saulescu, R., Jaliu, C., Munteanu, O., Cretescu, N. A Comparative Performance Analysis of Four Wind Turbines with Counter-Rotating Electric Generators, Applied Sciences 2022, 12(19):4233, p. 1-24, ISSN: 2076-3417, DOI: 10.3390/app12094233, WOS: 000794733500001 (**IF = 2,700**).

7. **Neagoe, M.**, Saulescu, R., Jaliu, C., Simionescu, P.A. A Generalized Approach to the Steady-State Efficiency Analysis of Torque-Adding Transmissions Used in Renewable Energy Systems, Energies 2020, 13, 4568, p. 1-18, ISSN: 1996-1073, DOI: 10.3390/en13174568, WOS: 000570321100001 (**IF = 3,004**).
8. Saulescu, R., Jaliu, **Neagoe, M.**, Ciobanu, D., Cretescu, N. Comparative analysis of torque-adding wind energy conversion systems with a counter-rotating vs. conventional electric generator, Frontiers in Energy Research 2023, 11, p. 1-14, ISSN: 2296-598X, DOI: 10.3389/fenrg.2023.1215509, WOS: 001049084500001 (**IF = 2,600**).
9. Saulescu, R., **Neagoe, M.**, Jaliu, C., Munteanu, O. A Comparative Performance Analysis of Counter-Rotating Dual-Rotor Wind Turbines with Speed-Adding Increasers, Energies 2021, 14, 2594, p. 1-24, ISSN: 1996-1073, DOI: 10.3390/en14092594, WOS: 000650300900001 (**IF = 3,252**).
10. **Neagoe, M.**, Saulescu, R., Jaliu, C., Munteanu, O. Amplificator de turație planetar reglabil reconfigurabil pentru turbine eoliene și metodă de reglare a acestuia, Brevet de invenție nr. RO 134401B1/28.02.2025.

Data: 8.04.2025 Prof. dr. ing. Mircea Neagoe

applied sciences

Article

Dynamic Analysis of a Single-Rotor Wind Turbine with Counter-Rotating Electric Generator under Variable Wind Speed

Mircea Neagoe [1], Radu Saulescu [2,*], Codruta Jaliu [1,*] and Ion Neagoe [3]

[1] Renewable Energy Systems and Recycling R&D Centre, Faculty of Product Design and Environment, Transilvania University of Brasov, 500036 Brasov, Romania; mneagoe@unitbv.ro
[2] Design of Mechanical Elements and Systems R&D Centre, Faculty of Product Design and Environment, Transilvania University of Brasov, 500036 Brasov, Romania
[3] Advanced Manufacturing Technologies and Systems R&D Centre, Faculty of Technological Engineering and Industrial Management, Transilvania University of Brasov, 500036 Brasov, Romania; neagoe_ion@unitbv.ro
* Correspondence: rsaulescu@unitbv.ro (R.S.); cjaliu@unitbv.ro (C.J.); Tel.: +40-268-413-000 (R.S.)

Abstract: This paper presents a theoretical study of the dynamic behaviour of a wind turbine consisting of a wind rotor, a speed increaser with fixed axes, and a counter-rotating electric generator, operating in variable wind conditions. In the first part, the dynamic analytical model of the wind turbine mechanical system is elaborated based on the dynamic equations associated with the component rigid bodies and the linear mechanical characteristics associated with the direct current (DC) generator and wind rotor. The paper proposes a method for identifying the coefficients of the wind rotor mechanical characteristics depending on the wind speed. The numerical simulations performed in Simulink-MATLAB by MathWorks on a case study of a 10 kW wind turbine highlight the variation with the time of the kinematic parameters (angular speeds and accelerations), torques and powers for wind system shafts, as well as the mechanical efficiency, both in transient and steady-state regimes, considering variable wind speed. The analytical and numerical results are helpful for researchers, designers, developers, and practitioners of wind turbines aiming to optimise their construction and functionality through virtual prototyping.

Keywords: renewable energy; wind turbine; counter-rotating electric generator; dynamic modelling; simulation; variable wind speed

Citation: Neagoe, M.; Saulescu, R.; Jaliu, C.; Neagoe, I. Dynamic Analysis of a Single-Rotor Wind Turbine with Counter-Rotating Electric Generator under Variable Wind Speed. *Appl. Sci.* **2021**, *11*, 8834. https://doi.org/10.3390/app11198834

Academic Editor: Daniel Villanueva Torres

Received: 29 August 2021
Accepted: 20 September 2021
Published: 23 September 2021

1. Introduction

In the global effort to achieve the ambitious targets for decarbonisation of the energy system, at a national and global level, wind energy plays a significant role now and a major one in the future. Thus, the European Union (EU) aims to move to 100% clean energy by 2050 as an important step in achieving climate neutrality, the energy sector being responsible for more than 75% of greenhouse gas emissions (GHG) at the European level, according to the European Green Deal [1]. This goal can be achieved by using renewable energy sources, a key role being granted to increasing wind production by improving wind energy systems, especially installed offshore. In all decarbonisation scenarios, which consider the high-level implementation of renewable energy systems, it is emphasized that the main source of electricity generation will be wind power by 2050 [1,2] with a share of over 36% of the total [3,4]. Thus, wind energy had a total installed capacity of 743 GW at the end of 2020 [5], with an increase to over 6000 GW foreseen by 2050 [4], as wind power remains an efficient and affordable technology of producing clean electricity in a safe and sustainable way. Energy management considering the variability of renewable energy sources and the reliability of networks and systems facing utility grid outages remains a challenge for energy systems with a high share of renewables [6–8].

The wind energy sector is gaining more and more popularity among researchers, developers and investors. They have paid attention to the behaviour of onshore and offshore wind systems and their components in different operating conditions. Their optimal design and modelling are permanent challenges in ensuring the high energy performance of wind systems, operating under variable wind conditions. Therefore, the dynamic behaviour of wind turbines is of significant interest as it influences significantly the conversion system functional performance, output power, and reliability.

The dynamic modelling of wind turbines in order to identify and control their behaviour or their functional optimization has drawn the attention of many researchers in recent decades. The research in this field is addressing either the dynamics of the entire wind turbine/farm or the dynamic modelling of a component of the wind conversion system: wind rotor, speed increaser, or electric generator. Different dynamic modelling approaches are presented in the literature, while the simulation is mainly performed with the MATLAB-Simulink software package.

Cottura et al. present in [9] the modelling of a floating wind turbine under a broad spectrum of sea and wind conditions. The dynamic model is compared with the FAST reference model (fatigue, aerodynamics, structures, and turbulence), a reference software for modelling offshore wind turbines, the errors between the two models being reported as being below two percent. A similar concept is presented in [10] where the hydrodynamic performance of the floating foundation of an offshore wind turbine is analysed based on Reynolds-Averaged Navier-Stokes simulations. The FAST dynamic model allows the performance investigation of the floating platform under operational and storm conditions. A rigid multibody dynamic model for a floating offshore wind turbine and its dynamic responses are presented in [11]. The authors use the Euler–Lagrange equations for system motion, while the dynamic response under four load cases is validated against the FAST model.

The dynamic of the onshore wind systems is addressed as well in the literature, referring mainly to general theoretical models, based on customised models that can be developed. For instance, Santoso and Le present in [12] a dynamic model that includes aerodynamic, mechanical, and electrical components of a turbine operating at a constant wind speed. The model is simulated in four case studies to prove its validity. Equivalent models of wind farms operating at constant wind speed are proposed in [13]. These dynamic models offer high accuracy of the dynamic response regarding the simulations of the energy system and a reduction in the simulation time compared to the detailed model of the actual wind farm.

A dynamic model of a fixed-pitch angle wind turbine simulator is presented in [14], which includes different wind turbine profiles for which the mechanical power characteristics of the wind turbine are assigned. The model allows defining the mechanical power and torque as functions of the wind speed. A similar concept is presented in [15], where the Blade Element Method is used to determine the power coefficient of a turbine consisting of a wind rotor, a speed increaser, and a conventional electric generator. The model considers the hydrodynamic data for the rotor, the inertia characteristics of the whole system, frictional losses, and the electromagnetic torque of the generator. Qi et al. propose in [16] a method to improve the dynamic response of a wind turbine by a torque error feed-forward control and the blade-pitch angle servo control. The mechanical system model is based on the FAST code, the results being validated on a five megawatt wind turbine. The dynamic behaviour of wind turbines under stormy wind conditions is presented in [17]. The authors use the beam theory to couple the wind turbine dynamic model to the unsteady aerodynamic model to generate the dynamic response of the system. The results are simulated on two wind turbines of two and six megawatts. The dynamic model of a wind turbine without a gearbox is presented in [18], the simulation performed in MATLAB-Simulink considering load flow, fluctuations in wind speed, and transient and output power.

The researchers in the field have paid particular attention to the dynamics of the gearbox, the literature proving that the dynamic behaviour of speed increasers is closely related to the dynamic behaviour of the wind systems. A gear transmission of Ravigneaux type is used in [19] to propose a dynamic analysis method based on a general algorithm for determining the transmission ratio, transmission torques, and efficiency. Another method for dynamic modelling uses numerical integration of Runge-Kutta type [20], and considers nonlinear dynamic characteristics of a speed increaser with one input and one output. Another nonlinear dynamic model is presented in [21], which considers a planetary speed increaser with an input and an output for which the load distribution on the gears is studied, the algorithm being based on the lumped parameters method. To improve the load-sharing capacity on the component gear pairs, Zhu et al. present in [22] a dynamic model of a planetary speed increaser with flexible pins. The dynamic behaviour of the wind system is also studied using the lumped parameter model, in which the stiffness of the bodies is predicted using the finite element method. Another approach is proposed by Fan et al. in [23] that discusses the dynamics of a speed increaser depending on the power vs. speed curve; the dynamic effect due to different input powers on the mechanical characteristics of the speed increaser is also investigated. A dynamic analysis of a planetary speed increaser is developed in [24] using the torsional multibody model, used to investigate the transient response of the transmission. Different planetary speed increasers for wind and hydro applications are proposed and dynamically analysed in [25,26] as transmissions with one input and one output. A new planetary speed increaser with two inputs and one output is proposed by Lin et al. [27] and its dynamic responses are simulated using the fourth order Runge-Kutta method. The time-domain dynamic response of heavy-duty planetary speed increasers is studied in [28] by using the lateral–torsional coupling modelling method; the method is validated on a two megawatt wind turbine gearbox. Wang et al. developed in [29] a dynamic model for a multistage planetary gear transmission by using the lumped parameter method to obtain the load-sharing coefficients for each planet gear pair under variable input speed and internal excitation.

Unlike the previously presented results that refer to gear transmissions used as speed increasers, ref. [30] proposes a new variant of a cycloidal planetary transmission for renewable energy systems and analyses its dynamic behaviour, the efficiency values being experimentally validated.

A general approach to the steady-state efficiency analysis of speed increasers with both one or two inputs and one or two outputs is proposed in [31]. The authors concluded that the in-parallel or split-power transmissions used in wind turbines with either two counter-rotating rotors or a counter-rotating generator have higher efficiency than serial transmissions.

Another approach in dynamic modelling is the use of controllers adapted for wind turbines with a double-fed induction generator, which allows the estimation in real time of dynamic behaviour compensating for the external disturbances action [32]. The optimal design of proportional-integral controllers integrated in on-grid permanent magnet synchronous generators from variable-speed wind turbines is addressed by Qais et al. in [33] by proposing a transient search optimization algorithm.

Aiming to improve the performance of the electric generators for wind turbines, a counter-rotating generator with permanent magnets for built environment applications is proposed and analysed in [34–36]; the counter-rotating generator is proved to have a higher efficiency than the conventional one, with a low starting torque, it is compact and scalable.

The literature survey concludes that the dynamic behaviour is performed only for systems with one input and one output or two inputs and one output, i.e., wind turbines with a conventional electric generator. In the vast majority of the presented research, the wind rotor and generator have nonlinear models, which lead to a dynamic model with a high complexity. In addition, some onshore theoretical models consider the wind turbines operating under constant wind speed. Generally, the numerical simulations are performed on high-power wind systems using Matlab-Simulink. As a result, the authors did not identify in the literature relevant results regarding the generalized dynamic modelling of the mechanical system for the class of wind turbines with single wind rotor and a counter-rotating electric generator, which would enable obtaining, in a simpler way, the dynamic response under variable wind speed.

The paper aims to cover the gap by proposing a novel algorithm for dynamic modelling of single-rotor wind systems that include a counter-rotating electric generator and a speed increaser with one input (connection to the wind rotor) and two outputs (connections to the rotor and stator of the electric generator), meant also to be used in real very attracting low-power applications, e.g., in the built environment. The power generated by the wind rotor is branched to the generator rotor and stator, a solution that brings several advantages compared to the conventional wind turbines (with fixed stator): higher mechanical efficiencies, a more compact speed increaser (with lower kinematic ratio), and a self-balancing electric generator in operation. The dynamic modelling is performed under variable wind conditions. It combines the classical equations associated with the rigid bodies with fixed-axis rotational motion (mechanical moments of inertia, kinematic transmission ratios, and the efficiency of the cylindrical gear set) with the linear equations associated with the mechanical characteristics for both the direct current (DC) generator and the wind rotor, respectively, on its quasilinear active working sector in operation. The linear equations of the wind rotor mechanical characteristic are expressed as functions of wind speed. The motion and efficiency equations in the dynamic regime are defined analytically and simulated for the case study of a 10 kW wind turbine, the numerical results validating the generalized theoretical model.

The paper is organised as follows: Section 2 presents the configuration of the wind turbine with counter-rotating generator and the analytical model for angular speeds and kinematic ratio; Section 3 is devoted to the dynamic analytical modelling; in Section 4 the numerical simulations and analyses are performed for a specific scenario; and Section 5 provides the conclusions.

2. Problem Formulation

Wind turbines with counter-rotating electric generator are characterised by a mechanical system with higher inertia versus the ones with conventional electric generator, due to the rotation of the generator stator, which usually is characterised by a higher mechanical moment of inertia than the generator rotor. Therefore, identifying the transient dynamic behaviour of these wind turbines when changing the wind speed is a challenge in expanding the implementation of wind turbine solutions with counter-rotating electric generators and also for their better operation.

The modelling of the dynamic response of wind turbines with counter-rotating electric generator was further developed for a generic wind turbine including a simple gearbox. The analysed wind turbine consisted of a wind rotor *R*, a fixed axes speed increaser *SI* with one input and two outputs, and a counter-rotating electric generator *G*, characterised by the rotation of the rotor *GR* and stator *GS* in opposite directions, Figure 1.

The speed increaser *SI* was derived from a cylindrical planetary gear set with one satellite gear, which functioned as a fixed axes mechanism obtained by connecting the satellite carrier *H* to frame 0. Thus, the mechanical power input in the speed increaser was achieved through a ring gear 2, which was connected to the wind rotor *R* and to the generator stator *GS*, which engaged with two or more evenly distributed gears 3. The gears 3 engaged simultaneously with gear 1, which ensured the transmission of mechanical power to the generator rotor *GR*. The ring gear 2 and gear 1 had the same revolute axis, namely the *central axis*. As a result, the input mechanical power was distributed on two branches to (Figure 1c):

- the generator rotor *GR*, through the speed increaser *SI*, with speed amplification;
- the generator stator *GS*, without changing the input speed due to the direct connection between the wind rotor *R* and the stator *GS*.

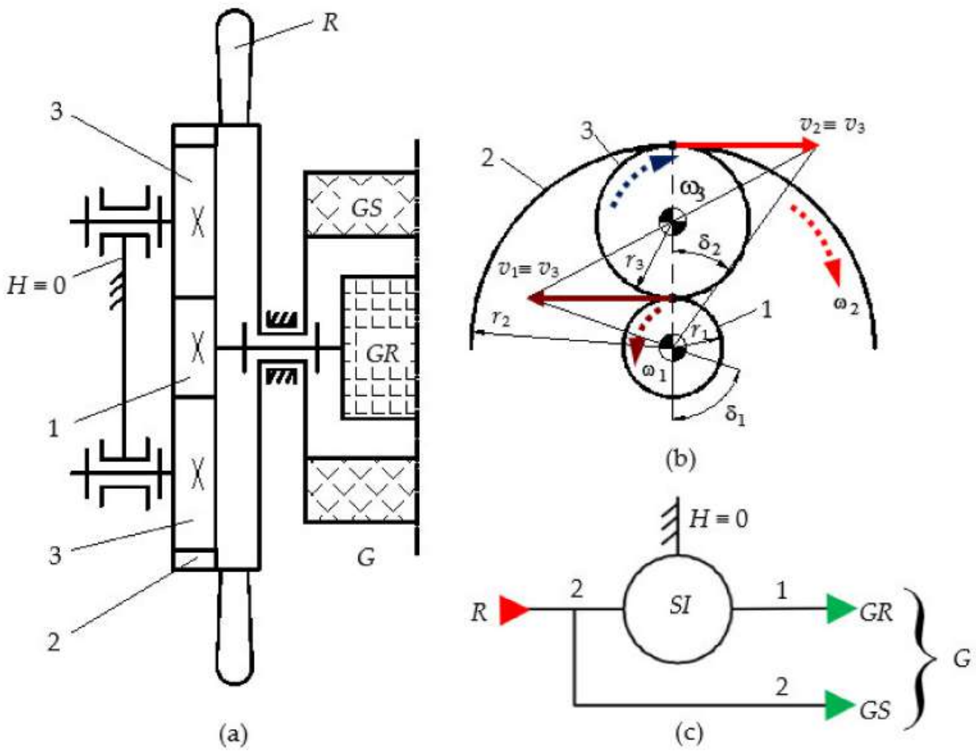

Figure 1. Single-rotor wind turbine with counter-rotating electric generator: (**a**) conceptual scheme; (**b**) kinematic scheme (upper-half front view); and (**c**) block scheme.

The angular speeds of the gears and the kinematic ratios, under the conditions of the branched transmission of mechanical power from the input $2 \equiv R$ to the outputs $1 \equiv GR$ and $2 \equiv GS$, can be obtained based on the scheme from Figure 1b:

$$\omega_1 = \frac{-v_1}{r_1} = -\tan\delta_1;\ \omega_1 = \omega_{GR} \tag{1}$$

$$\omega_2 = \frac{v_2}{r_2} = \tan\delta_2;\ \omega_2 = \omega_R = \omega_{GS} \tag{2}$$

$$i_{GR\_R} = \frac{\omega_{GR}}{\omega_R} = \frac{\omega_1}{\omega_2} = -\frac{\tan\delta_1}{\tan\delta_2} = -\frac{r_2}{r_1} = -\frac{z_2}{z_1} \tag{3}$$

$$i_{GS\_R} = \frac{\omega_{GS}}{\omega_R} = 1 \tag{4}$$

where ω_x is the angular speed of gear $x = 1 \ldots 3$; v_x—the peripheral linear speed on the pitch circle of radius r_x of gear $x = 1 \ldots 3$; $\delta_{1,2}$—the angle between the straight lines given by the center of rotation of gears 1, 2 and the origin and the tip, respectively, of the speed vector $v_{1,2}$; $z_{1,2}$—the teeth number of the gears 1, 2; i_{x_y}—the kinematic ratio (i.e., the ratio of angular speeds) when the rotation motion is transmitted from body x to body y.

In the operation of an electric generator, the relative angular speed of the rotor to the stator ω_G (referred to as the angular speed of the electric generator) is a characteristic parameter for the generated electric power:

$$\omega_G = \omega_{GR} - \omega_{GS} = \omega_1 - \omega_2 \tag{5}$$

As a result, the total amplification ratio of the angular speed i_{G_R} achieved by the wind turbine with counter-rotating generator can be determined with the following relation:

$$i_{G\_R} = \frac{\omega_G}{\omega_R} = \frac{\omega_{GR} - \omega_{GS}}{\omega_R} = \frac{-\tan\delta_1 - \tan\delta_2}{\tan\delta_2} = -1 - \frac{r_2}{r_1} = -\left(1 + \frac{z_2}{z_1}\right) \tag{6}$$

The dynamic modelling of the wind turbine from Figure 1 was performed under the following premises:

- the moving components (gears, the wind rotor, the rotor and stator of the electric generator) were rigid bodies with the mass distributed evenly and, also, geometrically symmetrical in relation to their own axis of rotation; therefore, the centre of mass of a body was a fixed point, located on the body fixed axis of rotation;
- only the frictional losses in the gearing were further considered, while the frictions in the revolute joints, materialised by bearings with low friction coefficients (due to the rolling friction), were neglected;
- the wind rotor and the electric generator were not adjusted during operation, which means that the pitch angle of the blades did not change in operation, and the adjustment parameters of the electric generator remained constant in operation;
- the wind rotor and the electric generator had known mechanical characteristics of linear type with constant coefficients. The mechanical characteristic of a wind rotor is a complex 2D curve, which can be approximated with a linear function in the steady-state regime. Moreover, the *DC* generators are characterised by a linear dependence between the driving torque and the angular speed of the electric generator ω_G;
- the electrical losses inside the generator were neglected in this study.

The main stages of the proposed dynamic response modelling of the wind turbine mechanical system are depicted in Figure 2 and further presented. Based on the conceptual diagram from Figure 1, the input parameters in this algorithm were the wind rotor radius, efficiencies of gear pairs and teeth numbers of the gears from the speed increaser, the torque-speed characteristic of the electric generator, and the inertial properties of the components. In the first stage, the kinematic modelling of the wind turbine mechanical system was performed by obtaining the transmitting functions for the angular speeds and the other angular speeds that are dependent on the independent speed of the wind rotor. For this mechanical system, three dynamic equations can be described, corresponding to the three rigid bodies to which the mechanical transmission can be reduced. The dynamic equations can be obtained by various approaches, in this case by using the Newton-Euler method. The mechanical characteristics (torque-angular speed dependence at a shaft level) of the wind rotor and the electric generator were added to the kinematic and dynamic equations of the mechanical system. This study considered the case of DC electric generators, characterized by linear characteristics modelled by linear functions, as well as by the equality in absolute value of the torques on its rotor and stator, both mobile with rotations in opposite directions. The mechanical characteristic of the wind rotor can be linearized on the active operating area, the coefficients of the linear function being dependent on the wind speed. These equations enable the calculation of the differential motion equation of the system that describes the behaviour in transient and steady-state regimes depending on the independent kinematic variable (the motion of the wind rotor).

The motion equation can be solved by using Simulink-Matlab software and obtains the system dynamic response (i.e., variation over time of the parameters of independent motion). Once the dynamic response is established, all the other kinematic parameters and torques that are associated with the mechanical transmission shafts are obtained explicitly based on the previous set of equations, including highlighting the changes in mechanical efficiency during wind turbine operation. The proposed algorithm is a general one and can be applied to any wind turbine with a single wind rotor and a counter-rotating electric generator, regardless of whether the mechanical characteristic of the wind rotor is linearized or not, the speed increaser has fixed axes or is of planetary type, and the generator is either a DC or an AC. For the sake of simplicity and better understanding, the simplified case of fixed axes speed increaser and linear mechanical characteristics is considered in this paper.

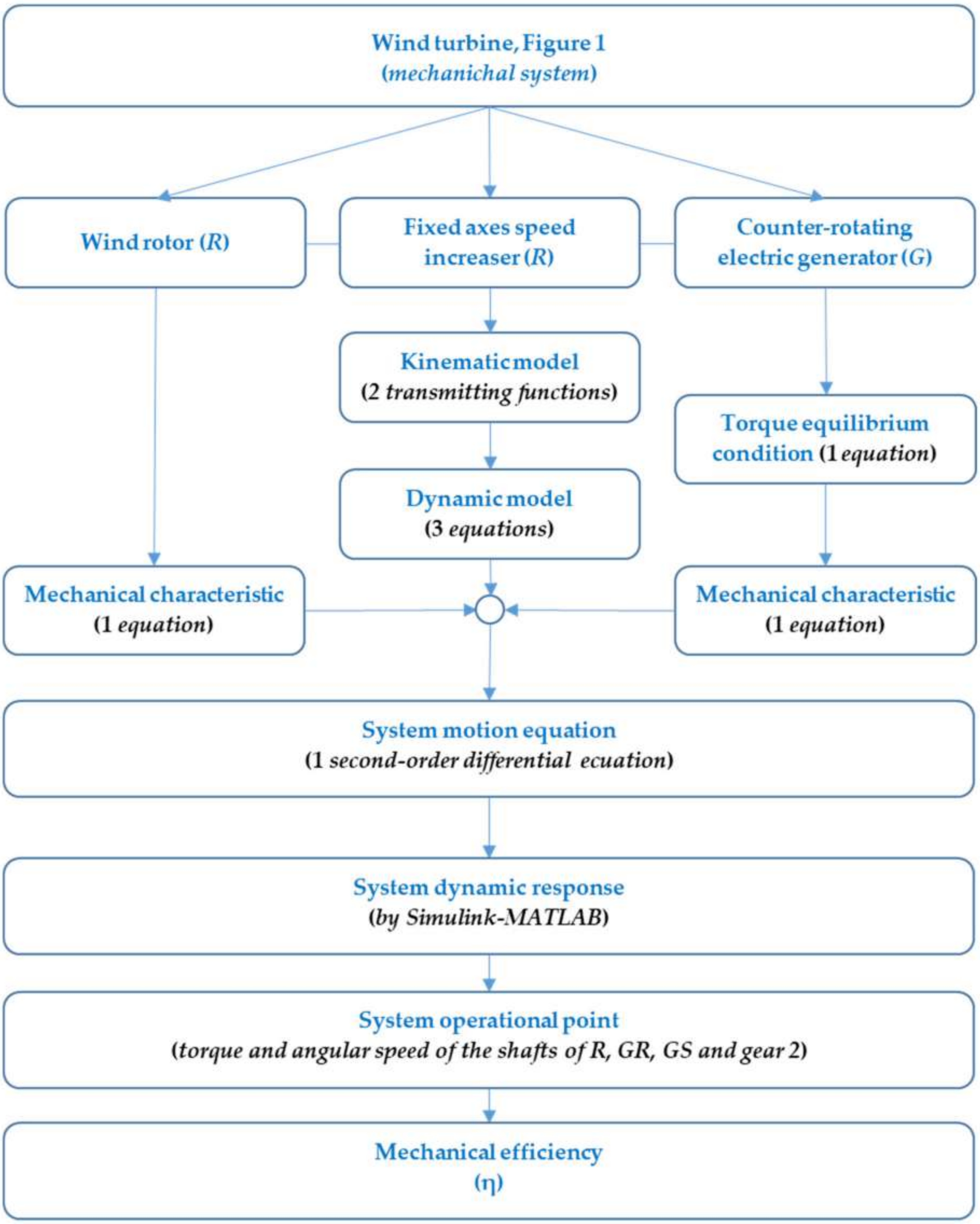

Figure 2. Flowchart of the proposed dynamic modelling for single-rotor wind turbines with counter-rotating electric generator.

3. Dynamic Modelling

The dynamic equations of a general system of motor(s)-mechanism-effector(s) type describe the system motion under the action of actuation and resistance forces/torques. The dynamic equations of a wind turbine under the premises mentioned in Section 2 are homogeneous linear differential equations of second order. The angular acceleration and speed of the wind rotor interfere with and define the independent motion of the mechanical system.

The dynamic modelling method uses the equations of the Newton-Euler formalism and implies the prior isolation of each body by replacing the connections between the bodies by the corresponding reaction forces. It is followed by the description of the Newton-Euler equations for each body, according to the general expression when the origin of the coordinate system attached to the body coincides with the body centre of mass cm [37]:

$$\begin{pmatrix} \mathbf{F} \\ \mathbf{T} \end{pmatrix} = \begin{pmatrix} m\mathbf{I}_3 & 0 \\ 0 & \mathbf{J_{cm}} \end{pmatrix} \begin{pmatrix} \mathbf{a_{cm}} \\ \boldsymbol{\varepsilon} \end{pmatrix} + \begin{pmatrix} 0 \\ \omega \times \mathbf{J_{cm}}\omega \end{pmatrix} \tag{7}$$

where $\mathbf{F}$ is the resultant force vector acting on the centre of mass, m—the body mass, $\mathbf{I}_3$—the 3×3 identity matrix, $\mathbf{a_{cm}}$—acceleration vector of the centre of mass, $\mathbf{T}$—resultant torque vector acting on the centre of mass, $\mathbf{J_{cm}}$—moment of inertia defined about the centre of mass, $\boldsymbol{\omega}$—angular speed vector of the body, and $\boldsymbol{\varepsilon}$—angular acceleration vector of the body.

In the case of symmetrical bodies with a fixed axis of rotation (i.e., the centre of mass cm is a fixed point on the axis of rotation), Equation (7) can be simplified in the following scalar form:

$$T = J \cdot \varepsilon \tag{8}$$

where T is the resultant torque acting on body, J—moment of inertia around the body motion axis, and ε—angular acceleration of the body.

3.1. Dynamic Equations of Component Bodies

Based on the scheme from Figure 1a, the considered wind turbine can be decomposed into the following rigid bodies:

- body B1: the assembly consisting of the sun gear 1, the generator rotor GR, and the connecting shaft, Figure 3a;
- body B2: the assembly wind rotor R—ring gear 2—generator stator GS, Figure 3b;
- a number s_3 of gears 3 and their shafts (body B3), evenly distributed around the central axis, Figure 3c.

The positive direction of the angular speed and torque vectors for all the bodies B1 ... B3 is defined to the right (Figure 1), while J_x denotes the axial moment of inertia of the body x = 1 ... 3, ω_x—the angular speed of the body x, and T_x—the resultant torque acting on the body x.

Thus, considering the body B1 characterised by the fixed-rigid connection between gear 1 and the generator rotor RG, the following equations can be written (Figure 3a):

$$\omega_1 = \omega_{GR} \tag{9}$$

$$J_1\varepsilon_1 = T_{GR} - T_1 \tag{10}$$

Similarly, the kinematic and dynamic equations of the B2 body, characterised by the connections $R \equiv 2 \equiv GS$, can be described by (Figure 3b):

$$\omega_R = \omega_2 = \omega_{GS} \tag{11}$$

$$J_2\varepsilon_2 = T_R - T_2 + T_{GS} \tag{12}$$

The mechanical power is transmitted from ring gear 2 to gear 1 through s_3 theoretically equal flows, corresponding to s_3 number of gears 3 that are mounted in parallel between gears 2 and 1. As a result, the body B3 is driven theoretically by a torque T_{32} defined by relation (13):

$$T_{32} = \frac{T_2}{s_3} i_{2\_3}\eta_{2\_3} \tag{13}$$

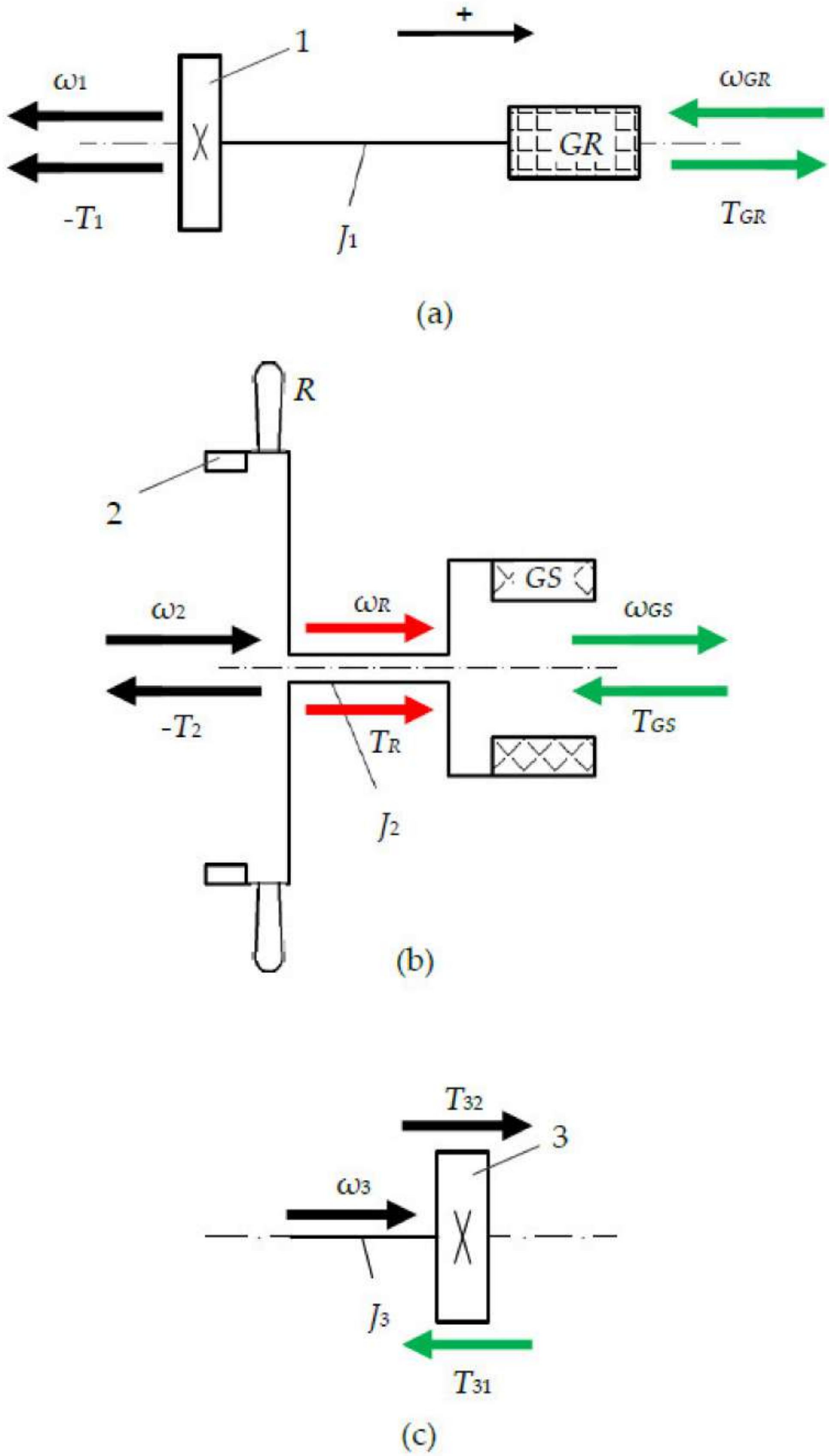

Figure 3. Dynamic scheme of: (**a**) body B1; (**b**) body B2; and (**c**) body B3.

which comes from the energetic equilibrium equation with friction for the gear pair 2–3:

$$T_2\omega_2\eta_{2\_3} = s_3 T_{32}\omega_3 \tag{14}$$

where $i_{2\_3} = \omega_2/\omega_3 = z_3/z_2$ is the kinematic ratio of the gear pair 2–3, and η_{2_3}—the efficiency of the gear pair 2–3.

Gear 3 is also subjected to a reaction torque T_{31} from gear 1:

$$T_{31} = \frac{T_1}{s_3} i_{1\_3}\eta_{3\_1}^{-1} \tag{15}$$

defined as well based on the energetic equilibrium equation with friction for the gear pair 3–1:

$$s_3 T_{31}\omega_3\eta_{3\_1} = T_1\omega_1 \tag{16}$$

where $i_{1\_3} = \omega_1/\omega_3 = -z_3/z_1$ is the kinematic ratio of the gear pair 1–3, and η_{3_1}—the efficiency of the gear pair 3–1.

As a result, the dynamic equation for the body B3 is:

$$J_3\varepsilon_3 = T_{32} + T_{31} \tag{17}$$

which by considering Equations (13) and (15) becomes:

$$s_3 J_3\varepsilon_3 = T_2 i_{2\_3}\eta_{2\_3} + T_1 i_{1\_3}\eta_{3\_1}^{-1} \tag{18}$$

Relation (18) models the transmission of mechanical power from gear 2 to gear 1 in the general case of considering the inertial effects of the body B3 and the impact of gear friction; if the mass of body 3 is neglected (i.e., $J_3 = 0$) or if the turbine is operating in a steady-state regime (i.e., $\varepsilon_3 = 0$), Equation (18) takes the particular form:

$$T_2 i_{2\_1}\eta_{2\_1} + T_1 = 0 \tag{19}$$

which expresses the energetic equilibrium condition of the speed increaser *SI* in the premise of considering friction in gear pairs, in which:

$$i_{2\_1} = \frac{\omega_2}{\omega_1} = i_{2\_3}\cdot i_{3\_1} = -\frac{z_1}{z_2} \tag{20}$$

and

$$\eta_{2\_1} = \eta_{2\_3}\cdot\eta_{3\_1} \tag{21}$$

3.2. Mechanical Characteristics

The set of dynamic equations of the three bodies B1 . . . B3 is completed with the linear mechanical characteristics with constant coefficients of the wind rotor and the counter-rotating electric generator, respectively:

- the wind rotor *R*

$$T_R = -a_R\omega_R + b_R,\ 0 \le \omega_R \le \frac{b_R}{a_R},\ a_R > 0,\ b_R > 0 \tag{22}$$

- the electric generator *G*

$$T_G = -a_G\omega_G + b_G,\ \omega_G \le \frac{b_G}{a_G},\ a_G > 0,\ b_G < 0 \tag{23}$$

where a_R, b_R, a_G, b_G are the constant coefficients under the steady-state regime, and, by definition, $T_G = T_{GR}$. Moreover, the functional specificity of an electric generator ensures the torque equilibrium condition between the rotor *GR* and the stator *GS*:

$$T_{GR} + T_{GS} = 0 \tag{24}$$

According to the chosen positive direction (see Figure 3), the mechanical characteristic of the wind rotor is active in quadrant I ($T_R > 0$ and $\omega_R > 0$), while for the electric generator in quadrant II, ($T_G > 0$ and $\omega_G < 0$) for absolute values of the angular speed ω_G larger than the critical value $|b_G/a_G|$, which delimits the operating modes as motor and generator of the *DC* machine, Figure 4. Therefore, in the dynamic analysis, the electric machine will be considered in idle functioning regime (i.e., $T_G = 0$) until the required operating speed as a generator is reached:

$$T_G = 0 \text{ for } \omega_G > \frac{b_G}{a_G} \tag{25}$$

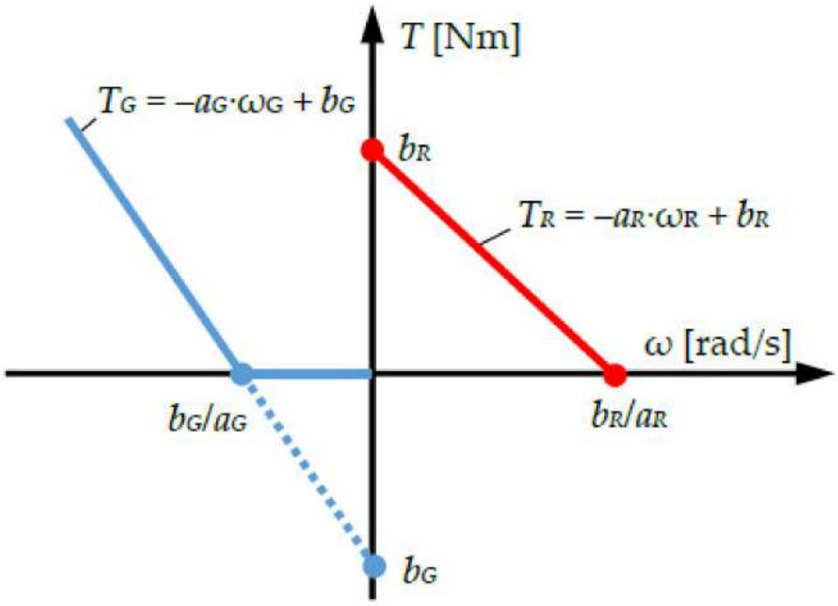

Figure 4. Linear mechanical characteristics of a wind rotor (*R*) and a *DC* generator (*G*).

In the present study, it was assumed that the electric generator was not adjusted during operation, and the pitch angle of the wind rotor blades was not changed. Instead, the mechanical characteristic of the wind rotor changes with the variation of the wind speed, as the mechanical power P_R generated at the wind rotor shaft depends on wind speed value [38]:

$$P_R = \frac{1}{2}\pi\rho C_p r_R^2 v_w^3 \tag{26}$$

where ρ is the air density, C_p—aerodynamic power coefficient, r_R—radius of the wind rotor, and v_w—the wind speed.

In the general case, the coefficient Cp depends on the wind speed v_w, the angular speed of the wind rotor ω_R, and the blade pitch angle β. Since, in this study, the pitch angle was considered constant β = 0°, the general relation of the power coefficient Cp [38–40] is obtained through particularisation in the following form:

$$C_p = c_1\left(\frac{c_2}{\lambda_i} - c_3\right) \cdot e^{-\frac{c_4}{\lambda_i}} + c_5\lambda \tag{27}$$

where λ is the tip speed ratio:

$$\lambda = \frac{\omega_R r_R}{v_w} \tag{28}$$

and

$$\frac{1}{\lambda_i} = \frac{1}{\lambda} - c_6 \tag{29}$$

where c_1 = 0.5176, c_2 = 116, c_3 = 5, c_4 = 21, c_5 = 0.0068, and c_6 = 0.035.

Thus, the mechanical characteristic of a wind rotor $T_R = T_R(\omega_R, v_w)$ can be described analytically by Equation (30):

$$T_R = \frac{P_R}{\omega_R} = \frac{1}{2}\pi\,\rho\, r_R^3 v_w^2 \left[\frac{c_1 v_w}{\omega_R r_R} \left(\frac{c_2 v_w}{\omega_R r_R} - c_2 c_6 - c_3 \right) \cdot e^{-c_4\left(\frac{v_w}{\omega_R r_R} - c_6\right)} + c_5 \right] \tag{30}$$

Considering the air density ρ = 1.225 kg/m^3, the mechanical characteristic of a wind rotor with the radius r_R = 5 m is illustrated in Figure 5 for different values of wind speed v_w. There is a distinct evolution of the torque T_R on the three zones A, B and C (Figure 5a), with approximately linear shapes, rounded at the transition from one zone to another. Thus, the torque T_R remains constant with the increase in the angular velocity ω_R up to a threshold value of the angular speed (which increases with the increase in the wind speed, zone A), followed by an ascending evolution to the maximum value (*max* T_R, zone B) and a lower slope decrease on zone C—the normal operating area of the wind rotor. It can also be noticed that the maximum power points (*max* P_R) are found in zone C, at higher values of the angular speed ω_R than those corresponding to the maximum torque points (*max* T_R). Moreover, regardless of wind speed, the maximum power points are located at the limit of the approximately linear sector of the mechanical characteristic from zone C. Therefore, it is reasonable to consider the hypothesis of mechanical characteristics of wind turbines as linear functions with constant coefficients at a given value of the wind speed, under the condition that the wind turbine operates at optimal angular speed values (corresponding to the maximum power point) or higher.

Considering the curves in zone C approximated by linear functions, described according to Equation (22), the influence of increasing wind speed on the wind rotor mechanical characteristic can be summarised as follows (Figure 5b):

- it causes the increase in the angular speed during idle operation (i.e, TR = 0), meaning the increase in the bR/aR value.
- it leads to the increase in the characteristic slope and to the increase in the bR value, implicitly.

As a result, both coefficients a_R and b_R are directly influenced by the wind speed and thus the wind rotor operates under a different mechanical characteristic when the wind changes its speed.

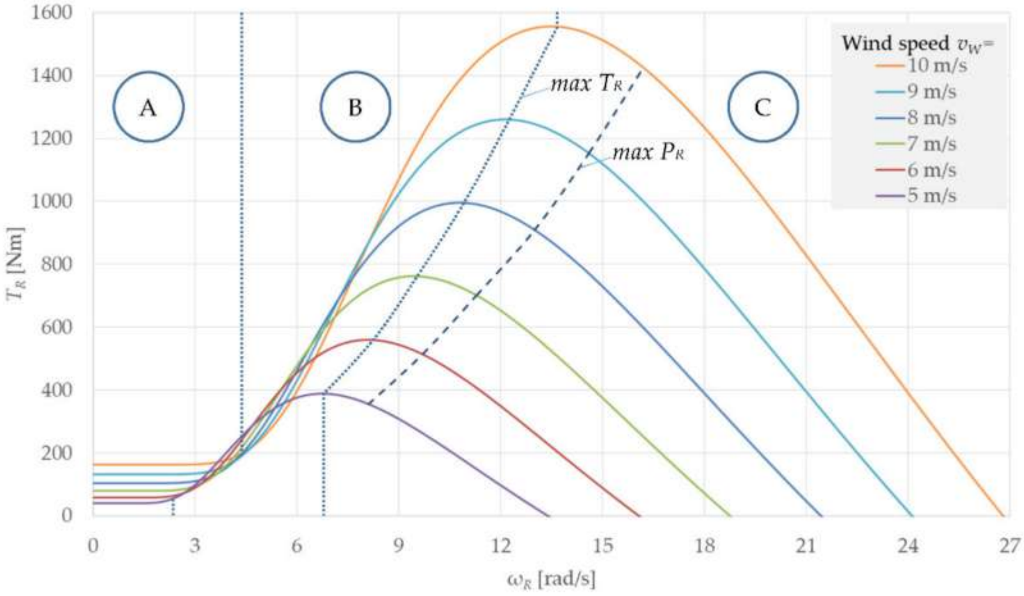

(a)

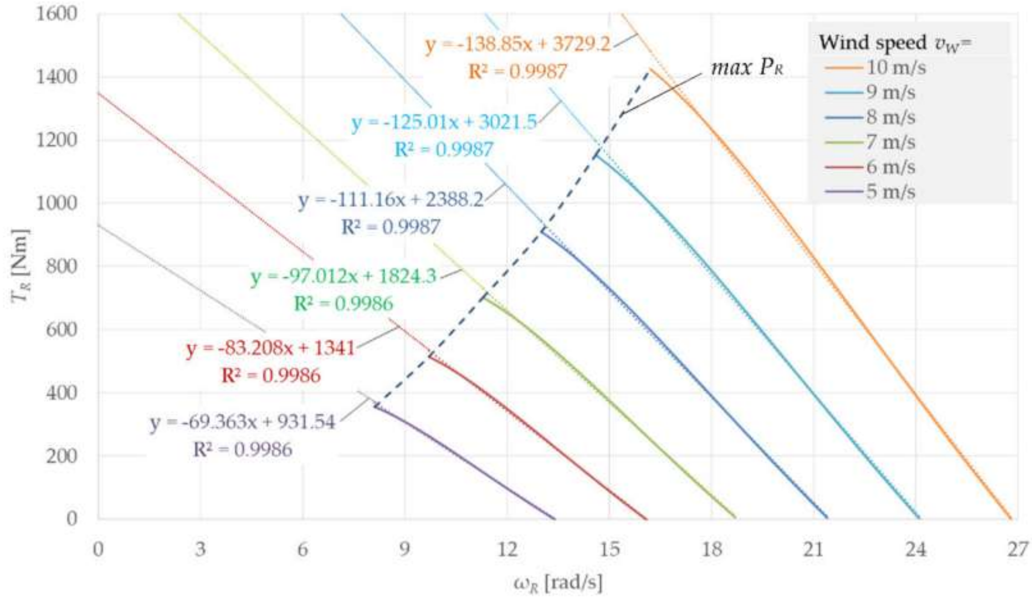

(b)

Figure 5. The influence of wind speed on the mechanical characteristic of a wind rotor: (**a**) mechanical characteristic zones; (**b**) linearized active sector of mechanical characteristics.

3.3. System Motion Equation

The wind system motion in the dynamic regime is described by a second-order differential equation represented as a function of the independent input motion of the wind rotor R, i.e., the angular speed $\omega_R = \dot{\varphi}_R$ and angular acceleration $\varepsilon_R = \ddot{\varphi}_R$, where φ_R is the angular displacement of the wind rotor, $\dot{\varphi}_R = d\varphi_R/dt$ and $\ddot{\varphi}_R = d^2\varphi_R/dt^2$.

According to Equations (10) and (18), the torques T_1 and T_2 are obtained:

$$T_1 = T_G - J_1\varepsilon_1 \tag{31}$$

$$T_2 = \frac{s_3 J_3 \varepsilon_3 - T_1 i_{1\_3} \eta_{3\_1}^{-1}}{i_{2\_3} \eta_{2\_3}} \tag{32}$$

and considering Equations (11), (12), and (31), the angular acceleration is obtained:

$$\varepsilon_R = \frac{T_R + T_G\left(\frac{i_{1\_2}}{\eta_{2\_1}} - 1\right)}{J_1\frac{i_{1\_2}^2}{\eta_{2\_1}} + J_2 + s_3 J_3 \frac{i_{3\_2}^2}{\eta_{2\_3}}} \quad (33)$$

in which the following obvious replacements are considered:

$$\varepsilon_1 = i_{1\_2}\varepsilon_2;\ \varepsilon_3 = i_{3\_2}\varepsilon_2;\ T_{GS} = -T_G \quad (34)$$

Equation (35) is obtained from Equations (23), (5), and (11):

$$T_G = -a_G(i_{1\_2} - 1)\omega_R + b_G \quad (35)$$

The motion equation of the wind system is obtained replacing Equations (22) and (35) in (33):

$$\varepsilon_R = \frac{-\left[a_R + a_G(i_{1\_2} - 1)\left(\frac{i_{1\_2}}{\eta_{2\_1}} - 1\right)\right]\omega_R + \left[b_R + b_G\left(\frac{i_{1\_2}}{\eta_{2\_1}} - 1\right)\right]}{J_1\frac{i_{1\_2}^2}{\eta_{2\_1}} + J_2 + s_3 J_3 \frac{i_{3\_2}^2}{\eta_{2\_3}}} \quad (36)$$

The following a priori known constant parameters interfere in the differential Equation (36):

$$a_R,\ b_R,\ a_G,\ b_G,\ J_1,\ J_2,\ J_3, i_{1\_2},\ i_{3\_2}, \eta_{2\_1}, \eta_{2\_3} \quad (37)$$

in which the parameters a_R and b_R are dependent on the wind speed, according to linear trend lines in Figure 5b.

The time variation of the independent parameters (φ_R, $\dot{\varphi}_R$, $\ddot{\varphi}_R$) is obtained solving Equation (36) under given initial conditions, which describes the evolution in time of the kinematic (displacements, angular speeds, and accelerations) and dynamic behaviour (torques, powers, and efficiency) of the wind system and its components. Equation (36) is numerically solved using Simulink-MATLAB by MathWorks, aspects of which are presented in Section 4.

3.4. Mechanical Efficiency

The energy loss due to friction in a mechanical system is expressed by mechanical efficiency, as a measure of how the mechanical input power is transmitted through the mechanism to the outputs. The mechanical efficiency is a variable quantity in the transient regime, significantly influenced by the system's inertial properties, which tends asymptotically towards a maximum value specific to the steady-state system operation.

Thus, the relation for the mechanical efficiency of the wind turbine is established starting from its definition, in which Equations (22) and (35) are replaced:

$$\eta = -\frac{T_G\omega_G}{T_R\omega_R} = -\frac{-a_G(i_{1\_2} - 1)\omega_R + b_G}{-a_R\omega_R + b_R}(i_{1\_2} - 1) \quad (38)$$

Equation (36) is solved as a function of ω_R and the mechanical efficiency in the transient regime is obtained after the replacement of the obtained solution in Equation (38):

$$\eta = \frac{(i_{1\_2} - 1)a_R b_G - (i_{1\_2} - 1)^2 a_G(b_R - \varepsilon_R J^*)}{\left(\frac{i_{1\_2}}{\eta_{2\_1}} - 1\right)a_R b_G - (i_{1\_2} - 1)\left(\frac{i_{1\_2}}{\eta_{2\_1}} - 1\right)a_G b_R - a_R\varepsilon_R J^*} \quad (39)$$

where J^* is the equivalent mechanical moment of inertia of the system reduced at body 2:

$$J^* = J_1\frac{i_{1\_2}^2}{\eta_{2\_1}} + J_2 + s_3 J_3\frac{i_{3\_2}^2}{\eta_{2\_3}} \quad (40)$$

Equation (39) shows the dependence of efficiency on the angular acceleration ε_R of the wind rotor; in a steady-state regime (i.e., $\varepsilon_R = 0$), the expression of the mechanical efficiency can be simplified as follows:

$$\eta = \eta_{2\_1} \frac{i_{1\_2} - 1}{i_{1\_2} - \eta_{2\_1}} \tag{41}$$

Unlike the conventional wind turbines with a wind rotor and conventional generator (with fixed stator), in which the speed increaser has the efficiency independent of the speed amplification ratio, the stationary mechanical efficiency of wind turbines with counter-rotating generator depends on both the efficiency of the speed increaser SI with fixed axes (i.e., $\eta_{2\_1} = \eta_{2\_3}\eta_{3\_1}$) and the kinematic ratio i_{1_2}, according to Equation (41). Given that the kinematic ratio i_{1_2} has a negative supraunitary value and $\eta_{2\_1} < 1$, it is obvious that $\eta > \eta_{2\_1}$. Thus, it can be concluded that wind turbines with counter-rotating generator have a better mechanical efficiency in a steady-state regime than the conventional systems that integrate the same speed increaser.

4. Results and Discussions

The numerical simulations of the dynamic model presented in Section 3, developed for the wind turbine with counter-rotating electric generator described in Section 2, aim to highlight the evolution in time of the mechanical power parameters (i.e., torque and angular speed) for input and output shafts, as well as the angular acceleration and the system mechanical efficiency, in the conditions of sudden changes of the wind speed. Thus, we considered a wind turbine with a rated power of 10 kW at a nominal wind speed of 8 m/s, characterised by the parameters from Table 1, in a operating scenario in which the wind turbine started under the action of a 8 m/s wind (stage I), after which the wind speed dropped sharply to 6 m/s after 8 s (stage II) and then returned to 8 m/s after 15 s (stage III). Since the linear model adopted for the mechanical characteristic of the wind rotor is valid only on the useful area of this characteristic (see Figure 5, zone C), in stage I the initial starting phase was ignored (which is not the object of this research) and the time of 0 s was chosen at the moment when the angular speed of the wind rotor reached the value corresponding to the maximum power *max* P_R.

Table 1. The parameters of the 10 kW wind turbine with counter-rotating generator.

Component	Parameter	Value	Unit
Wind rotor			
v_w = 8 m/s	a_R	111.16	Nm/s
	b_R	2388.2	Nm
v_w = 6 m/s	a_R	83.208	Nm/s
	b_R	1341	Nm
Speed increaser			
	i_{1_2}	−9	-
	i_{3_2}	2.25	-
	i_{1_3}	−4	-
	$\eta_{2\_3} = \eta_{3\_1}$	0.975	-
	η_{2-1}	0.9506	-
	s_3	3	-
Electric generator			
	a_G	3	Nm/s
	b_G	−395	Nm
Inertial parameters			
	J_1	2.5	kgm^2
	J_2	75	kgm^2
	J_3	0.25	kgm^2

The dynamic analytical model of the wind turbine was implemented in the Simulink module from Matlab by MathWorks. The obtained graphical results including the mechanical efficiency of the wind system are systematised in: Figure 6 for the input (wind rotor *R*) and output components (electric generator *G*), Figure 7 for the rotor *GR* and the stator *GS* of the electric generator, and the distributions of the torque and power of the wind rotor on the two branches towards the speed increaser input and towards the stator *GS* are illustrated in Figure 8.

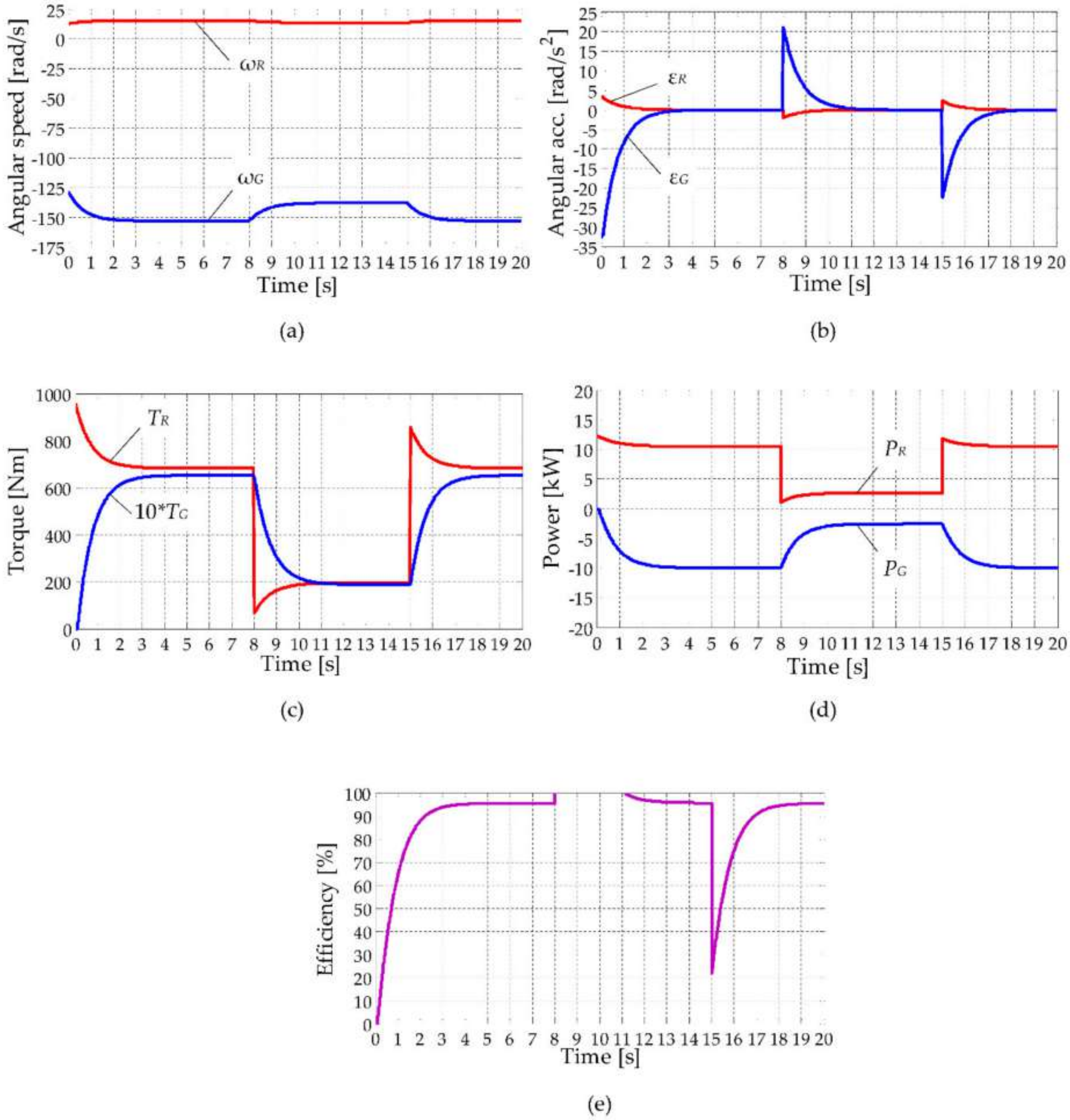

Figure 6. The dynamic behaviour of the wind rotor *R* and electric generator *G* in relation to wind speed modification: (**a**) angular speed; (**b**) angular acceleration; (**c**) torque; (**d**) mechanical power; and (**e**) mechanical efficiency.

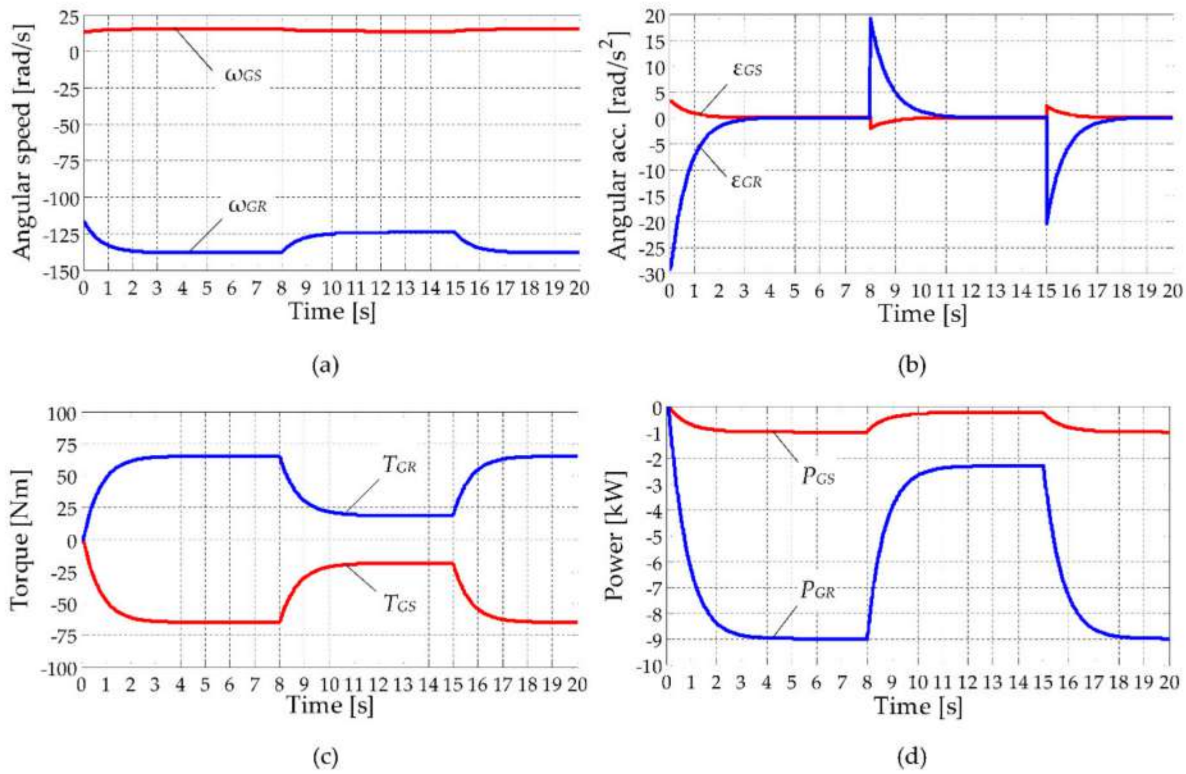

Figure 7. The dynamic behaviour of the generator rotor *GR* and stator *GS* in relation to wind speed modification: (**a**) angular speed; (**b**) angular acceleration; (**c**) torque; and (**d**) mechanical power.

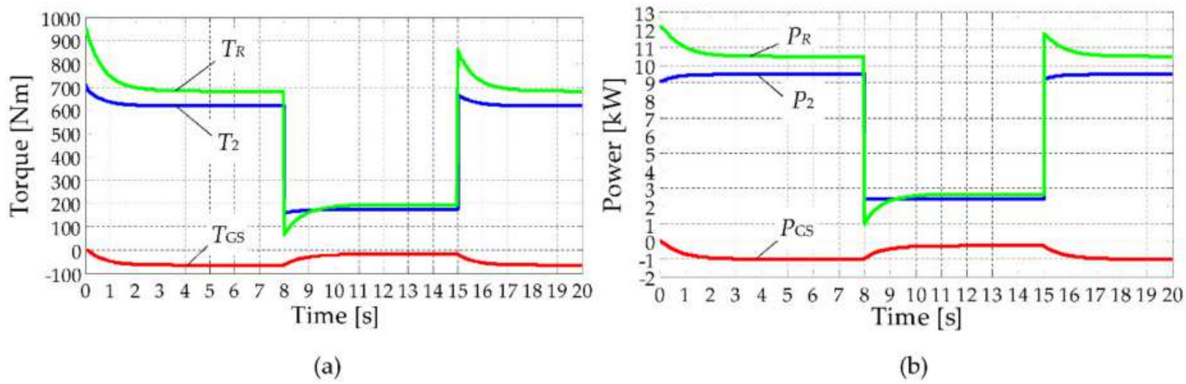

Figure 8. The dynamic distribution on gear 2 and the generator stator *GS* of the: (**a**) torque and (**b**) mechanical power generated by the wind rotor *R*.

In stage I of the considered operating scenario, the wind turbine passed through a transient period until entering the steady-state, i.e., characterised by constant values of the kinematic parameters and torques, Figure 6a–d. Typically, the beginning of the steady-state regime is identified when the angular accelerations become null, Figure 6b. In this transient stage, the system was accelerated, a significant part of the wind rotor power P_R was used to overcome the inertial resistance of the mechanical components and the accumulation of kinetic energy, implicitly.

The electric generator started producing electricity only when the speed ω_G became equal to the value b_G/a_G = 131.67 rad/s (see also Figure 4), shortly (about 0.1 s) after the entry of the wind rotor into the active area of its mechanical characteristic. At each operating time, the ratio between the angular speeds ω_G and ω_R and the ratio between the angular accelerations ε_G and ε_R, respectively, was constant and equal in this case to $i_{G\_R} = -10$.

In the steady-state operating regime during 4 to 8 s, the electric generator was operated with a power of 10 kW (Figure 6d) at an angular speed = 153.4 rad/s (Figure 6d).

The decrease in the wind speed to 6 m/s after 8 s of operation (Stage II) caused the change in the mechanical characteristic of the wind rotor (see Table 1) and also the crossing of a transient stage (of about 3 s) towards a new steady-state operation, Figure 6a–d. The significant decrease in the wind rotor power P_R to ~2.67 kW and of the driving power of the electric generator P_G to ~2.56 kW, i.e., a reduction of ~25% of the rated power when the wind speed has dropped to only 75% of its nominal value, is noted in Figure 6d. This significant decrease in power is due mainly to the large decrease in torques (Figure 6c) and less of the angular speeds (Figure 6a).

It is also worth noting the atypical evolution of the mechanical efficiency η, which became supraunitary under the conditions of the definition from Equation (37): according to Figure 6d, the power of the wind rotor P_R decreased suddenly with the decrease in the wind speed, but the power P_G changed progressively due to the active effect of the kinetic energy, accumulated in the previous stage, which was added to the mechanical energy produced by the wind rotor. The efficiency η in a steady-state regime was higher than the efficiency of the speed increaser (η_{2_1}), i.e., 95.53% vs. 95.06%.

In stage III of the numerical simulation scenario, the wind speed returned suddenly to the nominal value v_w = 8 m/s, after 15 s of operation. The variation in the functional parameters was relatively similar to the one from stage II, symmetrically to the horizontal axis. A sudden decrease in efficiency can be noted (Figure 6e) given that the power of the wind rotor was used at the beginning mainly to accelerate the mechanical system and less to increase the power P_G.

The evolution in time of the kinematic parameters and torques for the two mobile components of the electric generator, in the three stages of the simulation scenario, are presented in Figure 7. The generator rotor *GR* had an angular speed increased by $i_{GR\_R} = -9$ and higher than speed of the stator *GS*, implicitly ($i_{GS\_R} = 1$), Figure 6a. The angular accelerations ε_{GR} and ε_{GS} (Figure 7b) had similar evolutions to those illustrated in Figure 6b, given that $\varepsilon_{GS} = \varepsilon_R$ and $\varepsilon_{GR} = \varepsilon_G + \varepsilon_{GS}$, which are derived from Equations (11) and (5), respectively.

The symmetry of the torques curves for the two components of the electric generator (Figure 7c), characterised by the connection relationship from Equation (24), could also be observed. Since the torques T_{GS} and T_{GR} were equal in absolute value, the variation of the powers P_{GS} and P_{GR} depended significantly on the values of the angular speeds ω_{GS} and ω_{GR}. As a result, the leading share of power was brought by the rotor *GR*, characterised by an angular speed higher than the stator *GS* speed; at the same time, the rotor *GR* also had the most significant power drop with the decrease in wind speed in stage II, Figure 7d.

The torque T_R generated by the wind rotor *R* was dynamically distributed on two branches to gear 2 (speed increaser input) and the generator stator *GS*, the relation between these torques being influenced by the system inertia in the acceleration/deceleration phases, according to the dynamic relations from Equations (10), (12), and (18). Thus, in the transient phase of stage I, the torque T_R was used to accelerate the system and to balance the inertial resistances dynamically, implicitly, which were due to the mechanical moments of inertia J_1 and J_3, on the one hand, and J_2, on the other hand, Figure 8a. The resistances generated by the gearing friction forces also interfered in this process. Once the electric generator was put into operation, the resistant mechanical torque of the generator was added to the resistances mentioned above. The active effect of the kinetic energy accumulated in stage I can be observed at the beginning of stage II (Figure 8a), the torque T_2 being higher than T_R. Similar evolutions and conclusions can be found for the powers P_R, P_2, and P_{GS}, according to Figure 8b.

5. Conclusions

This paper presented a generalized dynamic modelling approach of the mechanical system of a single-rotor wind turbine with counter-rotating *DC* generator, which integrates a mechanical speed increaser on the power flow to the generator rotor *GR* and a direct connection of the generator stator *GS* to the wind rotor *R*. The proposed modelling algorithm considered, besides the dynamic equations of the component rigid bodies, the linear mechanical characteristics of the electric generator and wind rotor.

The analytical study and the numerical simulations of the considered case study in a functional scenario with three stages drew the following conclusions:

- The proposed dynamic modelling algorithm, synthetically explained in Figure 2 and detailed in Section 3, is a novel and general approach for the class of wind turbines with a single wind rotor and a counter-rotating electric generator. It enabled us to derive the motion equation and obtain the dynamic response and operating point of the mechanical system in a number and a well-defined sequence of steps, regardless of the type of components of the wind system.
- The proposed modelling for the linearization of the active sector of the mechanical characteristic of the wind rotor simplified the analytical modelling of the dynamic response, without introducing significant errors in relation to their nonlinear model regardless of the value of wind speed v_w: the obtained linear functions are characterized by higher values of the statistical parameter R-squared ($R^2 > 0.998$ for the case study of a 10 kW wind turbine, Figure 5b).
- The proposed analytical approach enabled us to identify the wind system dynamic behaviour at wind speed change both in a transient regime and a steady-state regime, in a particular case characterised by zero angular accelerations.
- The use of a counter-rotating generator in a wind turbine has the advantage of higher mechanical efficiency and kinematic ratio i_{G_R} than in a wind turbine of identical power that contains a conventional electric generator (with fixed stator).
- The proposed diagrams depicted in Figures 6–8, i.e., the variation of the mechanical power parameters, enabled us to draw valuable conclusions for the functional optimization of the wind turbine.

The authors aim to extend in future the simplified modelling of the mechanical characteristic of the wind rotor through a succession of linear functions covering the entire range of angular speed ω_R variation, which will enable the complete identification of the dynamic behaviour in the starting phase. We also intend to validate the theoretical results by using specialised rigs experimentally.

Author Contributions: Conceptualization, M.N. and R.S.; methodology, M.N., R.S. and C.J.; software, M.N. and R.S.; validation, M.N., R.S., C.J. and I.N.; formal analysis, M.N., R.S., C.J. and I.N.; investigation, M.N., R.S., C.J. and I.N.; writing—original draft preparation, M.N., R.S., C.J. and I.N.; writing—review and editing, M.N., R.S., C.J. and I.N.; visualization, M.N., R.S., C.J. and I.N.; supervision, M.N. and C.J. All authors have read and agreed to the published version of the manuscript.

Funding: This research received no external funding.

Institutional Review Board Statement: Not applicable.

Informed Consent Statement: Not applicable.

Conflicts of Interest: The authors declare no conflict of interest.

Nomenclature

a, b	Coefficients of mechanical characteristics
$\mathbf{a_{cm}}$	Acceleration vector of mass centre
B	Body
DC	Direct current
F	Force
G	Electric generator
GR	Electric generator rotor
GS	Electric generator stator
H	Satellite carrier
I	Kinematic ratio
$\mathbf{I}$	Identity matrix
J	Moment of inertia
J^*	Equivalent mechanical moment of inertia
m	Mass
P	Power
R	Wind rotor
r	Radius of the gear pitch circle
SI	Speed increaser
T	Torque
v	Linear speed
v_w	Wind speed
z	Gear teeth number
δ	Angle of the speed vector
ε	Angular acceleration
η	Mechanical efficiency
ω	Angular speed

References

1. European Commission. The European Green Deal. Available online: https://ec.europa.eu/info/sites/default/files/european-green-deal-communication_en.pdf (accessed on 15 September 2021).
2. European Commission. Energy. Roadmap 2050. Available online: https://ec.europa.eu/energy/sites/ener/files/documents/2012_energy_roadmap_2050_en_0.pdf (accessed on 15 September 2021).
3. International Renewable Energy Agency. Global energy transformation: A roadmap to 2050. Available online: https://www.irena.org/-/media/Files/IRENA/Agency/Publication/2018/Apr/IRENA_Report_GET_2018.pdf (accessed on 15 September 2021).
4. International Renewable Energy Agency. Global Renewables Outlook: Energy Transformation 2050. Available online: https://www.irena.org/publications/2020/Apr/Global-Renewables-Outlook-2020 (accessed on 15 September 2021).
5. Global Wind Energy Council (GWEC). Global Wind Report 2021. Available online: https://gwec.net/wp-content/uploads/2021/03/GWEC-Global-Wind-Report-2021.pdf (accessed on 15 September 2021).
6. Tostado-Véliz, M.; Icaza-Alvarez, D.; Jurado, F. A novel methodology for optimal sizing photovoltaic-battery systems in smart homes considering grid outages and demand response. *Renew. Energ.* **2021**, *170*, 884–896. [CrossRef]
7. Zamani, R.; Golshan, M.E.H.; Alhelou, H.H.; Hatziargyriou, N. A Novel Synchronous DGs Islanding Detection Method based on Online Dynamic Features Extraction. *Electr. Power Syst. Res.* **2021**, *195*, 107180. [CrossRef]
8. Alhelou, H.H.; Golshan, M.E.H.; Zamani, R.; Moghaddam, M.P.; Njenda, T.C.; Siano, P.; Marzband, M. An Improved UFLS Scheme based on Estimated Minimum Frequency and Power Deficit. In Proceedings of the IEEE Milan PowerTech, Milan, Italy, 23–27 June 2019; IEEE: Milan, Italy, 2019; pp. 1–6. [CrossRef]
9. Cottura, L.; Caradonna, R.; Ghigo, A.; Novo, R.; Bracco, G.; Mattiazzo, G. Dynamic Modeling of an Offshore Floating Wind Turbine for Application in the Mediterranean Sea. *Energies* **2021**, *14*, 248. [CrossRef]
10. Jiang, Y.; Hu, G.; Zong, Z.; Zou, L.; Jin, G. Influence of an Integral Heave Plate on the Dynamic Response of Floating Offshore Wind Turbine Under Operational and Storm Conditions. *Energies* **2020**, *13*, 6122. [CrossRef]
11. Bagherian, V.; Salehi, M.; Mahzoon, M. Rigid multibody dynamic modeling for a semi-submersible wind turbine. *Energ. Convers. Manag.* **2021**, *244*, 114399. [CrossRef]
12. Santoso, S.; Le, H. Fundamental time–Domain wind turbine models for wind power studies. *Renew. Energy* **2007**, *32*, 2436–2452. [CrossRef]
13. Fernández-Ramírez, L.; Saenz, J.; Jurado, F. Dynamic models of wind farms with fixed speed wind turbines. *Renew. Energy* **2006**, *31*, 1203–1230. [CrossRef]

14. Jansuya, P.; Kumsuwan, Y. Design of MATLAB/Simulink Modeling of Fixed-pitch Angle Wind Turbine Simulator. *Energy Procedia* **2013**, *34*, 362–370. [CrossRef]
15. Amarante Mesquita, A.L.; Amarante Mesquita, A.L.; Coutinho Palheta, F.; Pinheiro Vaz, J.R.; Girão de Morais, M.V.; Gonçalves, C. A methodology for the transient behavior of horizontal axis hydrokinetic turbines. *Energy Convers. Manag.* **2014**, *87*, 1261–1268. [CrossRef]
16. Qi, L.; Zheng, L.; Bai, X.; Chen, Q.; Chen, J.; Chen, Y. Nonlinear Maximum Power Point Tracking Control Method for Wind Turbines Considering Dynamics. *Appl. Sci.* **2020**, *10*, 811. [CrossRef]
17. Han, R.; Wang, L.; Wang, T.; Gao, Z.; Wu, J. Study of Dynamic Response Characteristics of the Wind Turbine Based on Measured Power Spectrum in the Eyewall Region of Typhoons. *Appl. Sci.* **2019**, *9*, 2392. [CrossRef]
18. Oyekola, P.; Mohamed, A.; Pumwa, J. Renewable Energy: Dynamic Modelling of a Wind Turbine. *Int. J. Innov. Technol. Explor. Eng.* **2019**, *9*, 9. [CrossRef]
19. Mathis, R.; Rémond, Y. Kinematic and dynamic simulation of epicyclic gear trains. *Mech. Mach. Theory* **2009**, *44*, 412–424. [CrossRef]
20. Xiang, L.; Gao, N.; Hu, A. Dynamic analysis of a planetary gear system with multiple nonlinear parameters. *J. Comput. Appl. Math.* **2017**, *327*, 325–340. [CrossRef]
21. Dong, H.; Zhang, C.; Wang, D.; Xu, S.; Qiu, J. Dynamic characteristics of gear box with PGT for wind turbine. *Procedia Comput. Sci.* **2017**, *109*, 801–808. [CrossRef]
22. Zhu, C.; Xu, X.; Liu, H.; Luo, T.; Zhai, H. Research on dynamical characteristics of wind turbine gearboxes with flexible pins. *Renew. Energy* **2014**, *68*, 724–732. [CrossRef]
23. Fan, Z.; Zhu, C.; Li, X.; Liang, C. The transmission characteristic for the improved wind turbine gearbox. *Energy Sci. Eng.* **2019**, *7*, 1368–1378. [CrossRef]
24. Shi, W.; Kim, C.; Chung, C.; Park, H. Dynamic Modeling and Analysis of a Wind Turbine Drivetrain Using the Torsional Dynamic Model. *Int. J. Precis. Eng. Manuf.* **2012**, *14*, 153–159. [CrossRef]
25. Jaliu, C.; Diaconescu, D.V.; Neagoe, M.; Saulescu, R. Dynamic features of speed increasers from mechatronic wind and hydro systems. Part I: Structure kinematics. In Proceedings of the EUCOMES 2008—The 2nd European Conference on Mechanism Science, Cassino, Italy, 17–20 September 2008; pp. 351–359. [CrossRef]
26. Jaliu, C.; Diaconescu, D.V.; Neagoe, M.; Saulescu, R. Dynamic features of speed increasers from mechatronic wind and hydro systems. Part II: Dynamic aspects. In Proceedings of the EUCOMES 2008—The 2nd European Conference on Mechanism Science, Cassino, Italy, 17–20 September 2008; pp. 361–368. [CrossRef]
27. Lin, A.-D.; Hung, T.-P.; Kuang, J.-H.; Tsai, H.-A. Power Flow Analysis on the Dual Input Transmission Mechanism of Small Wind Turbine Systems. *Appl. Sci.* **2020**, *10*, 7333. [CrossRef]
28. Wu, J.; Zhou, Y.; Jiang, W.; Chen, X. Time-Domain Dynamic Modeling and Analysis of Complex Heavy-Duty Gearbox Considering Floating Effect. *Appl. Sci.* **2021**, *11*, 6876. [CrossRef]
29. Wang, J.; Yang, S.; Liu, Y.; Mo, R. Analysis of Load-Sharing Behavior of the Multistage Planetary Gear Train Used in Wind Generators: Effects of Random Wind Load. *Appl. Sci.* **2019**, *9*, 5501. [CrossRef]
30. Neagoe, M.; Diaconescu, D.V.; Jaliu, C.; Pascale, L.; Saulescu, R.; Sisca, S. On a new cycloidal planetary gear used to fit mechatronic systems of RES. In Proceedings of the 11th International Conference on Optimization of Electrical and Electronic Equipment, Brasov, Romania, 22–24 May 2008; pp. 439–448. [CrossRef]
31. Neagoe, M.; Saulescu, R.; Jaliu, C.; Simionescu, P.A. A Generalized Approach to the Steady-State Efficiency Analysis of Torque-Adding Transmissions Used in Renewable Energy Systems. *Energies* **2020**, *13*, 4568. [CrossRef]
32. Song, Z.; Shi, T.; Xia, C.; Chen, W. A novel adaptive control scheme for dynamic performance improvement of DFIG-Based wind turbines. *Energy* **2012**, *38*, 104–117. [CrossRef]
33. Qais, M.H.; Hasanien, H.M.; Alghuwainem, S. Optimal Transient Search Algorithm-Based PI Controllers for Enhancing Low Voltage Ride-Through Ability of Grid-Linked PMSG-Based Wind Turbine. *Electronics* **2020**, *9*, 1807. [CrossRef]
34. Booker, J.; Mellor, P.H.; Wrobel, R.; Drury, D. A compact, high efficiency contra-rotating generator suitable for wind turbines in the urban environment. *Renew. Energy* **2010**, *35*, 2027–2033. [CrossRef]
35. Neagoe, M.; Saulescu, R.; Jaliu, C. Design and Simulation of a 1 DOF Planetary Speed Increaser for Counter-Rotating Wind Turbines with Counter-Rotating Electric Generators. *Energies* **2019**, *12*, 1754. [CrossRef]
36. Saulescu, R.; Neagoe, M.; Jaliu, C.; Munteanu, O. A Comparative Performance Analysis of Counter-Rotating Dual-Rotor Wind Turbines with Speed-Adding Increasers. *Energies* **2021**, *14*, 2594. [CrossRef]
37. Hahn, H. *Rigid Body Dynamics of Mechanisms. 1 Theoretical Basis*; Springer: Berlin/Heidelberg, Germany, 2002; ISBN 9783540423737.
38. Kong, X.; Ma, L.; Liu, X.; Abdelbaky, M.A.; Wu, Q. Wind Turbine Control Using Nonlinear Economic Model Predictive Control over All Operating Regions. *Energies* **2020**, *13*, 184. [CrossRef]
39. Petković, D.; Ćojbašić, Ž.; Nikolić, V. Adaptive neuro-fuzzy approach for wind turbine power coefficient estimation. *Renew. Sustain. Energy Rev.* **2013**, *28*, 191–195. [CrossRef]
40. Rahman, S.; Akther, S.; Hoque, H.E. Comparison of Different Pitch Controller in Wind Farm for Integrated Power System. *Am. J. Eng. Res.* **2018**, *7*, 288–299. [CrossRef]

Dynamic Modeling and Simulation of a Counter-Rotating Wind System with 1-DOF Planetary Speed Increaser

Mircea Neagoe[1](✉), Codruta Ileana Jaliu[1], and Radu Gabriel Saulescu[2]

[1] Renewable Energy Systems and Recycling R&D Center, Transilvania University of Brasov, Brasov, Romania
{mneagoe,cjaliu}@unitbv.ro

[2] Design of Mechanical Elements and Systems R&D Center, Transilvania University of Brasov, Brasov, Romania

Abstract. The paper presents a theoretical study on the dynamic behavior of a wind system composed by two counter-rotating wind rotors-planetary speed increaser-conventional generator. Its dynamic analytical model is developed by using the Newton–Euler method, in the assumption of rigid bodies and known linear mechanical characteristics of the two wind rotors and of the direct current generator. Numerical simulations were carried out in MATLAB-Simulink on a 700 kW wind turbine case study, which allowed highlighting the time variation of the kinematic parameters, torques and powers for the system shafts, both in transient and steady-state regimes. Analytical and numerical results are useful to researchers, designers and developers of wind turbines, who aim to optimize their construction and functionality through virtual prototyping.

Keywords: Renewable Energy · Wind System · Counter-Rotating Wind Turbine · Planetary Gearbox · Dynamic Modelling · Simulation

1 Introduction

The optimal design of wind energy systems faces permanent challenges in ensuring high energy performance, their dynamic behavior playing a significant role in relation to their functional performance, power output, reliability and lifetime. Dynamic modeling of wind turbines (WT), used for their behavior identification and control or functional optimization, has attracted the attention of many researchers in the last decades. Various dynamic modeling approaches are presented in the literature, while numerical simulation is mainly performed with the MATLAB-Simulink software package.

Numerous dynamic studies consider the wind system (WS) as a whole [1–9], based on the wind speed considered as main constant input parameter [3, 4, 7, 10]. Various mechanical characteristics of the wind rotors and the generator are considered in the system modeling, either of polynomial [1] or linear [6, 11].

The researchers paid special attention to the dynamics of speed increasers (SI) used in wind systems, their response being decisive for WS dynamic behavior. Most of the

M. Okada (Ed.): IFToMM WC 2023, MMS 149, pp. 1–11, 2024.
https://doi.org/10.1007/978-3-031-45709-8_72

speed increasers presented in literature are 1 degree-of-freedom (1-DOF) [2, 6, 11–18] and rarely 2-DOF transmissions [5, 19].

The most common dynamic modeling methods are Newton–Euler [6, 20] and Lagrange [8, 15–18, 21]. One of the software frequently used for numerical simulation of analytical dynamic models is Matlab-Simulink [2–4, 6, 7, 9, 10, 16, 17], which allows identifying the time variation of representative kinematic and dynamic parameters, such as angular speeds [3, 6–9], torques [3, 6–8, 21], powers [3, 6–8].

The development of dynamic models is needed for WS dynamic effect analysis and optimization. Moreover, according to the best knowledge of the authors, there are not relevant results in the literature on generalized dynamic modeling of the mechanical system for the WT class with counter-rotating wind rotors and conventional electric generator. The paper aims to cover this gap by developing a dynamic modeling algorithm for this WT class, through the Newton–Euler method, to identify the motion equation and to simulate numerically the dynamic behavior of a 700 kW wind turbine.

The rest of the paper is organized as follows: the formulation of the problem is introduced in Sect. 2, the kinematic and dynamic modeling algorithm of a counter-rotating WS with 1-DOF planetary speed increaser is detailed in Sect. 3, the numerical results obtained by simulating the analytical model in Matlab-Simulink are presented in Sect. 4, and the final conclusions are drawn in Sect. 5.

2 Problem Formulation

This study aims to present a specific algorithm for analytical dynamic modeling of a counter-rotating WS with 1-DOF planetary increaser and traditional electric generator (with fixed stator) and to identify its dynamic response in the start-up transient regime by numerical simulation of the theoretical model in the Matlab-Simulink software. In this respect, it is considered the WT depicted in Fig. 1 (half-upper side), composed by two wind rotors ($R1$—the upwind rotor, $R2$—the downwind rotor), an electric generator G and a 1-DOF cylindrical planetary speed increaser 1-2-3-4-5-H. The powers generated by the two wind rotors are summed up in the generator, a solution that brings the advantage of more power and a compact speed increaser (with a lower kinematic ratio) compared to conventional wind turbines (with a single wind rotor).

The considered SI is a planetary transmission derived from a novel solution proposed by the authors [22], composed of three central gears ($1 \equiv 0$, 2 and 3), a double satellite 4-5 and a satellite carrier H, with three external links: two inputs (H and 2) and an output 3 connected to the generator G. The rotors $R1$ and $R2$ are designed and adjusted to rotate in opposite directions and are connected to the speed increaser inputs. As a 1-DOF speed increaser, it has the property of increasing the output speed relative to the input speed, as well as summing up the torques generated by the two wind rotors. The 1-DOF planetary transmission with three external links has by default one independent external motion (of the upwind rotor $R1$) and two independent external torques (e.g., T_{R2} and T_G).

The dynamic modeling of the WS depicted in Fig. 1 is carried out by using the Newton–Euler method under the following assumptions:

- all system elements are geometrically symmetric rigid bodies with homogeneous spatially distributed mass;

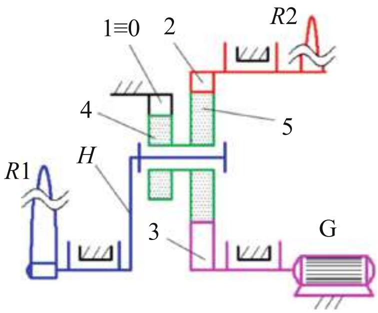

Fig. 1. Structural scheme of the 1-DOF wind system with two inputs and one output.

- the inertial effect of satellites 4-5 is reduced to the H element (i.e., the axial mechanical moment of inertia of the satellite carrier also includes the contribution of the satellites);
- the mechanical moments of inertia of the SI components are fully transferred to the shafts of the wind rotors and of the generator rotor. Thus, the planetary transmission can be modeled dynamically only with the help of static equations, without affecting the WS dynamic behavior;
- only the friction on gear pairs is considered (the friction in bearings is neglected);
- the nonlinear mechanical characteristic of the wind rotors is approximated by five successive linear functions, on five specific speed ranges;
- the generator is a direct current (DC) electric machine and has a linear mechanical characteristic, implicitly.

The WS dynamic response is simulated for a numerical case that allows the rotors $R1$ and $R2$ to operate simultaneously at their maximum power in steady-state, knowing that the downwind rotor $R2$ only benefits from a part of the input wind energy. Also, the system is controlled to activate the load (connecting the generator to the grid) only after the generator has reached the required speed. In these conditions, the time variation of some specific mechanical parameters (speed, torque and power), for all transmission shafts in start-up regime, is further addressed.

3 Kinematic and Dynamic Modeling

The WS (Fig. 1) has associated the block diagram from Fig. 2, in which the SI is modeled as a transmission composed by two planetary gear sets connected in parallel: a 1-DOF $PU1$ (1-4-5-3-H) and a 2-DOF $PU2$ (2-5-3-H). The block diagram shows the torques T_x and rotational speeds ω_x of the transmission shafts $x = 1, 2, 3, H$.

Figure 3 shows the dynamic schemes of the component subsystems obtained by isolating them from the analyzed WS (Fig. 1), where J_x represents the axial mechanical moment of inertia of a subsystem x, reduced to its shaft. The assumption of SI transmission without inertial masses (see Sect. 2) is considered.

Applying the method of isolating the component subsystems [11, 14], the following kinematic and dynamic correlations can be written for $PU1$, $PU2$ and the connections between them:

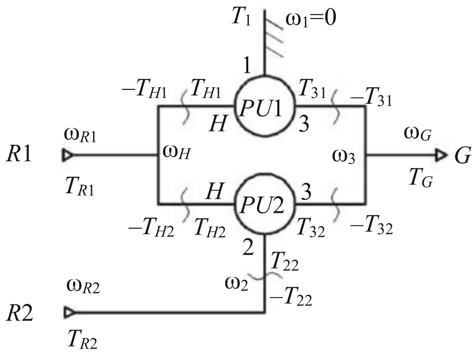

Fig. 2. Block scheme of the 1-DOF wind system with two inputs and one output.

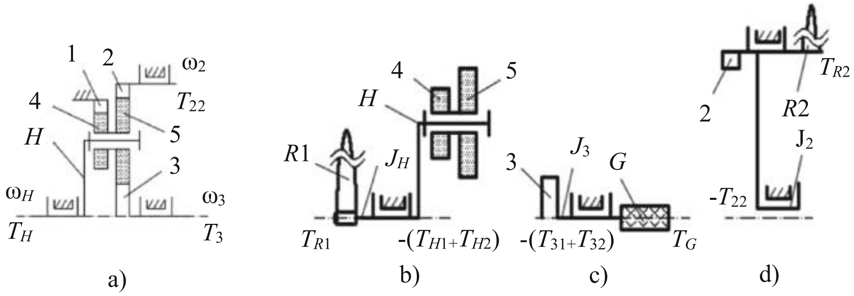

Fig. 3. Dynamic schemes for the WT subsystems: a) the speed increaser without inertial masses; b) the element H equipped with rotor $R1$ and satellite gears 4-5; c) the central gear 3 with the generator shaft, d) the central gear 2 and the rotor $R2$.

- specific equations of $PU1$ (1-4-5-3-H) and $PU2$ (2-5-3-H) (Fig. 3a):

$$UPI:\begin{cases}\omega_3-\omega_H(1-i_{01})=0\\ T_1+T_{31}i_{01}\eta_{01}^x=0\\ T_1+T_{31}+T_{H1}=0\end{cases},\quad UP2:\begin{cases}\omega_3-\omega_2 i_{02}-\omega_H(1-i_{02})=0\\ T_{22}+T_{32}i_{02}\eta_{02}^w=0\\ T_{22}+T_{32}+T_{H2}=0\end{cases}\tag{1}$$

- specific correlations for the wind rotor $R1$ and satellite carrier H (Fig. 3b):

$$\begin{cases}\omega_{R1}=\omega_H\\ J_H\varepsilon_H=T_{R1}-(T_{H1}+T_{H2})\end{cases}\tag{2}$$

- specific correlations for the generator G and gear 3 (Fig. 3c):

$$\begin{cases}\omega_3=\omega_G\\ J_3\varepsilon_3=T_G-(T_{31}+T_{32})\end{cases}\tag{3}$$

- specific correlations for the wind rotor $R2$ and gear 2 (Fig. 3d):

$$\begin{cases}\omega_{R2}=\omega_2\\ J_2\varepsilon_2=T_{R2}-T_{22}\end{cases}\tag{4}$$

where i_{01}, i_{02} and η_{01}, η_{02} are the internal kinematic ratios and internal efficiencies of the planetary units $PU1$ and $PU2$, respectively, and the superscripts x and w are the efficiency coefficients.

3.1 Kinematic Functions

Considering the motion of the primary rotor $R1$ as independent, based on the Eqs. (1)–(5) the expressions of the dependent angular velocities and accelerations (of shafts 2 and 3) can be obtained:

$$\omega_3 = \omega_H(1 - i_{01}), \quad \varepsilon_3 = \varepsilon_H(1 - i_{01}) \tag{5}$$

$$\omega_2 = \omega_H \frac{i_{02} - i_{01}}{i_{02}}, \quad \varepsilon_2 = \varepsilon_H \frac{i_{02} - i_{01}}{i_{02}} \tag{6}$$

3.2 Torque Functions and the Equation of Motion

The system of dynamic equations, obtained by extracting the torque equations from Eqs. (1)–(5), and considering the torques T_{R2} and T_G as independent, has as solution the expressions of the dependent torques (T_{22}, T_1, T_{H1}, T_{H2}, T_{31}, T_{32}, T_{R1}):

$$T_{22} = T_{R2} - J_2\varepsilon_H \frac{i_{02} - i_{01}}{i_{02}}, \quad T_1 = -T_G i_{01}\eta_{01}^x - T_{22}\frac{i_{01}\eta_{01}^x}{i_{02}\eta_{02}^w} + J_3\varepsilon_3 i_{01}\eta_{01}^x \tag{7}$$

$$T_{H1} = T_G\left(i_{01}\eta_{01}^x - 1\right) + T_{22}\left(\frac{i_{01}\eta_{01}^x - 1}{i_{02}\eta_{02}^w}\right) - J_3\varepsilon_3\left(i_{01}\eta_{01}^x - 1\right), \; T_{H2} = T_{22}\left(\frac{1}{i_{02}\eta_{02}^w} - 1\right) \tag{8}$$

$$T_{31} = T_G + T_{22}\frac{1}{i_{02}\eta_{02}^w} - J_3\varepsilon_3, \quad T_{32} = -T_{22}\frac{1}{i_{02}\eta_{02}^w} \tag{9}$$

$$T_{R1} = J_H\varepsilon_H + T_{H1} + T_{H2}. \tag{10}$$

The equation of motion of the wind system can be obtained by replacing relations (7)–(9) in Eq. (10):

$$\varepsilon_H = \frac{T_{R1} - T_G\left(i_{01}\eta_{01}^x - 1\right) - T_{R2}\left(\frac{i_{01}\eta_{01}^x}{i_{02}\eta_{02}^w} - 1\right)}{J_H - J_2\left(\frac{i_{02} - i_{01}}{i_{02}}\right)\left(\frac{i_{01}\eta_{01}^x}{i_{02}\eta_{02}^w} - 1\right) + J_3(i_{01} - 1)\left(i_{01}\eta_{01}^x - 1\right)} \tag{11}$$

where the external torques T_{R1}, T_G and T_{R2} have the expressions given by the mechanical characteristics (linear functions, see Sect. 2) of the wind rotors and generator:

$$T_{R1} = -a_{R1}\omega_{R1} + b_{R1}, \; T_{R2} = -a_{R2}\omega_{R2} + b_{R2}, \; T_G = -a_G\omega_G + b_G \tag{12}$$

where a_{R1}, b_{R1}, a_{R2}, b_{R2}, a_G and b_G are constant coefficients.

4 Results and Discussions

The numerical simulation of the WS dynamic behavior, modeled by the equation of motion (11), is carried out for the case study of a 700 kW wind turbine with rated wind speed of 14 m/s. The two wind rotors have diameters equal to 34 m. The intrinsic parameters of the speed increaser are: $i_{01} = -29$, $i_{02} = -17.4$, $\eta_{01} = \eta_{02} = 0.97^2 = 0.9409$, $x = -1$, $w = -1$. The mechanical characteristic of the electric generator is defined by the constant coefficients $a_G = 0.1$ kNs and $b_G = 6.22$ kN. The mechanical characteristics of the wind rotors are non-linear functions [6], and the solution of their approximation by linearization on five intervals was chosen. Since $R2$ rotates in the opposite direction to the $R1$, characterized by definition of positive values of the power parameters, it operates in quadrant 3 (both the moment and the angular velocity are negative, Fig. 4a), while the electric generator operates in quadrant 4, Fig. 4b.

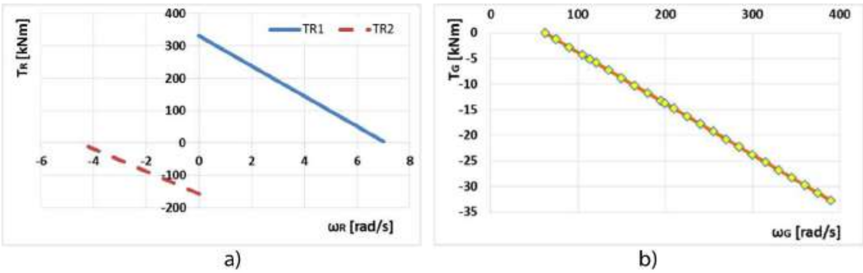

Fig. 4. Examples of linear mechanical characteristics of: a) wind rotors, b) DC electric generator.

4.1 Determination of the Mechanical Characteristics of Wind Rotors

For a constant wind speed, the torque generated by a wind rotor varies non-linearly with speed, Fig. 5: in the first part the torque increases slowly at low values (zone I), followed by an approximately linear increase (zone II) and then a transitional evolution (zones III and IV) to a final approximately linear shape of torque decreasing (zone V). Zones IV and V are exploited in operation, the maximum power point being located in zone IV, according to Fig. 5.

The mechanical characteristics of the two wind turbines are linearized in this study on the mentioned five zones, the values of the coefficients $a_{R1,2}$ and $b_{R1,2}$ being systematized in Table 1.

4.2 Dynamic Response

The WS analytical model, defined by Eqs. (5)–(12), was implemented in a Matlab-Simulink application and numerically simulated under the following assumptions:

- the system starts from rest at a constant wind speed $v_w = 14$ m/s (the rated wind speed), i.e. the mechanical characteristics of rotors $R1$ and $R2$ (with equal diameters of 17 m) from Table 1 are used;

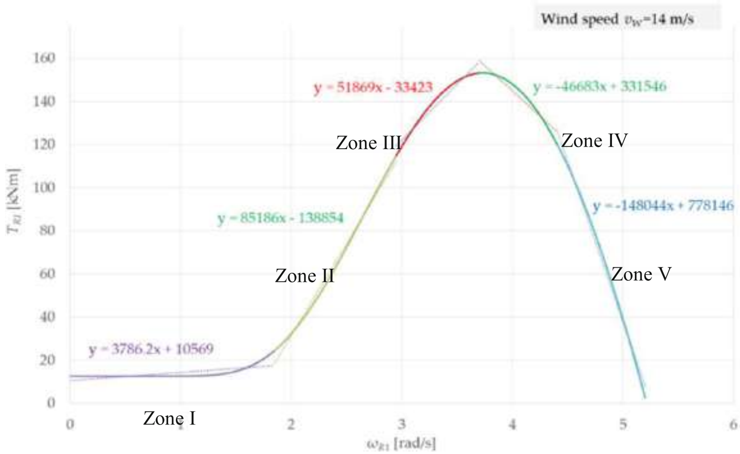

a)

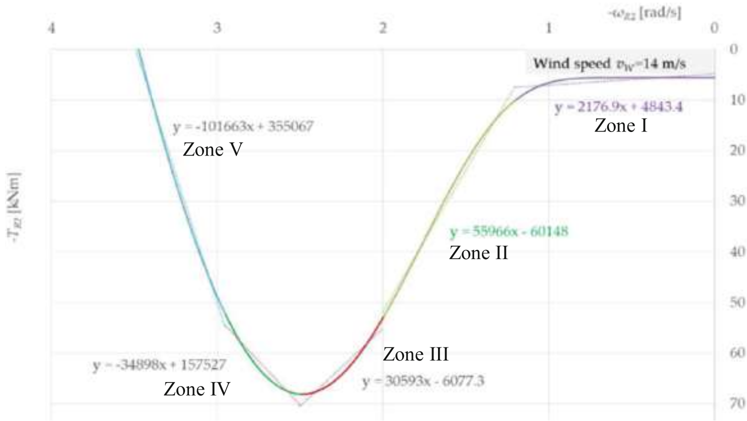

b)

Fig. 5. Torque versus speed curve (mechanical characteristic) of the wind rotor: a) $R1$ and b) $R2$.

Table 1. Coefficients of the mechanical characteristics of the rotors $R1$ and $R2$ on five zones.

Zone	Rotor $R1$		Rotor $R2$	
	a_{R1} [kNms]	b_{R1} [kNm]	a_{R2} [kNms]	b_{R2} [kNm]
I	− 3.7862	+ 10.569	− 2.1769	− 4.8434
II	− 85.186	− 138.854	− 55.966	+ 60.148
III	− 51.869	− 33.423	− 30.593	+ 6.0773
IV	+ 46.683	+ 331.546	+ 34.898	− 157.527
V	+ 148.044	778.146	+ 101.663	− 355.067

- the electric generator is activated (connected to power grid) after its speed reaches the value b_G / $a_G = 62.2$ rad/s, corresponding to the transition of the electric machine to generator mode;
- the wind system reaches the steady-state regime in zone IV (Fig. 5); its operating point corresponding to the maximum power point of the wind rotors.

The main results of the numerical simulation, in the transient regime of starting from rest at the rated wind speed, are depicted in Fig. 6, from which the following aspects can be highlighted:

- the starting time of the wind system is approx. 60 s, i.e. the time period the system to enter in steady-state (null accelerations);
- in the first 33.5 s, the system is increasingly accelerated as a result of the rotors traveling through zone I and partially zone II, having only inertial resistance as load;
- when $\omega_G = b_G$ / $a_G = 62.2$ rad/s (at time = 33.5 s, on zone II) the generator is connected to the power network and starts producing electricity; thus, the two wind rotors receive a new workload: the generator resistant torque, increasing linearly with generator speed;
- after generator activation, the system continues to increase the speed (Fig. 6a) until reaching the steady-state regime; the angular acceleration increases rapidly in zone II and then in zone III (entry time = 39.3 s), followed by a decreasing to zero after entering zone IV (at time = 42.2 s, Fig. 6b);
- the torques generated by the rotors $R1$ and $R2$ also increase rapidly on zones II and III, followed by a decrease on zone IV until the operating point is reached, Fig. 6c. Despite of equal diameters, the rotor $R1$ produces a torque ~ 3 times higher than $R2$ (the downwind rotor), that receive wind with significantly lower speed (~ 9.3 m/s) than $R1$ (14 m/s);
- the input and output powers have a similar variation to the torques; the upwind rotor $R1$ extracts ~ 3 times more power from the wind than $R2$. The powers of the rotors $R1$ and $R2$ are positive quantities (being input powers to the speed increaser), and the power of the generator is negative (output power);
- the wind system reaches in steady-state the operating point, power and efficiency at values specified in Table 2.

5 Conclusions

The paper presents an analytical dynamic modeling algorithm of a wind system from a novel class: WT with two counter-rotating rotors and 1-DOF speed increaser. The main output of the dynamic modeling is the equation of motion, expressed as a differential relationship between the independent motion (i.e., the angular velocity and acceleration of the rotor $R1$) and the independent external torques. The equation of motion was solved numerically and the WS dynamic behavior in transitory regime, including the identification of the operating point in the steady-state, was carried out in a specific application developed in the Matlab-Simulink software. The obtained analytical and numerical results allowed highlighting the following general conclusions:

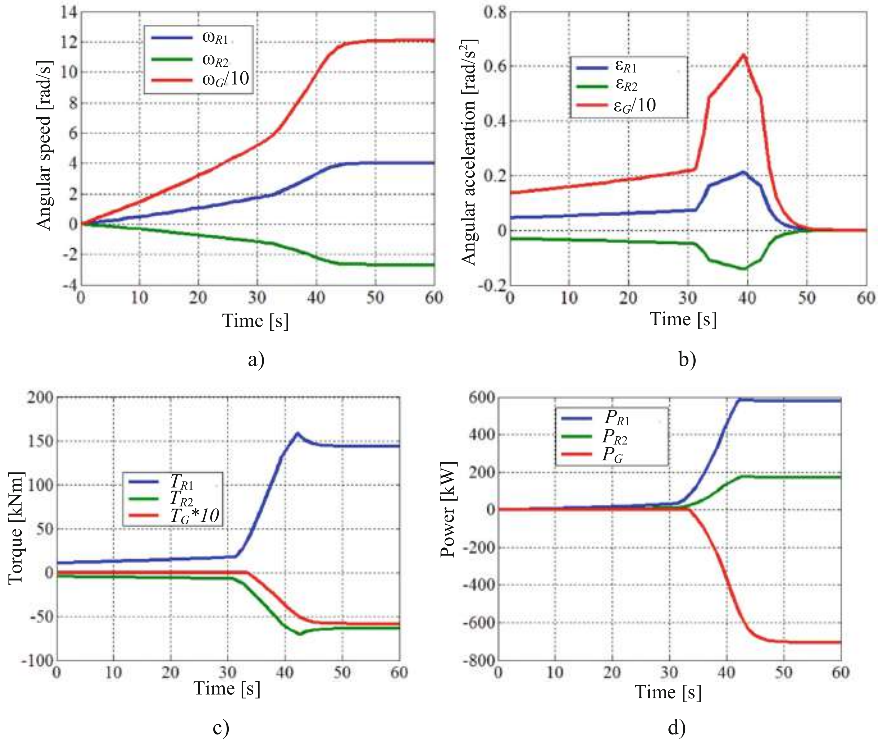

Fig. 6. Dynamic behavior of the wind system: a) angular velocities, b) angular accelerations, c) torques and d) powers.

Table 2. Kinematic and dynamic parameters at the operating point (in steady state).

Parameter	Rotor $R1$	Rotor $R2$	Generator G
Angular speed ω [rad/s]	4.024	− 2.683	120.733
Torque T [kNm]	143.673	− 63.897	− 5.854
Power P [kW]	578.140	171.433	− 706.771
Mechanical efficiency: $\eta = 94.24\%$			

- The proposed kinematic and dynamic modeling algorithm, based on the decomposition of the system into its components, the distribution of the moments of inertia of the speed increaser elements to its external shafts and the application of the Newton-Euler method, allowed to successfully obtain the differential equation of motion and all the correlations for torques, angular speeds and accelerations.

- The wind system crosses the transient regime in two phases: at the beginning, the wind turbine operates at idle and has only the inertial resistance as load; in the second phase, the generator is connected to the power grid to provide electricity, and hence a new load from the generator is accompanied the inertial load.
- The wind system stabilizes once entered into steady state regime; the values of its kinematic and static parameters represent the system operational point. In this regime only the generator load charges the system, the inertial load vanishes because of null accelerations.
- The developed model allows the identification of the values of all kinematic (velocities and angular accelerations) and dynamic (moments, powers) parameters in steady state, as well as their evolution during the transient regime.
- Wind turbines with counter-rotating rotors have the advantage of higher powers (approx. 30% higher) than traditional ones (with a single wind rotor), which is also confirmed by the paper results.

References

1. Abo-Khalil, A., Alyami, S., Sayed K., Alhejji A.: Dynamic modeling of wind turbines based on estimated wind speed under turbulent conditions. Energy **12** (2019). https://doi.org/10.3390/en12101907
2. Al-Hamadani, H., An, T., King, M., Long, H.: System dynamic modelling of three different wind turbine gearbox designs under transient loading conditions. Int. J. Precis. Eng. Manuf. **18**(11) (2017). https://doi.org/10.1007/s12541-017-0194-1
3. Erturk, E., Sivrioglu, S., Bolat, F.C.: Analysis model of a small scale counter-rotating dual rotor wind turbine with double rotational generator armature. Int. J. Renew. Energy Res. **8**(4) (2018). https://doi.org/10.20508/ijrer.v8i4.8235.g7549
4. Girsang, I,P., DhupiaS.J., Muljadi, E., Singh, M., Pao, Y.P.: Gearbox and drivetrain models to study dynamic effects of modern wind turbines. IEEE Trans. Ind. Appl. **50**(6) (2013). https://doi.org/10.1109/ECCE.2013.6646795
5. Lin, A.-D.; Hung, T.-P.; Kuang, J.-H.; Tsai, H.-A.: Power Flow analysis on the dual input transmission mechanism of small wind turbine systems. Appl. Sci. **10** (2020). https://doi.org/10.3390/app10207333
6. Neagoe, M., Saulescu, R., Jaliu, C., Neagoe, I.: Dynamic analysis of a single-rotor wind turbine with counter-rotating electric generator under variable wind speed. Appl. Sci. **11**, 8834 (2021). https://doi.org/10.3390/app11198834
7. Oyekola, P., Mohamed, A., Pumwa, J.: Renewable energy: dynamic modelling of a wind turbine. Int. J. Innov. Technol. Explor. Eng. **9** (2019). https://doi.org/10.35940/ijitee.A4411.119119
8. Teixeira, M.R., Ohara, M.F., Milhomens, D.M., de Paula S.A.: Dynamical behavior of a wind turbine power train considering a rotor-gearbox-generator coupled model. Eccomas Proceedia COMPDYN, 3543–3555 (2017). https://doi.org/10.7712/120117.5664.17890
9. Wang, B., Michon, M., Holehouse, R., Atallah, K.: Dynamic behaviour of a multi-MW wind turbine, 978-1-4673-7151-3/15/$31.00 IEEE (2015)
10. Jansuya, P., Kumsuwan, Y.: Design of MATLAB/Simulink modeling of fixed-pitch angle wind turbine simulator. Energy Procedia **34** (2013). https://doi.org/10.1016/j.egypro.2013.06.764

11. Neagoe, M., Saulescu, R., Jaliu, C.: Design and simulation of a 1 DOF planetary speed increaser for counter-rotating wind turbines with counter-rotating electric generators. Energies **12**, 1754 (2019). https://doi.org/10.3390/en12091754
12. Dewangan, P., Parey, A., Hammami, A., Chaari F., Haddar, M.: Dynamic characteristics of a wind turbine gearbox with amplitude modulation and gravity effect: theoretical and experimental investigation. Mech. Mach. Theory **167** (2022). https://doi.org/10.1016/j.mechmachtheory.2021.104468
13. Fan, Z., Zhu, C., Li, X., Liang, C.: The transmission characteristic for the improved wind turbine gearbox. Energy Sci. Eng. **7** (2019). https://doi.org/10.1002/ese3.356
14. Neagoe, M., Saulescu, R., Jaliu, C., Simionescu, P.A.: A generalized approach to the steady-state efficiency analysis of torque-adding transmissions used in renewable energy systems. Energies **13**, 4568 (2020). https://doi.org/10.3390/en13174568
15. Shi, W. Kim, C.-W., Chung, C.-W., Park, H.-C.: Dynamic modeling and analysis of a wind turbine drivetrain using the torsional dynamic model. Int. J. Precis. Eng. Manuf. **14** (2012). https://doi.org/10.1007/s12541-013-0021-2
16. Shi, W., Ning, D., Ma, Z., Ren, N., Park H.: Parametric study of drivetrain dynamics of a wind turbine using the multibody dynamics. Int. J. Mech. Eng. Appl. **7**(2) (2019). https://doi.org/10.11648/j.ijmea.20190703.11
17. Shi, W., Park, H.-C., Na, S., Song, J., Ma, S., Kim, C.-W.: Dynamic analysis of three-dimensional drivetrain system of wind turbine. Int. J. Precis. Eng. Manuf.Precis. Eng. Manuf. **15**, 7 (2014). https://doi.org/10.1007/s12541-014-0476-9
18. Xiang, L., Gao, N., Hu, A.: Dynamic analysis of a planetary gear system with multiple non-linear parameters. J. Comput. Appl. Math. **327** (2017). https://doi.org/10.1016/j.cam.2017.06.021
19. Saulescu, R., Neagoe, M., Jaliu, C., Munteanu, O.: A comparative performance analysis of counter-rotating dual-rotor wind turbines with speed-adding increasers. Energies **14** (2021). https://doi.org/10.3390/en14092594
20. Zhao, M., Ji, J.: Dynamic analysis of wind turbine gearbox components. Energies **9** (2016). https://doi.org/10.3390/en9020110
21. Park, Y., Shi, W., Park, H.: Effect of the variable gear mesh model in dynamic simulation of a drive train in the wind turbine. Eng. Rev. (2020) https://doi.org/10.30765/er.1496
22. Neagoe, M., Saulescu, R., Jaliu, C., Munteanu, O., Cretescu, N.: Monomobile counter-rotating wind system. Patent no RO 131512B1 (2022)

applied sciences

Article

Dynamic Response of a Single-Rotor Wind Turbine with Planetary Speed Increaser and Counter-Rotating Electric Generator in Starting Transient State

Radu Saulescu [1] and Mircea Neagoe [2,*]

[1] Design of Mechanical Elements and Systems R&D Centre, Faculty of Product Design and Environment, Transilvania University of Brasov, 500036 Brasov, Romania; rsaulescu@unitbv.ro
[2] Renewable Energy Systems and Recycling R&D Centre, Faculty of Product Design and Environment, Transilvania University of Brasov, 500036 Brasov, Romania
* Correspondence: mneagoe@unitbv.ro; Tel.: +40-268-413-000

Abstract: The paper addresses the dynamic modeling and numerical simulation of a novel single-rotor wind system with a planetary speed increaser and counter-rotating direct current (DC) generator, patented by authors, during the transient stage from rest. The proposed analytical dynamic algorithm involves the decomposition of the wind system into its component rigid bodies, followed by the description of their dynamic equations using the Newton–Euler method. The linear mechanical characteristics of the DC generator and wind rotor are added to these dynamic equations. These equations allow for the establishment of the close-form equation of motion of the wind system and, implicitly, the time variation of the mechanical power parameters. Numerical simulations of the obtained analytical dynamic model were performed in MATLAB-Simulink in start-up mode from rest for the case study of a 100 kW wind turbine. These results allowed highlighting the time variation of angular velocities and accelerations, torques, and powers for all system shafts, both in the transient regime and steady-state. The implementation, in this case, of the counter-rotating generator indicates a 6.4% contribution of the mobile stator to the generator's total power. The paper's results are useful in the design, virtual prototyping, and optimization processes of modern wind energy conversion systems.

Keywords: renewable energy; wind turbines; counter-rotating electric generator; dynamic modeling; simulation; transient regime; steady-state

Academic Editor: Wei Huang

Received: 3 November 2024
Revised: 18 December 2024
Accepted: 25 December 2024
Published: 29 December 2024

Citation: Saulescu, R.; Neagoe, M. Dynamic Response of a Single-Rotor Wind Turbine with Planetary Speed Increaser and Counter-Rotating Electric Generator in Starting Transient State. *Appl. Sci.* **2025**, *15*, 191. https://doi.org/10.3390/app15010191

1. Introduction

Wind turbines can shut down during operation, typically due to lack of wind, high wind speeds, or need for maintenance, and followed afterward by their transition from rest to operation state. The start-up of medium-large wind turbines is carried out automatically and in a controlled manner, and prior knowledge of their dynamics is typically employed in controllers. Thus, dynamic behavior in transient regimes represents a challenge for researchers and an advantage for designers in the optimization of the control system and wind system design [1–3].

An important issue in approaching the wind system dynamics concerns the assumption of variable wind speed and identification of system dynamic behavior in transient regimes owing to the change in wind speed or starting from rest. Dynamic studies refer to both the wind system as a whole [2–7] and its component subsystems, such as electric generators [8] or mechanical gear transmission [9–11] with the role of speed increasers with fixed axes [2,12], mobile axes [7,13–17] or combined [18–26]. The overwhelming majority of speed increasers are monomobile (single degree of freedom, 1-DOF) mechanical transmissions [2,16,19,20,23–25,27,28] and rarely differential (2-DOF) transmissions [5,17]. The dynamic response of wind systems can be electrical or mechanical, depending on the type of power pursued: electrical or mechanical power, respectively.

Aiming at improving the performance of electric generators, in conjunction with their overall size reduction, various counter-rotating type generators [2,17,20,29,30] are addressed in literature: with permanent magnets [31], with liquid metals [32], DFIG (Double Fed Induction Generator) that uses a back-to-back Pulse-Width converter Modulation (PWM) for bidirectional control [8], etc.

Dynamic analysis of wind systems and their subsystems requires the use of specific software such as FAST v8.16 (Fatigue, Aerodynamics, Structures, and Turbulence) for aero-elastic dynamic modeling [1,33,34], MATLAB-Simulink [1,2,18,24,35,36], with results having errors below 2% compared to FAST, Ansys 15.0 [15], SIMPACK [33,34] based on dynamic multibody modeling, PSCAD/EMDTC [37], etc. These software packages allow the identification of various representative dynamic parameters related to mechanical efficiency [2,16,38], shaft speeds [3,36,38] and torques [38–40], mechanical powers [3,29,38], and for electrical response: current intensity [36,38] and voltage [38].

Modeling the dynamic response of a wind system requires also knowledge of the mechanical characteristics of both the wind rotor and the electric generator. In literature, these features are modeled as nonlinear [8,27,33] or linear [2,20] functions. Thus, Neagoe et al. [2] addressed the dynamic modeling and simulation of a 10 kW wind turbine with a single wind rotor and counter-rotating generator, equipped with a classical transmission with fixed axes, by considering only one linearized zone of the WR mechanical characteristic: the working zone. The dynamic numerical simulations cover scenarios of wind speed changes during operation by maintaining the operating point on this working zone. However, this research did not consider the starting phase from rest or optimizing the generator's load entry. Similarly, a single linear function for the working zone is proposed for power flow modeling in the steady state of a dual-rotor wind turbine with a counter-rotating generator [20].

In most cases, the dynamic response is an analytical or grapho-analytical result, the most common dynamic modeling methods applied for wind turbines being Newton–Euler [1,2,13,41–43], Lagrange + Runge–Kutta [6,22,28,39,40], lumped parameter theory [10,26,44] or polynomial chaos [12]. Generally, the approaches of WT dynamics consider the gearbox effect in a simplified model by neglecting the rotation of the satellite gears in planetary transmissions.

The dynamic behavior of a wind energy conversion system also depends on the moment when the electric generator is connected to the grid: either from the beginning [2,29,35,45] or at a time after start-up [36,41]. Oyekola et al. [36] stated that synchronous or DC motors can be operated as induction generators if their shaft rotation speed overcomes the synchronous speed. However, this study did not address the optimization problem or the impact of the generator connecting time to the grid on the system's dynamic behavior.

Based on this literature review, the following gaps emerge:

- Choosing an appropriate model of the mechanical characteristics specific to the operating condition of the wind system is still a challenging issue;
- The rotation of the satellite gears from planetary speed increasers is typically neglected;
- The choice of the optimal time for connecting the electric generator to the grid.

Aiming at dealing with these gaps and deepening the understanding of the optimal functioning of a wind system, the present study brings contributions and focuses mainly on the following aspects:

(a) The dynamic modeling is carried out analytically by applying the Newton–Euler method and the MATLAB-Simulink R2014a software in numerical simulations;
(b) The functional compatibility of the wind system is ensured by the planetary speed increaser, whose input is connected to the wind rotor, and its two outputs are connected to the generator rotor and stator, respectively;
(c) The satellite's own rotation was considered in dynamic modeling by using an equivalent axial moment of inertia;
(d) The mechanical moments of inertia of the transmission components were reduced at the shafts of the wind rotor and the electric generator;
(e) The nonlinear mechanical characteristic of the wind rotor is linearized on four zones;
(f) The dynamic system response is given by a simulation module that allows the generator to connect to the grid after the wind rotor enters the maximum power zone. This simulator also allows the identification of the dynamic behavior of the considered subsystems through specific parameters such as power, torque, speed, and efficiency.

Based on the actual reported results, to the best of our knowledge, the dynamic behavior of this type of wind system with a counter-rotating generator and planetary speed increaser has not been significantly addressed in the literature. Aiming to cover this literature gap, the paper proposes a generalized algorithm for close-form dynamic modeling of single-rotor wind turbine class with planetary speed increaser and counter-rotating generator, patented by authors [46].

The subsequent sections of the paper are organized as follows: Section 2 introduces the conceptual and block diagrams of a counter-rotating wind turbine and formulates the dynamic modeling problem. Section 3 details the proposed generalized algorithm for analytical dynamic modeling. Numerical results for a 100 kW wind turbine are presented and discussed in Section 4, and the paper concludes in Section 5.

2. Problem Formulation

Designing wind systems with counter-rotating generators is challenging owing to the branched power flow in planetary transmissions from a single input to dual outputs. The generalized modeling and numerical simulation of the dynamic response of this wind turbine (WT) type is addressed in this paper. Without reducing the generality, a case study of a 1-DOF wind system is considered (Figure 1), consisting of a wind rotor *R*, a planetary speed increaser (*SI*) with one input (satellite-carrier *H*) and two outputs (gears 1 and 2) connected to a counter-rotating electric generator *G*. The rotor *GR* and the stator *GS* of the generator are both mobile and rotate in opposite directions.

The block scheme in Figure 1b highlights the interactions between the three key components of the wind system: mechanical power is transmitted from the wind rotor *R* via the shaft *H* to the speed increaser *SI*, which distributes the output power to both the rotor *GR* and stator *GS*. Obviously, the two power outputs are not independent, the rotor and stator of the generator being permanently characterized in operation by equal and opposite torques (i.e., $T_{GS} = -T_{GR}$).

The speed increaser is a planetary mechanical transmission with cylindrical gears (1–5, Figure 1), three of which are sun gears (1, 2, and $5 \equiv 0$), and the solidarized gears 3 and 4 form a double satellite. In practical applications, the planetary transmission includes $n_s \geq 2$ equiangularly arranged double satellites (3–4).

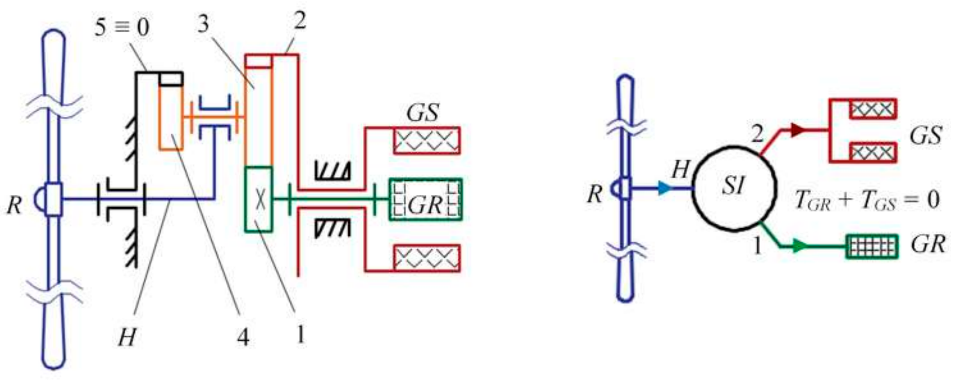

(**a**) (**b**)

Figure 1. Single-rotor wind turbine with counter-rotating electric generator: (**a**) conceptual scheme; (**b**) block scheme.

The power input of the speed increaser (i.e., the satellite carrier H) is solidarized with the wind rotor R. Satellites 3–4 engage on the one hand with a fixed ring gear 5 and on the other hand with the sun gear 1, connected with the generator rotor GR, and with the ring gear 2, coupled to the generator stator GS. The angular speed of a counter-rotating generator G (ω_G) is given by the relative speed of the rotor GR with respect to the stator GS:

$$\omega_G = \omega_{GR} - \omega_{GS} = \omega_1 - \omega_2. \tag{1}$$

As a result, the kinematic amplification ratios, which describe the transmission of the rotational speed from the wind rotor to the generator rotor (i_{a1}) and to the generator stator (i_{a2}), respectively, and the total amplification ratio (i_{aG}) achieved by the wind turbine, can be established through the following relations:

$$i_{a1} = \frac{\omega_1}{\omega_H};\ i_{a2} = \frac{\omega_2}{\omega_H};\ i_{aG} = \frac{\omega_1 - \omega_2}{\omega_H} = i_{a1} - i_{a2}, \tag{2}$$

where ω_x is the angular velocity of the body x = 1, 2, H; i_{ay}—the amplification ratio from the input R to the element y = 1, 2, G.

The dynamic modeling of the analyzed 1-DOF wind system aims to identify its equation of motion $\varepsilon_R = f(\omega_R,\ J_x,\ cst)$, where J_x is the mechanical axial moment of inertia of the body x = 1, 2, H, and cst represents the set of other constant parameters. The motion of the input shaft (of the wind rotor R) is considered as an independent kinematic variable of the wind turbine. By solving this differential equation, the time variation of the torques and kinematic variables (velocities and angular accelerations) related to all system shafts is obtained; the numerical simulations are performed under the assumption of starting the system from rest at a specified constant wind speed.

In the proposed dynamic modeling, the following working premises are considered:

(1) The rotational elements have geometric symmetry with respect to their own axis of motion, and they are rigid bodies with uniformly distributed mass; as a result, the mass center of a body is located on its own axis of rotation;
(2) The inertial masses of the mobile elements in the planetary transmission are reduced to their outer shafts; thus, the correlations of the torques in the planetary units coincide with those of static conditions;
(3) Only the gearing friction losses are considered, neglecting the friction in bearings;
(4) The pitch angle of WR blades does not change during operation; therefore, the adjustment parameters of the wind rotor remain constant during operation;

(5) As 1-DOF transmission is employed, the system has one independent motion attributed to the input element, i.e., the wind rotor;

(6) A direct current (DC) generator is used, and implicitly, its mechanical characteristic is a linear function with constant coefficients; during generator operation, the balancing condition of the torques of the rotor *GR* (T_{GR}) and of the stator *GS* (T_{GS}) is described by: $T_{GR} + T_{GS} = 0$;

(7) The mechanical characteristic of the wind rotor is modeled over four rotational speed intervals by linear functions with constant coefficients, obviously at a constant wind speed.

Dynamic modeling of the WT mechanical system from Figure 1 is based on the block scheme depicted in Figure 2a, in which the planetary speed increaser is modeled by two planetary units (PU) I (*H*-5-4-3-1) and II (*H*-5-4-3-2), connected in parallel.

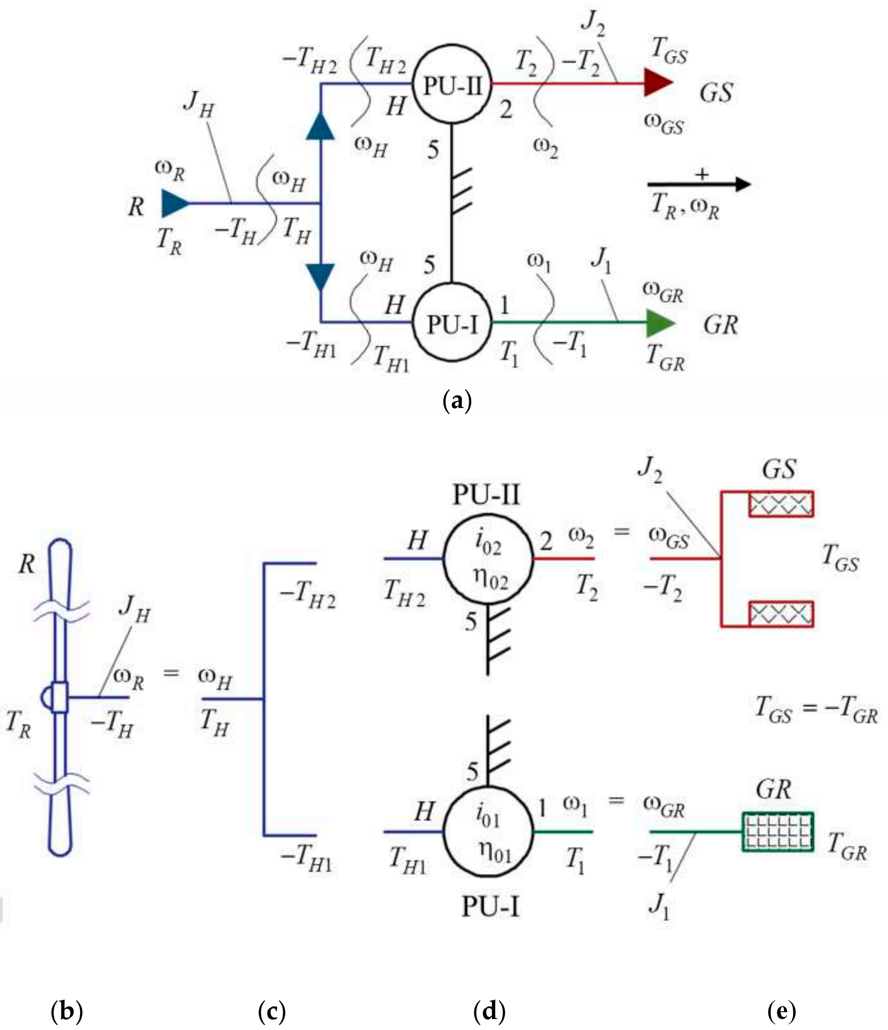

Figure 2. (**a**) Block scheme of the wind turbine and its decomposition into components: (**b**) wind rotor; (**c**) intermediate shaft; (**d**) planetary units; and (**e**) generator rotor and stator.

By decomposing the wind system from Figure 2a, the six structural components represented in Figure 2b–e are obtained, characterized by specific kinematic and dynamic equations, according to the methodology detailed in Section 3. In the proposed approach, the axial moments of inertia of the components are reduced on the outer shafts of the planetary transmission (i.e., the shafts of the *R*, *GR*, and *GS* bodies) [37]. Thus, the torque equations for the components in Figure 2c,d can be described by the classical relations established under steady-state conditions and for the other components, depicted in Figure 2b,e,—under dynamic conditions.

The axial moment of inertia of the n_s satellites 3–4, mounted in parallel, is reduced to the satellite-carrier H axis based on the principle of equalizing their kinetic energy. The satellite body has a combined rotation (around its own axis) and revolution (around the fixed sun axis) motion; its kinetic energy is considered equal to that of a virtual body with motion around the sun axis having an equivalent moment of inertia J_{sH}:

$$K_s = \frac{1}{2}n_s\left(m_s v_{Gs}^2 + J_s {\omega_s}^2\right) = \frac{1}{2}J_{sH}\omega_H^2, \tag{3}$$

$$J_{sH} = n_s m_s\left(\frac{v_{Gs}}{\omega_H}\right)^2 + n_s J_s\left(\frac{\omega_s}{\omega_H}\right)^2, \tag{4}$$

in which

$$\frac{\omega_s}{\omega_H} = \frac{\omega_H + \omega_{sH}}{\omega_H} = 1 + \frac{\omega_{sH}}{\omega_H} = 1 + \frac{\omega_{sH}}{\omega_{H5}} = 1 - \frac{\omega_{sH}}{\omega_{5H}} = 1 - i_{45},\ v_{Gs} = \omega_H \cdot r_H, \tag{5}$$

yielding to

$$J_{sH} = n_s\left(m_s r_H^2 + J_s(1 - i_{45})^2\right), \tag{6}$$

where m_s and J_s are the mass and the axial mechanical moment of a satellite 3–4, respectively (Js is established with respect to the own axis of rotation), r_H is the radius of satellite axis arrangement on the carrier H, and i_{45} is the kinematic ratio of the gear pair with fixed axes 4–5 (i.e., $i_{45} = z_5/z_4$, where z_4 and z_5 are the numbers of teeth of gears 4 and 5, respectively).

Next, the main steps of the dynamic modeling algorithm are presented, based on dynamic equations of the transmission external shafts, modeled by the Newton–Euler method, the kinematic and static equations of both planetary units I and II, and the mechanical characteristics of the wind rotor and counter-rotating electric generator.

3. Dynamic Modelling

The dynamic equations of the wind system components in the mentioned working premises are linear differential equations of the second order with constant coefficients; they can be obtained by applying the Newton–Euler method considering the positive direction of angular velocity and torque vectors according to Figure 2.

According to premise (2), the following kinematic and static equations can be written for the two planetary units PU-I and PU-II [16], see Figure 2d:

$$\text{PU-I}: \begin{cases} \omega_1 = \omega_H(1 - i_{01}) \\ \omega_H T_{H1}\eta_1 + \omega_1 T_1 = 0 \end{cases} \quad \text{PU-II}: \begin{cases} \omega_2 = \omega_H(1 - i_{02}) \\ \omega_H T_{H2}\eta_2 + \omega_2 T_2 = 0 \end{cases} \tag{7}$$

where T_x is the resultant torque acting on the element x; i_{01}, i_{02}, and η_1, η_2 are the internal kinematic ratio and the efficiency of PU-I and PU-II, respectively, and $T_H = T_{H1} + T_{H2}$—Figure 2b.

The relations for the kinematic ratios and transmission efficiencies, specified in Table 1, can be easily derived from Equation (7).

According to the block diagram in Figure 2 and Equation (2), Table 2 illustrates the dynamic schemes of the three WT components, resulting from the decomposition of the wind system into distinctive rigid bodies, as well as their related kinematic and dynamic equations.

Table 1. Transmission ratios and efficiencies.

PU	$i_{01,2}$	$i_{a1,2}$	$\eta_{1,2}$
I	$-\frac{z_5}{z_4}\cdot\frac{z_3}{z_1}$	$1-i_{01}$	$\frac{1-i_{01}}{1-i_{01}/\eta_{01}}$
II	$\frac{z_5}{z_4}\cdot\frac{z_3}{z_2}$	$1-i_{02}$	$\frac{1-i_{02}}{1-i_{02}/\eta_{02}}$

z_j is the no. of teeth of the gear j = 1. . .5 (see Figure 1); η_{01}, η_{02}—internal efficiency of PU-I and PU-II, respectively; $\eta_{01} = \eta_{02} = \eta_g^2$, where η_g is the efficiency of a gear pair with fixed axes.

Table 2. Schemes and dynamic equations of the WT components.

Body	Dynamic Schemes	Equations
	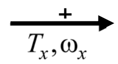	
$R \equiv H$ Figure 2a	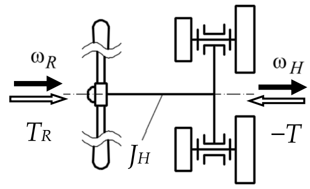	$\omega_H = \omega_R$ $J_H\varepsilon_H = T_R - T_H$
$1 \equiv GR$ Figure 2e	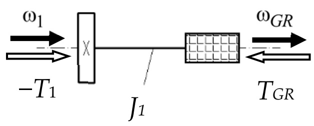	$\omega_1 = \omega_{GR}$ $\omega_1 = \omega_H \cdot i_{a1}$ $\varepsilon_1 = \varepsilon_H \cdot i_{a1}$ $J_1\varepsilon_1 = -T_1 + T_{GR}$
$2 \equiv GS$ Figure 2e	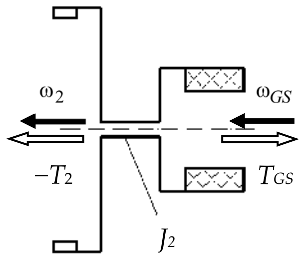	$\omega_2 = \omega_{GS}$ $\omega_2 = \omega_H \cdot i_{a2}$ $\varepsilon_2 = \varepsilon_H \cdot i_{a2}$ $J_2\varepsilon_2 = -T_2 + T_{GS}$

ε_x is the angular acceleration of the body x = 1, 2, H; $J_H = J_R + J_{shR} + J_{sH}$, $J_1 = J_{g1} + J_{sh1} + J_{GR}$, $J_2 = J_{g2} + J_{sh2} + J_{GS}$, where g—gear and sh—shaft.

The set of equations in Table 2 is augmented by the linear mechanical characteristics with constant coefficients of the wind rotor (R) and generator (G):

$$T_R = -a_R\omega_R + b_R;\ T_G = -a_G(\omega_{GR} - \omega_{GS}) + b_G, \tag{8}$$

where a_R, b_R, a_G, b_G are constant coefficients under steady-state conditions, and by definition $T_G = T_{GR}$.

The mechanical characteristic of a wind rotor is a nonlinear function [33,35], which can, however, be acceptably approximated by straight line segments; in this study, four-zone nonlinear characteristic modeling was adopted (Figure 3): zones I and II are used at start-up, zone III includes the point of maximum power P_{max}, and zones III and IV designate the working zones of the wind rotor. Obviously, the coefficients a_R, b_R in Equation (8) are replaced specifically by a_{Ri}, b_{Ri}, i = 1. . .4 for each of the four zones I. . .IV.

Obviously, linearizing the WT mechanical characteristic leads to inaccuracies in the calculated torque T_R, as qualitatively shown in Figure 3. For the case study presented in Section 4, the most significant torque errors are recorded in zone III, with a relative error value of less than 3.4% (its maximum value near the midpoint of zone III, Figure 3), an acceptable level in numerical simulation of such a complex system.

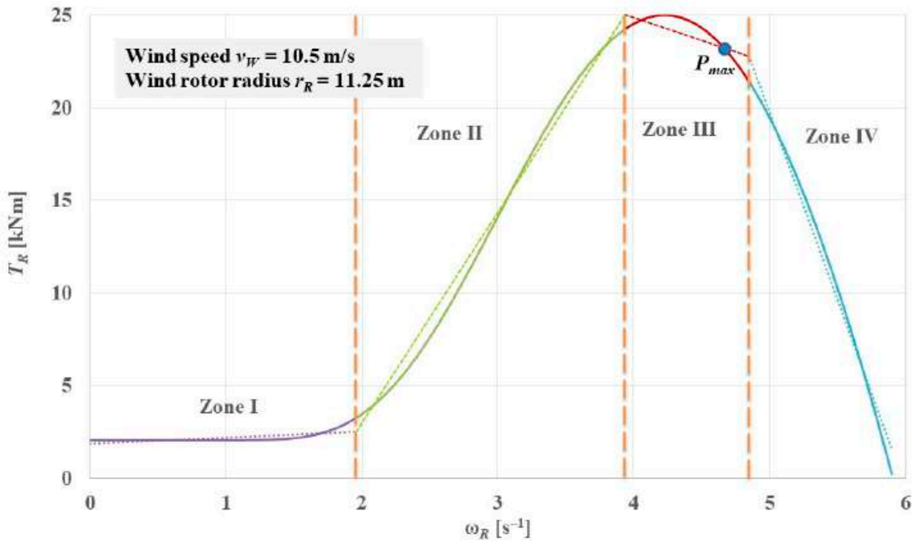

Figure 3. The mechanical characteristic of a wind rotor modeled by four linearized zones.

Substituting the gear ratio and efficiency relations from Table 1 into the kinematic, static, and dynamic equations from Table 2 and corroborating with Rels. (4) and (5), the equation of motion is obtained:

$$\varepsilon_R = \frac{\omega_R\left[a_G\left(i_{a1}i_{a2}(\eta_1+\eta_2) - \eta_2 i_{a1}^2 - \eta_1 i_{a2}^2\right) - a_R\eta_1\eta_2\right] + b_G\left(\eta_2 i_{a1} - \eta_1 i_{a2}\right) + b_R\eta_1\eta_2}{J_1 i_{a1}^2\eta_2 + J_2 i_{a2}^2\eta_1 + J_H\eta_1\eta_2}. \quad (9)$$

This equation of motion is a nonhomogeneous second-order differential equation in one variable (independent motion parameter:ω_R, where $\varepsilon_R = \frac{d\omega_R}{dt}$). This differential equation is solved by numerical integration in MATLAB-Simulink R2014a under known initial conditions: the starting from rest is considered ($\omega_{R(t=0)} = 0$), and the electric machine is coupled to the grid (i.e., the load is activated) when it switches to generator mode ($\omega_G > \frac{b_G}{a_G}$).

The dynamic behavior in a transient regime can be determined by solving the equation of motion (9), obtained using Rels. (7), (8), and Table 2; based on the solution of independent motion, it becomes possible to derive the time evolution of power parameters for all transmission shafts.

4. Results and Discussions

Using the previously presented dynamic model, a numerical response is targeted for a 100 kW wind system with parameter values provided in Table 3.

Table 3. Constant intrinsic parameters of the wind system.

z_i	i_0	i_a	a [kNms] b [kNm]	η	J [kgm^2]
$z_1 = 19$ $z_2 = 135$ $z_3 = 58$ $z_4 = 20$ $z_5 = 97$	$i_{01} = -14.8052$ $i_{02} = 2.0837$	$i_{a1} = 15.8052$ $i_{a2} = -1.0837$ $i_{aG} = 16.8889$	$a_{R1} = -0.328$, $b_{R1} = 1.866$ $a_{R2} = -11.536$, $b_{R2} = -20.533$ $a_{R3} = 2.298$, $b_{R3} = 34.014$ $a_{R4} = 20.259$, $b_{R4} = 121.065$ $a_G = 0.368$, $b_G = 27.975$	$\eta_g = 0.9560$ $\eta_1 = 0.9195$ $\eta_2 = 0.8468$	$J_1 = 0.1 \cdot 10^3$ $J_2 = 1 \cdot 10^3$ $J_H = 200 \cdot 10^3$

The wind turbine has a nominal power of 100 kW, generated by a wind rotor with a diameter of 22.5 m at a nominal wind speed of 10.5 m/s. The start-up of the wind system is performed from rest, and the electric generator load is applied at the time when $\omega_G = b_G/a_G = 76\ \mathrm{s}^{-1}$. Thus, the wind system goes through three phases:

(1) In the first phase, the mechanical energy generated by the wind rotor is used exclusively to overcome inertial resistance (implicitly, to accelerate the system);

(2) In the second phase, when the generator is coupled to the grid, the generator-resistant torque is added to the inertial load;

(3) In the third phase, the wind turbine enters into a steady state (i.e., zero accelerations), obtaining the operating point described by the values of the angular velocities and torques, as well as the powers of all the shafts of the wind system, Table 4.

Table 4. Operating point of the wind system in steady-state.

Shaft	Torque [kNm]	Angular Speed [s^{-1}]	Power [kW]
R ≡ H	23.208	4.704	109.17
H1	21.600	4.704	101.61
H2	1.608	4.704	7.56
1 ≡ GR	−1.256	74.317	−93.34
2 ≡ GS	1.256	−5.097	−6.40
G	−1.256	79.414	−99.75

The results of the numerical simulation in MATLAB-Simulink R2014a, based on the equation of motion (9) and all the other equations of the analytical model, are depicted in Figures 4–6. The diagrams in these figures highlight the two moments of time delimiting the three phases of the WT transition from rest to steady-state: the electric generator enters the load at ≈260 s, and the stabilization of the system takes place at ≈280 s (i.e., the starting time).

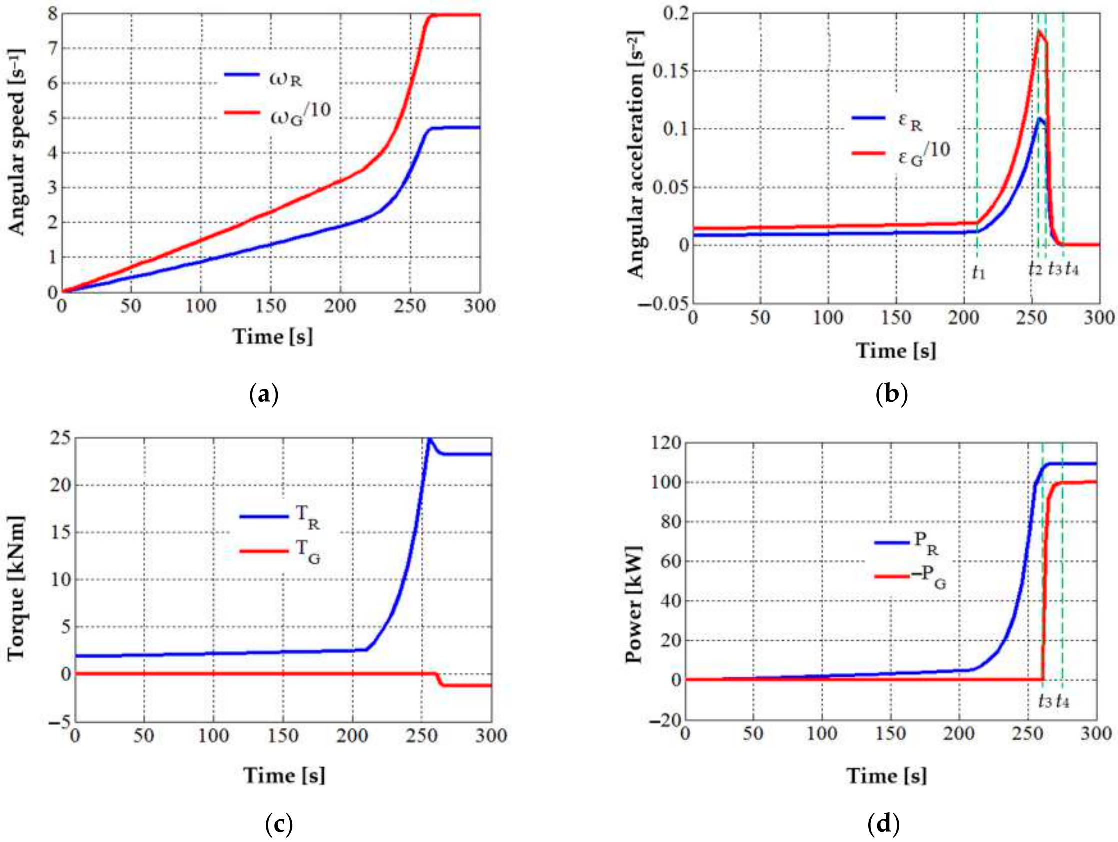

Figure 4. The wind system dynamic response: (**a**) input vs. output angular speeds; (**b**) input vs. output angular accelerations; (**c**) wind rotor vs. generator torques; (**d**) wind rotor vs. generator powers.

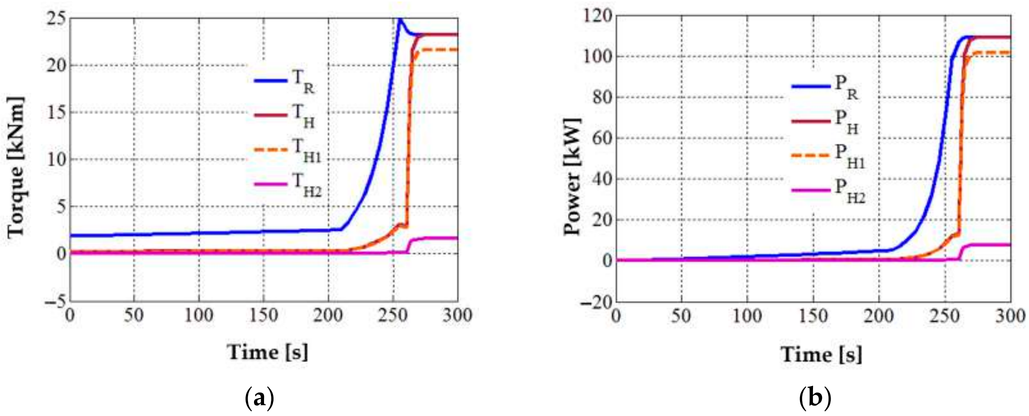

Figure 5. The dynamic response at the wind rotor side: (**a**) wind rotor vs. input torques; (**b**) wind rotor vs. input powers.

Figure 4 shows comparatively the time variations of the kinematic parameters, torques, and powers from the system input vs. output. Worth noting the quasi-linear variation of all input parameters and output motions in the first part of the start-up phase 1, characterized by $T_G = 0$ (i.e., the generator runs idle) and wind rotor operation on the zone I (see Figure 3). Since the torque generated by the wind rotor has low values at start-up ($T_R \approx 2$ kNm, Figure 4c), the system requires a long time (≈220 s) of slow increase in speed (Figure 4a) and implicitly in angular acceleration (Figure 4b) as a result of inertial resistance. Once the wind rotor enters zone II (time $t_1 \approx 220$ s), the system is rapidly accelerated as a result of the greater torque extracted by the wind rotor from the wind. The wind rotor torque reaches its maximum value at the end of zone II (at time $t_2 \approx 255$ s), followed by a torque decrease into zone III for ≈5 s. At time $t_3 \approx 260$ s, the electric generator enters the load (i.e., the wind system goes into phase 2), as the operating conditions of the DC electric machine as a generator are being met: $\omega_G \geq b_G/a_G = 76\ \mathrm{s}^{-1}$, Figure 4a. The generator torque increases rapidly up to the value $T_G = 1.25$ kNm (Figure 4c), with the decrease to zero of the angular acceleration (Figure 4b) and implicitly the entry of the system into steady-state (at time $t_4 \approx 280$ s).

In phase 3, the generator power stabilizes at $P_G \approx -100$ kW, the mechanical power extracted from the wind being $P_R = 109.4$ kW, Figure 4d; implicitly, the transmission efficiency has the value: $\eta_{WT} = -P_G/P_R = -T_G \cdot \omega_G/(T_R \cdot \omega_R) = 0.9138$. The efficiency η_{WT} has a value close to the value η_1 and is significantly higher than η_2 (see Table 3); thus, the advantage of power branching in complex mechanisms compared to the serial connection of component mechanisms is also well emphasized.

Figure 5 shows the distribution of torques and mechanical power on the inputs of planetary units I and II, as well as the influence of inertia on the WT dynamic behavior. In the first part of phase 1, a significant difference between the driving torque T_R and the resistant torque T_H is noted (Figures 2 and 5a). This fact is owing to the insignificant values of the torques T_{H1} and T_{H2}, also caused by the reduced inertial resistances of the output shafts (the values of the moments of inertia J_1 and J_2 being much lower compared to J_H: $J_H \approx 2000 \cdot J_1 \approx 200 \cdot J_2$, see Figure 2, Tables 2 and 3); this reduced inertial effect of the output shafts is also confirmed by their relatively reduced values of angular accelerations. As a result, the torque T_R is mostly used to overcome the inertial load of the input shaft *H*. Once the generator enters the load, the T_{H1} torque increases much faster than T_{H2}, becoming the major component of T_H in the steady state. Although the *GR* rotor and *GS* stator torques are equal in steady-state, the significant difference between T_{H1} and T_{H2} is explained by the large differences in the amplification ratios $i_{a1} = 15.8052$ and $i_{a2} = -1.0837$ (see Table 3) corresponding to the two power branches. The power variation on the input shafts (Figure 5b) follows a similar evolution as the input torques (Figure 5a): most of the wind rotor power (over 93%) is directed to the planetary unit I and, implicitly, to the *GR* rotor—the body with the highest rotation speed.

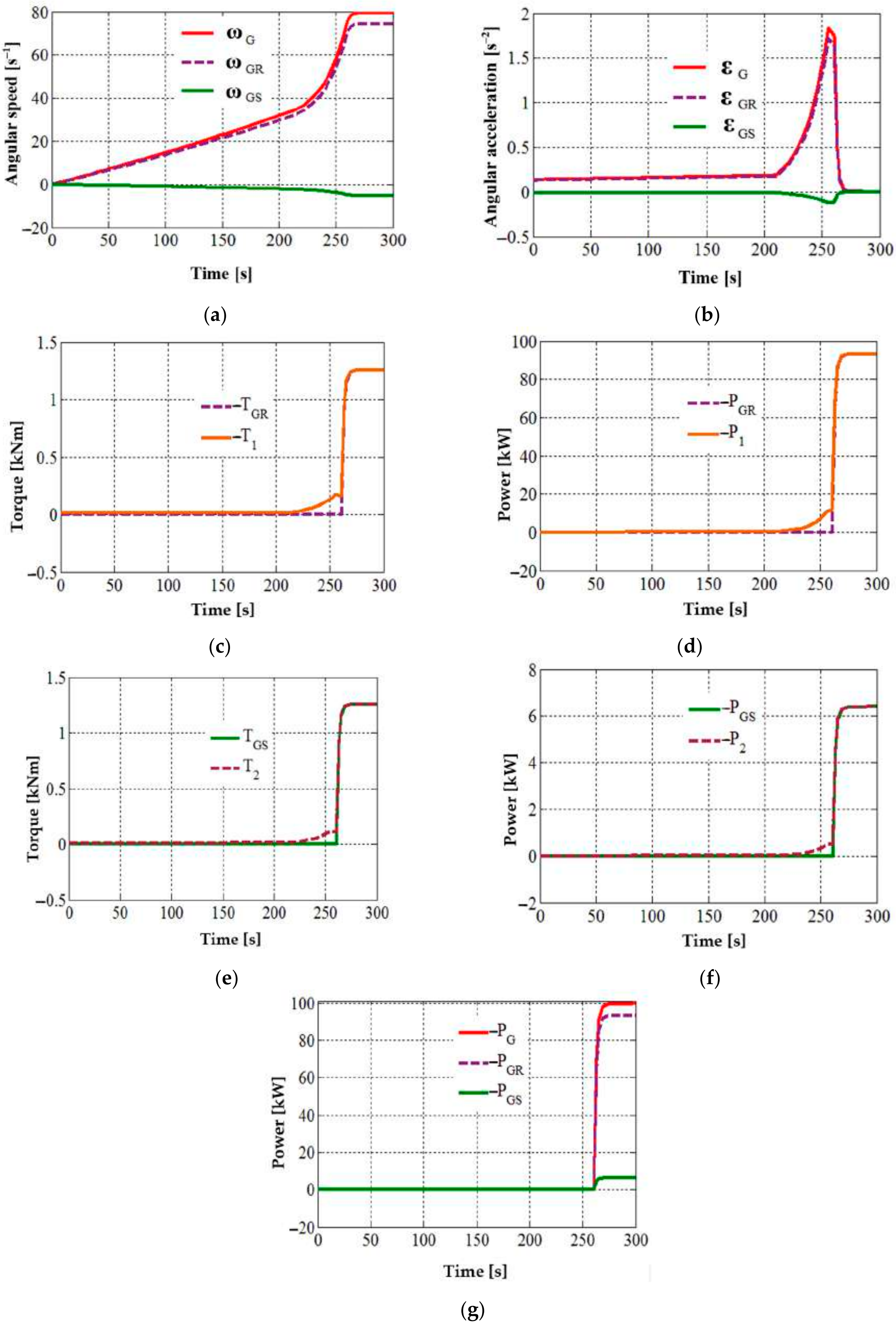

Figure 6. The dynamic response at the generator side: (**a**) generator angular speeds; (**b**) generator angular accelerations; (**c**) generator rotor vs. output 1 torques; (**d**) generator rotor vs. output 1 powers; (**e**) generator stator vs. output 2 torques; (**f**) generator stator vs. output 2 powers; (**g**) mechanical powers.

Figure 6 illustrates the WT dynamic behavior at the output side, characterized by the branched power transmission via the rotor *GR* and the stator *GS*, respectively; the contribution of the mobile stator to the overall performance of the wind system is particularly highlighted. The output angular speeds and accelerations (Figure 6a,b) have a linear dependence on the independent motion of the wind rotor; according to the relations in Table 2, they follow the variation profile of the angular velocity ω_R and acceleration ε_R, respectively (Figure 4a,b), with values amplified with the ratios i_{a1}, i_{a2}, and i_{aG}, respectively. Note the much lower speed and acceleration of the *GS* stator compared to the *GR* rotor, and finally, the smaller power contribution from the *GS* stator vs. *GR* rotor due to the large inequality: $|i_{a2}| << i_{a1}$. Obviously, this situation can be improved by optimizing the ratio between i_{a2} and i_{a1}, as well as the large ratio between the inertia of the *GS* stator and the *GR* rotor.

At the time the generator enters the load (≈ 260 s), the torques T_1 (Figure 6c) and T_2 (Figure 6e), respectively, the powers P_1 (Figure 6d) and P_2 (Figure 6f) reflect the inertial impact of the output shafts (1 and 2). Although the two shafts have different moments of inertia ($J_2 = 10J_1$, see Table 3), the large acceleration difference in favor of shaft $1 \equiv GR$ makes the inertial resistance of shaft 1 greater than that of shaft 2 (maximum 0.172 vs. 0.118 kNm) in phase (1). In steady-state, the high angular velocity of the *GR* rotor allows it to receive a much higher power compared to the *GS* stator (i.e., $|P_{GR}| = 93.34$ kW > $|P_{GS}| = 6.40$ kW). Thus, the power contribution of the *GS* stator to the total power of the generator is ~ 6.4% (Figure 6g), the largest share of the power flow being distributed to the *GR* rotor.

The results of the dynamic numerical simulations, based on the analytical dynamic model developed in this study, allow the identification of the WT dynamic behavior in the transient regime during starting-up from rest, as well as the values of the operating point parameters in steady-state.

5. Conclusions

The paper proposes a generalized algorithm for dynamic modeling of the wind system class of type: single-rotor, 1-DOF planetary transmission, and counter-rotating generator.

The counter-rotating generator requires a dual-output speed increaser, leading to a branched power flow configuration where the input power is distributed to the two parallel-connected planetary units. The analytical equation of motion is derived by combining the dynamic equations of the shafts, the mechanical characteristics of the wind rotor and electric generator, and the kinematic and static equations of the planetary gear transmission, which together describe the complex interactions within this system. This system of equations allows the analytical establishment of the wind system equation of motion and implicitly its operating point by numerical solution in transient mode and in steady-state.

The analytical study and the results of the numerical simulations carried out on a case study of a wind turbine with a rated power of 100 kW allowed us to draw the following conclusions:

- The proposed generalized modeling algorithm allows obtaining analytically the equation of motion of the wind system, formulated as a nonhomogeneous differential equation of the second order in a single independent variable, describing the wind rotor motion;
- By numerically solving the equation of motion, using the MATLAB-Simulink R2014a software, the dynamic response of the wind system in transient mode and the operating point in steady-state are obtained;
- The analysis of the dynamic response in transient mode, when starting from rest at constant wind speed, allowed the identification of the starting time of the wind system,

as well as the stresses induced by the inertial load alone and by its combination with the generator load;

- Unlike the case of traditional wind turbines, equipped with a conventional generator with a fixed stator, the counter-rotating generator allows an additional input of power brought by the mobile stator *GS*; in the analyzed case, the additional power supply by *GS* in steady-state is ~6.4%.

The proposed generalized algorithm can be applied, with rigorous adaptations, to other types of wind systems, regardless of their complexity: with one or more wind rotors, with conventional or counter-rotating electric generators, with fixed-axis or planetary speed increaser. Likewise, the developed MATLAB-Simulink R2014a model can also be applied iteratively for the purpose of constructive-functional optimization of this particular type of wind system, as well as in the simulation scenarios of variable operational conditions determined by the change in wind speed.

The authors intend to address in the future the dynamic optimization of such wind systems and the validation of theoretical results through the experimental research of some functional models on specialized testing rigs.

6. Patents

Saulescu, R., Neagoe, M., Visa, M., Jaliu, C., Munteanu, O., Totu, I. Cretescu, N. Monomobile planetary speed increaser with two counter-rotating outputs, Patent no RO 131740 B1, 29 November 2023.

Author Contributions: Conceptualization, M.N. and R.S.; methodology, M.N. and R.S.; software, R.S. and M.N.; validation, M.N. and R.S.; formal analysis, M.N. and R.S.; investigation, R.S. and M.N.; resources, R.S. and M.N.; data curation, M.N. and R.S.; writing—original draft preparation, M.N. and R.S.; writing—review and editing, M.N.; visualization, R.S.; supervision, M.N. All authors have read and agreed to the published version of the manuscript.

Funding: This research received no external funding.

Institutional Review Board Statement: Not applicable.

Informed Consent Statement: Not applicable.

Data Availability Statement: The original contributions presented in this study are included in the article. Further inquiries can be directed to the corresponding author.

Conflicts of Interest: The authors declare no conflict of interest.

Nomenclature

a_G	speed coefficient in the generator mechanical characteristic
a_R	speed coefficient in the wind rotor mechanical characteristic
b_G	torque term in the generator mechanical characteristic
b_R	torque term in the wind rotor mechanical characteristic
DOF	degree of freedom
DC	direct current
DFIG	double fed induction generator
FAST	fatigue, aerodynamics, structures, and turbulence
g	gear
G	electric generator
GR	generator rotor
GS	generator stator
H	satellite carrier
i	kinematic ratio

i_0	internal kinematic ratio
i_a	speed amplification ratio
J	mechanical axial moment of inertia
K_s	kinetic energy
m	mass
n_s	number of satellites
P	power
PWM	pulse-width converter modulation
PU	planetary unit
r	radius
R	wind rotor
t	time
T	torque
η	efficiency
η_0	internal efficiency
η_g	efficiency of a gear pair
ω	angular speed
ε	angular acceleration
SI	speed increaser
sh	shaft
v	linear speed
WR	wind rotor
WT	wind turbine
z_j	number of teeth of gear j

References

1. Cottura, L.; Caradonna, R.; Ghigo, A.; Novo, R.; Bracco, G.; Mattiazzo, G. Dynamic Modeling of an Offshore Floating Wind Turbine for Application in the Mediterranean Sea. *Energies* **2021**, *14*, 248. [CrossRef]
2. Neagoe, M.; Saulescu, R.; Jaliu, C.; Neagoe, I. Dynamic Analysis of a Single-Rotor Wind Turbine with Counter-Rotating Electric Generator under Variable Wind Speed. *Appl. Sci.* **2021**, *11*, 8834. [CrossRef]
3. Sanchez, R.; Medina, A. Wind turbine model simulation: A bond graph approach. *Simul. Model. Pract. Theory* **2014**, *41*, 28–45. [CrossRef]
4. Al-Hamadani, H.; An, T.; King, M.; Long, H. System Dynamic Modelling of Three Different Wind Turbine Gearbox Designs under Transient Loading Conditions. *Int. J. Precis. Eng. Manuf.* **2017**, *18*, 11. [CrossRef]
5. Lin, A.-D.; Hung, T.-P.; Kuang, J.-H.; Tsai, H.-A. Power Flow Analysis on the Dual Input Transmission Mechanism of Small Wind Turbine Systems. *Appl. Sci.* **2020**, *10*, 7333. [CrossRef]
6. Rubio, J.J.; Soriano, L.A.; Yu, W. Dynamic Model of a Wind Turbine for the Electric Energy Generation. *Math. Probl. Eng.* **2014**, *2014*, 409268. [CrossRef]
7. Wang, B.; Michon, M.; Holehouse, R.; Atallah, K. Dynamic Behaviour of a Multi-MW Wind Turbine. In Proceedings of the IEEE Energy Conversion Congress and Exposition (ECCE), Montreal, QC, Canada, 20–24 September 2015; ISBN 978-1-4673-7151-3.
8. Abo-Khalil, A.; Alyami, S.; Sayed, K.; Alhejji, A. Dynamic Modeling of Wind Turbines Based on Estimated Wind Speed under Turbulent Conditions. *Energy* **2019**, *12*, 1907. [CrossRef]
9. Dewangan, P.; Parey, A.; Hammami, A.; Chaari, F.; Haddar, M. Dynamic characteristics of a wind turbine gearbox with amplitude modulation and gravity effect: Theoretical and experimental investigation. *Mech. Mach. Theory* **2022**, *167*, 104468. [CrossRef]
10. Dong, H.; Zhang, C.; Wang, D.; Xu, S. Dynamic characteristics of gear box with PGT for wind turbine. *Procedia Comput. Sci.* **2017**, *109*, 801–808. [CrossRef]
11. Fan, Z.; Zhu, C.; Li, X.; Liang, C. The transmission characteristic for the improved wind turbine gearbox. *Energy Sci. Eng.* **2019**, *7*, 1368–1378. [CrossRef]
12. Mabrouk, I.B.; Hami, A.E.; Walha, L.; Zghal, B.; Haddar, M. Dynamic response analysis of Vertical Axis Wind Turbine geared transmission system with uncertainty. *Eng. Struct.* **2017**, *139*, 170–179. [CrossRef]
13. Li, D.; Zhao, Y. A dynamic-model-based fault diagnosis method for a wind turbine planetary gearbox using a deep learning network. *Prot. Control. Mod. Power Syst.* **2022**, *7*, 22. [CrossRef]
14. Mathis, R.; Rémond, Y. Kinematic and dynamic simulation of epicyclic gear trains. *Mech. Mach. Theory* **2009**, *44*, 412–424. [CrossRef]

15. Mohsine, A.; Mostapha, B.E.; Alaoui, R.E.; Daoudi, K. Comparative Study in the Structural and Modal Analysis of a Wind Turbine Planetary Gear Based on Material Reduction Criteria Using FEM. *Int. J. Renew. Energy Res.* **2019**, *9*, 2. [CrossRef]
16. Neagoe, M.; Saulescu, R.; Jaliu, C.; Simionescu, P.A. A Generalized Approach to the Steady-State Efficiency Analysis of Torque-Adding Transmissions Used in Renewable Energy Systems. *Energies* **2020**, *13*, 4568. [CrossRef]
17. Saulescu, R.; Neagoe, M.; Jaliu, C.; Munteanu, O. A Comparative Performance Analysis of Counter-Rotating Dual-Rotor Wind Turbines with Speed-Adding Increasers. *Energies* **2021**, *14*, 2594. [CrossRef]
18. Girsang, I.P.; Dhupia, S.J.; Muljadi, E.; Singh, M.; Pao, Y.P. Gearbox and Drivetrain Models to Study Dynamic Effects of Modern Wind Turbines. *IEEE Trans. Ind. Appl.* **2013**, *50*, 3777–3786. [CrossRef]
19. Li, Z.; Wen, B.; Peng, Z.; Dong, X.; Qu, Y. Dynamic modeling and analysis of wind turbine drivetrain considering the effects of non-torque loads. *Appl. Math. Model.* **2020**, *83*, 146–168. [CrossRef]
20. Neagoe, M.; Saulescu, R.; Jaliu, C. Design and Simulation of a 1 DOF Planetary Speed Increaser for Counter-Rotating Wind Turbines with Counter-Rotating Electric Generators. *Energies* **2019**, *12*, 1754. [CrossRef]
21. Nejad, A.R.; Guo, Y.; Gao, Z.; Moan, T. Development of a 5 MW Reference Gearbox for Offshore Wind Turbines. *Wind Energy* **2016**, *9*, 6. [CrossRef]
22. Ren, Z.; Zhou, S.; Wen, B. Dynamic coupled vibration analysis of a large wind turbine gearbox transmission system. *J. Vibroengineering* **2015**, *7*, 6.
23. Shi, W.; Kim, C.-W.; Chung, C.-W.; Park, H.-C. Dynamic Modeling and Analysis of a Wind Turbine Drivetrain Using the Torsional Dynamic Model. *Int. J. Precis. Eng. Manuf.* **2012**, *14*, 153–159. [CrossRef]
24. Shi, W.; Ning, D.; Ma, Z.; Ren, N.; Park, H. Parametric Study of Drivetrain Dynamics of a Wind Turbine Using the Multibody Dynamics. *Int. J. Mech. Eng. Appl.* **2019**, *7*, 2. [CrossRef]
25. Shi, W.; Park, H.-C.; Na, S.; Song, J.; Ma, S.; Kim, C.-W. Dynamic Analysis of Three-Dimensional Drivetrain System of Wind Turbine. *Int. J. Precis. Eng. Manuf.* **2014**, *15*, 7. [CrossRef]
26. Wang, J.; Yang, S.; Liu, Y.; Mo, R. Analysis of Load-Sharing Behavior of the Multistage Planetary Gear Train Used in Wind Generators: Effects of Random Wind Load. *Appl. Sci.* **2019**, *9*, 5501. [CrossRef]
27. Farias, M.G.; Galhardo, A.B.M.; Vaz, R.P.J.; Pinho, T.J. A steady-state based model applied to small wind turbines. *J. Braz. Soc. Mech. Sci. Eng.* **2019**, *41*, 209. [CrossRef]
28. Xiang, L.; Gao, N.; Hu, A. Dynamic analysis of a planetary gear system with multiple nonlinear parameters. *J. Comput. Appl. Math.* **2017**, *327*, 325–340. [CrossRef]
29. Erturk, E.; Sivrioglu, S.; Bolat, F.C. Analysis Model of a Small Scale Counter-Rotating Dual Rotor Wind Turbine with Double Rotational Generator Armature. *Int. J. Renew. Energy Res.* **2018**, *8*, 4. [CrossRef]
30. Wrobel, R.; Drury, D.; Mellor, P.D.; Booker, J.D. Contra-Rotating Modular Wound Permanent Magnet Generator for a Wind Turbine. In Proceedings of the 2008 4th IET Conference on Power Electronics, Machines and Drives (PEMD 2008), York, UK, 2–4 April 2008; pp. 330–334. [CrossRef]
31. Booker, J.D.; Mellor, P.H.; Wrobel, R.; Drury, D. A compact, high efficiency contra-rotating generator suitable for wind turbines in the urban environment. *Renew. Energy* **2010**, *35*, 2027–2033. [CrossRef]
32. Egorov, A.V.; Kaizer, Y.F.; Lysyannikov, A.V.; Kuznetsov, A.V.; Shram, V.G.; Pavlov, A.I.; Smirnov, M.Y.; Kuznetsova, P.A. Counter-rotating electric generator for wind power plants with liquid metal energy transfer. *J. Phys. Conf. Ser.* **2021**, *2094*, 052018. [CrossRef]
33. Dong, W.; Xing, Y.; Moan, T. Time Domain Modeling and Analysis of Dynamic Gear Contact Force in a Wind Turbine Gearbox with Respect to Fatigue Assessment. *Energies* **2012**, *5*, 4350–4371. [CrossRef]
34. Xing, Y.; Guo, Y.; Keller, J.; Moan, T. Model Fidelity Study of Dynamic Transient Loads in a Wind Turbine Gearbox. In Proceedings of the WINDPOWER Conference 2013, Chicago, IL, USA, 5–8 May 2013. Available online: https://www.osti.gov/biblio/1078065 (accessed on 7 October 2024).
35. Jansuya, P.; Kumsuwan, Y. Design of MATLAB/Simulink Modeling of Fixed-pitch Angle Wind Turbine Simulator. *Energy Procedia* **2013**, *34*, 362–370. [CrossRef]
36. Oyekola, P.; Mohamed, A.; Pumwa, J. Renewable Energy: Dynamic Modelling of a Wind Turbine. *Int. J. Innov. Technol. Explor. Eng.* **2019**, *9*, 9. [CrossRef]
37. Santoso, S.; Le, H. Fundamental time–domain wind turbine models for wind power studies. *Renew. Energy* **2007**, *32*, 2436–2452. [CrossRef]
38. Teixeira, M.R.; Ohara, M.F.; Milhomens, D.M.; de Paula, S.A. Dynamical Behavior of a Wind Turbine Power Train Considering a Rotor-Gearbox-Generator Coupled Model. In Proceedings of the 6th ECCOMAS Thematic Conference on Computational Methods in Structural Dynamics and Earthquake Engineering, Rhodes Island, Greece, 15–17 June 2017; pp. 3543–3555. [CrossRef]
39. Park, Y.; Shi, W.; Park, H. Effect of the Variable Gear Mesh Model in Dynamic Simulation of a Drive Train in the Wind Turbine. *Eng. Rev.* **2020**, *41*, 113–124. [CrossRef]

40. Park, Y.; Park, H.; Ma, Z.; You, J.; Shi, W. Multibody Dynamic Analysis of a Wind Turbine Drivetrain in Consideration of the Shaft Bending Effect and a Variable Gear Mesh Including Eccentricity and Nacelle Movement. *Front. Energy Res.* **2021**, *8*, 604414. [CrossRef]
41. Fernández, M.L.; Saenz, J.R.; Jurado, F. Dynamic models of wind farms with fixed speed wind turbines. *Renew. Energy* **2006**, *31*, 1203–1230. [CrossRef]
42. Song, Z.; Shi, T.; Xia, C.; Chen, W. A novel adaptive control scheme for dynamic performance improvement of DFIG-Based wind turbines. *Energy* **2012**, *38*, 104–117. [CrossRef]
43. Zhao, M.; Ji, J. Dynamic Analysis of Wind Turbine Gearbox Components. *Energies* **2016**, *9*, 110. [CrossRef]
44. Zhu, C.; Xu, X.; Liu, H.; Luo, T.; Zhai, H. Research on dynamical characteristics of wind turbine gearboxes with flexible pins. *Renew. Energy* **2014**, *68*, 724–732. [CrossRef]
45. Yi, P.; Zhang, C.; Guo, L.; Shi, T. Dynamic modeling and analysis of load sharing characteristics of wind turbine gearbox. *Adv. Mech. Eng.* **2015**, *7*, 3. [CrossRef]
46. Saulescu, R.; Neagoe, M.; Visa, M.; Jaliu, C.; Munteanu, O.; Totu, I.; Cretescu, N. Monomobile Planetary Speed Increaser with Two Counter-Rotating Outputs. RO 131740 B1, 29 November 2023.

Available online at www.sciencedirect.com
ScienceDirect
Energy Reports 8 (2022) 1154–1169
www.elsevier.com/locate/egyr

TMREES22-Fr, EURACA, 09 to 11 May 2022, Metz-Grand Est, France

Comparative energy performance analysis of four wind turbines with counter-rotating rotors in steady-state regime

Mircea Neagoe[a], Radu Saulescu[b,*]

[a] *Renewable Energy Systems and Recycling R&D Center, Transilvania University of Brasov, 500036 Brasov, Romania*
[b] *Design of Mechanical Elements and Systems R&D Center, Transilvania University of Brasov, 500036 Brasov, Romania*

Received 13 June 2022; accepted 19 July 2022
Available online 5 August 2022

Abstract

In the worldwide effort to decarbonize the electricity generation, increasing the energy performance of renewable energy conversion systems is a continuing global concern and challenge for stakeholders. In this context, the paper presents the results of a comparative study on energy performance of four counter-rotating wind turbines of different types. In this regard, the authors propose a new reconfigurable structure of a counter-rotating wind system, able of operating in four distinct cases: with traditional electric generator (with fixed stator) or counter-rotating generator, with monomobile (torque adding) or bimobile (speed adding) speed increaser. These functional cases are obtained by the appropriate command of two intermittent clutches. A generalized algorithm for kinematic and static analytical modeling of the reconfigurable wind system in steady-state regime is proposed in the first part. Also, a new approach for optimizing the main design parameters, such as the ratio of wind rotor diameters, is detailed. The numerical simulations of the obtained closed-form model, for optimized value set of design parameters and various wind speed values, showed a slight energy advantage of using counter-rotating generators and monomobile transmissions, but accompanied by drawback of increased complexity. The main results of the paper, *i.e.* the new reconfigurable wind system concept and its analytical steady-state model of speeds, torques and efficiency, are useful for researchers and practitioner interested in developing optimized counter-rotating wind turbines.

Peer-review under responsibility of the scientific committee of the TMREES22-Fr, EURACA, 2022.

Keywords: Wind turbine; Counter-rotating rotors; Speed increaser; Counter-rotating generator; Energy performance; Steady-state regime

1. Introduction

The counter-rotating wind turbines (CRWT) are a recent alternative with higher energy performance to the conventional wind systems (with single wind rotor and electric generator with fixed stator). A large number of research works have been recently devoted to CRWTs by studying various factors influencing their performances. As shown in [1,2], counter-rotating wind systems require certain distances between counter-rotating wind rotors

* Corresponding author.
E-mail address: rsaulescu@unitbv.ro (R. Saulescu).

https://doi.org/10.1016/j.egyr.2022.07.092

Peer-review under responsibility of the scientific committee of the TMREES22-Fr, EURACA, 2022.

Nomenclature

a_G	speed coefficient in the generator mechanical characteristic
a_R	speed coefficient in the wind rotor mechanical characteristic
b_G	torque term in the generator mechanical characteristic
b_R	torque term in the wind rotor mechanical characteristic
C1,2	clutch 1,2
C_P	aerodynamic power coefficient
CRWT	counter-rotating wind turbine
DC	direct current
DOF	degree of freedom
G	electric generator
GR	generator rotor
GS	generator stator
H	satellite carrier
HAWT	horizontal-axis wind turbine
i	kinematic ratio
i_0	internal kinematic ratio
$\overline{i_0}$	internal static ratio
i_a	speed amplification ratio
k_G	ratio of the parameters b_G and a_G
k_R	ratio of the downwind and upwind rotors radius
k_ω	ratio of the angular speeds of the wind rotors
L	number of external links
P	power
P_{G0}	rated power of wind turbine
PGS	planetary gear set
$R1/R2$	upwind/downwind rotor
r_R	radius of the wind rotor
SI	speed increaser
T	torque
$\widetilde{T}$	torque value at the operating point
v_R	speed of equivalent uniform flow at the rotor *R*
v_w	undisturbed wind speed
v_{w0}	rated wind speed
z	number of gear teeth
β	blade pitch angle
η	efficiency
η_0	internal efficiency
λ	tip speed ratio
ρ	air density
ω	angular speed
$\widetilde{\omega}$	angular speed value at the operating point

with equal [2–4] or different [5–8] diameters, and may include counter-rotating generators [1,9–11]. An important performance parameter of wind systems is the power coefficient (C_P); in the case of counter-rotating rotors with the same diameter, C_P increases theoretically from 0.59 (Betz's limit) to 0.64 [2,4,7,12–14], which represents an improvement of 8%–9% when the distance between the rotors is close to the radius of the rotor, and 7% when the diameter of the upwind rotor is 25% of the downwind rotor diameter [6]. It was found experimentally that the wind turbine rotational speed of the wind turbine is also influenced by the blade pitch angle β; thus, as β increases, the rotational speed decreases, which leads to a decrease in the power coefficient [3,7,12,15]. The annual energy production can be increased by using counter-rotating turbines by about 43.5% [12] or by about 21% at a nominal wind speed of 10.6 m/s [7]. Whang [16] demonstrated that his proposed counter-rotating wind system can generate energy as efficiently as a conventional 3-blade system, but at a slower rotor speed, which means lower noise operation.

The integration of two counter-rotating rotors can improve the performance of wind turbine systems with conventional generator, even in low power systems. These CRWTs integrate a speed increaser with two inputs and one output. This topic has been theoretically approached in various works [17–20], in which dynamic aspects or power flow were analyzed in the case of 1-DOF (degree of freedom) or 2-DOF speed increaser, thus allowing the reduction of rotor size while increasing the energy input.

Also worth noting that the parallel transmission of mechanical power from wind turbines to the electric generator has a better efficiency than serial transmission. A specific algorithm for the conceptual synthesis of speed increasers integrated in wind energy conversion systems was proposed in [21], as a useful tool in the design process of wind turbines: with single *vs.* two counter-rotating wind rotors, with 1-DOF *vs.* 2-DOF speed increaser, and conventional *vs.* counter-rotating electric generator.

The use of counter-rotating electric generators is a relatively recent approach in the domain of wind turbines. Thus, variants of generators with permanent magnets, connected directly to the wind rotors, have been proposed [9, 10]. A three-phase synchronous electric generator with counter-rotating armatures, with 1 kW rated power at rated speed of 750 rpm, was analyzed in [10]. Popescu et al. highlighted both the difficulties in execution with a high degree of complexity, as well as a number of advantages, such as: the increase of the relative speed between the armatures of the electric generator, and the increase of the power extracted from the wind, respectively. Further development was proposed by Yanan et al. [11], which introduces a new type of twin-rotor wind turbine and electrically excited synchronous generator. Another variant of electric generator used in a counter-rotating turbine is the induction turbine (TRIAS) [22], intended for applications that supply power directly to the grid, which allows a reduction of losses by about 27% compared to a conventional generator.

Increasing the performance of wind turbines is the main goal in their optimization process. Herzog [14] stated that a wind speed loss of 1% leads to a 3% decrease in power; moreover, he showed that the upwind rotor extracts 74% of the power, while the downwind rotor only 26%. The fact that a counter-rotating turbine is more efficient at lower rotor rotational speeds has been demonstrated in [4], which states that $C_P = 0.37$ at tip speed ratio $\lambda = 6$, while a counter-rotating system reaches $C_P = 0.39$ at $\lambda = 5$. Kumar [23] also showed that compared to [7], for an increase in the distance between the two rotors from 0.5 to 0.65 times the rotor diameter, it reaches a maximum power increase of 9.67%. Mitulet [24] confirmed that two counter-rotating rotors with different diameters (2.46 m upwind rotor and 2.66 m downwind rotor) increase the output power in the range of 37–45.2%, depending on the wind speed. No [25] presented detailed procedures for modeling the dynamics and aerodynamics of the 1 MW wind turbine system.

Aiming at highlighting their performances, wind systems with counter-rotating rotors and/or counter-rotating generators have been investigated *vs.* conventional systems. Farahani [26] analyzed a two-input wind system, in which the main (upwind) rotor has twice the diameter of the downwind rotor. Climescu [27] and Saulescu [28] considered different operating situations for wind turbines with one *vs.* two counter-rotating rotors, with *vs.* without speed increaser (1-DOF or 2-DOF) and electric generator with fixed *vs.* mobile stator. Their dynamic behavior was investigated and compared, concluding that the use of counter-rotating turbines for applications with Class 1 wind potential allows energy generation at lower nominal speed than in conventional cases. Similar comparative analyzes were also presented in [29]; it concluded that the counter-rotating turbine solution ensured more compact rotors and higher efficiency of mechanical transmission (81.7% compared to 71.3% for the considered conventional turbine). A variable wind speed dynamic approach was presented in [30] for a 10 kW turbine consisting of a wind rotor, speed increaser and counter-rotating electric generator.

The literature presents various studies, in general, on particular solutions of counter-rotating wind systems, without identifying significant results on optimizing the ratio of wind rotor diameters, respectively the impact of the type of electric generator and the type of speed increaser on the energy performance of the wind system. As a result, the main purpose of the paper is to propose, model and optimize a novel wind system capable of transforming wind energy into electricity with high efficiency, by considering the class of wind turbines with counter-rotating wind turbines, counter-rotating generator and planetary speed increaser. Thus, a new reconfigurable counter-rotating wind system is proposed in Section 2, for which four distinct operating cases of 1-DOF or 2-DOF turbines are considered, with traditional (with fixed stator) or counter-rotating generator. The kinematic and static analytical modeling of this reconfigurable wind system is presented in Section 3, and the optimization of the system design parameters is addressed in Section 4. A relevant numerical example is described in Section 5, along with discussions on the results obtained for four cases. The conclusions of the paper are drawn in Section 6.

2. Problem formulation

The proposed comparative analysis addresses four categories of horizontal-axis wind turbines (HAWT) with two counter-rotating coaxial rotors $R1$ and $R2$, which integrate a single degree of freedom (1-DOF) or differential (2-DOF) speed increaser (*SI*) and a conventional (with fixed stator, $GS \equiv 0$, Fig. 1a) or counter-rotating electric generator (in which the rotor *GR* and the stator *GS* are mobile and rotate in opposite directions, Fig. 1b). By convention, $R1$ is the upwind rotor and $R2$ - the downwind rotor. The two rotors $R1$ and $R2$ can have the same or different diameters, and the speed increaser is usually a planetary transmission. It is already known that branched (in parallel) transmission of mechanical power from wind rotors to the generator is achieved with higher efficiencies than serial transmission [20]. Based on these considerations, the energy performance of the counter-rotating wind turbines, under similar operating conditions, can be significantly different depending on their category; thus, identifying their behavior is a challenge for researchers and a goal for designers in determining the optimal solution.

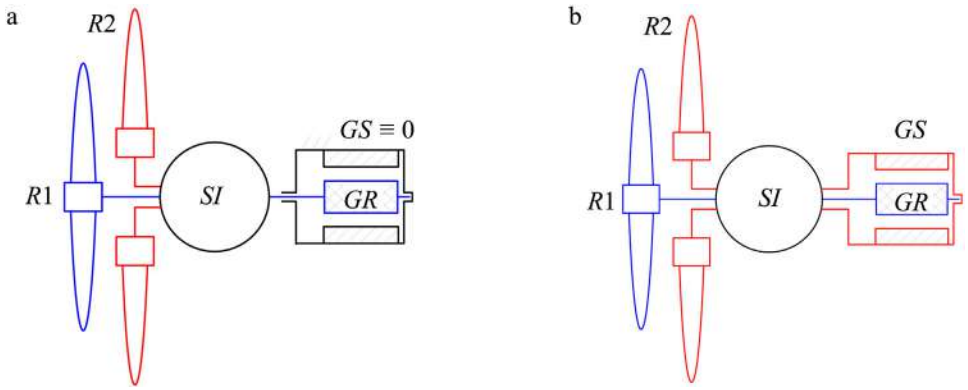

Fig. 1. Conceptual scheme of wind turbines with counter-rotating rotors and: (a) conventional generator; (b) counter-rotating generator.

The problem of modeling and identifying the energy performance of the four counter-rotating wind systems is addressed in the following hypotheses:

- the wind turbines have the same set of wind rotors and the electric generators have identical characteristics;
- the wind rotors $R1$ and $R2$ have optimized uneven diameters, according to a proposed approach;
- the rotors $R1$ and $R2$ rotate in opposite directions;
- the pitch angle β of the rotor blades is considered at constant value: $\beta = 0°$, for both $R1$ and $R2$ rotors;
- the *GR* rotor and the mobile *GS* stator rotate in opposite directions, thus leading to an increased speed of the electric generator (defined as the relative speed between *GR* and *GS*). For inertial reasons, the speed of the *GR* rotor is typically higher than that of the *GS* stator;
- the speed increaser is based on a reconfigurable planetary transmission with two inputs, which can operate both as 1-DOF and 2-DOF mechanism, with one or two outputs, by the appropriate control of two intermittent clutches $C1$ and $C2$, Fig. 2;
- without reducing the generality of the proposed method, for the sake of simplicity of the analytical approach, it is considered that the wind turbines are equipped with two wind rotors and electric generators of direct current, whose mechanical characteristics are linear functions with constant coefficients;

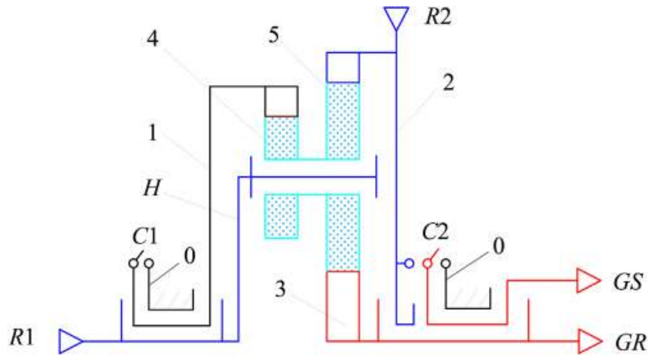

Fig. 2. Structural scheme of the proposed reconfigurable counter-rotating wind system (upper half section).

- the modeling and functional simulation of the four wind turbines are performed in stationary conditions, at three wind speeds: the rated speed, a speed close to the cut-in value and an intermediate speed.

The proposed speed increaser (Fig. 2) is a planetary transmission with cylindrical gears, consisting of two sun ring gears 1 and 2, which mesh with the satellite gears 4 and 5, and a sun external gear 3 engaged with the satellite gear 5. The transmission has two inputs (of mechanical power), due to the connection of the satellite carrier H to the rotor $R1$ and the gear 2 to the rotor $R2$. It can have a single output to the generator rotor ($3 \equiv GR$) or two outputs ($3 \equiv GR$ and $2 \equiv GS$). The transmission can also operate as a 1-DOF drive (by attaching the gear 1 to the base 0) or 2-DOF (when the gear 1 moves idle). Thus, the speed increaser is a transmission with adjustable configuration, property ensured by means of the clutches $C1$ and $C2$, for which the following coding is introduced:

- $C1 = 0$ – the clutch $C1$ is engaged, *i.e.,* $1 \equiv 0$; $C1 = 1$ – the clutch $C1$ is disengaged, *i.e.* the gear 1 has idle motion;
- $C2 = 0$ – the double clutch $C2$ is engaged with the base 0, *i.e.* $GS \equiv 0$; $C2 = 1$ – the clutch $C2$ is engaged with the gear 2, *i.e.* $GS \equiv 2$.

The complex *SI* in Fig. 2 can be decomposed into two planetary gear sets $PGS1$ (1-4-5-3-H) and $PGS2$ (2-5-3-H), respectively, each characterized by an internal kinematic ratio $i_{01,2}$ and an internal efficiency $\eta_{01,2}$(Fig. 3).

The main parameters of the energy performance considered in this study refer to the mechanical power provided by the wind rotors, the mechanical power driving the generator and the transmission efficiency. These energy performance parameters can be identified by applying the algorithm depicted in Fig. 4, considering in a general approach the following four operating cases ensured by the proposed planetary transmission:

- Case A: bimobile (differential) transmission with two inputs and two outputs (2-DOF, $L = 4$; $C1 = 1$ & $C2 = 1$ => $\omega_1 \neq 0$, $T_1 = 0$),$\omega_2 = \omega_{GS}$;
- Case B: monomobile transmission with two inputs and two outputs (1-DOF, $L = 4$; $C1 = 0$ & $C2 = 1$ => $\omega_1 = 0$, $T_1 \neq 0$), $\omega_2 = \omega_{GS}$;
- Case C: bimobile transmission with two inputs and one output (2-DOF, $L = 3$, C1 = 1 & C2 = 0 => $\omega_1 \neq 0$,$\omega_1 \neq 0$, $T_1 = 0$, $\omega_2 \neq \omega_{GS}$, $\omega_{GS} = 0$);
- Case D: monomobile transmission with two inputs and one output (1-DOF, $L = 3$, C1 = 0 & C2 = 0 => $\omega_1 = 0$, $T_1 \neq 0$, $\omega_2 \neq \omega_{GS}$, $\omega_{GS} = 0$).

3. Wind system modeling

The kinematic and static modeling of the mechanical systems, corresponding to the four wind turbines, uses the block diagram from Fig. 3, which specifies the torques T_x and the angular velocities ω_x related to the isolated subsystems (*PGS* and shafts); this modeling is based on the general relationships in the theory of gears [31]. Thus, starting from the definition of the internal kinematic ratios i_{01} and i_{02}, and assuming that all gears have the same

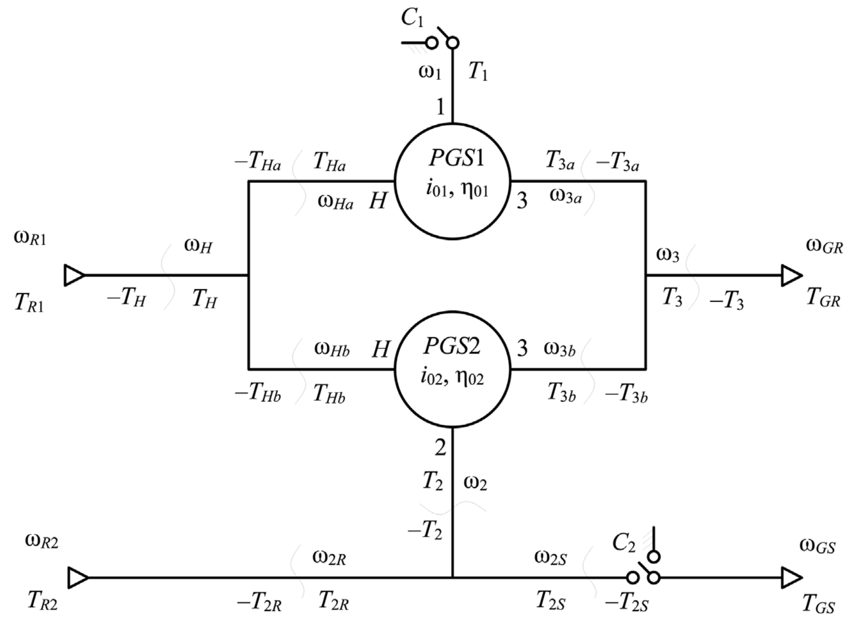

Fig. 3. Block scheme of the reconfigurable wind system.

module, the numbers of teeth are modeled by:

$$\begin{cases} i_{01} = i_{31}^H = \dfrac{\omega_{3H}}{\omega_{1H}} = -\dfrac{z_5}{z_3}\dfrac{z_1}{z_4} \\ i_{02} = i_{32}^H = \dfrac{\omega_{3H}}{\omega_{2H}} = -\dfrac{z_2}{z_3} \\ z_1 - z_4 = z_5 + z_3 = z_2 - z_5 \end{cases} \Rightarrow \begin{cases} z_1 = z_3 \dfrac{i_{01}\,(1 - i_{02})}{2i_{01} - i_{02} - 1} \\ z_2 = -z_3 i_{02} \\ z_4 = z_3 \left(\dfrac{1 - i_{02}}{2}\right)\left(\dfrac{1 + i_{02}}{2i_{01} - i_{02} - 1}\right) \\ z_5 = -z_3 \dfrac{1 + i_{02}}{2} \end{cases} \tag{1}$$

where z_3, i_{01} and i_{02} are considered independent design variables.

As the wind rotors should rotate in opposite directions in all operation cases (*i.e.*, $\omega_{R1}/\omega_{R2} < 0$), it is necessary that $|i_{01}| > |i_{02}|$, which leads to the restriction: $z_2 > z_1$(by default: $z_5 > z_4$).

According to Fig. 3, the planetary speed increaser is characterized by the following analytical correlations related to its isolated subsystems:

- input shafts:

$$\begin{cases} \omega_{R1} = \omega_H \\ T_{R1} - T_H = 0 \end{cases} \text{ and } \begin{cases} \omega_{R2} = \omega_{2R} \\ T_{R2} - T_{2R} = 0 \end{cases} \tag{2}$$

- internal shafts:

$$\begin{cases} \omega_H = \omega_{Ha} = \omega_{Hb} \\ T_H - T_{Ha} - T_{Hb} = 0 \end{cases}, \begin{cases} \omega_2 = \omega_{2R} = \omega_{2S} \\ T_{2R} - T_2 + T_{2S} = 0 \end{cases} \text{ and } \begin{cases} \omega_3 = \omega_{3a} = \omega_{3b} \\ T_3 - T_{3a} - T_{3b} = 0 \end{cases} \tag{3}$$

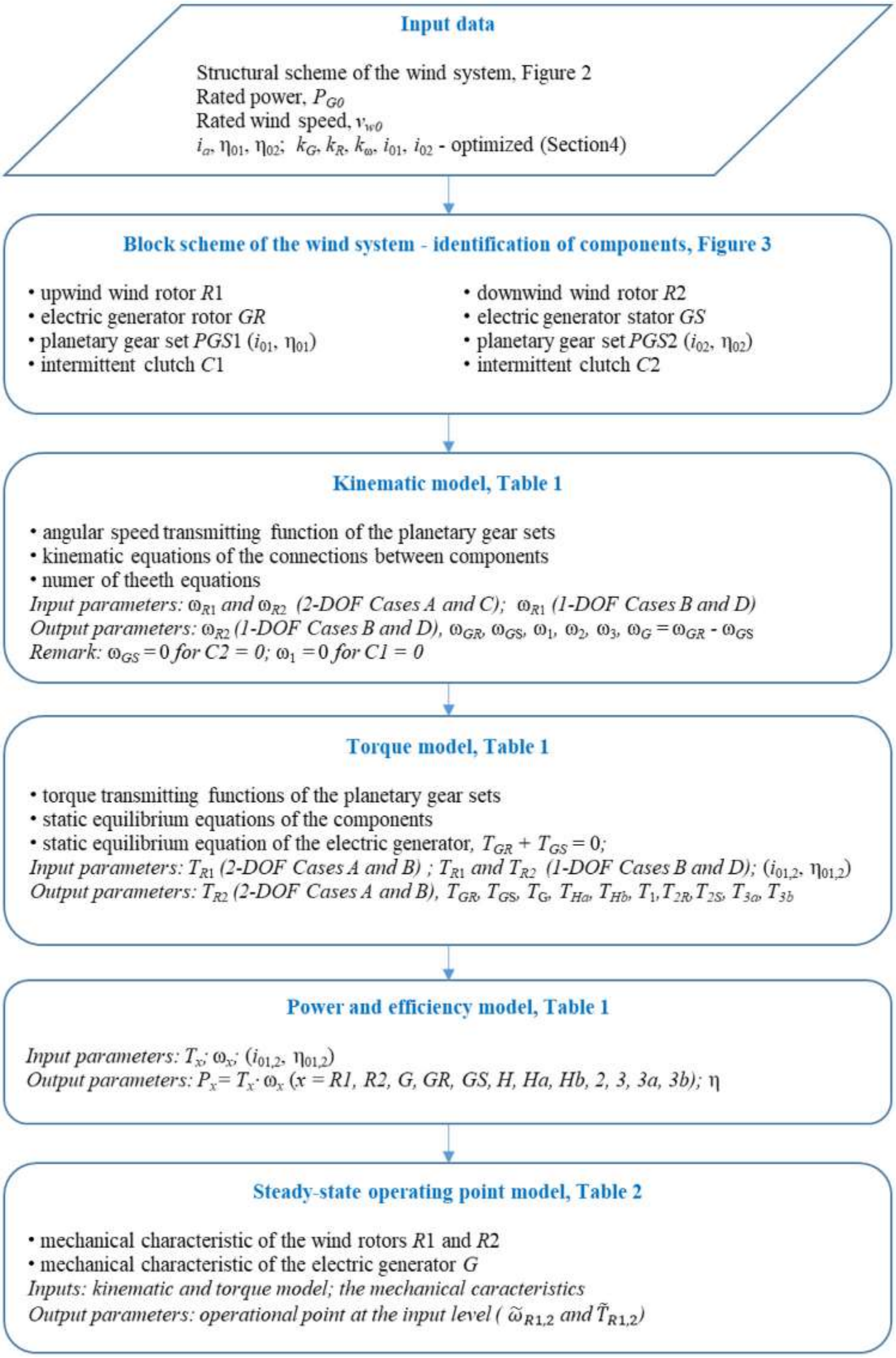

Fig. 4. Flowchart of the proposed analytical modeling of the reconfigurable wind system.

• planetary gear sets:

$$PGS1:\begin{cases}\omega_3-\omega_1 i_{01}-\omega_H\left(1-i_{01}\right)=0\\ T_1+T_{3a}i_{01}\eta_{01}^{x_1}=0\\ T_1+T_{3a}+T_{Ha}=0\end{cases}\quad\text{and}\quad PSG2:\begin{cases}\omega_3-\omega_2 i_{02}-\omega_H\left(1-i_{02}\right)=0\\ T_2+T_{3b}i_{02}\eta_{02}^{x_2}=0\\ T_2+T_{3b}+T_{Hb}=0\end{cases}\tag{4}$$

in which:

$$x_1=\operatorname{sgn}\left(\omega_{3H}T_{3a}\right)=\operatorname{sgn}\left(\frac{\omega_{3H}T_{3a}}{-\omega_{31}T_{3a}}\right)=\operatorname{sgn}\left(\frac{i_{01}}{1-i_{01}}\right)=-1\tag{5}$$

$$x_2=\operatorname{sgn}\left(\omega_{3H}T_{3b}\right)=\operatorname{sgn}\left(\frac{\omega_{3H}T_{3b}}{-\omega_{32}T_{3b}}\right)=\operatorname{sgn}\left(\frac{i_{02}}{1-i_{02}}\right)=-1\tag{6}$$

The general relations (4) have the following particular forms: Cases A and C, in which $\omega_1\neq 0, T_1=0$ and implicitly $T_{3a}=0, T_{Ha}=0$, *i.e.* $PGS1$ operates idle; Cases B and D, in which $\omega_1=0, T_1\neq 0$ and implicitly $\omega_3-\omega_H\left(1-i_{01}\right)=0$, *i.e.* $PGS1$ becomes a 1-DOF planetary gear set.

• transmission connections with the generator stator and rotor:

$$\begin{cases}\omega_3=\omega_{GR}\\ T_{GR}-T_3=0\end{cases}\quad\text{and}\quad\begin{cases}\omega_{2S}=\omega_{GS}\\ T_{GS}-T_{2S}=0\end{cases}\tag{7}$$

• the equations of the global wind system:

$$\begin{cases}\left(\omega_{R1}T_{R1}+\omega_{R2}T_{R2}\right)\eta+\omega_{GR}T_{GR}+\omega_{GS}T_{GS}=0\\ T_{R1}+T_{R2}+T_1+T_{GR}+T_{GS}=0\end{cases}\tag{8}$$

• electric generator equations:

$$\begin{cases}\omega_G=\omega_{GR}-\omega_{GS}\\ T_G=T_{GR}=-T_{GS}\end{cases}\tag{9}$$

in which, by convention, the angular speed of the electric generator is defined as the relative speed between its rotor and stator, and the generator torque is considered the torque of the rotor *GR* (equal and opposite to the torque of the *GS* stator).

The relations (2)...(9) allow the analytical determination of the expressions of torques and angular velocities for all shafts of the wind system (Table 1): in Cases A and C, depending on the independent variables ($\omega_{R1},\ T_{R1},\ \omega_{R2}$), and in Cases B and D, depending on ($\omega_{R1},\ T_{R1},\ T_{R2}$) parameters.

The operating point of the analyzed wind systems (*i.e.* the values of kinematic and static parameters in steady state regime for all shafts) can be determined based on the relationships in Table 1 and on the linear mechanical characteristics with constant coefficients of wind rotors and electric generator (see Fig. 5):

- the wind rotors $R1$ and $R2$

$$T_{R1}=-a_{R1}\omega_{R1}+b_{R1}, 0\leq\omega_{R1}\leq\frac{b_{R1}}{a_{R1}},\ a_{R1}>0, b_{R1}>0\tag{10}$$

$$T_{R2}=-a_{R2}\omega_{R2}+b_{R2},\frac{b_{R2}}{a_{R2}}\leq\omega_{R2}\leq 0, a_{R2}>0, b_{R2}<0\tag{11}$$

- the electric generator G

$$T_G=-a_G\omega_G+b_G, \omega_G>\frac{b_G}{a_G},\ a_G>0, b_G>0\tag{12}$$

where the values of the parameters $a_{R1,2}$ and $b_{R1,2}$ depend on the properties of the wind rotors and they change with the wind speed.

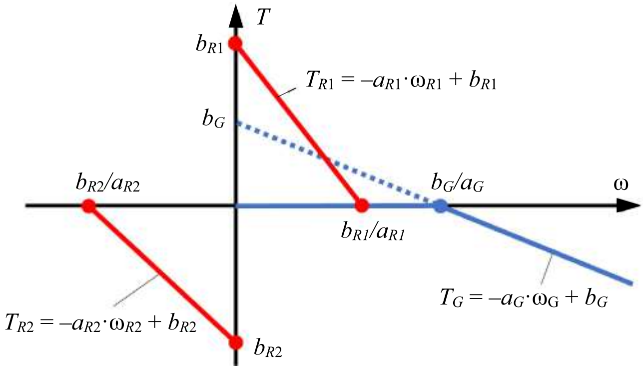

Fig. 5. Linear mechanical characteristics of the wind rotors (*R*1 and *R*2) and the *DC* generator (G).

Table 1. Analytical expressions of kinematic and static parameters of the four CRWTs.

Parameter	Case A (2-DOF, $L=4$)	Case B (1-DOF, $L=4$)	Case C (2-DOF, $L=3$)	Case D (1-DOF, $L=3$)
ω_{R2}	ω_{R2}	$\omega_{R1}\left(i_{02}-i_{01}\right)/i_{02}$	ω_{R2}	$\omega_{R1}\left(i_{02}-i_{01}\right)/i_{02}$
ω_1	$\omega_{R1}\frac{i_{01}-i_{02}}{i_{01}}+\omega_{R2}\frac{i_{02}}{i_{01}}$	0	$\omega_{R1}\frac{i_{01}-i_{02}}{i_{01}}+\omega_{R2}\frac{i_{02}}{i_{01}}$	0
ω_{GS}	ω_{R2}	$\omega_{R1}\left(i_{02}-i_{01}\right)/i_{02}$	0	0
ω_{GR}	$\omega_{R1}\left(1-i_{02}\right)+\omega_{R2}i_{02}$	$\omega_{R1}\left(1-i_{01}\right)$	$\omega_{R1}\left(1-i_{02}\right)+\omega_{R2}i_{02}$	$\omega_{R1}\left(1-i_{01}\right)$
ω_G	$\left(\omega_{R1}-\omega_{R2}\right)\left(1-i_{02}\right)$	$\omega_{R1}i_{01}\left(1-i_{02}\right)/i_{02}$	$\omega_{R1}\left(1-i_{02}\right)+\omega_{R2}i_{02}$	$\omega_{R1}\left(1-i_{01}\right)$
T_{R2}	$-T_{R1}$	T_{R2}	$-T_{R1}\overline{i_{02}}/\left(\overline{i_{02}}-1\right)$	T_{R2}
T_1	0	$-T_{R1}-T_{R2}$	0	$\left[T_{R1}\overline{i_{02}}+T_{R2}\left(\overline{i_{02}}-1\right)\right]\overline{i_{01}}/\left[\overline{i_{02}}\left(\overline{i_{01}}-1\right)\right]$
T_{Ha}	0	$\left(T_{R1}+T_{R2}\right)\left(\overline{i_{01}}-1\right)/\overline{i_{01}}$	0	$\left[T_{R1}\overline{i_{02}}+T_{R2}\left(\overline{i_{02}}-1\right)\right]/\overline{i_{02}}$
T_{Hb}	T_{R1}	$\left[T_{R1}-T_{R2}\left(\overline{i_{01}}-1\right)\right]/\overline{i_{01}}$	T_{R1}	$-T_{R2}\left(\overline{i_{02}}-1\right)/\overline{i_{02}}$
T_{3a}	0	$\left(T_{R1}+T_{R2}\right)/\overline{i_{01}}$	0	$-\left[T_{R1}\overline{i_{02}}+T_{R2}\left(\overline{i_{02}}-1\right)\right]/\left[\overline{i_{02}}\left(\overline{i_{01}}-1\right)\right]$
T_{3b}	$T_{R1}/\left(\overline{i_{02}}-1\right)$	$\left[T_{R1}-T_{R2}\left(\overline{i_{01}}-1\right)\right]/\left[\overline{i_{01}}\left(\overline{i_{02}}-1\right)\right]$	$T_{R1}/\left(\overline{i_{02}}-1\right)$	$-T_{R2}/\overline{i_{02}}$
T_2	$-T_{R1}\overline{i_{02}}/\left(\overline{i_{02}}-1\right)$	$-\left[T_{R1}-T_{R2}\left(\overline{i_{01}}-1\right)\right]\overline{i_{02}}/\left[\overline{i_{01}}\left(\overline{i_{02}}-1\right)\right]$	$-T_{R1}\overline{i_{02}}/\left(\overline{i_{02}}-1\right)$	T_{R2}
T_{GR}	$T_{R1}/\left(\overline{i_{02}}-1\right)$	$\left[T_{R1}\overline{i_{02}}+T_{R2}\left(\overline{i_{02}}-\overline{i_{01}}\right)\right]/\left[\overline{i_{01}}\left(\overline{i_{02}}-1\right)\right]$	$T_{R1}/\left(\overline{i_{02}}-1\right)$	$-\left[T_{R1}\overline{i_{02}}+T_{R2}\left(\overline{i_{02}}-\overline{i_{01}}\right)\right]/\left[\overline{i_{02}}\left(\overline{i_{01}}-1\right)\right]$
η	$\frac{1-i_{02}}{1-\overline{i_{02}}}$	$\frac{T_{R1}\overline{i_{02}}+T_{R2}\left(\overline{i_{02}}-\overline{i_{01}}\right)}{T_{R1}i_{02}+T_{R2}\left(i_{02}-i_{01}\right)}\cdot\frac{i_{01}\left(i_{02}-1\right)}{\overline{i_{01}}\left(\overline{i_{02}}-1\right)}$	$\frac{\omega_{R1}\left(i_{02}-1\right)-\omega_{R2}i_{02}}{\omega_{R1}\left(\overline{i_{02}}-1\right)-\omega_{R2}\overline{i_{02}}}$	$\frac{T_{R1}\overline{i_{02}}+T_{R2}\left(\overline{i_{02}}-\overline{i_{01}}\right)}{T_{R1}i_{02}+T_{R2}\left(i_{02}-i_{01}\right)}\,\frac{i_{02}\left(i_{01}-1\right)}{\overline{i_{02}}\left(\overline{i_{01}}-1\right)}$

Notes: $\overline{i_{01}}=i_{01}\eta_{01}^{x_1}$, $\overline{i_{02}}=i_{02}\eta_{02}^{x_2}$; $x_1=-1, x_2=-1, \omega_2=\omega_{R2}$, $\omega_3=\omega_{GR}$, $\omega_H=\omega_{R1}$; $T_H=T_{R1}$, $T_{2R}=T_{R2}$, $T_3=T_{2S}=T_{GR}=-T_{GS}$.

The Eq. (2)…(12) define a determined linear system whose solution represents the torques and angular speeds related to the wind system shafts, to which its efficiency η is added, Table 1. Thus, the expressions of the kinematic and static parameters of the operating point for the input shafts (of the wind rotors $R1$ and $R2$) are presented in Table 2, used to calculate all the other wind system parameters, according to the relations in Table 1. These expressions have been obtained using the Maple software and include the constant coefficients of the mechanical characteristics (a_G and $a_{R1,2}$, b_G and $b_{R1,2}$) and the internal kinematic ratios (i_{01} and i_{02}), which are subject to optimization in the design process.

4. Optimal synthesis of CRWT design parameters

The main design parameters of the wind turbines come from the three basic components: (a) the radius r_{R1} and r_{R2} of the $R1$ and $R2$ wind rotors, respectively; (b) the internal kinematic ratios i_{01} and i_{02} of the planetary gear sets; (c) the coefficients a_G and b_G of the generator mechanical characteristic. The values of these parameters can be optimized at the level of the reconfigurable wind system based on functional harmonization of the wind rotors and the electric generator.

4.1. Optimization of the wind rotor radius ratio

In certain applications, the wind rotors have equal diameters, which leads to a sub-optimal use of the downwind rotor due to the reduction of wind speed at its level, as will be emphasized in Section 5. The rotor radius ratio

Table 2. Operating point parameters for the wind rotor shafts.

Case A (2-DOF, $L = 4$)
$\widetilde{\omega}_{R1} = \frac{(\overline{i_{02}}-1)[(b_{R1}+b_{R2})a_G(i_{02}-1)-a_{R2}b_G]+a_{R2}b_{R1}}{(\overline{i_{02}}-1)(a_{R1}+a_{R2})a_G(i_{02}-1)+a_{R1}a_{R2}}$; $\widetilde{\omega}_{R2} = -\frac{a_{R1}\widetilde{\omega}_{R1}-b_{R1}-b_{R2}}{a_{R2}}$
$\widetilde{T}_{R1} = \frac{(\overline{i_{02}}-1)[(a_{R2}b_{R1}-a_{R1}b_{R2})a_G(i_{02}-1)-a_{R1}a_{R2}b_G]}{(\overline{i_{02}}-1)(a_{R1}+a_{R2})a_G(i_{02}-1)+a_{R1}a_{R2}}$; $\widetilde{T}_{R2} = -a_{R2}\widetilde{\omega}_{R2} + b_{R2}$
Case B (1-DOF, $L = 4$)
$\widetilde{\omega}_{R1} = \frac{i_{02}[b_{R1}\overline{i_{02}}+b_{R2}(\overline{i_{02}}-\overline{i_{01}})-b_G\overline{i_{01}}(\overline{i_{02}}-1)]}{a_{R1}i_{02}\overline{i_{02}}+a_{R2}(i_{02}-i_{01})(\overline{i_{02}}-\overline{i_{01}})+a_G i_{01}\overline{i_{01}}(i_{02}-1)(\overline{i_{02}}-1)}$; $\widetilde{\omega}_{R2} = \widetilde{\omega}_{R1}\,(i_{02} - i_{01})\,/\,i_{02}$
$\widetilde{T}_{R1} = \frac{a_{R1}b_G i_{02}\overline{i_{01}}(\overline{i_{02}}-1)-a_{R1}b_{R2}i_{02}(\overline{i_{02}}-\overline{i_{01}})+a_G b_{R1}i_{01}\overline{i_{01}}(i_{02}-1)(\overline{i_{02}}-1)+a_{R2}b_{R1}(i_{02}-i_{01})(\overline{i_{02}}-\overline{i_{01}})}{a_{R1}i_{02}\overline{i_{02}}+a_{R2}(i_{02}-i_{01})(\overline{i_{02}}-\overline{i_{01}})+a_G i_{01}\overline{i_{01}}(i_{02}-1)(\overline{i_{02}}-1)}$
$\widetilde{T}_{R2} = a_{R2}\,(i_{01} - i_{02})\,\widetilde{\omega}_{R1}/i_{02} + b_{R2}$
Case C (2-DOF, $L = 3$)
$\widetilde{\omega}_{R1} = \frac{(\overline{i_{02}}-1)(a_G b_{R2}i_{02}-a_{R2}b_G)+a_G b_{R1}i_{02}\overline{i_{02}}+a_{R2}b_{R1}}{(\overline{i_{02}}-1)(i_{02}-1)a_G a_{R2}+a_G a_{R1}i_{02}\overline{i_{02}}+a_{R1}a_{R2}}$; $\widetilde{\omega}_{R2} = -\frac{\overline{i_{02}}(a_{R1}\widetilde{\omega}_{R1}-b_{R1})-b_{R2}(\overline{i_{02}}-1)}{a_{R2}(\overline{i_{02}}-1)}$
$\widetilde{T}_{R1} = -\frac{(\overline{i_{02}}-1)[(a_{R1}b_{R2}-a_{R2}b_{R1})a_G i_{02}+a_{R2}(a_G b_{R1}-a_{R1}b_G)]}{(\overline{i_{02}}-1)(i_{02}-1)a_G a_{R2}+a_G a_{R1}i_{02}\overline{i_{02}}+a_{R1}a_{R2}}$; $\widetilde{T}_{R2} = -a_{R2}\widetilde{\omega}_{R2} + b_{R2}$
Case D (1-DOF, $L = 3$)
$\widetilde{\omega}_{R1} = \frac{i_{02}[b_{R1}\overline{i_{02}}+b_{R2}(\overline{i_{02}}-\overline{i_{01}})-b_G\overline{i_{02}}(\overline{i_{01}}-1)]}{a_{R1}i_{02}\overline{i_{02}}+a_{R2}(i_{02}-i_{01})(\overline{i_{02}}-\overline{i_{01}})+a_G i_{02}\overline{i_{02}}(i_{01}-1)(\overline{i_{01}}-1)}$; $\widetilde{\omega}_{R2} = \widetilde{\omega}_{R1}\,(i_{02} - i_{01})\,/\,i_{02}$
$\widetilde{T}_{R1} = \frac{a_{R1}b_G i_{02}\overline{i_{02}}(\overline{i_{01}}-1)-a_{R1}b_{R2}i_{02}(\overline{i_{02}}-\overline{i_{01}})+a_G b_{R1}i_{02}\overline{i_{02}}(i_{01}-1)(\overline{i_{01}}-1)+a_{R2}b_{R1}(i_{02}-i_{01})(\overline{i_{02}}-\overline{i_{01}})}{a_{R1}i_{02}\overline{i_{02}}+a_{R2}(i_{02}-i_{01})(\overline{i_{02}}-\overline{i_{01}})+a_G i_{02}\overline{i_{02}}(i_{01}-1)(\overline{i_{01}}-1)}$
$\widetilde{T}_{R2} = a_{R2}\,(i_{01} - i_{02})\,\widetilde{\omega}_{R1}/i_{02} + b_{R2}$

$k_R = r_{R2}/r_{R1}$ can be optimized provided that both rotors operate simultaneously at maximum power (*i.e.*, at the maximum value of the aerodynamic power coefficient C_P) and to provide equal torques in absolute value (as required in Case A, see Table 1).

The mechanical power P_R at a wind rotor shaft is modeled by the relation [26]:

$$P_R = \frac{1}{2}\pi\rho C_p r_R^2 v_w^3 \tag{13}$$

where ρ is the air density ($\rho = 1.225$ kg/m^3).

The power coefficient C_P depends on the tip speed ratio λ and the pitch angle of the blades β; in the assumption $\beta = 0°$, the expression of the power coefficient C_P becomes [26]:

$$C_P = c_1\left(\frac{c_2}{\lambda_i} - c_3\right)\cdot e^{-\frac{c_4}{\lambda_i}} + c_5\lambda,\ \frac{1}{\lambda_i} = \frac{1}{\lambda} - c_6,\ \lambda = \frac{\omega_R r_R}{v_R} \tag{14}$$

where $c_1 = 0.5176$, $c_2 = 116$, $c_3 = 5$, $c_4 = 21$, $c_5 = 0.0068$, $c_6 = 0.035$.

The wind rotor mechanical characteristic results as follows [30] :

$$T_{R1,2} = \frac{P_{R1,2}}{\omega_{R1,2}} = \frac{1}{2}\pi\,\rho\, r_{R1,2}^3 v_{R1,2}^2\left[\frac{c_1 v_{R1,2}}{\omega_{R1,2}r_{R1,2}}\left(\frac{c_2 v_{R1,2}}{\omega_{R1,2}r_{R1,2}} - c_2c_6 - c_3\right)\cdot e^{-c_4\left(\frac{v_{R1,2}}{\omega_{R1,2}r_{R1,2}}-c_6\right)} + c_5\right]. \tag{15}$$

The maximum mechanical power P_{Rmax} of a wind rotor at any wind speed, regardless of the rotor radius, results for the maximum value of the coefficient C_P(*i.e.* $C_{P\max} = 0.47952$), obtained for $\lambda^* = 8.100$ as a solution of the equation $dC_P/d\lambda = 0$:

$$c_5\lambda^3 + e^{c_4\left(c_6-\frac{1}{\lambda}\right)}c_1\left[c_2c_4 - (c_2 + c_3c_4 + c_2c_4c_6)\,\lambda\right] = 0. \tag{16}$$

Considering the average wind speed on the downwind rotor as modeled in [25]:

$$v_{R2} = v_{R1}\sqrt[3]{1 - \frac{19}{27}\frac{r_{R1}^2}{r_{R2}^2}} \tag{17}$$

the two counter-rotating wind rotors have in operation the same torque at their maximum power points (as required in case A, Table 1), *i.e.* $P_{R1max}/\omega_{R1}^* = P_{R2max}/\ \omega_{R2}^*$, if:

$$\left(\frac{r_{R2}}{r_{R1}}\right)^2\left[1 - \frac{19}{27}\left(\frac{r_{R1}}{r_{R2}}\right)^2\right]\frac{\omega_{R1}^*}{\omega_{R2}^*} = 1,\ \omega_{R1,2}^* = \frac{\lambda^* v_{R1,2}}{r_{R1,2}} \tag{18}$$

Table 3. Values of the CRWT design parameters.

Parameter	r_{R1}	r_{R2}	i_{01}	i_{02}	η_{01}	η_{02}	a_G	b_G
Value	20 m	23.4 m	−29.157	−17.5	0.9506	0.9506	0.0525 kN ms	2.100 kNm
$k_R = 1.17,\ k_\omega = 1.488,\ i_a = 46,\ b_G/a_G = 40\ \mathrm{s}^{-1},\ z_1 = 258,\ z_2 = 350,\ z_3 = 20,\ z_4 = 73,\ z_5 = 165$								

yielding to the equation:

$$k_R^3\left[1-\frac{19}{27}\frac{1}{k_R^2}\right]^{\frac{2}{3}}=1 \tag{19}$$

with the solution:

$$k_R = r_{R2}/r_{R1} = 1.17055. \tag{20}$$

It should be noted that in this situation the ratio of input rotational speeds, $k_\omega = -\omega_{R1}^*/\omega_{R2}^*$:

$$k_\omega = \frac{r_{R2}}{r_{R1}}\frac{v_{R1}}{v_{R2}} = k_R\frac{1}{\sqrt[3]{1-\frac{19}{27}\frac{1}{k_R^2}}} = 1.488 \tag{21}$$

has a constant value irrespective of wind speed.

4.2. Optimization of the internal kinematic ratios

The wind rotors $R1$ and $R2$ can operate simultaneously at their maximum power, including in the case of 1-DOF wind systems (Cases B and D), if:

$$\omega_{R2} = \omega_{R1}\left(i_{02}-i_{01}\right)/i_{02} = -\omega_{R1}/k_\omega \Rightarrow i_{01} = \frac{1+k_\omega}{k_\omega}i_{02} = 1.672 i_{02}. \tag{22}$$

Also, in the design phase in case A, a certain amplification speed ratio $i_a = \omega_G/\omega_{R1}$ can be required and thus the following condition is fulfilled:

$$i_{02} = 1 - i_a/(1+k_\omega). \tag{23}$$

4.3. Optimization of the electric generator parameters

The choice of the electric generator (based on the coefficients a_G and b_G) has a major impact on the behavior of the wind system, being directly influenced by the operating point of the wind rotors and implicitly influence the output power. For the rated wind speed, the angular speed ($\widetilde{\omega}_{R1}$) of the rotor $R1$ at maximum power (and implicitly for the rotor $R2$ and the electric generator) can be determined by following the steps in Sections 4.1 and 4.2. Thus, according to Table 2, a first relation between the coefficients a_G and b_G is obtained; by imposing the ratio $k_G = b_G/a_G$ which ensures the generator operation (*i.e.*, $\widetilde{\omega}_G > k_G$), a determined system of two independent equations and (a_G, b_G) is thus derived.

5. Numerical results and discussions

The numerical analysis of the reconfigurable wind system in Fig. 2 aims to identify the energy behavior of the four wind turbines (Cases A, B, C and D), in steady-state regime, for various values of wind speed, starting from the analytical model presented in Section 3.

The set of input data (values of the design parameters) in Table 3, established according to the algorithm in Section 4, is further considered. The rated power P_{G0} of wind turbines is close to 1 MW at the rated wind speed $v_{w0} = 12$ m/s.

The mechanical characteristic of wind rotors, Eq. (15), is a nonlinear function. However, it presents a quasi-linear profile on the normal operating range of the rotor, *i.e.* for angular speed higher than the one corresponding to the

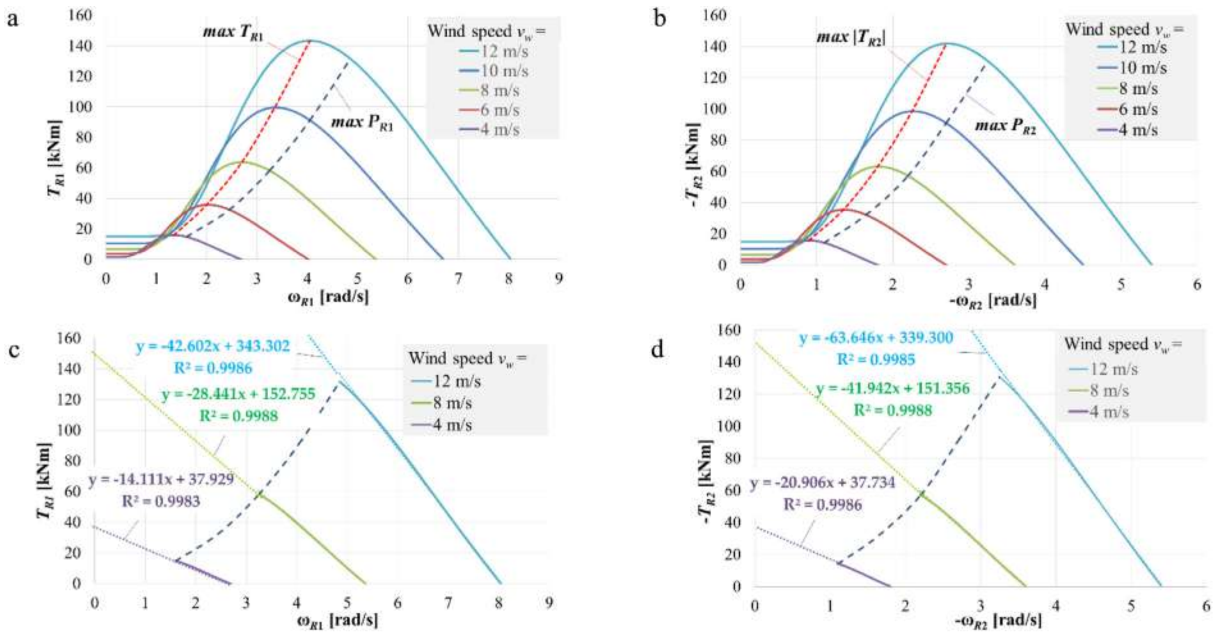

Fig. 6. Nonlinear model of mechanical characteristics for: (a) the $R1$ rotor; (b) the $R2$ rotor; linearized mechanical characteristics on the operating zone for: (c) the $R1$ rotor; (d) the $R2$ rotor.

maximum power point, see Figs. 6a and 6b. The expressions of the linearized mechanical characteristics, for the operating areas of the rotors $R1$ and $R2$, are exemplified in Figs. 6c and 6d for three values of undisturbed wind speed: 12 m/s (rated wind speed), 8 m/s (intermediate speed), and 4 m/s (close to cut-in speed).

The operating points of the four wind turbines were numerically simulated in Maple based on the input parameter values as stated in Table 3; in this approach, the relationships in Tables 1 and 2 were used, which allowed the calculation of the powers on the wind system shafts and of the efficiency. Thus, for the rated wind speed (12 m/s), the power flows are depicted in Fig. 7 and the values of torques, angular speeds and powers on the input ($R1$ and $R2$) and output (G) shafts are represented comparatively in Fig. 8.

The power flows (Fig. 7) are convergent from the inputs (rotors $R1$ and $R2$) towards outputs (GR and GS), excepting the Case D (Fig. 7d) where a close-circuit power flow occurred and, consequently, a loss of useful power is registered. It can be highlighted the negative effect of close-circuit power flow on the energy performance in Case D, the output power decreasing for an increased input power compared with Case C.

The output power $P_G = P_{GR} + P_{GS}$ is higher for the systems with counter-rotating generator (Cases A and B) by ∼1.5% compared with Cases C and D (traditional generator), performance ensured by the system ability to extract more power from wind, *i.e.* the input powers P_{R1} and P_{R2} are higher (by ∼1.25… 2.5%, Figs. 7 and 8a).

As well, the Cases A and B are characterized by higher efficiencies: ∼95.32% *vs.* 95.22% (Case C) and 95.05% (Case D). The higher values of the wind rotor powers in Cases A and B come from the increase of the torques (Fig. 8b) and also a slighter rise of the output angular speed ω_G (Fig. 8c).

The torques (Fig. 8b) and the angular speeds (Fig. 8c) at the generator are simultaneously higher in the Cases A and B than in C and D. Because higher torques are transmitted in the Cases A and B, as a disadvantage, the shafts of these transmissions should have higher diameters than in Cases C and D. Despite of its higher diameter, the downwind rotor $R2$ generates less power (approx. 65%) than the upwind rotor $R1$ due to a decrease in wind speed (to approx. 9.5 m/s, *i.e.* at 79% of the undisturbed wind speed) after crossing the $R1$ rotor.

The wind turbine with counter-rotating generator and 1-DOF transmission (Case B) provides slightly higher power than the 2-DOF one (Case A): 0.15% *vs.* 0.1%. In contrast, the 2-DOF transmissions have the advantage of less complexity, *i.e.* *PGS* 1 does not interfere with power transmission and thus gears 1 and 4 can be eliminated.

The wind speed influences significantly the energy performance of the analyzed wind turbines, the output power P_G decreasing rapidly with the reduction of the speed, Fig. 9. Thus, the operation of turbines at $v_w = 8$ m/s (2/3 of

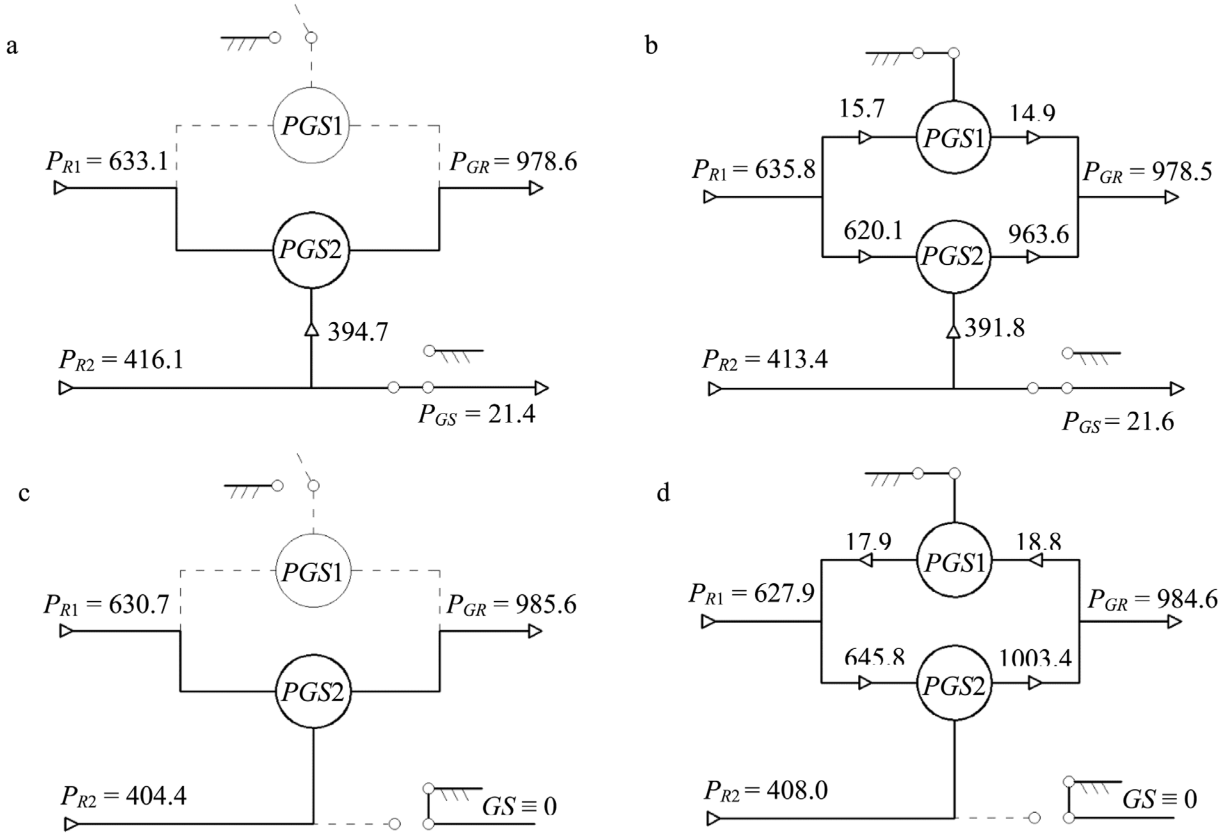

Fig. 7. Power flow (in kW) through the speed increaser for rated wind speed ($v_w = 12$ m/s): (a) Case A (2-DOF, $L = 4$); (b) Case B (1-DOF, $L = 4$); (c) Case C (2-DOF, $L = 3$); (d) Case D (1-DOF, $L = 3$).

the rated speed) is accompanied by a decrease in power to about 1/3 of the rated power. The power supply becomes insignificant at $v_w = 4$ m/s. It can be noticed that the output power differences between the four cases diminishes with the decrease of wind speed and they are practically negligible for wind speeds less than 8 m/s.

6. Conclusions

The paper presents the analytical modeling and the numerical simulation results of the obtained close-form model for four wind turbines with two coaxial counter-rotating rotors with horizontal axis, a reconfigurable planetary transmission and a counter-rotating/traditional generator, aiming at highlighting their comparative performances. The investigation of the energy behavior of the four wind turbines, in steady-state regime at various values of wind speed, allowed drawing the following conclusions:

- The wind turbines with counter-rotating generator operate at higher powers than those with conventional generator; however, they have the disadvantage of increased complexity due to the mobile stator and its additional connections to the transmission.
- The 1-DOF wind turbines generally outperform 2-DOF ones, but they have the disadvantage of higher speed increaser complexity and can be subject of close circuit power flow.
- The downwind rotor $R2$ generates less power (approx. 65%) compared to the upwind rotor $R1$, where $k_R = 1.17$.
- Given the optimization of the design parameter values, according to the algorithm proposed in the paper, the differences in energy performance between the four cases are practically insignificant. However, these differences may become relevant for other value sets of the design parameters, such as for the k_R ratio.

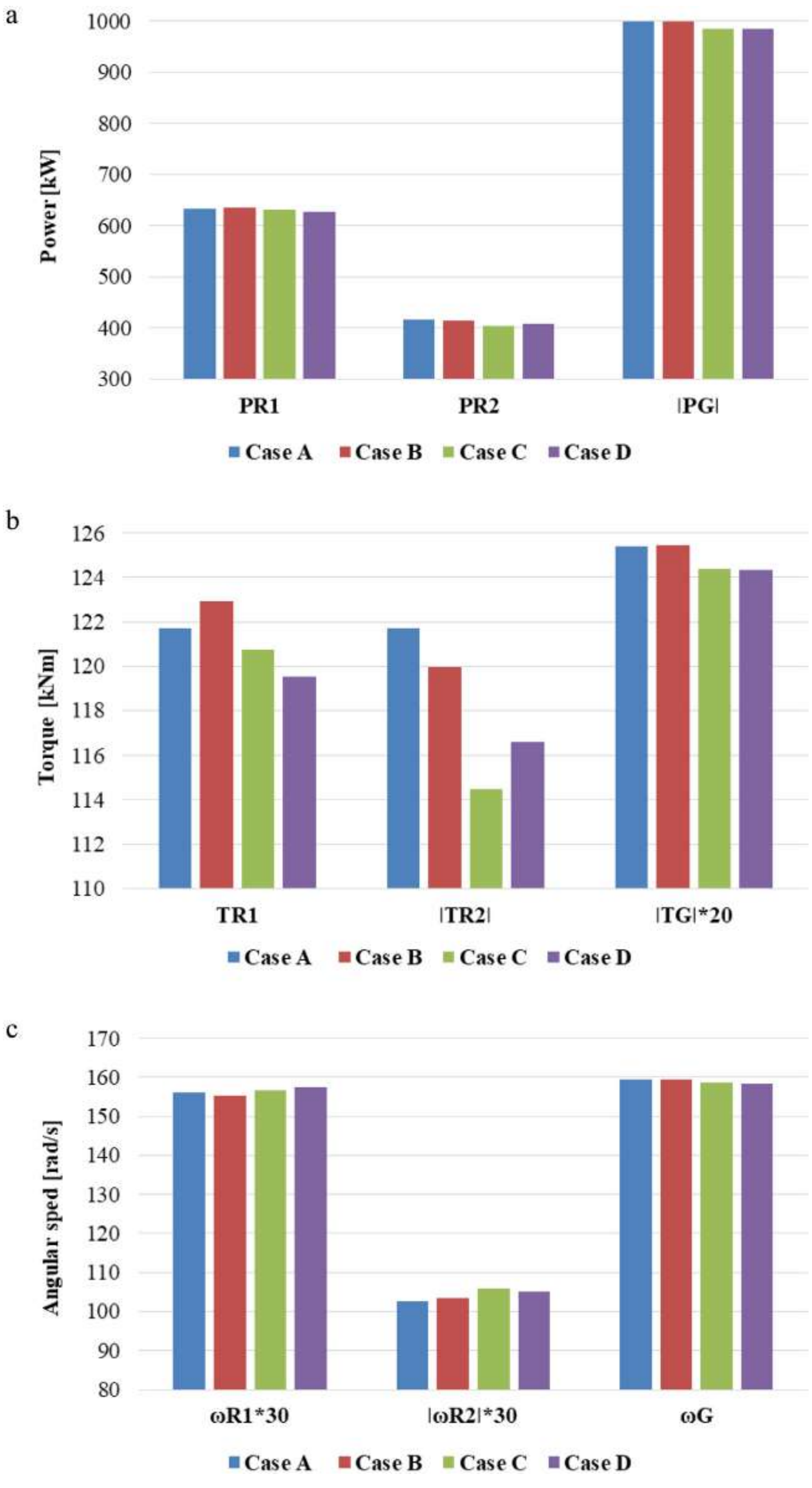

Fig. 8. Values obtained for the four turbines at rated wind speed ($v_w = 12$ m/s) for: (a) power; (b) torques; (c) angular velocities.

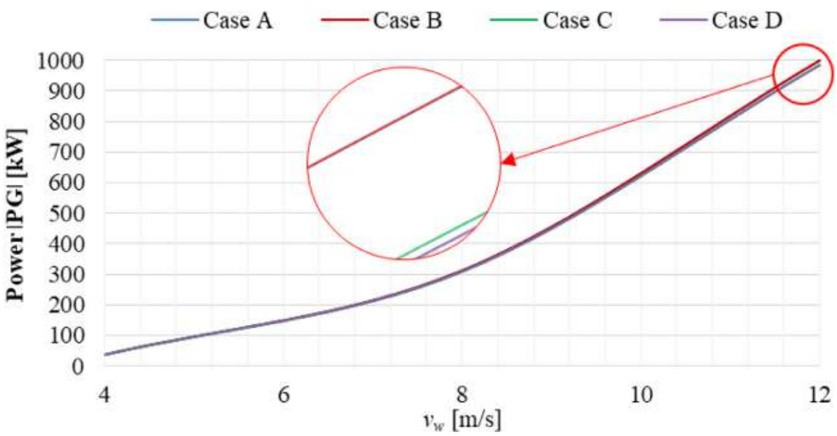

Fig. 9. Variation of the generator power with the wind speed for the analyzed four turbines.

- The choice in a practical application of one of the four wind turbine types requires a preliminary multicriteria analysis, in which other criteria should be considered in addition to energy performance, such as: complexity, cost, reliability, etc.

This steady-state analysis of CRWTs is to be extended by virtual prototyping under dynamic conditions, considering the impact of wind speed variation on their transient behavior. Also, an important step on the path to commercialization is the validation of conceptual solutions through experimental testing using specialized stands, the development of which is a future priority of the authors.

Declaration of competing interest

The authors declare that they have no known competing financial interests or personal relationships that could have appeared to influence the work reported in this paper.

Data availability

Data will be made available on request.

References

[1] Oprina Gabriela, Chihaia Rares, El-Leathey LA, Nicolaie S, Babutanu CA, Voina A. A review on counter-rotating wind turbines development. J Sustain Energy 2016;7:91–8.
[2] Newman Barry. Multiple actuator-disc theory for wind turbines. J Wind Eng Ind Aerodyn 1986;24:215–25.
[3] Erturk Ercan, Sivrioglu Selim, Bolat Fevzi. Analysis model of a small scale counter-rotating dual rotor wind turbine with double rotational generator armature. Int J Renew Energy Res 2018;8:1849–58.
[4] Hoang Anh Dung, Yang Chang-Jo. Design and performance evaluation of a 10 kW scale counter-rotating wind turbine rotor. J Korean Soc Mar Environ Saf 2014;20(1):104–12.
[5] Kanemoto Toshiaki, Galal Ahmed. Development of intelligent wind turbine generator with tandem wind rotors and double rotational armatures (1st report, superior operation of tandem wind rotors). JSME Int J Ser B 2006;49(2):450–7.
[6] Rosenberg Aaron, Selvaraj Suganthi, Sharma Anupam. A novel dual-rotor turbine for increased wind energy capture. J Phys Conf Ser 2014;524(1):1–10.
[7] Jung Sung Nam, No Tae-Soo, Ryu Ki-Wahn. Aerodynamic performance prediction of a 30 kW counter-rotating wind turbine system. Renew Energy 2005;30:631–44.
[8] Li Zhiqiang, Wu Yunke, Hong Jie, Zhang Zhihong, Chen Wenqi. The study on performance and aerodynamics of micro counter-rotating HAWT. Energy 2018;161:939–54.
[9] Kutt Filip, Blecharz Krzysztof, Karkosinski Dariusz. Axial-flux permanent-magnet dual-rotor generator for a counter-rotating wind turbine. Energies 2020;13(2833):1–15.
[10] Popescu Mihail, Oprina Gabriela, Mitulet Andreea, Nicolaie Sergiu, Chihaia Rares, Nedelcu Adrian, et al. Aspects regarding the application of electric generators to wind energy conversion using counter rotating turbines. In: Proceedings of the 8th international symposium on advanced topics in electrical engineering. 2013, p. 1–4.

[11] Yanan Li, Jia'an Zhang, Zhijun Li, Peng Yang, Huajun Wang. Design and verification of a novel double rotor without stator windturbine generation system. Energy Rep 2021;7:161–72.
[12] Shen Wen Zhong, Zakkam VAK, Sørensen Jensa, Appa K. Analysis of counter-rotating wind turbines. J Phys Conf Ser 2007;75(012003):1–9.
[13] Galvão Francisco Leme. Topics on wind turbine aerodynamic design. In: Proceedings of COBEM 2009 20th international congress of mechanical engineering. 2009, p. 1–10.
[14] Herzog Raoul, Schaffarczyk Alois Peter, Wacinski Andrzej, Zürcher O. Performance and stability of a counter–rotating windmill using a planetary gearing: Measurements and simulation. In: Proceedings of the european wind energy conference & exhibition. 2010, p. 1–8.
[15] Romański Leszek, Bieniek Jerzy, Komarnicki Piotr, Dębowski Marcin, Detyna Jerzy. Operational tests of a dual-rotor mini wind turbine. Eksploatacja Niezawodnosc – Maint Reliab 2016;18(2):201–9.
[16] Whang Cho, Kooksun Lee, Ick Choy, Juhoon Back. Development and experimental verification of counter-rotating dual rotor/dual generator wind turbine: Generating, yawing and furling. Renew Energy 2017;114:644–54.
[17] Saulescu Radu, Jaliu Codruta, Munteanu Olimpiu, Climescu Oliver. Planetary gear for counter-rotating wind turbines. Appl Mech Mater 2014;658:135–40.
[18] Lin Ah-Der, Hung Tsung-Pin, Kuang Jao-Hwa, Tsai Hsiu-An. Power flow analysis on the dual input transmission mechanism of small wind turbine systems. Appl Sci 2020;10(7333):1–5.
[19] Neagoe Mircea, Saulescu Radu, Jaliu Codruta. Design and simulation of a 1 DOF planetary speed increaser for counter-rotating wind turbines with counter-rotating electric generators. Energies 2019;12(1754):1–19.
[20] Neagoe Mircea, Saulescu Radu, Jaliu Codruta, Simionescu Petru. A generalized approach to the steady-state efficiency analysis of torque-adding transmissions used in renewable energy systems. Energies 2020;13(4568):1–18.
[21] Saulescu Radu, Neagoe Mircea, Jaliu Codruta. Conceptual synthesis of speed increasers for wind turbine conversion systems. Energies 2018;11(2257):1–33.
[22] Habash Riadh, Groza Voicu, Guillemette Pierre. Performance optimization of a dual-rotor wind turbine system. In: Proceedings of IEEE electrical power & energy conference. 2010, p. 451–6.
[23] Kumar Santhana, Bensingh Joseph, Abraham A. Computational analysis of 30 Kw contra rotor wind turbine. ISRN Renew Energy 2012;1–5, Article ID 939878.
[24] Mitulet Lucia-Andreea, Oprina Gabriela, Chihaia Rares-Andrei, Nicolaie Sergiu, Nedelcu Adrian, Popescu Mihail. Wind tunnel testing for a new experimental model of counter-rotating wind turbine. Procedia Eng 2015;100:1141–9.
[25] No Taesoo, Kim Ji-Eun, Moon Ji-Hong, Kim Sujin. Modeling, control, and simulation of dual rotor wind turbine generator system. Renew Energy 2009;34:2124–32.
[26] Farahani Ehsan, Hosseinzadeh Nasser, Ektesabi Motamed. Comparison of fault-ride-through capability of dual and single-rotor wind turbines. Renew Energy 2012;48:473–81.
[27] Climescu Oliver, Jaliu Codruta, Saulescu Radu. Comparative analysis of horizontal small scale wind turbines for a specific application. In: Proceedings of the 14th IFToMM world congress. 2015, p. 545–50.
[28] Saulescu Radu, Neagoe Mircea, Jaliu Codruta, Munteanu Olimpiu. A comparative performance analysis of counter-rotating dual-rotor wind turbines with speed-adding increasers. Energies 2021;14(2594):1–21.
[29] Saulescu Radu, Neagoe Mircea, Jaliu Codruta, Munteanu Olimpiu. Comparative analysis of two wind turbines with planetary speed increaser in steady-state. Appl Mech Mater 2016;823(2016):355–60.
[30] Neagoe Mircea, Saulescu Radu, Jaliu Codruta, Neagoe Ion. Dynamic analysis of a single-rotor wind turbine with counter-rotating electric generator under variable wind speed. Appl Sci 2021;11(8834):1–21.
[31] Miloiu Gheorghe, Dudita Florea, Diaconescu Dorin. Modern Mechanical Transmissions. Bucharest: Ed. Tehnica; 1980, Romania [in Romanian].

energies

MDPI

Article

Design and Simulation of a 1 DOF Planetary Speed Increaser for Counter-Rotating Wind Turbines with Counter-Rotating Electric Generators

Mircea Neagoe [1], Radu Saulescu [2] and Codruta Jaliu [1,*]

[1] Renewable Energy Systems and Recycling R&D Centre, Transilvania University of Brasov, Brasov 500036, Romania; mneagoe@unitbv.ro

[2] Design of Mechanical Elements and Systems R&D Centre, Transilvania University of Brasov, Brasov 500036, Romania; rsaulescu@unitbv.ro

* Correspondence: cjaliu@unitbv.ro; Tel.: +40-268-413-000

Received: 30 March 2019; Accepted: 6 May 2019; Published: 9 May 2019

Abstract: The improvement of wind turbine performance poses a constant challenge to researchers and designers in the field. As a result, the literature presents new concepts of wind turbines (WTs), such as: counter-rotating wind turbines (CRWTs) with two coaxial wind rotors revolving in opposite directions, WTs with higher-efficiency and downsized transmission systems, or WTs with counter-rotating electric generators (CREGs). Currently, there are a few solutions of WTs, both containing counter-rotating components; however, they can only be used in small-scale applications. Aiming to extend the use of WTs with counter-rotating wind rotors (CRWRs) and CREGs to medium- and large-scale applications, this paper introduces and analyzes a higher-performance WT solution, which integrates two counter-rotating wind rotors, a 1 degree of freedom (DOF) planetary speed increaser with four inputs and outputs, and a counter-rotating electric generator. The proposed system yields various technical benefits: it has a compact design, increases the output power (which makes it suitable for medium- and large-scale wind turbines) and allows a more efficient operation of the electric generator. The kinematic and static computing methodology, as well as the analytical models and diagrams developed for various case studies, might prove useful for researchers and designers in the field to establish the most advantageous solution of planetary speed increasers for the CRWTs with CREGs. Moreover, this paper extends the current database of WT speed increasers with an innovative concept of 1 DOF planetary gearbox, which is subject to a patent application.

Keywords: wind turbine; counter-rotating wind rotors; counter-rotating electric generator; speed increaser; kinematic and static modelling; operating point

1. Introduction

In recent years, wind power has increasingly become a feasible alternative in providing electrical energy to fossil fuels, although it is site-dependent and its conversion is influenced by the equipment performance. Therefore, the increase of wind turbine (WT) efficiency and the better use of onsite wind potential are goals which definitely pose a major challenge to researchers and designers in the field. Different theoretical approaches and technical solutions have been developed and used to reduce energy loss in WT conversion system; e.g., increasing nominal power or improving the conversion of wind energy into electrical energy.

Over the years, research in the field of WTs has covered more and more issues regarding the improvement of their performance by introducing new concepts of WTs with variations in both shape and number of rotors and/or blades, by designing more efficient and downsized transmission systems for WTs, or by integrating new solutions of electric generators, etc. [1–8]. Thus, the range of WT solutions that are currently available on the market has been steadily enlarged, from single-rotor to counter-rotating systems, capable of operating with either horizontal or vertical axis [1,2,9,10], and equipped with innovative mechanical transmissions and efficient electric generators. Consequently, the literature presents new concepts of WTs that meet the requirements for increased performance and optimal use of wind potential, such as large-capacity WTs using multiple, smaller rotors in different spatial arrangements [11], counter-rotating wind turbines (CRWTs) with two coaxial wind rotors revolving in opposite directions [10,12,13], or counter-rotating electric generators (CREGs) composed by both mobile rotors and stators turning with opposite speeds, which increase the output power of WTs. Moreover, for the speed of wind rotors (which is generally low) to comply with the speed parameters of the electric generator, a gearbox—operating as a speed increaser—may be integrated into WT conversion systems. Thus, both the wind rotor(s) and the electric generator can operate at their maximum efficiency. The speed increasers for WTs can be of fixed-axes [3,14,15] or planetary type [12,16–27], the latter being mainly used to produce high kinematic ratios, as is the case with counter-rotation wind systems [23,24]. Other solutions of WT gearboxes are variable-ratio transmissions [28] and hybrid planetary transmissions with incorporated control systems [29,30].

The analysis of the WT solutions presented in the literature in recent years allows their systematization according to the type of the components that are integrated in the WT conversion systems (i.e., wind rotors, transmission, and electric generator). The common WT is a single-rotor system, with 1 degree of freedom (DOF) fixed axes or planetary transmission and a classical generator. The use of counter-rotating motions with either the wind rotors or the electric generator improves WT performance. The counter-rotating solutions span a variety of WT systems, as follows: (a) WTs with CRWRs + 1 DOF gearbox + classical generator [13,18,31,32]; (b) WTs with CRWRs + 2 DOF gearbox + classical generator [2,4,5,7–9,16,21,22,25,26,32–37]; (c) WTs with single wind rotor + 1 DOF gearbox + CREG [1,20,32,38]; (d) WTs with CRWRs + 1 DOF gearbox + CREG [19,32,39,40]; and (e) WTs with CRWRs + 2 DOF gearbox + CREG [32]. The use of (a) and (b) types of WTs leads to an increase in efficiency of up to 64% during the steady-state regime versus the single-rotor type [2,4,7–9,16,32–35], and to an automatic adjustment of rotors speed to the wind behavior [2,36]. Due to the relatively low capacity of the CREGs, solution (c) is suitable to be implemented in the built environment. This type of electric generators—characterized by increased efficiency as compared to the classical ones—can be combined with wind rotors with two rows of blades, which are more efficient than those with a single row of blades, leading to wind systems with higher electrical power than the conventional ones. The behavior of such electric generators under dynamic conditions and their optimal functioning are approached in [41,42]. Solutions (d) and (e) are hardly tackled in the literature. Type (d) WTs presented in [39,40] are low-capacity systems, which contain complex fixed-axes gearboxes placed between the CRWRs and the CREG. A similar solution, though with a less complex transmission system, is proposed by the authors and described in [19]. Type (e) WT is presented merely as a concept in [32].

To conclude, the latest research in the field presents and analyzes—in a wide range of specialized studies—the performance of WTs with either CRWRs or CREGs. The solutions including both counter-rotating components are seldom addressed and are only suitable for low-capacity applications. The main drawbacks of the CRWTs refer to the mechanical complexity, complex aerodynamic characteristics, and higher initial cost compared to the single-rotor WTs. The dynamic behavior of CRWTs depend on the arrangement of wind rotors: on the same or on opposite sides of the tower; higher dynamic challenges are raised by the first case of CRWTs due to the influence of the wind rotors on the airflows. The gearboxes integrated in these WTs have a complex structure consisting of spur gear trains [40] or spur and bevel gear trains [39] with fixed axes and relatively low amplification kinematic ratios.

With regard to the WT operation, the studies in the literature approach various topics, such as: the impact of design parameters on WT performance, the increase in efficiency by using appropriate control algorithms and strategies [43,44], the analysis of WT optimal design [32,37], or the comparison of different types of WTs in terms of energy output [24,28,29,45]. The dynamic analysis of CRWTs is approached in [46,47], while numerical simulations of the aerodynamic performance of a CRWT are presented in [5,9,48,49]. Different adaptive methods for fast optimal pitch angle control of the WTs under variable wind speeds are proposed in the literature, e.g., by using artificial neural network (ANN) controllers, fuzzy logic based controllers, or hybrid ANN-fuzzy controllers [50].

Aiming to extend the use of type (d) WTs to medium- and large-scale applications, this paper introduces and analyzes a higher-performance WT solution, which integrates two CRWRs, a 1 DOF planetary speed increaser with four inputs and outputs, and a CREG. The proposed system with counter-rotating components has a compact design, increases the output power, and allows a more efficient operation of the electric generator. The system structure, the kinematic and static properties and correlations of the proposed speed increaser are described in Section 2. The kinematic modeling of the planetary gearbox is presented in Section 3, while torque values and efficiency are analytically modeled in Section 4. WT power flows, efficiency and operating point in steady state regime are further analyzed in four different cases of the speed increaser functioning. Besides the proposed analysis methodology and analytical models for efficiency and output power, the paper extends the database of speed increasers for WTs with an innovative 1 DOF planetary transmission concept, which is subject to a patent application.

2. Problem Formulation

The general scheme of a CRWT containing a CREG and a 1 DOF speed increaser is presented in in Figure 1. The two rotors *R*1 and *R*2 are rotating in opposite directions; similarly, the electric generator rotor (*GR*) and the electric generator stator (*GS*) have opposite rotations, thus increasing the relative speed between them. The 1 DOF speed increaser (with the mechanism degree of freedom $M = 1$) has four external links ($L = 4$, Figure 1b), the inputs being connected to the two wind rotors, while the outputs to the rotor and stator of the electric generator.

The electric generator with fixed stator and mobile rotor which is rotating with a speed equal to the relative speed of the CREG will be further referred to as equivalent electric generator.

Conventionally, the main input of the speed increaser is connected to the main wind rotor *R*1, while the secondary input to the wind rotor *R*2; the two outputs are connected to the rotor *GR* and stator *GS* of the counter-rotating electric generator.

The 1 DOF speed increasers have the properties of summing up the input torques generated by the wind rotors *R*1 and *R*2, as well as transmitting an independent external motion (in this case, the speed of the main wind rotor *R*1) to the other three external links, in a determined way. Therefore, these speed increasers take up the mechanical power from two wind rotors with counter-rotating motions and transmit it to the counter-rotating electric generator, on the condition of summing up the input torques and the increase of the electric generator speed as well.

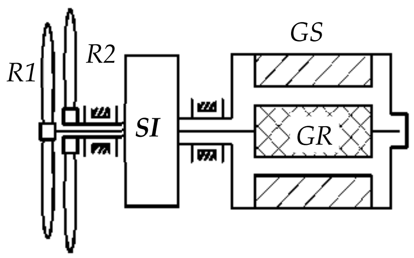

(**a**)

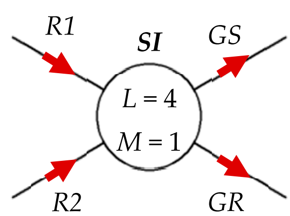

(**b**)

Figure 1. Counter-rotating wind turbine with counter-rotating electric generator: (**a**) general conceptual scheme; (**b**) block scheme of the speed increaser (*SI*) with two inputs and two outputs (*R*1—main wind rotor, *R*2—secondary wind rotor, *GR*—electric generator rotor, *GS*—electric generator stator, *L*—number of mechanism inputs and outputs, M—mechanism degree of freedom).

The 1 DOF planetary speed increaser has the following kinematic and static properties:

(a) conventionally, the angular speed ω_{R1} is considered as the independent parameter, while the input speed ω_{R2} and the output speeds ω_{GR} and ω_{GS} depend on ω_{R1}. Due to the counter-rotating motion between the generator rotor *GR* and stator *GS*, the relative speed ω_{eg}, given by:

$$\omega_{eg} = \omega_{GR} - \omega_{GS} \tag{1}$$

is higher than the speed of a classical generator with fixed stator (ω_{GR}).

(b) it has one transmission function of the external torques, defined by the qualitative relation:

$$c_1 T_{R1} + c_2 T_{R2} + c_3 T_{GR} + T_{GS} = 0 \tag{2}$$

where c_i, $i = 1 \ldots 3$ are constant coefficients.

The static property of the 1 DOF speed increaser, i.e., the weighted summation of the two torques generated by the two wind rotors *R*1 and *R*2:

$$T_{GR} = (c_1 T_{R1} + c_2 T_{R2})/(1 - c_3) \tag{3}$$

is obtained knowing that the electric generator operation is characterized by:

$$T_{GS} = -T_{GR}. \tag{4}$$

Based on the previous qualitative properties, the paper focuses on identifying the possible functioning cases of the planetary speed increaser and, implicitly, of the wind turbine, as well as on the dependence of its performance on two main parameters:

the amplification ratio:

$$i_{aR1-eg} = \omega_{eg}/\omega_{R1} \tag{5}$$

and the input torques ratio:

$$k_t = -T_{R2}/T_{R1}. \tag{6}$$

Considering the general case illustrated in Figure 1, the paper highlights the performance and features of this new type of WTs through an example that integrates a new planetary speed increaser (Figure 2), which is subject to patent application. This speed increaser is obtained by linking in parallel a bevel transmission with fixed axes 2–1″−1′−3 (denoted by *I*, Figure 3) and a 2 DOF planetary spur gear set with one satellite gear 4-5-6-*H* (denoted by *II*). The bevel gear 3 transmits the motion to the sun ring gear 4, which is connected to the generator stator GS, while the carrier H takes the motion from the main wind rotor *R*1. The secondary wind rotor *R*2 drives the ring gear 4 and, thus, the stator GS. The shaft of the rotor *GR* is connected to the shaft of the sun gear 6 in the planetary gear set II.

The component transmissions, the internal and external links of the planetary speed increaser and the torques on the WT shafts are presented in the block scheme depicted in Figure 3, which is associated with the conceptual scheme illustrated in Figure 2.

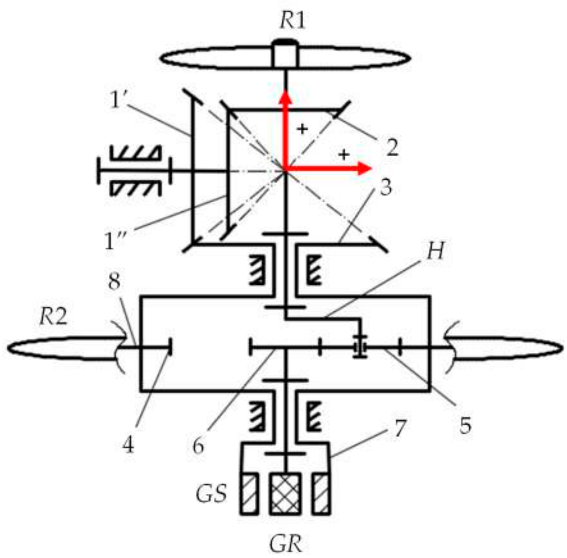

Figure 2. The conceptual scheme of a wind system containing: two counter-rotating wind rotors, a 1 degree of freedom (DOF) speed increaser and a counter-rotating electric generator.

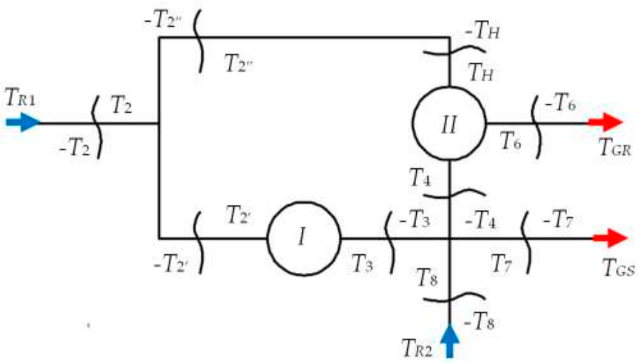

Figure 3. The block scheme of the 1 DOF planetary speed increaser.

The kinematic and static transmission functions of the speed increaser can be determined on the basis of the kinematic and static equations (correlations), which characterize the isolated transmissions *I* and *II*, and the internal and external links according to the block scheme in Figure 3 [18,21,23]:

- The correlations for the input shafts:

$$2 = R1 : \begin{cases} \omega_2 = \omega_{R1} \\ T_{R1} - T_2 = 0 \end{cases}, \tag{7}$$

$$8 = R2 : \begin{cases} \omega_8 = \omega_{R2} \\ T_{R2} - T_8 = 0 \end{cases} \tag{8}$$

- The correlations for the output shafts:

$$6 = GR : \begin{cases} \omega_6 = \omega_{GR} \\ T_{GR} - T_6 = 0 \end{cases} \tag{9}$$

$$7 = GS : \begin{cases} \omega_7 = \omega_{GS} \\ T_{GS} - T_7 = 0 \end{cases} \tag{10}$$

- The correlations for the bevel mechanism with fixed axes *I*:

$$I:\begin{cases} i_{01} = i_{32'} = \frac{\omega_3}{\omega_{2'}} = \frac{\omega_3}{\omega_{1'}}\frac{\omega_{1''}}{\omega_2} = -\frac{z_{1'}}{z_3}\frac{z_2}{z_{1''}} \quad => \quad \omega_3 = i_{01}\omega_{2'} \\ \omega_{2'}T_{2'}\eta_{01}^{w} + \omega_3 T_3 = 0 \quad => \quad T_{2'} = -\frac{i_{01}T_3}{\eta_{01}^{w}} \end{cases} \tag{11}$$

for $k_t \leq 1$, $w = +1$, and $k_t > 1$, $w = -1$, while $\eta_{01} = \eta_{21'}\eta_{1''3}$ is the interior efficiency of transmission *I*, $\eta_{21'}$ and $\eta_{1''3}$ are the efficiencies of the two component bevel gear pairs, z_i—the teeth number of the component gears, i = 1′, 1″, 2, 3.

- The correlations for the planetary gear set *II* [12,24]:

$$II:\begin{cases} i_{02} = \frac{\omega_{6H}}{\omega_{4H}} = -\frac{z_4}{z_6} \\ \omega_6 - \omega_4 i_{02} - \omega_H(1 - i_{02}) = 0 \\ T_6\omega_{6H}\eta_{02}^{x} + T_4\omega_{4H} = 0;\ x = \mathrm{sgn}(\omega_{6H}T_6) = \mathrm{sgn}\left(\frac{i_{02}}{1-i_{02}}\right) = -1 \\ T_H + T_4 + T_6 = 0 \end{cases} \tag{12}$$

where sgn is the sign function and i_{02} the interior kinematic ratio of the planetary gear set *II*.

- The correlations for the connections between the planetary gear set *II* and the bevel transmission *I*:

$$2 = 2' = 2'' : \begin{cases} \omega_{2'} = \omega_{2''} = \omega_2 \\ T_2 - T_{2'} - T_{2''} = 0 \end{cases} \tag{13}$$

$$2'' = H : \begin{cases} \omega_{2''} = \omega_H \\ T_{2''} - T_H = 0 \end{cases} \tag{14}$$

$$3 = 4 = 7 = 8 : \begin{cases} \omega_3 = \omega_4 = \omega_7 = \omega_8 \\ -T_3 - T_4 + T_7 + T_8 = 0 \end{cases} \tag{15}$$

- The correlations for the external links:

$$\begin{cases} \omega_{eg} = \omega_{GR} - \omega_{GS} \\ (\omega_{R1}T_{R1} + \omega_{R2}T_{R2})\eta_{tot} + \omega_{GR}T_{GR} + \omega_{GS}T_{GS} = 0 \\ T_{eg} = T_{GR} = -T_{GS} \\ T_{R2} = -k_t T_{R1},\ k_t \geq 0 \end{cases} \tag{16}$$

where ω_{eg} represents the speed of the equivalent electric generator.

Based on the previous correlations, the kinematic and static modeling of the proposed planetary gearbox (Figure 2) is further presented, along with the power flow and efficiency analysis for four functioning cases of the speed increaser, defined according to the input torques ratio: (a) $k_t = 0$, (b) $0 < k_t < 1$ (c) $k_t = 1$, (d) $k_t > 1$. The torque generated by a wind rotor can be controlled by adjusting the pitch angle of the blades, which is considered in the paper through the adjustable parameter k_t.

3. Kinematic Modeling

The aim of the kinematic modeling is to find out the kinematic transmitting functions of the speed increaser by considering the power flows from inputs to outputs and based on the equations that characterize both the isolated transmissions and the internal and external links, according to the block scheme in Figure 3.

The speed transmitting function from the main wind rotor *R*1 to the generator rotor *GR* can be expressed by:

$$\omega_{GR} = \omega_{R1} i_{a\,R1-GR} \tag{17}$$

$$i_{a\,R1-GR} = i_{02} i_{01} + (1 - i_{02}) \tag{18}$$

where $i_{a\,R1-GR}$ is the amplification kinematic ratio for the main power flow; wind rotor *R1*—generator rotor *GR*, based on the following speed relations:

$$\omega_6 = \omega_4 i_{02} + \omega_H (1 - i_{02}),\ \omega_4 = i_{01} \omega_{R1},\ \omega_H = \omega_{R1}. \tag{19}$$

The speed transmitting function and the amplification kinematic ratio $i_{a\,R1-GS}$ on the power flow; main wind rotor *R*1—generator stator *GS*, can be obtained:

$$\omega_{GS} = \omega_{R1} i_{a\,R1-GS} \tag{20}$$

$$i_{a\,R1-GS} = i_{01} \tag{21}$$

Similarly, the speed transmitting function from the secondary wind rotor *R*2 to the generator rotor *GR* can be derived as follows:

$$\omega_{GR} = \omega_{R2} i_{a\,R2-GR}, \tag{22}$$

$$i_{a\,R2-GR} = i_{02} + (1 - i_{02}) \frac{1}{i_{01}} \tag{23}$$

where $i_{a\,R2-GR}$ is the amplification kinematic ratio for the secondary power flow; wind rotor *R*2—generator rotor *GR*. The angular speed of the generator stator *GS* in relation with the secondary wind rotor *R*2 speed can be also established:

$$\omega_{GS} = \omega_{R2} i_{a\,R2-GS} \tag{24}$$

$$i_{a\,R2-GS} = 1 \tag{25}$$

Therefore, the kinematic parameters that characterize the two power flows from the wind rotors to the equivalent electric generator are expressed by:

$$\omega_{eg} = \omega_{R1} i_{a\,R1-eg} \tag{26}$$

$$i_{a\,R1-eg} = i_{a\,R1-GR} - i_{a\,R1-GS} = (1 - i_{02})(1 - i_{01}) \tag{27}$$

for the main flow, and:

$$\omega_{eg} = \omega_{R2} i_{a\,R2-eg}, \tag{28}$$

$$i_{a\,R2-eg} = \frac{(1 - i_{02})(1 - i_{01})}{i_{01}} \tag{29}$$

for the secondary flow.

4. Modeling of Torques and Efficiency

The efficiency of the speed increaser η_{tot} depends on the efficiency values of the two component transmissions, being influenced by the power flows and the torques on each branch, according to the k_t ratio. By considering the block scheme in Figure 3, the speed increaser efficiency can be obtained on the basis of the following algorithm:

1. The torques transmitting function for the main power flow *R*1-*eg* is established by:

$$T_{R1} = -T_3 \frac{i_{01}}{\eta_{01}} + T_H, \tag{30}$$

where the torques T_3 and T_H are given by:

$$T_3 = -\left[k_t T_{R1} + T_{GR}\left(1 - \frac{i_{02}}{\eta_{02}}\right)\right] \tag{31}$$

$$T_H = T_{GR}\left(\frac{i_{02}}{\eta_{02}} - 1\right) \tag{32}$$

Therefore, the torque T_{R1} can be expressed as follows:

$$T_{R1} = -T_{GR}\frac{\left(1 - \frac{i_{01}}{\eta_{01}}\right)\left(1 - \frac{i_{02}}{\eta_{02}}\right)}{1 - \frac{i_{01}}{\eta_{01}}k_t}. \tag{33}$$

2. The torques transmitting function for the secondary power flow *R2-eg* is established by the following relation:

$$T_{R2} = -k_t T_{R1} = T_{GR}\frac{\left(1 - \frac{i_{01}}{\eta_{01}}\right)\left(1 - \frac{i_{02}}{\eta_{02}}\right)}{k_t - \frac{i_{01}}{\eta_{01}}}. \tag{34}$$

3. The speed increaser efficiency η_{tot} is further determined:

$$\eta_{tot} = -\frac{\omega_{GR}T_{GR} + \omega_{GS}T_{GS}}{\omega_{R1}T_{R1} + \omega_{R2}T_{R2}} = \frac{(1 - i_{01})(1 - i_{02})\left(1 - \frac{i_{01}}{\eta_{01}}k_t\right)}{\left(1 - \frac{i_{01}}{\eta_{01}}\right)\left(1 - \frac{i_{02}}{\eta_{02}}\right)(1 - i_{01}k_t)}. \tag{35}$$

The relations for the kinematic and static parameters that are used in describing the wind turbine with 1 DOF planetary speed increaser, as detailed in the block scheme in Figure 3, are shown in Table 1.

Table 1. The relations for the kinematic and static parameters as functions of the input parameters (ω_{R1}, T_{R1}).

<table>
<tr><td colspan="6">$\omega_2 = \omega_{2'} = \omega_{2''} = \omega_H = \omega_{R1}$</td></tr>
<tr><td>T_2</td><td colspan="2">$T_{2'}$</td><td colspan="2">$T_{2''}$</td><td>T_H</td></tr>
<tr><td>T_{R1}</td><td colspan="2">$T_{R1}\frac{i_{01}(k_t-1)}{\eta_{01}-i_{01}}$</td><td colspan="2">$T_{R1}\frac{\eta_{01}-i_{01}k_t}{\eta_{01}-i_{01}}$</td><td>$T_{R1}\frac{\eta_{01}-i_{01}k_t}{\eta_{01}-i_{01}}$</td></tr>
<tr><td colspan="6">$\omega_3 = \omega_4 = \omega_8 = \omega_9 = \omega_{R2} = \omega_{GS} = \omega_{R1}i_{01}$</td></tr>
<tr><td>T_3</td><td>T_4</td><td>T_8</td><td>T_9</td><td>T_{R2}</td><td>T_{GS}</td></tr>
<tr><td>$T_{R1}\frac{\eta_{01}(1-k_t)}{\eta_{01}-i_{01}}$</td><td>$-T_{R1}\frac{\frac{i_{02}}{\eta_{02}}\left(1-\frac{i_{01}}{\eta_{01}}k_t\right)}{\left(1-\frac{i_{01}}{\eta_{01}}\right)\left(1-\frac{i_{02}}{\eta_{02}}\right)}$</td><td>$T_{R1}\frac{1-\frac{i_{01}}{\eta_{01}}k_t}{\left(1-\frac{i_{01}}{\eta_{01}}\right)\left(1-\frac{i_{02}}{\eta_{02}}\right)}$</td><td>$-T_{R1}k_t$</td><td>$-T_{R1}k_t$</td><td>$T_{R1}\frac{1-\frac{i_{01}}{\eta_{01}}k_t}{\left(1-\frac{i_{01}}{\eta_{01}}\right)\left(1-\frac{i_{02}}{\eta_{02}}\right)}$</td></tr>
<tr><td colspan="4">$\omega_6 = \omega_{GR} = \omega_{R1}[i_{02}i_{01} + (1 - i_{02})]$</td><td colspan="2">$\omega_{eg} = \omega_{R1}(1 - i_{01})(1 - i_{02})$</td></tr>
<tr><td colspan="2">T_6</td><td colspan="2">T_{GR}</td><td colspan="2">T_{eg}</td></tr>
<tr><td colspan="2">$-T_{R1}\frac{1-\frac{i_{01}}{\eta_{01}}k_t}{\left(1-\frac{i_{01}}{\eta_{01}}\right)\left(1-\frac{i_{02}}{\eta_{02}}\right)}$</td><td colspan="2">$-T_{R1}\frac{1-\frac{i_{01}}{\eta_{01}}k_t}{\left(1-\frac{i_{01}}{\eta_{01}}\right)\left(1-\frac{i_{02}}{\eta_{02}}\right)}$</td><td colspan="2">$-T_{R1}\frac{1-\frac{i_{01}}{\eta_{01}}k_t}{\left(1-\frac{i_{01}}{\eta_{01}}\right)\left(1-\frac{i_{02}}{\eta_{02}}\right)}$</td></tr>
<tr><td colspan="6">Remark: the relations are valid for $k_t \le 1$. For $k_t > 1$,η_{01} has to be replaced by $1/\eta_{01}$.</td></tr>
</table>

5. Numerical Simulations and Interpretation

Based on the previous analytical relations, some relevant numerical results regarding the influence of the amplification kinematic ratio i_{aR1_eg} and the k_t ratio on the main kinematic and static parameters, on the transmission efficiency and output power, as well as on the power flow through the speed increaser are further presented.

The numerical simulations are focused on three main functional aspects:

(a) The correlative influence of the amplification kinematic ratio i_{aR1_eg} and the k_t ratio on the speed increaser efficiency; in this regard, a unitary input power at the main wind rotor is used, e.g., P_{R1} = 1 kW ($\omega_{R1} = 1\ s^{-1}$, $T_{R1} = 1\ kNm$).

(b) The power flow distinct cases depending on the k_t ratio values, for a particular value of the kinematic ratio, i.e., $i_{aR1\_eg} = 18$: four functional cases are identified, and detailed in the subchapter 5.2 under the assumptions of considering and neglecting the friction in the gear pairs.
(c) The operating point of the wind system for the previous four functional cases.

A numerical example of the planetary speed increaser characterized by $i_{02} = -8$, $\eta_{01} = 0.9604$ and $\eta_{02} = 0.9506$ are further considered as basic solution in all the performed simulations. The variation of the amplification kinematic ratio i_{aR1_eg}, dependent on both the interior kinematic ratios of the transmissions *I* and *II*, is analyzed in this paper only by changing the kinematic ratio i_{01} of the bevel transmission and by maintaining the kinematic ratio i_{02} at a constant value ($i_{02} = -8$). Several scenarios of adjusting the torque generated by the secondary wind rotor (i.e., the k_t ratio) are discussed, considering that the speed increaser has a closed loop power flow. The power flow and the operating point simulations are carried out for $i_{01} = -1$.

5.1. The Influence of the Amplification Kinematic Ratio and the Input Torques Ratio

The amplification kinematic ratio of the main power flow i_{aR1-eg} depends on the interior kinematic ratios i_{01} and i_{02}, according to rel. (27), and it can significantly influence the speed increaser efficiency for different values of the input toques ratio k_t. Thus, starting from the basic speed increaser solution, a variation of the amplification kinematic ratio $i_{aR1-eg} = 18 \ldots 144$ (Figure 4) is obtained by changing the value of the interior kinematic ratio in the range $i_{01} = -1 \ldots -15$. These results highlight the following properties of the speed increaser:

- the η_{tot} efficiency does not depend on the i_{aR1-eg} ratio in the case $k_t = 1$, i.e., the input torques T_{R1} and T_{R2} are equal in absolute value, the efficiency being at its maximum value $\eta_{tot} = 0.956$, Figure 4a,b;
- for lower values of the k_t parameter ($k_t < 0.1$), the η_{tot} efficiency decreases continuously with the increase of the amplification kinematic ratio, Figure 4b; the η_{tot} efficiency has a growing trend for higher subunit values ($0.1 < k_t < 1$) and in the range of high values of the amplification ratio, Figure 4b;
- if the secondary wind rotor generates higher torques than the main rotor, $|T_{R2}| > T_{R1}$ (i.e., $k_t > 1$), the η_{tot} efficiency increases continuously with the increase of the amplification kinematic ratio (Figure 4b, $k_t = 1.2$).

The results of the numerical simulations for different values of the k_t ratio in the case of the basic solution ($i_{01} = -1$, $i_{02} = -8$) are presented in Figure 5; accordingly, the following conclusions can be drawn:

- the transmission efficiency increases with the increase of the k_t ratio until the secondary wind rotor torque becomes equal to that of the main rotor ($k_t = 1$), after which it decreases continuously with the increase of k_t ratio, regardless of the value of the amplification ratio (Figure 5a,b);
- the useful mechanical power P_{eg} at the equivalent generator input has a linear variation with respect to k_t (Figure 5c,d), being directly dependent on the power introduced in the system by the secondary wind rotor $R2$.

Therefore, this type of wind turbine can be designed to function with high amplification kinematic ratios and efficiency, mainly when the input torques ratio k_t is maintained around the unitary value.

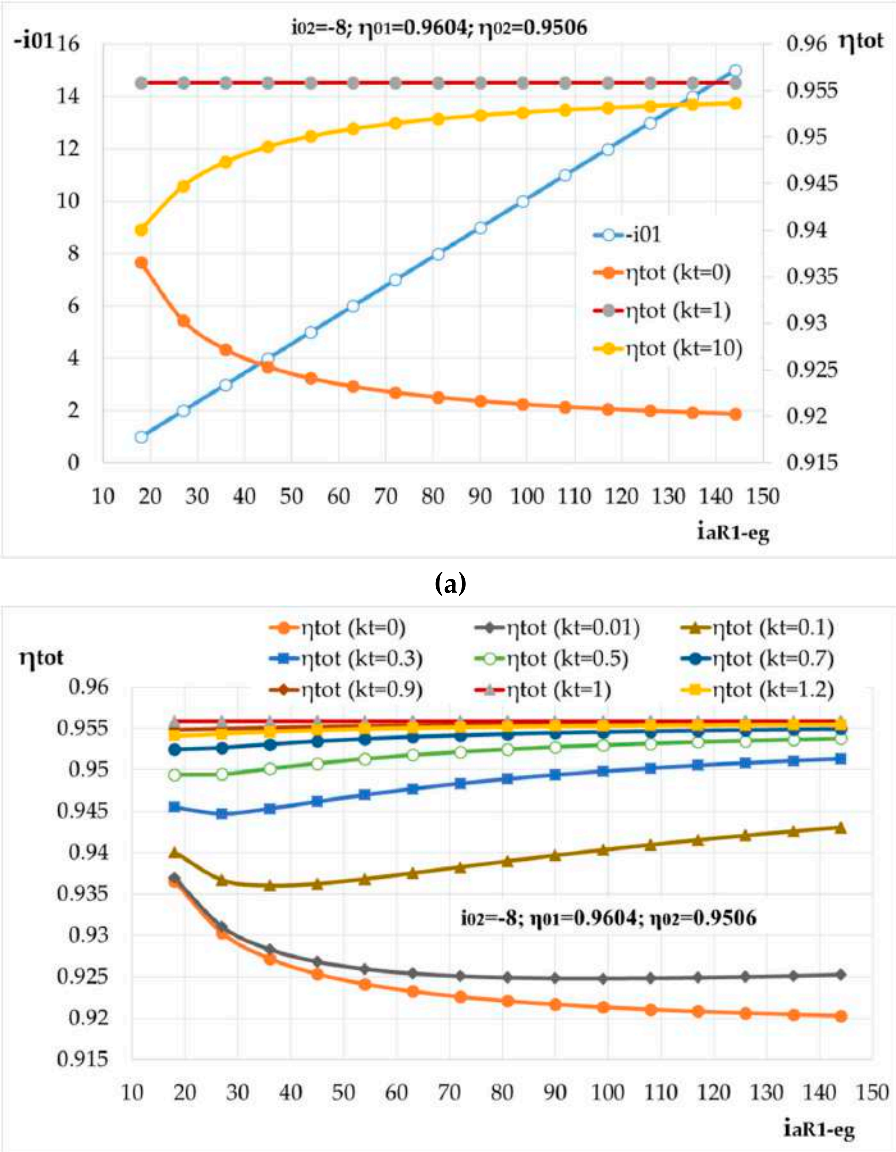

(a)

(b)

Figure 4. The variation of the speed increaser efficiency as a function of the amplification kinematic ratio: (**a**) for three representative values of the k_t ratio; (**b**) for $k_t \leq 1.2$.

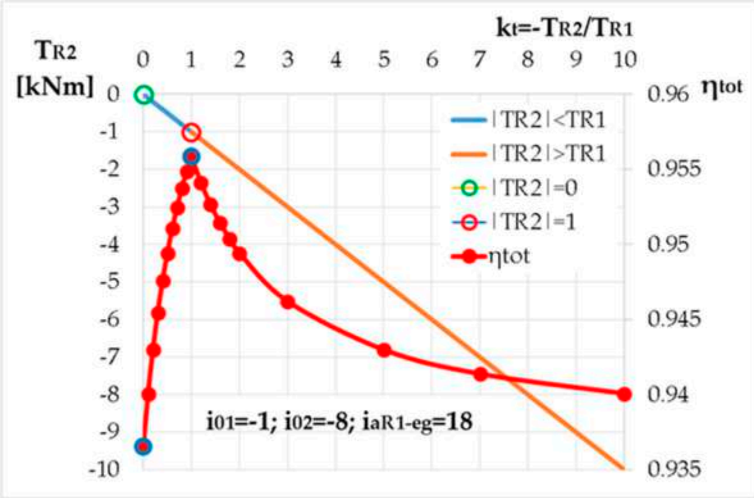

(a)

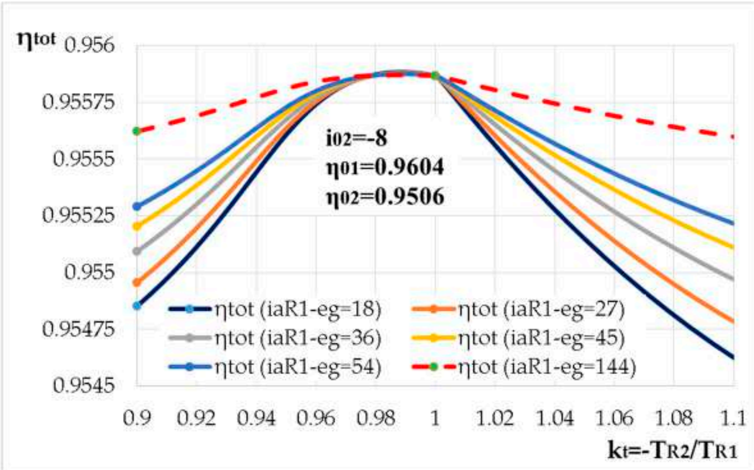

(b)

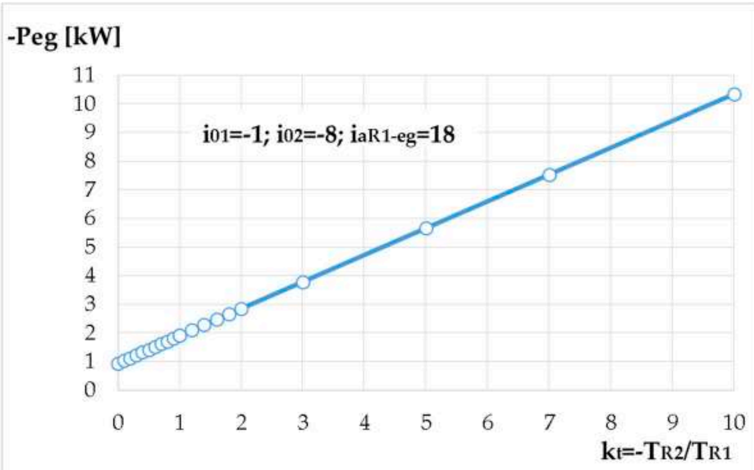

(c)

Figure 5. *Cont*.

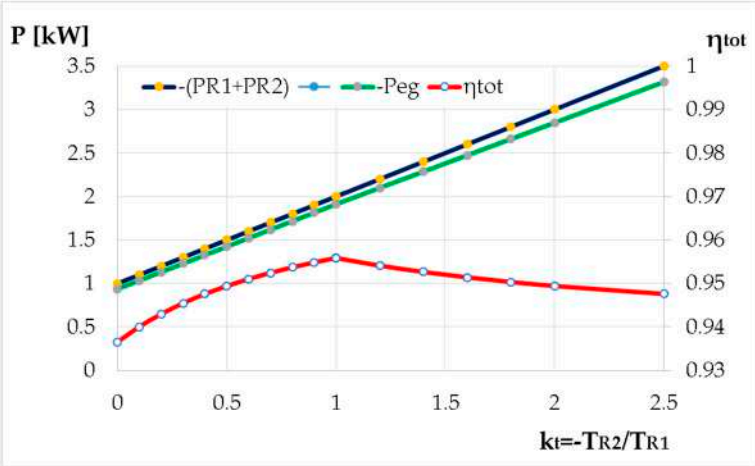

(d)

Figure 5. The influence of the k_t ratio on the speed increaser efficiency and on the output power P_{eg}: (**a**) the T_{R2} torque and η_{tot} efficiency variations; (**b**) the η_{tot}efficiency variation around the maximum value for different values of the $i_{aR1\text{-}eg}$ ratio; (**c**) the power P_{eg} variation; (**d**) the powers and efficiency variations for $k_t < 2.5$.

5.2. Power Flow

Power transmitting from inputs to outputs can be done in an open or closed loop flow according to the k_t values, the power flow configuration also influencing the speed increaser efficiency. For equal torques of the two wind rotors ($k_t = 1$), the power transmitted by the bevel transmission *I* becomes null (i.e., $T_{2'} = 0$) and, therefore, it represents the limit value at which the change of the power flow direction through this transmission occurs.

Considering the basic solution of the planetary speed increaser ($i_{01} = -1$, $i_{02} = -8$, $\eta_{01} = 0.9604$, $\eta_{02} = 0.9506$), the power flows without friction (Figure 6) and with friction (Figure 7) are analyzed in four distinct functional cases depending on the value of the k_t ratio:

- **Case 1**: the torque of the secondary wind rotor is null $T_{R2} = 0$, i.e., $k_t = 0$, Figures 6a and 7a. This situation occurs when the secondary wind turbine is set so as not to generate mechanical power, the gearbox thus running with one input and two outputs at the efficiency value $\eta_{tot} = 0.937$, in case of considering friction (Figure 7a);
- **Case 2**: $k_t = 1$, Figures 6b and 7b. In this situation, the bevel transmission *I* is no longer involved in the mechanical power transmitting and, thus, decoupling of the two power inputs occurs: the power generated by the main wind rotor *R*1 is entirely transmitted to the generator rotor *GR*, the secondary wind rotor *R*2 ensures the power requirements for the generator stator *GS*, and the power difference is transmitted to the *GR* rotor. In this case, the gearbox efficiency becomes $\eta_{tot} = 0.956$, Figure 7b.
- **Case 3**: $0 < k_t < 1$, Figures 6c and 7c. The power of the main wind rotor *R*1 branches through the two transmissions *I* and *II*, the flow through the bevel mechanism I merges with the power flow of the wind rotor *R*2, which is then distributed to the generator stator *GS* and to the generator rotor *GR*. In this case, for a power of the *R*2 rotor equal to 0.5 of the *R*1 rotor power; according to Figure 7c, a gearbox efficiency of $\eta_{tot} = 0.949$ is obtained.
- **Case 4**: $k_t > 1$, Figures 6d and 7d. In this case, the power generated by the secondary wind rotor *R*2 is transmitted in a branched way to the stator *GS* and to the rotor *GR* by both transmissions *I* and *II*. As a result, the power flow through the transmission I is reversed with respect to case 3, a part of the power generated by the secondary wind rotor *R*2 being summed up with that of the main rotor *R*1 and then transmitted to the generator rotor *GR* through the planetary gear set *II*. For the numerical example, the planetary transmission efficiency is $\eta_{tot} = 0.952$, Figure 7d.

According to the numerical example, the planetary gearbox operates with higher efficiency for values of the secondary wind rotor torques around the limit value $(k_t \approx 1)$, which corresponds to close values of the two input torques. In the particular case $k_t = 1$, the torque transmitted by the bevel transmission *I* becomes null and, therefore, it has the role of a kinematic mechanism.

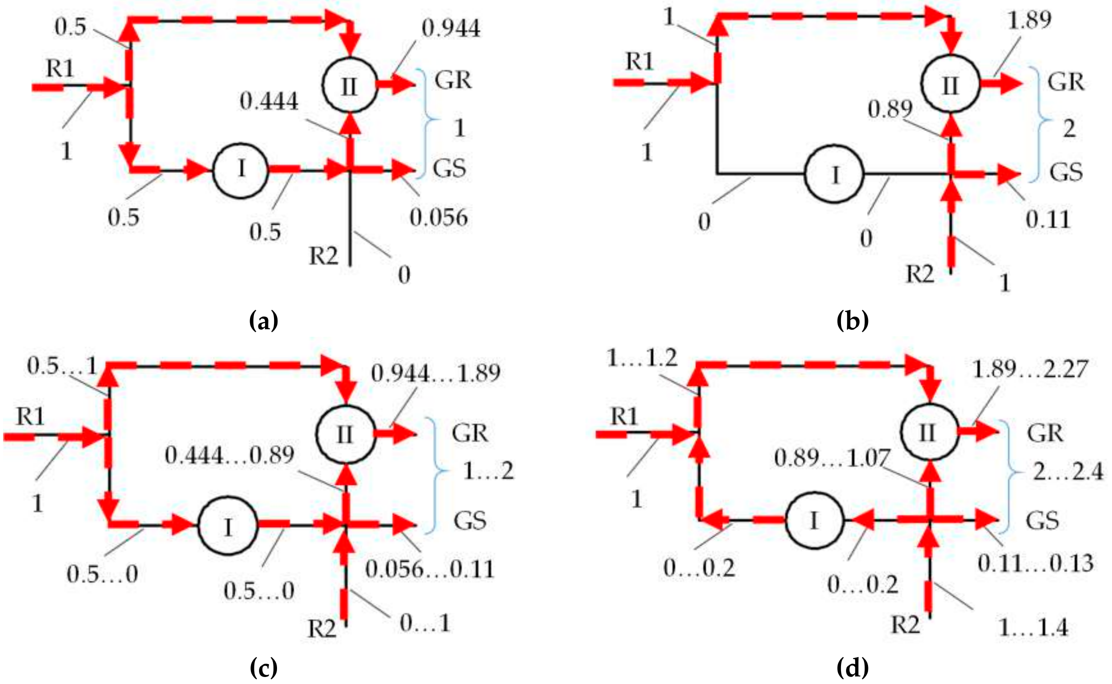

Figure 6. Power flow in the premise of neglecting friction for the case: (**a**) $k_t = 0$; (**b**) $k_t = 1$, (**c**) $0 < k_t < 1$; (**d**) $k_t \geq 1$.

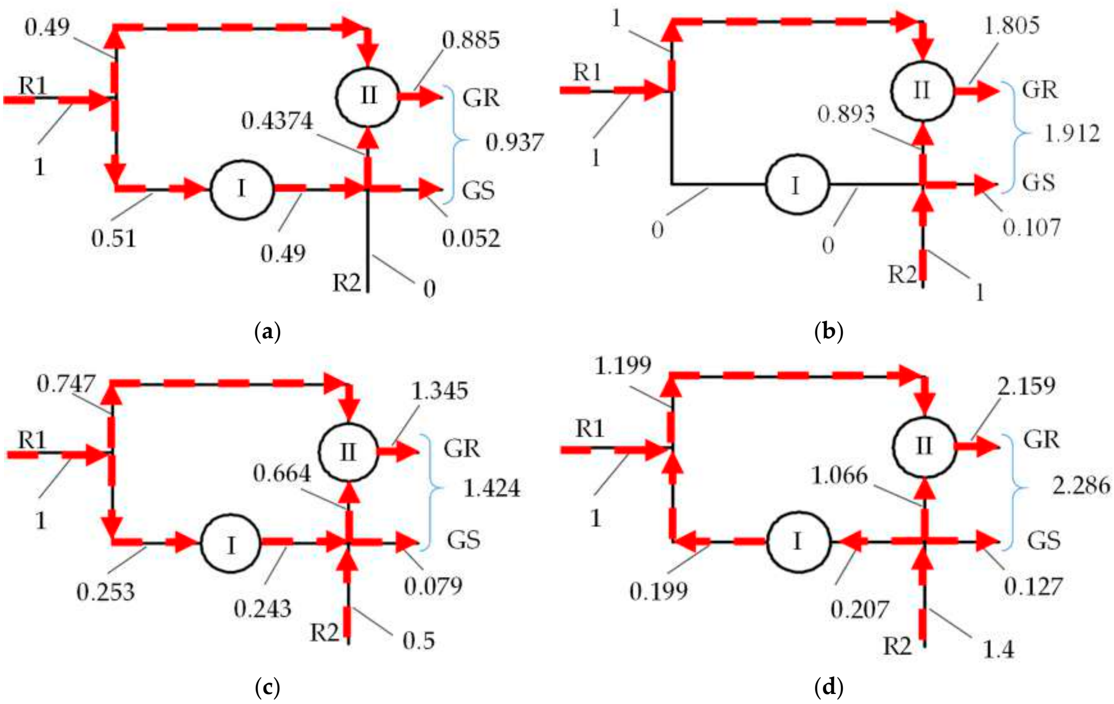

Figure 7. Power flow in the premise of considering friction for the case: (**a**) $k_t = 0$; (**b**) $k_t = 1$; (**c**) $k_t = 0.5$ (< 1); (**d**) $k_t = 1.4$ (> 1).

5.3. Operating Point

The stationary operating point of a wind system of the type: two CRWR-1 DOF speed increaser-CREG, Figures 1 and 2, can be determined if the transmitting functions of the speed increaser are known: three kinematic functions, relations (17), (20), and (24) and 1 function for torques, relation (33), the mechanical characteristics of the two wind rotors and the mechanical characteristic of the equivalent electric generator. The equality relation in absolute value between the torques of the rotor *GR* and the stator *GS*, according to Equation (16), is added to the previous seven independent equations. The values of the eight kinematic and static external parameters, associated to the four external links described in Figure 3, which present the operating point in the WT steady-state regime, can be obtained from these eight equations.

The hypothesis of linear mechanical characteristics for both wind rotors and the equivalent electric generator is considered in this paper—a situation encountered in practice at direct current (DC) electric generators.

Considering that the torque of the secondary wind rotor and, implicitly, its mechanical characteristics can be adjusted through the k_t ratio, the calculation of the operating point will be further exemplified in four representative cases k_t = [0; 0.5; 1; 1.4].

The mechanical characteristics of wind rotors can be expressed as follows:

$$T_{R1,2} = -a_{R1,2}\omega_{R1,2} + b_{R1,2} \tag{36}$$

and can be reduced to the equivalent output shaft (*es*) of the speed increaser (the shaft 6 ≡ *GR* having the torque unmodified, and the speed equal to the relative speed between the rotor and the stator of the electric generator), obtaining a linear equation of the type:

$$T_{es} = -a_{es}(\omega_{GR} - \omega_{GS}) + b_{es}, \tag{37}$$

where $a_{R1,2}$, $b_{R1,2}$, a_{es}, and b_{es} are constant coefficients and $T_{es} = T_{GR}$. Note that the interior kinematic ratios of the speed increaser (i_{01} and i_{02}) are known, and the coefficients a_{R2}, b_{R2}, a_{es}, and b_{es} depend on the k_t ratio.

Considering the relation of ω_{R1} derived from rel. (1) and (26):

$$\omega_{R1} = \frac{\omega_{GR} - \omega_{GS}}{(1 - i_{02})(1 - i_{01})} \tag{38}$$

the T_{es} expression is obtained:

$$T_{es} = T_{R1}D = -\frac{a_{R1}D}{(1 - i_{02})(1 - i_{01})}(\omega_{GR} - \omega_{GS}) + b_{R1}D, \tag{39}$$

where

$$D = -\frac{1 - \frac{i_{01}}{\eta_{01}}k_t}{\left(1 - \frac{i_{01}}{\eta_{01}}\right)\left(1 - \frac{i_{02}}{\eta_{02}}\right)}. \tag{40}$$

The coefficients of the mechanical characteristics of the two wind rotors *R*1 and *R*2, reduced to the output equivalent shaft *es* of the speed increaser are obtained according to Equations (37) and (39):

$$a_{es} = \frac{a_{R1}D}{(1 - i_{02})(1 - i_{01})}, \quad b_{es} = b_{R1}D. \tag{41}$$

Knowing the mechanical characteristic of the equivalent electric generator:

$$-T_{eg} = a_{eg}\omega_{eg} - b_{eg} \tag{42}$$

where a_{eg} and b_{eg} are constant coefficients, the operating point of the wind turbine in steady-state regime can be obtained by solving the following system:

$$\begin{cases} T_{es} = -a_{es}\omega_{es} + b_{es} \\ -T_{eg} = a_{eg}\omega_{eg} - b_{eg} \\ -T_{es} + T_{eg} = 0 \\ \omega_{es} = \omega_{eg} = \omega_{GR} - \omega_{GS} \end{cases} \tag{43}$$

The coordinates of the operating point on the equivalent output shaft (ω_{es}, T_{es}) are thus obtained:

$$\omega_{es} = \frac{b_{eg} - b_{es}}{a_{eg} - a_{es}}, \tag{44}$$

$$T_{es} = -a_{es}\omega_{es} + b_{es} \tag{45}$$

The values of all kinematic and static, external and internal parameters of the wind system can be further determined by means of the numerical values of the coordinates $(\omega_{es},\ T_{es})$, calculated with the relations (44) and (45).

For a numerical case of the wind turbine type presented in Figure 2, the values of the constant parameters and of the operating point coordinates are tabulated (see Table 2 below) for four values of the k_t ratio. The operation point parameters can be graphically obtained by reducing the mechanical characteristics of the two wind rotors to the equivalent output shaft *es* (Figure 8).

Table 2. Functional parameters of the wind turbine in steady-state regime.

WT Component	Constant Parameters	Variable Parameters	k_t			
			0	**0.5**	**1**	**1.4**
Main wind rotor $R1$	a_{R1}= 0.386 kNms b_{R1}= 73.5 kNm	ω_{R1} [s^{-1}]	4.71	5.42	6.13	6.94
		T_{R1} [kNm]	71.68	71.40	71.13	70.82
		P_{R1} [kW]	337.61	386.99	436.03	491.49
Secondary wind rotor $R2$		ω_{R2} [s^{-1}]	0	−5.42	−6.13	−6.94
		T_{R2} [kNm]	0	−35.70	−71.13	−99.15
		P_{R2} [kW]	0	193.49	436.03	688.10
Speed increaser	i_{aR1-eg}= 18	η_{tot}	0.9366	0.9494	0.9559	0.9171
Equivalent output shaft		a_{es} [kNms]	−0.0011	−0.0017	−0.0023	−0.0027
		b_{es} [kNm]	−3.8243	−5.8153	−7.8063	−9.3360
Equivalent electric generator	a_{eg} = 0.15 kNms b_{eg} = 9 kNm	ω_{eg} [s^{-1}]	84.77	97.54	110.41	120.07
		T_{eg} [kNm]	−3.73	−5.65	−7.55	−9.01
		P_{eg} [kW]	−316.21	−551.11	−833.60	−1081.80

The results obtained by simulating the operating point also highlight the possibility of increasing the mechanical power at the generator input by increasing the k_t ratio, Figure 8. The optimal wind turbine operation (i.e., with maximum efficiency) is achieved for torques of the secondary wind rotor $R2$ adjusted to quasi-equal values of the main wind rotor $R1$ torques (i.e., $k_t \approx 1$), Table 2.

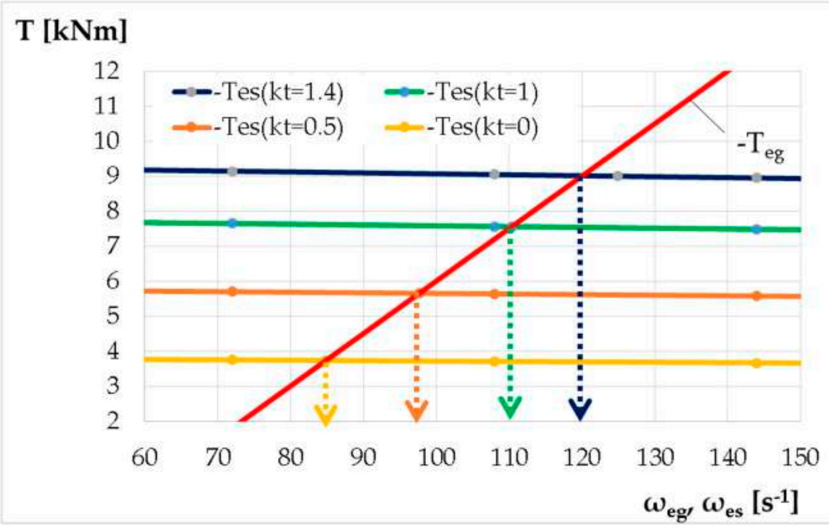

Figure 8. Graphical determination of the running point parameters on the equivalent output shaft for the four analyzed cases (k_t = 0; 0.5; 1; 1.4).

6. Conclusions

The performance of a new, patent-pending solution of a 1 DOF planetary transmission is analyzed in this paper, meant to increase the speeds and torques in the counter-rotating wind turbines with counter-rotating electric generator. The speed increaser is obtained by parallel connection of a two-step bevel transmission with a 2 DOF planetary gear set. This example was used to explain the proposed kinematic and static modeling algorithm that allows identifying the speed increaser efficiency and performance of the wind turbine which integrates this type of gearbox, by solving the stationary operating point problem.

Using the properties of 1 DOF transmissions with two inputs and two outputs of summing up the torques/powers and distributing an external speed in a determined way, the proposed transmission allows both an increase in the relative speed between the electric generator rotor and stator, and additional power/torque input brought by the secondary wind turbine.

Beyond the advantage of increasing power, the use of these wind turbines with counter-rotating components allows a more efficient operation of the electric generator by providing increased speeds along with a compact design. The results presented in the form of kinematic and static computing methodology, analytical models, and diagrams developed for various case studies may prove useful for researchers and designers in the field to establish advantageous solutions of planetary speed increasers for counter-rotating wind turbines that integrate electric generators with mobile stators in which speed needs to be increased proportionally with the power increase.

Author Contributions: Conceptualization, M.N., R.S. and C.J.; methodology, M.N., R.S. and C.J.; software, M.N., R.S. and C.J.; validation, M.N., R.S. and C.J.; formal analysis, M.N. and R.S.; investigation, M.N., R.S. and C.J.; resources, M.N., R.S. and C.J.; data curation, M.N., R.S. and C.J.; writing-original draft preparation, M.N., R.S. and C.J.; writing—review and editing, M.N.; visualization, M.N., R.S. and C.J.; supervision, M.N.; project administration, M.N.

Funding: This research received no external funding.

Conflicts of Interest: The authors declare no conflict of interest.

Nomenclature

WT	Wind turbine	DOF	Degree of freedom
CRWT	Counter-rotating wind turbine	M	Mechanism degree of freedom
CRWR	Counter-rotating wind rotors	GR	Electric generator rotor
CREG	Counter-rotating electric generator	GS	Electric generator stator
$R1$	Main wind rotor	L	Number of mechanism inputs and outputs
$R2$	Secondary wind rotor	eg	Equivalent electric generator
SI	Speed Increaser	i_a	Amplification kinematic ratio
ω	Angular speed	η_0	Transmission interior efficiency
T	Torque	i_0	Transmission interior kinematic ratio
k_t	Input torques ratio	η_{tot}	Efficiency of the speed increaser
z	Gear teeth number	es	Equivalent output shaft of the transmission
H	Planetary carrier	$P_{R1,2}$	Power of the wind rotor R1,2

References

1. Booker, J.D.; Mellor, P.H.; Wrobel, R.; Drury, D. A compact, high efficiency contra-rotating generator suitable for wind turbines in the urban environment. *Renew. Energy* **2010**, *35*, 2027–2033. [CrossRef]
2. Sapre, R.; Murkute, H.; Agrawal, R. Comparison between single axis wind turbine and counter wind turbine—A case study. *Glob. J. Eng. Appl. Sci.* **2012**, *2*, 144–146.
3. Vișa, I.; Jaliu, C.; Duta, A.; Neagoe, M.; Comsit, M.; Moldovan, M.; Ciobanu, D.; Burduhos, B.; Saulescu, R. *The Role of Mechanisms in Sustainable Energy Systems*; Transilvania University of Brașov Publishing House: Brașov, Romania, 2015; pp. 281–316. ISBN 978-606-19-0571-3.
4. Appa, K. *Energy Innovations Small Grant (EISG) Program (Counter Rotating Wind Turbine System)*; EISG Final Report; EISG: Shores, CA, US, 2002; Available online: http://www.eai.in/ref/invent/upload/00-09%2520FAR%2520Appendix%2520A.pdf (accessed on 11 June 2017).
5. Jung, S.; No, T.; Ryu, K. Aerodynamic performance prediction of a 30kW counter-rotating wind turbine system. *Renew. Energy* **2005**, *30*, 631–644. [CrossRef]
6. McKenna, R.; Leye, P.O.; Fichtner, W. Key challenges and prospects for large wind turbines. *Renew. Sustain. Energy Rev.* **2016**, *53*, 1212–1221. [CrossRef]
7. Lee, S.; Kim, H.; Lee, S. Analysis of aerodynamic characteristics on a counter-rotating wind turbine. *Curr. Appl. Phys.* **2010**, *10*, S339–S342. [CrossRef]
8. Hwang, B.; Lee, S.; Lee, S. Optimization of a counter-rotating wind turbine using the blade element and momentum theory. *J. Renew. Sustain. Energy* **2013**, *5*, 052013. [CrossRef]
9. Lee, S.; Kim, H.; Son, E.; Lee, S. Effects of design parameters on aerodynamic performance of a counter-rotating wind turbine. *Renew. Energy* **2012**, *42*, 140–144. [CrossRef]
10. Didane, D.H.; Rosly, N.; Zulkafli, M.F.; Shamsudin, S.S. Performance evaluation of a novel vertical axis wind turbine with coaxial contra-rotating concept. *Renew. Energy* **2015**, *115*, 353–361. [CrossRef]
11. Shin, C. Multi-Unit Rotor Blade System Integrated Wind Turbine. U.S. Patent No 5876181, 2 March 1999.
12. Climescu, O.; Saulescu, R.; Jaliu, C. Specific features of a counter-rotating transmission for renewable energy systems. *Environ. Eng. Manag. J.* **2011**, *10*, 1105–1113. [CrossRef]
13. Oprina, G.; Chihaia, R.A.; El-Leathey, L.A.; Nicolaie, S.; Băbuțanu, C.A.; Voina, A. A review on counter-rotating wind turbines development. *J. Sustain. Energy* **2016**, *7*, 91–98.
14. Marjanovic, N.; Isailovic, B.; Marjanovic, V.; Milojevic, Z.; Blagojevic, M.; Bojic, M. A practical approach to the optimization of gear trains with spur gears. *Mech. Mach. Theory* **2012**, *53*, 1–16. [CrossRef]
15. Bevington, C.M.; Bywaters, G.L.; Coleman, C.C.; Costin, D.P.; Danforth, W.L.; Lynch, J.A.; Rolland, R.H. Wind Turbine Having a Direct-Drive Drivetrain. U.S. Patent 7431567B1, 7 October 2008.
16. Climescu, O.; Jaliu, C.; Saulescu, R. Comparative Analysis of Horizontal Small Scale Wind Turbines for a Specific Application. In Proceedings of the 14th IFToMM World Congress, Taipei, Taiwan, 25–30 October 2015. [CrossRef]
17. Mesquita, A.L.A.; Palheta, F.C.; Pinheiro Vaz, J.R.; Girão de Morais, M.V.; Gonçalves, C. A methodology for the transient behavior of horizontal axis hydrokinetic turbines. *Energy Convers. Manag.* **2014**, *87*, 1261–1268. [CrossRef]

18. Neagoe, M.; Saulescu, R.; Jaliu, C.; Cretescu, N. Novel Speed increaser used in counter-rotating wind turbines. In *New Advances in Mechanisms, Mechanical Transmissions and Robotics, Mechanisms and Machine Science 46*; Springer: Berlin, Germany, 2017; pp. 143–151.
19. Saulescu, R.; Neagoe, M.; Jaliu, C. *Improving the Energy Performance of Wind Turbines Implemented in the Built Environment Using Counter-Rotating Planetary Transmissions*; Materials Science and Engineering—IOP Conference Series: Materials Science and Engineering; IOP Publishing Ltd.: Bristol, UK, 2016.
20. Saulescu, R.; Neagoe, M.; Munteanu, O.; Cretescu, N. *Performance Analysis of a Novel Planetary Speed Increaser Used in Single-Rotor Wind Turbines with Counter-Rotating Electric Generator*; Materials Science and Engineering—IOP Conference Series: Materials Science and Engineering; IOP Publishing Ltd.: Bristol, UK, 2016.
21. Saulescu, R.; Jaliu, C.; Neagoe, M. Structural and Kinematic Features of a 2 DOF Speed Increaser for Renewable Energy Systems. *Appl. Mech. Mater.* **2016**, *823*, 367–372. [CrossRef]
22. Saulescu, R.; Neagoe, M.; Jaliu, C.; Munteanu, O. Comparative analysis of two wind turbines with planetary speed increaser in steady-state. *Appl. Mech. Mater.* **2016**, *823*, 355–360. [CrossRef]
23. Saulescu, R.; Jaliu, C.; Munteanu, O.; Climescu, O. Planetary Gear for Counter-rotating Wind Turbines. *Appl. Mech. Mater.* **2014**, *658*, 135–140. [CrossRef]
24. Saulescu, R.; Jaliu, C.; Climescu, O.; Diaconescu, D. On the use of 2 DOF planetary gears as "speed increaser" in small hydros and wind turbines. In Proceedings of the ASME 2011 International Design Engineering Technical Conferences & Computers and Information in Engineering Conference, Washington DC, USA, 25–31 August 2011.
25. Wacinski, A.; Sàrl, E. Drive Device for a Windmill Provided with Two Counter–Rotative Propellers. U.S. Patent No. 7384239, 10 June 2008.
26. Herzog, R.; Schaffarczyk, A.P.; Wacinski, A.; Zürcher, O. Performance and stability of a counter–rotating windmill using a planetary gearing: Measurements and Simulation. In Proceedings of the European Wind Energy Conference & Exhibition, Warsaw, Poland, 20–23 April 2010; Available online: https://www.researchgate.net/publication/236683548 (accessed on 15 June 2017).
27. Brander, M. Bi-Directional Wind Turbine. U.S. Patent 2008/0197639 A1, 23 March 2008.
28. Qiu, J.; Liu, B.; Dong, H.; Wang, D. Type Synthesis of Gear-box in Wind Turbine. *Procedia Comput. Sci. C* **2017**, *109*, 809–816. [CrossRef]
29. Hall, J.F.; Mecklenborg, C.A.; Chen, D.; Pratap, S.B. Wind energy conversion with a variable-ratio gearbox: Design and analysis. *Renew. Energy* **2011**, *36*, 1075–1080. [CrossRef]
30. Vidal, Y.; Acho, L.; Luo, N.; Zapateiro, M.; Pozo, F. Power Control Design for Variable-Speed Wind Turbines. *Energies* **2012**, *5*, 3033–3050. [CrossRef]
31. Zhamalov, A.Z.; Obozov, A.D.; Kunelbaev, M.M.; Baikadamova, L.S. Capacity and Power Characteristics of Disk Generator with Counter-Rotation of Double-Rotor Wind Turbine. *Middle-East J. Sci. Res.* **2013**, *15*, 1655–1662. [CrossRef]
32. Saulescu, R.; Neagoe, M.; Jaliu, C. Conceptual Synthesis of Speed Increasers for Wind Turbine Conversion Systems. *Energies* **2018**, *11*, 2257. [CrossRef]
33. Newman, B.G. Actuator-disc theory for vertical-axis wind turbines. *J. Wind Eng. Ind. Aerodyn.* **1983**, *15*, 347–355. [CrossRef]
34. Farahani, E.M.; Hosseinzadeh, N.; Ektesabi, M. Comparison of fault-ride-through capability of dual and single-rotor wind turbines. *Renew. Energy* **2012**, *48*, 473–481. [CrossRef]
35. No, T.S.; Kim, J.E.; Moon, J.H.; Kim, S.J. Modelling, control, and simulation of dual rotor wind turbine generator system. *Renew. Energy* **2009**, *34*, 2124–2132. [CrossRef]
36. Kubo, K.; Hano, Y.; Mitarai, H.; Hirano, K.; Kanemoto, T.; Galal, A.M. Intelligent wind turbine unit with tandem rotors (discussion of prototype performances in field tests). *Curr. Appl. Phys.* **2010**, *10*, S326–S331. [CrossRef]
37. Chantharasenawong, C.; Suwantragul, B.; Ruangwiset, A. Axial Momentum Theory for Turbines with Co-axial Counter Rotating Rotors. In Proceedings of the Commemorative International Conference of the Occasion of the 4th Cycle Anniversary of KMUTT Sustainable Development to Save the Earth: Technologies and Strategies Vision 2050: (SDSE2008), Bangkok, Thailand, 11–13 December 2008.
38. Kanemoto, T.; Galal, A.M. Development of intelligent wind turbine generator with tandem wind rotors and double rotational armatures. *JSME Int. J. Ser. B* **2006**, *49*, 450–457. [CrossRef]

39. Caiozza, J. Wind Driven Electric Generator Apparatus. U.S. Patent 7227276 B2, 5 June 2007.
40. Winderl, W. Wind Operated Generator. U.S. Patent 4039848, 2 August 1977.
41. Duong, M.Q.; Leva, S.; Mussetta, M.; Le, K.H. A Comparative Study on Controllers for Improving Transient Stability of DFIG Wind Turbines During Large Disturbances. *Energies* **2018**, *11*, 480. [CrossRef]
42. Duong, M.Q.; Grimaccia, F.; Leva, S.; Mussetta, M.; Le, K.H. Improving Transient Stability in a Grid-Connected Squirrel-Cage Induction Generator Wind Turbine System Using a Fuzzy Logic Controller. *Energies* **2015**, *8*, 6328–6349. [CrossRef]
43. Barambones, O. Sliding Mode Control Strategy for Wind Turbine Power Maximization. *Energies* **2012**, *5*, 2310–2330. [CrossRef]
44. Zhu, Y.; Cheng, M.; Hua, W.; Wang, W. A Novel Maximum Power Point Tracking Control for Permanent Magnet Direct Drive Wind Energy Conversion Systems. *Energies* **2012**, *5*, 1398–1412. [CrossRef]
45. Hau, E. *Wind Turbines: Fundamentals, Technologies, Application, Economics*, 2nd ed.; Springer: Berlin/Heidelberg, Germany, 2006; pp. 253–3018. ISBN 978-3-540-24240-6.
46. Jelaska, D.; Podrug, S.; Perkusic, M. A novel hybrid transmission for variable speed wind turbines. *Renew. Energy* **2015**, *83*, 78–84. [CrossRef]
47. Zhao, M.; Ji, J. Dynamic analysis of wind turbine gearbox components. *Energies* **2016**, *9*, 110. [CrossRef]
48. Moghadassian, B.; Rosenberg, A.; Sharma, A. Numerical Investigation of Aerodynamic Performance and Loads of a Novel Dual Rotor Wind Turbine. *Energies* **2016**, *9*, 571. [CrossRef]
49. Sultan, T.; Gour, A.; Mukeshpandey. Differentiation analysis of single and dual rotor wind turbine torque transmission system. *Int. J. Mech. Eng. Robot. Res.* **2014**, *3*, 585–588.
50. Marugán, A.P.; Márquez, F.P.G.; Perez, J.M.P.; Ruiz-Hernández, D. A survey of artificial neural network in wind energy systems. *Appl. Energy* **2018**, *228*, 1822. [CrossRef]

applied sciences

MDPI

Article

A Comparative Performance Analysis of Four Wind Turbines with Counter-Rotating Electric Generators

Mircea Neagoe [1], Radu Saulescu [2], Codruta Jaliu [1], Olimpiu Munteanu [1] and Nadia Cretescu [1,*]

[1] Renewable Energy Systems and Recycling R&D Centre, Faculty of Product Design and Environment, Transilvania University of Brasov, 500036 Brasov, Romania; mneagoe@unitbv.ro (M.N.); cjaliu@unitbv.ro (C.J.); omunt@unitbv.ro (O.M.)

[2] Design of Mechanical Elements and Systems R&D Centre, Faculty of Product Design and Environment, Transilvania University of Brasov, 500036 Brasov, Romania; rsaulescu@unitbv.ro

* Correspondence: ncretescu@unitbv.ro; Tel.: +40-268-413-000

Abstract: Wind energy conversion systems play a major role in the transition to carbon-neutral power systems, and obviously, a special attention is paid in identifying the most effective solutions for a higher valorization of the local wind potential. In this context, this paper presents a comparative study on the energy performances of wind turbines (WTs) that include a counter-rotating electric generator. Starting from an innovative concept proposed by the authors for a reconfigurable wind turbine with three clutches, four cases of WTs with counter-rotating generators are studied: a system with three wind rotors (WRs) and a 2-DOF (degrees of freedom) planetary speed increaser (Case A), with two counter-rotating WRs and a 1-DOF (Case B) or a 2-DOF (Case C) speed increaser and a 1-DOF single rotor wind system (Case D). An analytical archetype model for angular speeds, torques, powers and efficiency of the reconfigurable planetary speed increaser, corresponding to the general case with three inputs (Case A), was firstly derived. The analytical models of the other three cases (B, C and D) were results by customizations of the archetype model according to the kinematic- and static-specific effects of engaging/disengaging the clutches. The simulation of the analytical models for a numerical representative example with two variable parameters (input speed ratio k_ω and input torque ratio k_t) allows highlighting the influence of various parameters (number of WRs, speed increaser DOF, k_ω and k_t) on the input powers, power that flows through the planetary transmission and mechanical power supplied to the electric generator, as well as on the transmission efficiency. The obtained results show that the output power increases with the increase of the number of wind rotors, the transmission efficiency is the maximum for $k_t = 1$ and the speed amplification ratio increases with the ratio k_ω.

Keywords: renewable energy; wind turbine; wind rotor; counter-rotating electric generator; speed increaser; steady-state modeling; efficiency; power flow

check for updates

Citation: Neagoe, M.; Saulescu, R.; Jaliu, C.; Munteanu, O.; Cretescu, N. A Comparative Performance Analysis of Four Wind Turbines with Counter-Rotating Electric Generators. *Appl. Sci.* **2022**, *12*, 4233. https://doi.org/10.3390/app12094233

Academic Editor: José A. F. O. Correia

Received: 12 March 2022
Accepted: 18 April 2022
Published: 22 April 2022

1. Introduction

The importance of replacing fossil fuel-based energy with clean energy in the concern for the sustainable development of human society is well-known, achieving green economic growth in the context of reducing its impact on climate change. Thus, the generation of electricity with renewable energy systems can reduce global greenhouse gas emissions to a large extent while reducing environmental pollution.

A significant share of clean electricity is obtained by converting wind kinetic energy by using wind turbines (WTs). In order to be accessible and feasible, wind turbines must meet several specific requirements, the conversion efficiency of wind energy into electricity being one of the most important technical issues. Therefore, it is necessary to optimize wind turbines by designing and developing efficient solutions; thus, the following main directions of scientific research have been identified in the literature:

- the design and development of novel solutions for wind turbines or their main components and an estimation of their performances;
- increasing the efficiency and/or energy performance of existing WTs;
- functional optimization of existing WT subsystems.

Special attention is also paid in the literature to the comparative study of various types of wind turbines: conventional (with a single wind rotor and electric generator with a fixed stator) and unconventional: dual- and multi-rotor WTs, with counter-rotating generators, with diverse types of speed increasers, etc.

The design of new or improved wind turbines is a constant concern of researchers and developers in the field. Thus, Oprina et al. [1] conducted a literature review of the main results on counter-rotating wind turbines (CRWTs) in terms of the design and methods for estimating their performances. Didan et al. [2] investigated experimentally the performance of a novel vertical axis counter-rotating wind turbine, and Pacholczyk et al. [3] analyzed a new small CRWT considering the influence of distance between the two wind rotors, its performance being highlighted using the computational fluid dynamics (CFD) method. An original small CRWT with a vertical shaft was proposed by West in a patent [4], in which the input motions of the two rotors are added by means of a gear transmission; a novel torque-adding CRWT was proposed by Neagoe et al. [5], considering also adding speed in the counter-rotating generator. Saulescu et al. presented in [6] an algorithm for the conceptual synthesis of systems with one or two counter-rotating wind rotors and with conventional or counter-rotating electric generators. Another way to increase the performances of wind turbines addressed the counter-rotating wind systems by implementing a counter-rotating double-sided flux switching permanent magnet generator, as proposed by Mirnikjoo et al. [7] and tested by Kutt [8]. A novel concept of CRWTs, including a 1-DOF (degree of freedom) planetary speed increaser with two inputs and one output, was proposed by Neagoe et al. in [9]. The design of multi-rotor and multi-generator WTs with a lattice tower was presented in [10]. Cho et al. [11] proposed, developed and experimentally tested an integrated control algorithm for a new dual-rotor wind turbine with a counter-rotating generator, designed to maximize the output power of the wind turbine. Jelaska et al. [12] proposed a wind system with two inputs and one output, one input being connected to a wind rotor and the other input to a motor aiming at maintaining a constant speed at the electric generator shaft. Unlike the previous studies, which refer to low- and medium-power systems, Qiu et al. [13] presented the main types of wind systems with one input and high output capacity. The performances of a CRWT with a conventional generator were analyzed by Saulescu et al. in [14] based on a steady-state operating point; the same authors approached in [15] the analysis of the efficiency of several speed increasers for systems with two inputs and one output with different mounting situations. Vasel-Be-Hagh et al. [16] analyzed the performance of a CRWT farm, and Blanco et al. investigated theoretically and experimentally the performance (power coefficient) of a vertical axis Savonius wind turbine integrating an innovative rotor with Fibonacci spiral geometry [17].

The performances of existing wind turbines have been studied by many researchers considering various indicators (capacity factor, availability, failure rate, downtime, power coefficient, efficiency, reliability, etc.) and using a wide range of data and methods, such as those systematized by Pfaffel et al. [18], the empirical mode decomposition method [19,20] or methods such as experiments and the Lattice Boltzmann model combined with Large Eddy Simulation [21] applied to a horizontal axis counter-rotating wind turbine. The performances of dual-rotor (co- and counter-rotating) wind turbines were highlighted also by Lam et al. in [22], ideas that were further developed by Lipian et al. [23] and Bani-Hani et al. [24]. The performance of a CRWT was discussed by Erturk et al. [25] in the case of implementing a counter-rotating generator, while Pamuji et al. compared rotary systems with two or three wind rotors [26]. Neagoe et al. analyzed in [27] the stationary operating point of a 2-DOF CRWT with a counter-rotating generator. Fan et al. [28] analyzed the influence of three-stage transmission vibrations on the performance of horizontal axis wind systems operating in low-wind speed areas. Chaichana et al. studied in a wind tunnel the effect of the speed ratios of two counter-rotating rotors of a vertical axis wind turbine [29]; on the same CRWT type, Didane et al. [30] investigated the aerodynamic characteristics, power and torque coefficients. In [31], Didane et al. highlighted the performance of a CRWT with Darius H-type rotors using three-dimensional CFD models based on the K-omega Shear Stress Transport turbulence model; the same method was applied by Cao et al. [32] for a similar turbine on a floating platform. The performance of a horizontal axis CRWT with identical front and rear rotors was highlighted by Ilmunandar et al. in [33], while Koehuan et al. [34] analyzed the performance of the same wind turbine type by considering the ratio of wind rotor diameters as a dimensionless parameter.

The main WT subsystems addressed extensively by researchers are wind rotors, electric generators and speed increasers. Li et al. studied in [35] the effect of the number of blades on the aerodynamic forces of a vertical axis wind turbine, while the design of the WT blade shapes and their influence on the power coefficient in static and dynamic conditions were addressed in [36]. Mirnikjoo et al. investigated the performance of a counter-rotating electric generator [37].

Several representative speed reducers for which the power flow was reversed (and, hence, used as a speed increaser) were analyzed by Jaliu et al. in [38], while Saulescu et al. [39] proposed and modeled a speed increaser able to be operated with one input and one or two outputs. Other novel solutions of planetary speed increasers have been presented and analyzed in the literature: a 2-DOF hybrid transmission for variable speed wind turbines [12] and a two-input one-output cylindrical planetary gear set with satellites in a series [40]. The dynamic properties of a speed increaser and the steady-state operating point were highlighted by Herzog et al. [41] by studying the behavior of a wind turbine with counter-rotating rotors using a wind tunnel and the CFD method. Bharani et al. [42] classified the gearbox technologies for horizontal axis wind systems into three categories (planetary gearbox, continuous variable transmission and magnetic gearbox) and studied their performances based on indicators such as the torque output, tracking accuracy and durability. Qiu et al. summarized the gear mechanisms used in wind turbines [13]. Recent technologies and development trends of mechanical transmissions were systematized by Nejad et al. [43], and Concli et al. analyzed the behavior of the gear teeth using artificial neural networks [44] or the load capacity and its influence on the condition of the teeth [45]. The dynamic behavior of speed increasers was addressed by Wu et al. [46] by modeling the lateral-torsional coupling of the transmission of a large wind turbine. Lee et al. [47] proposed a testing rig, patented by the authors, used to investigate the mechanical power flow of a speed increaser into a high-speed wind turbine, while Lin et al. developed a new concept of a speed increaser with a parallel power flow implemented in a wind turbine with two inputs and one output [48].

Several studies have compared the efficiency of counter-rotating vs. conventional WTs, concluding that counter-rotating systems can generate up to 40% more electricity. Thus, Climescu et al. [49] analyzed the dynamics of counter-rotating vs. conventional wind systems with a cylindrical gearbox. Saulescu et al. approached comparatively the stationary operating point for wind turbines with two counter-rotating rotors vs. one rotor and 1-DOF vs. 2-DOF speed increasers [50], wind systems with one rotor and counter-rotating vs. traditional (with fixed stator) electric generator [51] and wind systems with two counter-rotating rotors and counter-rotating vs. a traditional generator [52]. Farahani et al. [53] showed comparatively the dynamic behavior of a CRWT in several operating situations.

Considering the variability of wind speed during the year, the optimization of wind energy harvesting and the transformation as efficient as possible into electricity are major challenges for research in the field. Dual- or multi-rotor wind turbines with counter-rotating generators are a promising recent technology still insufficiently explored for large-scale development and implementation. This research is also part of this knowledge development effort by proposing a comparative analysis of the energy performance of four wind turbines with a counter-rotating electric generator that integrate a planetary speed increaser with an innovative variable structure patented by the authors. This transmission allows the wind turbine to operate with one, two or three counter-rotating WRs by means of three clutches.

The manuscript is organized as follows: Section 2 is devoted to problem formulation and presents the four studied configurations (cases) of the WTs with a counter-rotating generator. Section 3 details the analytical modeling method and presents the kinematic, static, power and efficiency results in the four cases derived from a general model. For a representative numerical set, Section 4 presents the simulation results and discussions on the analyzed WT performances. The final conclusions of the paper are drawn in Section 5.

2. Problem Formulation

The wind systems with counter-rotating generators (*WSCGs*) have superior conversion efficiencies compared to conventional generators (with fixed stator) due to the branched transmission of mechanical power and higher relative speed between the rotor (GR) and the stator (GS) of the electric generator (G). A counter-rotating generator has both armatures (GR and GS) movable and rotates in opposite directions; usually, due to inertial reasons, the generator rotor has a higher speed than the stator. However, the energy performance of *WSCGs* is significantly influenced by the number of WRs, as well as by the speed increaser type. In order to highlight the influence of the number of WRs (inputs) and of the structural degree of freedom, a comparison between *WSCGs* with 1-DOF or 2-DOF speed increasers with one input (i.e., with one *WR* and the total number of external connections L = 3, implicitly), two inputs (two *WRs* and L = 4) and three inputs (three *WRs* and L = 5) is further approached. To this end, a planetary transmission with a variable structure, based on three clutches and derived from a solution for which the authors have a patent application [54], is proposed; by appropriate combinations of clutch engaging and disengaging, the transmission can operate in various structures, of which four cases were selected (Figure 1):

- Case A: 2-DOF (differential) transmission with three inputs (2-DOF, L = 5, and three *WRs*);
- Case B: 1-DOF (monomobile) transmission with two inputs (1-DOF, L = 4, and two *WRs*);
- Case C: 2-DOF transmission with two inputs (2-DOF, L = 4, and two *WRs*);
- Case D: 1-DOF transmission with one input (1-DOF, L = 3, and one *WR*).

As a result, the energy performances of *WSCG*s with two or three wind rotors can be directly compared with those of conventional wind turbines (with one wind rotor), highlighting the specific differences of cases with 1-DOF vs. 2-DOF transmissions.

The approach starts from a "variable" structure, based on setting the clutches C1 ... C3 (Figure 1); this structure contains: three wind rotors (a permanent primary rotor $R1$ and two secondary rotors $R2$ and $R3$ activated by clutches C2 and C3, respectively), a planetary gear set with bevel gears I $\equiv$ 2-1″-1′-3-H_1 (equipped with clutch C1 for blocking the satellite carrier H_1) and a differential cylindrical planetary gear set II $\equiv$ 4-5-6-H_2 with two counter-rotating outputs, 6 and 7, secured to the rotor *GR* and the stator *GS*, respectively.

The primary rotor $R1$ is coupled to the bevel gear (2), which is assembled on the carrier H_2. The power generated by $R1$ is distributed on two branches to the planetary gear set II through the bevel sun gear (3), assembled into the ring sun gear (4) and directly to the carrier H_2; further, the power is transmitted by gear set II to the rotor $GR \equiv 6$ and stator $GS \equiv 7$, respectively.

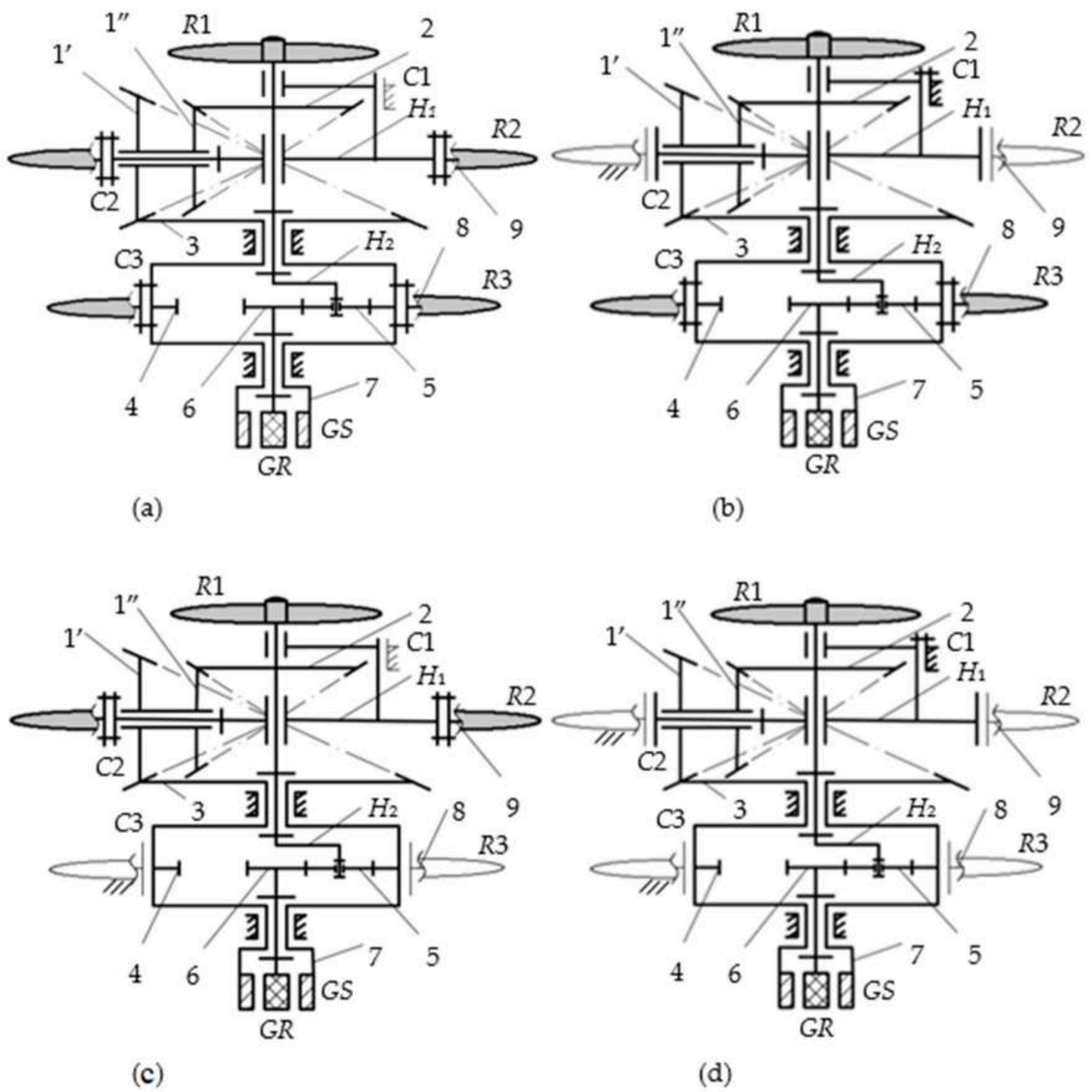

Figure 1. Schemes of the *WSCGs* with a "variable" structure: (**a**) *C*1 = 0, *C*2 = *C*3 = 1: Case A (2-DOF, L = 5); (**b**) *C*1 = *C*3 = 1, *C*2 = 0: Case B (1-DOF, L = 4); (**c**) *C*1 = *C*3 = 0, *C*2 = 1: Case C (2-DOF, *L* = 4); (**d**) *C*1 = 1, *C*2 = *C*3 = 0: Case D (1-DOF, *L* = 3).

Denoting a disengaged clutch by *Ci* = 0 and an engaged clutch by *Ci* = 1 (*i* = 1, 2, 3), the structures related to Cases A, B, C and D can be described as follows:

- Case A, Figure 1a: *C*1 = 0, *C*2 = *C*3 = 1, 2-DOF transmission with three inputs and two outputs (*L* = 5);
- Case B, Figure 1b: *C*1 = *C*3 = 1, *C*2 = 0, 1-DOF transmission with two inputs and two outputs (*L* = 4); for *C*1 = 1, the bevel transmission I is a 1-DOF gear set with fixed axes, and, for *C*2 = 0, the rotor *R*2 idles and torque $T_{R2} = 0$, implicitly. In order to facilitate the kinematic modeling, it is considered that the clutch disengaging, afferent to a rotor *R*, is accompanied by fixing the rotor to the base, i.e., the rotational speed $\omega_R = 0$;
- Case C, Figure 1c: *C*1 = *C*3 = 0, *C*2 = 1, 2-DOF transmission with two inputs and two outputs (*L* = 4); analogous to Case B, for *C*3 = 0, the rotor *R*3 becomes inactive and blocked, i.e., $T_{R3} = 0$ and $\omega_{R3} = 0$;
- Case D, Figure 1d: *C*1 = 1, *C*2 = *C*3 = 0, 1-DOF transmission with one input and two outputs (*L* = 3); analogous with Cases B and C, the rotors *R*2 and *R*3 become

inactive and blocked for $C2 = C3 = 0$, i.e., $T_{R2} = 0$, $\omega_{R2} = 0$ and $T_{R3} = 0$, $\omega_{R3} = 0$, respectively.

The four variants of *WSCGs* (Figure 1) use the same speed increaser under the following premises:

- homologous gears of the four *WSCGs* have the same number of teeth z_i, $i = 1', 1'', \ldots, 6$;
- homologous gear pairs with fixed axes have the same efficiency;
- the three wind rotors have the possibility to modify the pitch angle of their blades to adjust the input powers, the angular speeds and the input torques implicitly while considering a constant wind speed (i.e., a steady-state regime);
- in order to facilitate the kinematic modeling, it is considered that the clutch disengaging for a wind rotor is accompanied by the rotor locking at the base, which means that both the rotor torque and speed become null.

Under these premises, the problem addressed in the paper refers to the analytical modeling of the parameters considered as the main comparison criteria: the kinematic amplification ratio of the speed from the primary rotor $R1$ to the generator G (i_a), the transmission efficiency (η) and the mechanical power transmitted to the electric generator (P_G), as well as the power flow. For simplicity, the meaning of the symbols used in the equations is detailed in the Nomenclature section, without repeating it in the text.

3. Closed-Form Modeling

The kinematic and static models of the *WSCGs* illustrated in Figure 1 can be derived based on the block diagrams from Figure 2. The following correlations [55] can be written by decomposing the complex transmissions into gear sets I and II, according to the block diagrams in Figure 2:

- Planetary gear set I:

$$\mathrm{I}: \begin{cases} i_{32}^{H_1} = i_{01} = \frac{\omega_{3H_1}}{\omega_{2H_1}} = -\frac{z_{1'}}{z_3}\frac{z_2}{z_{1''}} \\ \omega_3 = \omega_2 i_{01} - \omega_{H_1}(1 - i_{01}) \quad \Rightarrow \quad i_{32} = i_{01} + \frac{\omega_{H_1}}{\omega_2}(1 - i_{01}) \\ T_3 i_{01} \eta_{01}^{x} + T_{2'} = 0 \\ T_3 + T_{2'} + T_{H_1} = 0 \end{cases} \tag{1}$$

where $x = \pm 1$, depending on the direction of the power flow transmission through the fixed axis mechanisms associated with the planetary gear set, obtained by reversing the motion with respect to H_1 [55]. For Case A (Figure 1a) and Case B (Figure 1b), the sign of x depends on the ratio $k_t = -T_{R3}/T_{R1}$: for $k_t > 1$, $x = +1$, and for $k_t < 1$, $x = -1$. For Cases C (Figure 1c) and D (Figure 1d), $x = -1$.

- Planetary gear set II:

$$\mathrm{II}: \begin{cases} i_{64}^{H_2} = i_{02} = \frac{\omega_{6H_2}}{\omega_{4H_2}} = -\frac{z_4}{z_6} \\ \omega_6 = \omega_4 i_{02} + \omega_{H2}(1 - i_{02}) \quad \Rightarrow \quad i_{64} = i_{02} + \frac{\omega_{H_2}}{\omega_4}(1 - i_{02}) \\ T_6 i_{02} \eta_{02}^{w} + T_4 = 0 \\ T_6 + T_4 + T_{H_2} = 0 \end{cases} \tag{2}$$

where the sign of the exponent w is obtained as follows [55]:

$$w = \mathrm{sgn}(\omega_{6H_2} T_6) = \mathrm{sgn}\left(\frac{i_{02}}{1 - i_{02}}\right) = -1 \tag{3}$$

where sgn is the signum function.

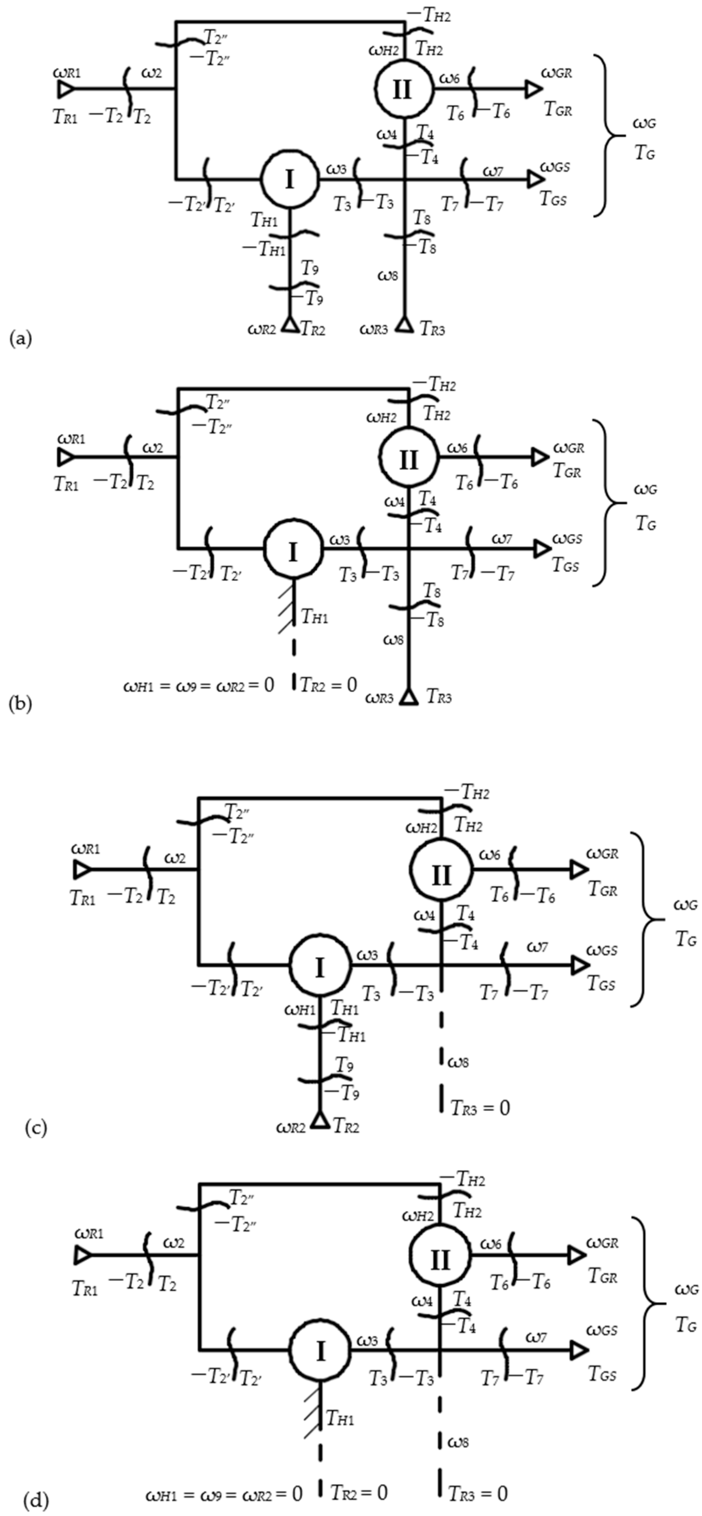

Figure 2. Block diagrams of the transmissions from Figure 1: (**a**) Case A (Figure 1a); (**b**) Case B (Figure 1b); (**c**) Case C (Figure 1c); (**d**) Case D (Figure 1d).

The kinematic and static modeling in the general case (Case A) is further presented considering Equations (1) and (2), to which the kinematic and static correlations related to the connections between the planetary gear sets, the wind rotors and the electric generator are added. The relations for the other three functional cases (B, C and D) are obtained by customizing the analytical archetype model obtained in Case A.

3.1. Kinematic Modeling

The transmission with three inputs (Case A, Figure 1a) is characterized by two independent external speeds; for instance, ω_{R1} and ω_{R2}. For simplicity, it is preferable to use the input speed ratio $k_\omega = -\omega_{R2}/\omega_{R1}$ as an independent variable instead of the speed ω_{R2}. According to Figure 2a, the following correlations related to the connections between the *WSCG* components can be added to the kinematic equations in Systems (1) and (2):

$$\begin{cases} \omega_{R1} = \omega_2 = \omega_{H_2} \\ \omega_{R2} = \omega_9; \quad \omega_{R2} = -k_\omega \omega_{R1} \\ \omega_9 = \omega_{H_1} \\ \omega_3 = \omega_4 = \omega_7 = \omega_8 \\ \omega_7 = \omega_{GS}; \; \omega_8 = \omega_{R3} \\ \omega_6 = \omega_{GR} \\ \omega_G = \omega_{GR} - \omega_{GS} \end{cases} \tag{4}$$

The obtained set of 14 independent equations with 16 unknown parameters allows the description of the 14 dependent kinematic variables (ω_{R2}, ω_{R3}, ω_{GR}, ω_{GS}, ω_G, ω_2, ω_3, ω_4, ω_6, ω_7, ω_8, ω_9, ω_{H_1} and ω_{H_2}), depending on the independent variables ω_{R1} and k_ω.

The other three cases (B, C and D) can be modeled kinematically based on the relations previously obtained for the archetype model, in which the following particularizations occur:

- Case B: $C1 = 1$, $C2 = 0$ and $\omega_{R2} = 0$; implicitly: $\omega_9 = \omega_{H1} = 0$ (Figure 2b);
- Case C: $C3 = 0$ and $\omega_{R3} = 0$; implicitly: $\omega_8 = 0$ and $\omega_7 = \omega_4 = \omega_3 \ (\neq 0)$ (Figure 2c);
- Case D: $C1 = 1$, $C2 = C3 = 0$ and $\omega_{R2} = 0 = \omega_{R3} = 0$; implicitly: $\omega_9 = \omega_{H1} = 0$, $\omega_8 = 0$ and $\omega_7 = \omega_4 = \omega_3 \ (\neq 0)$ (Figure 2d).

The transmission amplification ratio i_a can be obtained with the relation:

$$i_a = \frac{\omega_G}{\omega_{R1}} \tag{5}$$

The kinematic correlations of the speed increasers from Figure 1, systematized in Table 1, can be obtained by solving the set of kinematic Equations (1), (2), (4) and (5) and considering the previous particularizations. It can be observed that, except for the speed ω_{R3}, the relations are identical for Cases A and C (2-DOF variants) and B and D (1-DOF variants), respectively.

Table 1. The analytical expressions of the dependent kinematic parameters and the amplification kinematic ratio corresponding to the four cases (Figures 1 and 2).

	Case A	**Case C**	**Case B**	**Case D**
ω_{R2}	$-\omega_{R1}k_\omega$	$-\omega_{R1}k_\omega$	0	0
ω_{R3}	$\omega_{R1}[i_{01} - k_\omega(1 - i_{01})]$	0	$\omega_{R1}i_{01}$	0
ω_{GR}	$\omega_{R1}[i_{02}(i_{01} - 1)(1 + k_\omega) + 1]$		$\omega_{R1}[i_{02}(i_{01} - 1) + 1]$	
ω_{GS}	$\omega_{R1}[i_{01} - k_\omega(1 - i_{01})]$		$\omega_{R1}i_{01}$	
ω_G	$\omega_{R1}(1 - i_{01})(1 - i_{02})(1 + k_\omega)$		$\omega_{R1}(1 - i_{01})(1 - i_{02})$	
i_a	$(1 - i_{01})(1 - i_{02})(1 + k_\omega)$		$(1 - i_{01})(1 - i_{02})$	

3.2. Torque Modeling in the Steady-State Regime

The following set of static equations in steady-state conditions is obtained based on the torque equations that come from the modeling of the two planetary gear sets, according to Equations (1) and (2), and the equations of static equilibrium for the shafts isolated from the *WSCG*—Case A (Figure 2a):

$$\begin{cases} T_{R1} - T_2 = 0 \\ T_2 - T_{2'} - T_{2''} = 0;\ T_{2'} = -\overline{i_{01}}T_3;\ T_{2''} = T_{H_2} \\ -T_3 - T_4 + T_7 + T_8 = 0 \\ T_9 - T_{H_1} = 0;\ T_{H_1} = \left(\overline{i_{01}} - 1\right)T_3;\ T_{H_2} = \left(\overline{i_{02}} - 1\right)T_6 \\ T_4 = -\overline{i_{02}}T_6 \\ T_{R2} - T_9 = 0;\ T_{R3} - T_8 = 0;\ T_{R3} = -k_t T_{R1} \\ T_{GR} - T_6 = 0;\ T_{GS} - T_7 = 0;\ T_G = T_{GR} = -T_{GS} \end{cases} \tag{6}$$

where $\overline{i_{01}} = i_{01}\eta_{01}^{x}$, $\overline{i_{02}} = i_{02}\eta_{02}^{w}$. Thus, a system of 16 linear equations with 16 dependent torques (T_{R2}, T_{R3}, T_{GR}, T_{GS}, T_G, T_2, $T_{2'}$, $T_{2''}$, T_3, T_4, T_6, T_7, T_8, T_9, T_{H_1} and T_{H_2}) and two independent variables T_{R1} and T_{R3}, replaced by T_{R1} and the input torques ratio $k_t = -T_{R3}/T_{R1}$, is obtained. Relations (6) are valid for the other three cases by considering the following customizations:

- Case B: *C*2 = 0, $T_{R2} = 0$, and implicitly, $T_9 = 0$ and $T_{H_1} \neq 0$ (Figure 2b);
- Case C: *C*3 = 0, $T_{R3} = 0$, and implicitly, $T_8 = 0$ (Figure 2c);
- Case D: *C*2 = *C*3 = 0, $T_{R2} = 0$ and $T_{R3} = 0$, and implicitly, $T_8 = 0$, $T_9 = 0$ and $T_{H_1} \neq 0$ (Figure 2d).

Solving linear system (6), by taking into account the particularities of each case, leads to the torque expressions systematized in Table 2. It can be noticed that the torques in Table 2 have identical expressions in Cases A and B and C and D, respectively, except for the zero input torques; in addition, the torque relations for Cases C and D are obtained through the customization of Cases A and B by considering $k_t = 0$.

Table 2. Expressions of *WSCG* torques related to the four cases (Figures 1 and 2).

	Case A	Case B	Case C	Case D
T_{R2}	$T_{R1}(k_t - 1)$	0	$-T_{R1}$	0
T_{R3}	$-T_{R1}k_t$		0	0
T_{GR}	$-T_{R1}\frac{\left(1-k_t\overline{i_{01}}\right)}{\left(\overline{i_{01}}-1\right)\left(\overline{i_{02}}-1\right)}$		$-T_{R1}\frac{1}{\left(\overline{i_{01}}-1\right)\left(\overline{i_{02}}-1\right)}$	
T_{GS}	$T_{R1}\frac{\left(1-k_t\overline{i_{01}}\right)}{\left(\overline{i_{01}}-1\right)\left(\overline{i_{02}}-1\right)}$		$T_{R1}\frac{1}{\left(\overline{i_{01}}-1\right)\left(\overline{i_{02}}-1\right)}$	
$T_{2'}$	$-T_{R1}\frac{\overline{i_{01}}(k_t-1)}{\overline{i_{01}}-1}$		$T_{R1}\frac{\overline{i_{01}}}{\overline{i_{01}}-1}$	
$T_{2''}$	$-T_{R1}\frac{1-k_t\overline{i_{01}}}{\overline{i_{01}}-1}$		$-T_{R1}\frac{1}{\overline{i_{01}}-1}$	
T_3	$T_{R1}\frac{k_t-1}{\overline{i_{01}}-1}$		$-T_{R1}\frac{1}{\overline{i_{01}}-1}$	
T_4	$T_{R1}\frac{\overline{i_{02}}\left(1-k_t\overline{i_{01}}\right)}{\left(\overline{i_{01}}-1\right)\left(\overline{i_{02}}-1\right)}$		$T_{R1}\frac{\overline{i_{02}}}{\left(\overline{i_{01}}-1\right)\left(\overline{i_{02}}-1\right)}$	
T_{H_1}	$T_{R1}(k_t - 1)$		$-T_{R1}$	

Notes: $T_2 = T_{R1}$, $T_G = T_{GR}$, $T_6 = T_{GR}$, $T_7 = T_{GS}$, $T_8 = T_{R3}$, $T_9 = T_{R2}$ and $T_{H_2} = T_{2''}$.

3.3. Power and Efficiency Modeling in Steady-State Regime

The mechanical power on the speed increaser shafts can be analytically determined by taking into account the kinematic results from Table 1 and the static ones from Table 2, depending on the independent parameters T_{R1}, ω_{R1}, k_t and k_ω. The obtained power relations (i.e., the power $P_i = T_i \cdot \omega_i$ on the *i* shaft, *i* = 1, 2, . . .) are systematized in Table 3 for the four studied cases.

Table 3. *WSCG* power and efficiency expressions for the four cases (Figures 1 and 2).

	Case A	Case B	Case C	Case D
P_{R2}	$-\omega_{R1}T_{R1}k_{\omega}(k_t-1)$	0	$-\omega_{R1}T_{R1}k_{\omega}$	0
P_{R3}	$-\omega_{R1}T_{R1}k_t[i_{01}-k_{\omega}(1-i_{01})]$	$-\omega_{R1}T_{R1}k_t i_{01}$	0	0
P_{GR}	$-\omega_{R1}T_{R1}\frac{\left(1-k_t\overline{i_{01}}\right)[i_{02}(i_{01}-1)(1+k_{\omega})+1]}{\left(\overline{i_{01}}-1\right)\left(\overline{i_{02}}-1\right)}$	$-\omega_{R1}T_{R1}\frac{\left(1-k_t\overline{i_{01}}\right)[i_{02}(i_{01}-1)+1]}{\left(\overline{i_{01}}-1\right)\left(\overline{i_{02}}-1\right)}$	$-\omega_{R1}T_{R1}\frac{i_{02}(i_{01}-1)(1+k_{\omega})+1}{\left(\overline{i_{01}}-1\right)\left(\overline{i_{02}}-1\right)}$	$-\omega_{R1}T_{R1}\frac{i_{02}(i_{01}-1)+1}{\left(\overline{i_{01}}-1\right)\left(\overline{i_{02}}-1\right)}$
P_{GS}	$\omega_{R1}T_{R1}\frac{\left(1-k_t\overline{i_{01}}\right)[i_{01}-k_{\omega}(1-i_{01})]}{\left(\overline{i_{01}}-1\right)\left(\overline{i_{02}}-1\right)}$	$\omega_{R1}T_{R1}\frac{i_{01}\left(1-k_t\overline{i_{01}}\right)}{\left(\overline{i_{01}}-1\right)\left(\overline{i_{02}}-1\right)}$	$\omega_{R1}T_{R1}\frac{i_{01}-k_{\omega}(1-i_{01})}{\left(\overline{i_{01}}-1\right)\left(\overline{i_{02}}-1\right)}$	$\omega_{R1}T_{R1}\frac{i_{01}}{\left(\overline{i_{01}}-1\right)\left(\overline{i_{02}}-1\right)}$
P_G	$-\omega_{R1}T_{R1}\frac{(1-i_{01})(1-i_{02})(1+k_{\omega})\left(1-k_t\overline{i_{01}}\right)}{\left(\overline{i_{01}}-1\right)\left(\overline{i_{02}}-1\right)}$	$-\omega_{R1}T_{R1}\frac{(1-i_{01})(1-i_{02})\left(1-k_t\overline{i_{01}}\right)}{\left(\overline{i_{01}}-1\right)\left(\overline{i_{02}}-1\right)}$	$-\omega_{R1}T_{R1}\frac{(1-i_{01})(1-i_{02})(1+k_{\omega})}{\left(\overline{i_{01}}-1\right)\left(\overline{i_{02}}-1\right)}$	$-\omega_{R1}T_{R1}\frac{(1-i_{01})(1-i_{02})}{\left(\overline{i_{01}}-1\right)\left(\overline{i_{02}}-1\right)}$
P_2	$T_{R1}\omega_{R1}$	$T_{R1}\omega_{R1}$	$T_{R1}\omega_{R1}$	$T_{R1}\omega_{R1}$
$P_{2'}$	$-\omega_{R1}T_{R1}\frac{\overline{i_{01}}(k_t-1)}{\overline{i_{01}}-1}$	$-\omega_{R1}T_{R1}\frac{\overline{i_{01}}(k_t-1)}{\overline{i_{01}}-1}$	$\omega_{R1}T_{R1}\frac{\overline{i_{01}}}{\overline{i_{01}}-1}$	$\omega_{R1}T_{R1}\frac{\overline{i_{01}}}{\overline{i_{01}}-1}$
$P_{2''}$	$-\omega_{R1}T_{R1}\frac{1-k_t\overline{i_{01}}}{\overline{i_{01}}-1}$	$-\omega_{R1}T_{R1}\frac{1-k_t\overline{i_{01}}}{\overline{i_{01}}-1}$	$-\omega_{R1}T_{R1}\frac{1}{\overline{i_{01}}-1}$	$-\omega_{R1}T_{R1}\frac{1}{\overline{i_{01}}-1}$
P_3	$\omega_{R1}T_{R1}\frac{[i_{01}-k_{\omega}(1-i_{01})](k_t-1)}{\overline{i_{01}}-1}$	$\omega_{R1}T_{R1}\frac{i_{01}(k_t-1)}{\overline{i_{01}}-1}$	$-\omega_{R1}T_{R1}\frac{i_{01}-k_{\omega}(1-i_{01})}{\overline{i_{01}}-1}$	$-\omega_{R1}T_{R1}\frac{i_{01}}{\overline{i_{01}}-1}$
P_4	$\omega_{R1}T_{R1}\frac{\overline{i_{02}}\left(1-k_t\overline{i_{01}}\right)[i_{01}-k_{\omega}(1-i_{01})]}{\left(\overline{i_{01}}-1\right)\left(\overline{i_{02}}-1\right)}$	$\omega_{R1}T_{R1}\frac{i_{01}\overline{i_{02}}\left(1-k_t\overline{i_{01}}\right)}{\left(\overline{i_{01}}-1\right)\left(\overline{i_{02}}-1\right)}$	$\omega_{R1}T_{R1}\frac{\overline{i_{02}}[i_{01}-k_{\omega}(1-i_{01})]}{\left(\overline{i_{01}}-1\right)\left(\overline{i_{02}}-1\right)}$	$\omega_{R1}T_{R1}\frac{i_{01}\overline{i_{02}}}{\left(\overline{i_{01}}-1\right)\left(\overline{i_{02}}-1\right)}$
η	$\frac{(i_{01}-1)(i_{02}-1)\left(1-k_t\overline{i_{01}}\right)}{\left(\overline{i_{01}}-1\right)\left(\overline{i_{02}}-1\right)(1-k_t i_{01})}$		$\frac{(i_{01}-1)(i_{02}-1)}{\left(\overline{i_{01}}-1\right)\left(\overline{i_{02}}-1\right)}$	

Notes: $P_2=P_{R1}$, $P_6=P_{GR}$, $P_7=P_{GS}$, $P_8=P_{R3}$, $P_9=P_{R2}$, $P_{H_1}=P_{R2}$ and $P_{H_2}=P_{2''}$.

Starting from the efficiency expression in Case A, in the hypothesis of wind rotors operating as motors (i.e., $P_{Ri} > 0$, i = 1, 2, 3):

$$\eta = -\frac{P_G}{P_{R1} + P_{R2} + P_{R3}} = -\frac{\omega_{GR} T_{GR} + \omega_{GS} T_{GS}}{\omega_{R1} T_{R1} + \omega_{R2} T_{R2} + \omega_{R3} T_{R3}} \tag{7}$$

the efficiencies of the other speed increasers (Cases B, C and D) are obtained by customization; the analytical relations for the efficiency in the four cases are also systematized in Table 3.

4. Numerical Simulations and Discussions

The *WSCG* analytical model, described by the relations in Tables 1–3, contains eight independent parameters: the interior kinematic ratios i_{01} and i_{02}, the interior efficiencies η_{01} and η_{02}, the primary wind rotor power parameters (ω_{R1} and T_{R1}) and the ratios k_ω and k_t. The numerical simulations are based on the input data from Table 4, where i_{01}, i_{02}, η_{01} and η_{02} are constant parameters of the mechanical transmission, k_ω and k_t are independent parameters used as variable simulation ratios whose values can be controlled by appropriately adjusting the pitch angles of the wind rotor blades.

Table 4. Input data for the numerical simulations of the analytical model.

Planetary Gear Set	i_0	η_0	$k_\omega = -\frac{\omega_{R2}}{\omega_{R1}}$	$k_t = -\frac{T_{R3}}{T_{R1}}$
I	−1.5	0.8836 (=0.94^2)	−0.5 . . . 1	-
II	−5	0.925 (=0.95^2)	-	0 . . . 1.5

The numerical simulations are performed under the following assumptions:

- Both secondary rotors (R2 and R3) rotate in opposite directions to the primary rotor R1 (by exception, rotor R2 may also have the rotation direction of rotor R1, a situation highlighted in Section 4.1);
- The powers of rotors R1, R2 and R3 are input powers for the transmission, i.e., $P_{R1} > 0$, $P_{R2} > 0$ and $P_{R3} > 0$ (but there are also exceptions in which rotor R2 becomes the brake, i.e., $P_{R2} < 0$, as highlighted in Section 4.2);
- The counter-rotating electric generator G is characterized by the operating speed $\omega_G = \omega_{GR} - \omega_{GS}$, the torque $T_G = T_{GR} = -T_{GS}$ and by the mechanical power $P_G = T_G \omega_G$ (considered as the transmission output power, i.e., $P_G = T_G \omega_G < 0$, Figure 2);
- In order to simplify the comparative energy analysis of the selected cases, the mechanical characteristics related to the wind rotors and the generator are disregarded; as a result, the power of the primary rotor R1 will be further considered as the reference power, and the other powers will be expressed by ratios of the type P_x / P_{R1}, whatever the x shaft, called reduced powers (at the primary rotor).

4.1. Transmission Input Powers and Efficiency

The analysis of the diagrams depicted in Figures 3–6 allows the following particularities to emerge:

(a) The ratios k_ω and k_t directly influence the operation state of the secondary wind rotors R2 and R3 and the mechanical power flow through the planetary transmission implicitly; thus, for Case A, the variation ranges of these ratios for which the wind system operation makes sense are further analyzed, i.e., the secondary wind rotors R2 and R3 are motor sources (P_{R2} > 0 and P_{R3} > 0).

(b) In the premise P_{R1} > 0, the angular speed and the torque of the rotor R2 (controlled by k_ω and k_t) also influence the power of the secondary wind rotor R3 (Figures 3 and 4).

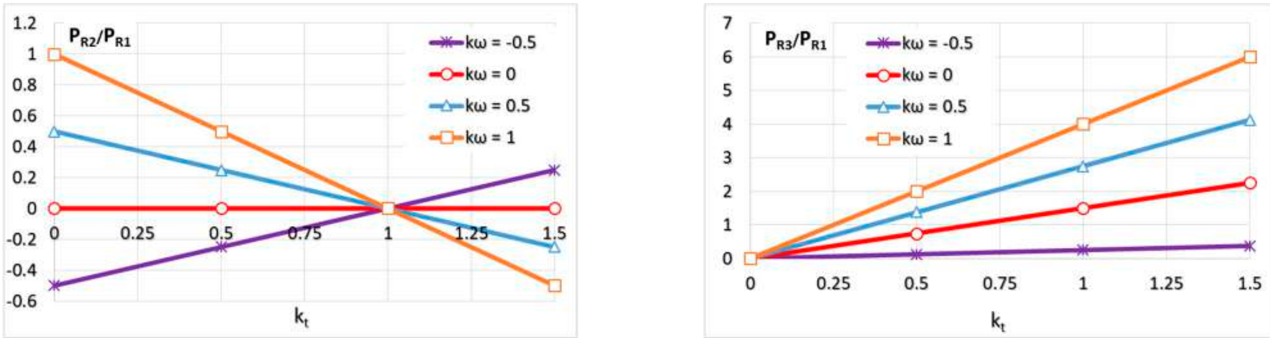

(**a**) (**b**)

Figure 3. Reduced input power variations depending on the ratio k_t for various values of ratio k_ω: (**a**) reduced power of the wind rotor R2; (**b**) reduced power of the wind rotor R3 (Case A).

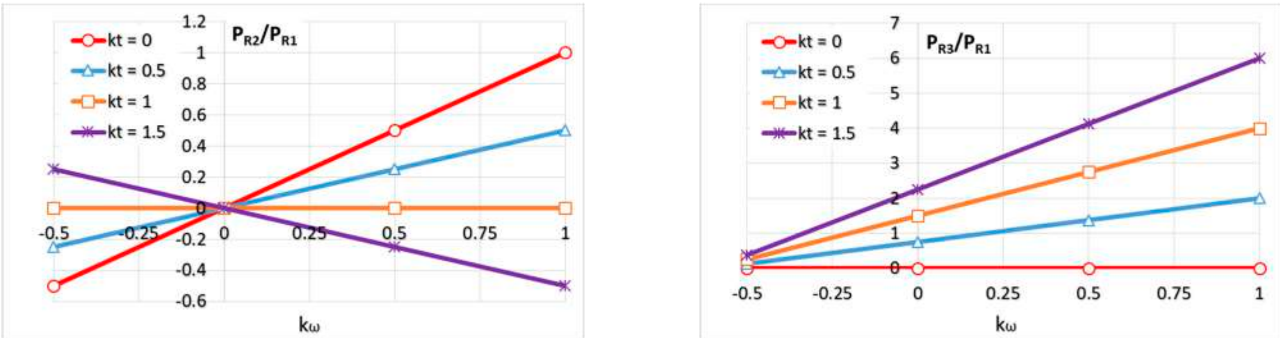

(**a**) (**b**)

Figure 4. Reduced input power variations depending on the ratio k_ω for various values of ratio k_t: (**a**) reduced power of the wind rotor R2; (**b**) reduced power of the wind rotor R3 (Case A).

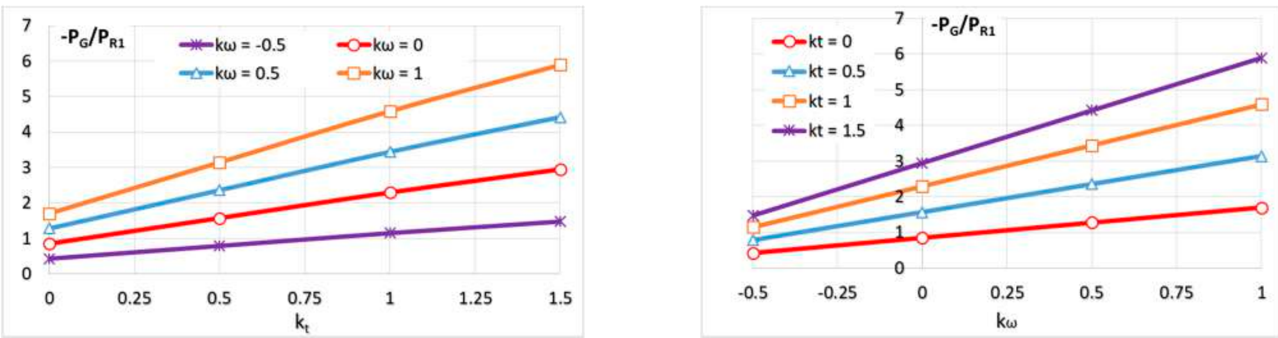

(**a**) (**b**)

Figure 5. Variations of the electric generator reduced power, depending on: (**a**) the ratio k_t; (**b**) the ratio k_ω (Case A).

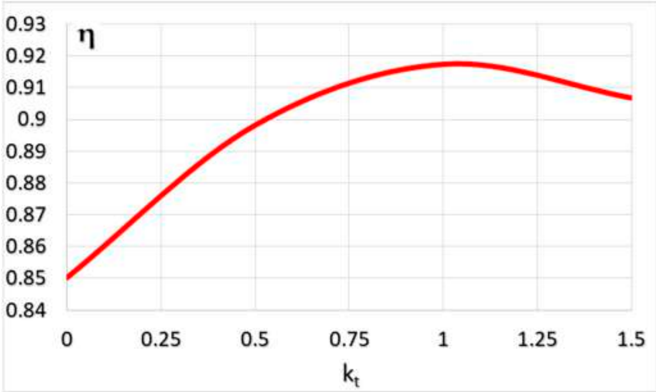

Figure 6. Variations of the planetary transmission efficiency, depending on k_t (Case A).

(c) Rotor $R2$ is the most reactive to the variations of k_ω and k_t, which can change its state from the motor mode ($P_{R2} > 0$) to the brake mode ($P_{R2} < 0$) (Figures 3a and 4a); additionally, the power of rotor $R2$ is cancelled for $k_t = 1$, irrespective of the k_ω value.

(d) At normal operations ($k_\omega > 0$), rotor $R2$ works in the motor mode only for $k_t < 1$, becoming a brake for $k_t > 1$; for $k_\omega < 0$ (i.e., rotor $R2$ rotates in the same direction as the primary rotor $R1$), $R2$ becomes the motor only if $k_t > 1$ (see the line $k_\omega = -0.5$ in Figure 3a).

(e) Rotor $R3$ always operates in the motor mode ($P_{R3} > 0$), irrespective of the k_t and k_ω values (Figures 3b and 4b); the power P_{R3} increases linearly with the increase of k_t, while the slope of line P_{R3} increases with k_ω.

(f) The maximum power generated by rotor $R3$ ($P_{R3} = 6P_{R1}$ for $k_t = 1.5$ and $k_\omega = 1$, Figure 3b) is significantly higher than the maximum power of rotor $R2$ ($P_{R2} = P_{R1}$ for $k_t = 0$ and $k_\omega = 1$, Figure 3a).

(g) The mechanical power received by the generator increases linearly with the increase of the ratios k_t and k_ω (Figure 5), even in the brake mode of rotor $R2$ ($P_{R2} < 0$ for $k_t > 1$ and $k_\omega > 0$, Figure 3a).

(h) The transmission efficiency does not depend on the ratio k_ω (see Table 3), but it is influenced by ratio k_t, with a maximum value of 0.917 for $k_t = 1$ (Figure 6), i.e., when the energy contribution of rotor $R2$ is zero ($P_{R2} = 0$, Figure 3a).

In conclusion, as k_t and k_ω increase, the mechanical power supplied to the electric generator increases as well, with a higher input brought about by wind rotor $R3$ (Figures 3 and 4). The diagrams depicted in Figures 3–6 allow highlighting the particular cases in which the ratios k_t and k_ω become null; by customization, the type A systems become types B ($k_\omega = 0$), C ($k_t = 0$) and D ($k_\omega = 0$, $k_t = 0$).

4.2. Power Flow

In all four cases, the speed increaser contains a branched circuit of mechanical power, and the direction of the power flow in each branch depends on the k_t and k_ω values; moreover, the three-rotor version (Case A) allows obtaining the other three cases by appropriate customizations: Case B ($\omega_{R2} = \omega_9 = \omega_{H_1} = 0$), Case C ($T_{R3} = T_8 = 0$) and Case D ($\omega_{R2} = \omega_9 = \omega_{H_1} = 0$ and $T_{R3} = T_8 = 0$).

The power flow is further analyzed comparatively, considering the input data from Table 4 and certain representative values $k_\omega \in \{0, 0.5, 1\}$ and $k_t \in \{0, 0.5, 1, 1.5\}$. According to Table 3, the powers in Case A depend on both the ratio k_t and k_ω; in Case B, only on k_t, and in Case C, only on k_ω, while, in Case D, they are not influenced by these ratios.

- Case A

Six distinct simulation variants, defined by the distinct combinations of the k_t and k_ω values, are addressed in Case A (see Figure 2a). The numerical results on the power flow are depicted in Figure 7, and the values of certain representative parameters are shown in Table 5. Based on the obtained data, the following aspects can be highlighted:

- The secondary rotors $R2$ and $R3$ influence each other when the pitch angle changes, their powers depending on both ratios k_ω (adjustment for $R2$) and k_t (adjustment for $R3$).
- Ratio k_t significantly influences both the power values and the directions of the power flows as follows:
  - $k_t = 0$: that is, Case C, in which the energetic contribution of rotor $R3$ is zero, such as $T_{R3} = 0$;
  - $0 < k_t < 1$ (red lines, Figure 7a,b): the powers of rotors $R1$, $R2$ and $R3$ flow branched and convergent towards the rotor and stator of the generator;

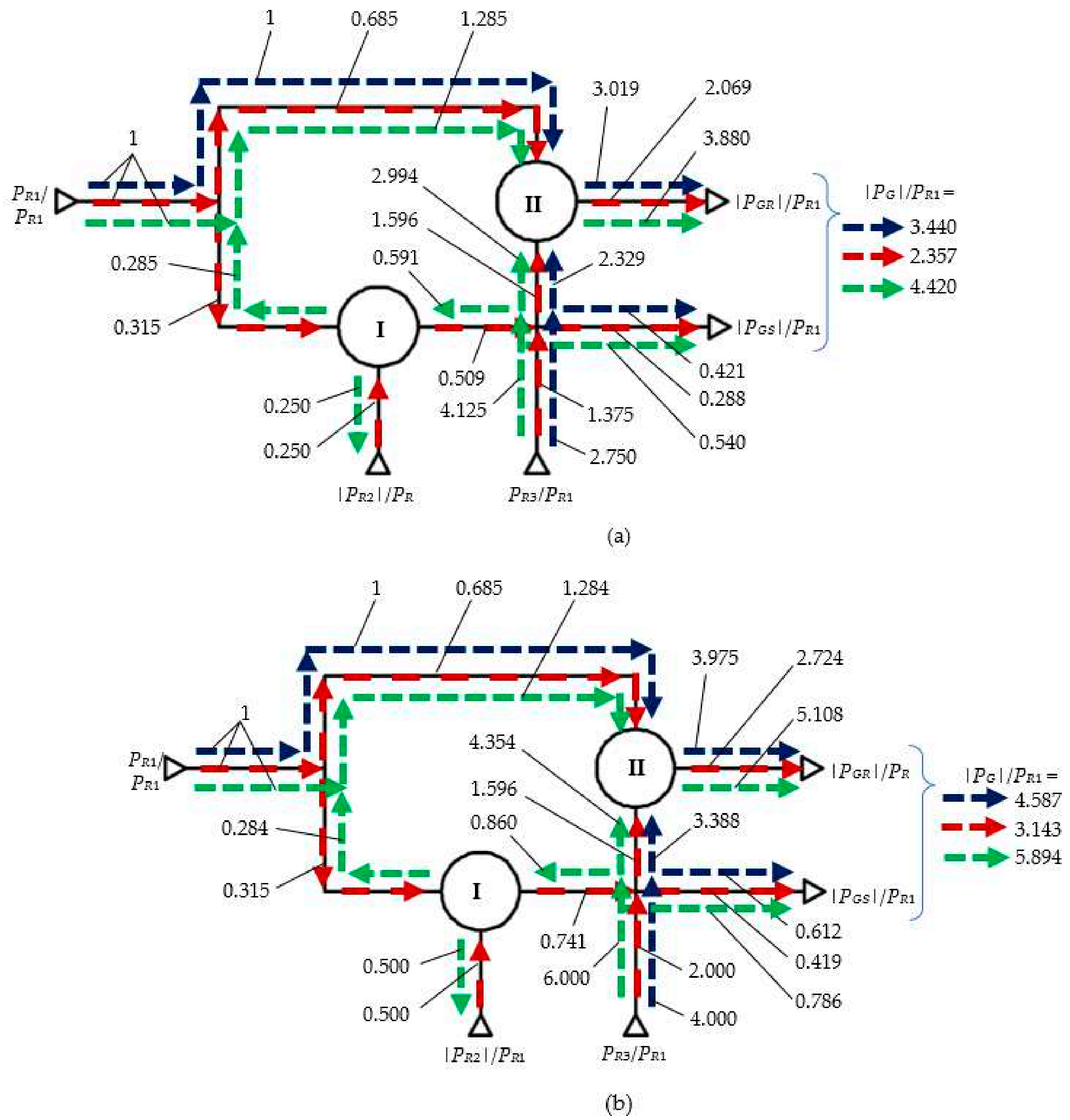

Figure 7. Reduced power flows of the 2-DOF and $L = 5$ system (Case A) for: (**a**) $k_t = 0.5$ (red), 1 (blue), 1.5 (green) and $k_\omega = 0.5$; (**b**) $k_t = 0.5$ (red), 1 (blue), 1.5 (green) and $k_\omega = 1$.

- $k_t = 1$ (blue lines, Figure 7a,b): in this limit situation (when $T_{R2} = 0$ and $P_{R2} = 0$, see Tables 2 and 3), rotor *R*2 and the planetary gear set I are idling, and the power of rotor *R*1 flows through gear set II to *GR*, while the power of the rotor *R*3 branches into two flows: one directly to *GS* and another, through gear set II, to *GR*. It can be noticed that both the mechanical power of the generator and the transmission efficiency are higher compared with the previous situation ($0 < k_t < 1$);
- $k_t > 1$ (green lines, Figure 7a,b): the power flow of rotor *R*1 is transmitted entirely through gear set II to *GR*, while the power of rotor *R*3 branches into four streams: a first flow directly to *GS*, a second flow through gear set II to *GR*, a third flow through gear sets I and II also towards *GR* and a fourth flow through gear set I towards rotor *R*2, which passes in the brake mode, with the reversal of the power flow direction through planetary gear set I; although rotor *R*2 becomes the brake (reverse direction of P_{R2} flow), the power received by the generator increases, while the transmission efficiency decreases (see Table 5).
  - The power $|P_G|$ received by the electric generator increases with the increase of the ratio k_t.
  - The power supply to the mobile stator *GS* increases with the increase of ratio k_ω (i.e., from 10% P_G for $k_\omega = 0$ to 13.3% P_G for $k_\omega = 1$).
  - The amplification ratio i_a does not depend on ratio k_t and increases with the increase of ratio k_ω (i.e., from 15 for $k_\omega = 0$ to 30 for $k_\omega = 1$, Table 5).
- Case B

Case B (Figure 2b) is derived from Case A by engaging clutch C1 (i.e., C1 = 1) and disengaging clutch C2 (i.e., C2 = 0 => $T_{R2} = 0$), accompanied by rotor *R*2 blocking ($\omega_{R2} = 0$ => $k_\omega = 0$). Comparing the best scenarios in Case A ($k_\omega = 1$ and $k_t = 1$) and in Case B ($k_t = 1$, see Table 5 and Figure 8): the rotor *R*3 power decreases about 2.66 times, the total input power and the output power decrease two times and the power input of the stator *GS* decreases to 10% of P_G.

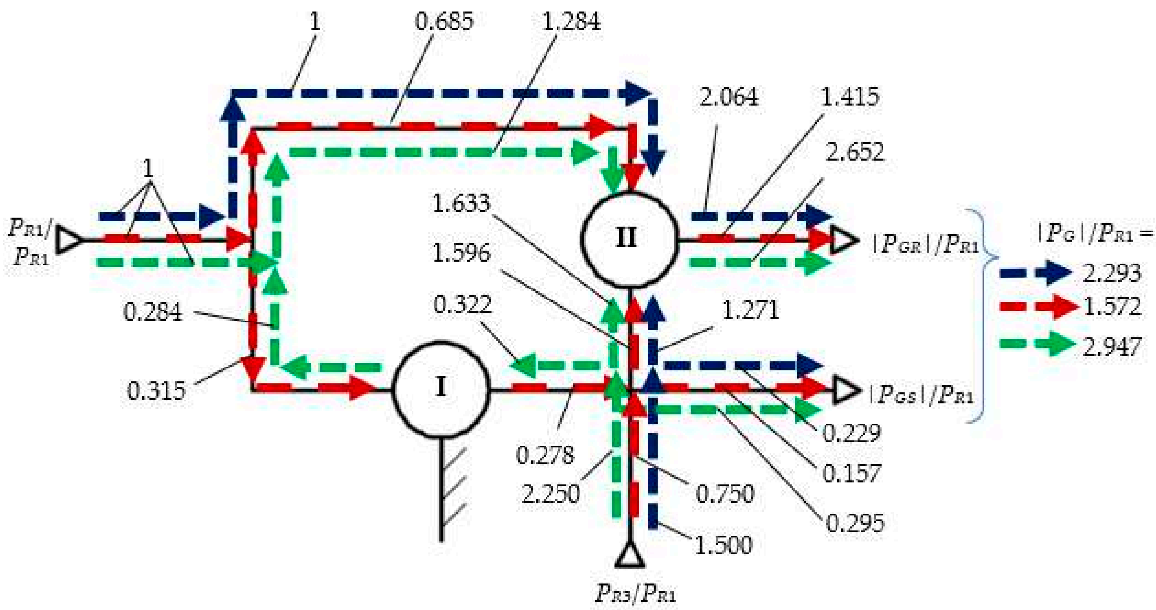

Figure 8. Reduced power flows of the 1-DOF and $L = 4$ system (Case B) for: $k_t = 0.5$ (red), 1 (blue) and 1.5 (green).

- Case C

Case C (Figure 2c) is obtained from Case A by eliminating rotor *R*3 ($T_{R3} = 0$ => $k_t = 0$) and the flows related to it; according to Figure 9, the flow corresponding to the value $k_\omega = 0$ is missing, because in this situation, Case C turns into Case D.

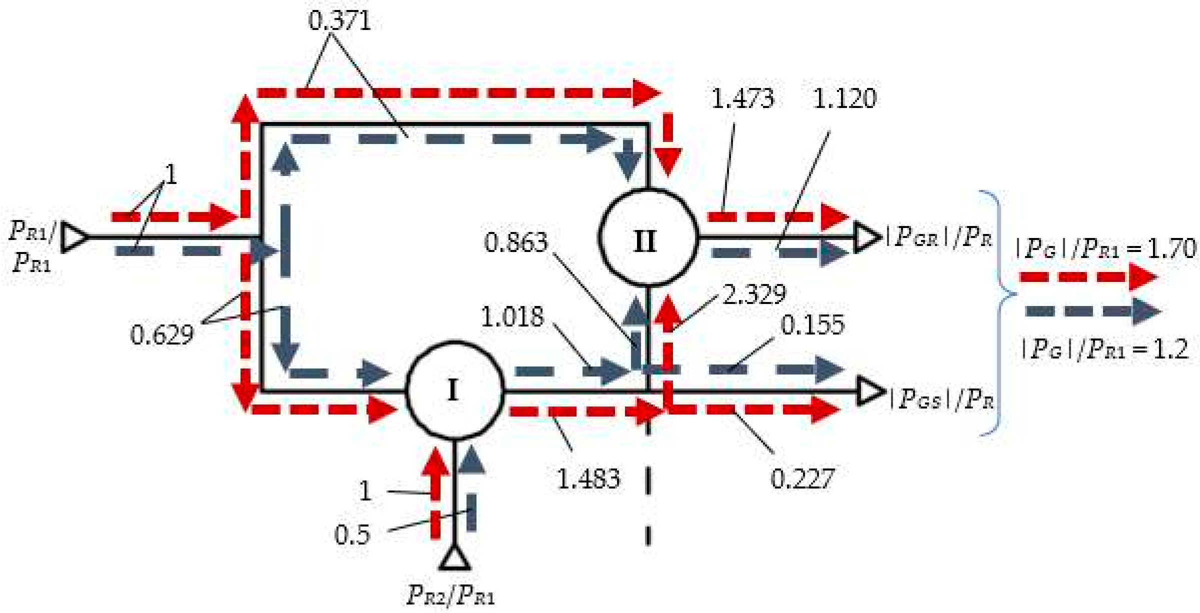

Figure 9. Reduced power flows of the 2-DOF and L = 4 system (Case C) for $k_\omega = 0.5$ (blue) and 1 (red).

Table 5. Performances of the four *WSCGs* for certain representative numerical scenarios.

Case	DOF	No WRs	k_t	k_ω	i_a	P_{R2}/P_{R1}	P_{R3}/P_{R1}	P_{in}/P_{R1}	$\lvert P_G \rvert/P_{R1}$	η	P_{GS}/P_G
A	2	3	0.5	1	30	0.500	2.000	3.500	3.143	0.898	13.3%
			1	1	30	0	4.000	5.000	4.587	0.917	13.3%
			1	0.5	22.5	0	2.750	3.750	3.440	0.917	12.2%
B	1	2	0.5	0	15	0	0.750	1.750	1.572	0.898	10.0%
			1	0	15	0	1.500	2.500	2.293	0.917	10.0%
C	2	2	0	0.5	22.5	0.500	0	1.500	1.275	0.850	12.2%
			0	1	30	1.000	0	2.000	1.700	0.850	13.3%
D	1	1	0	0	15	0	0	1.000	0.850	0.850	10.0%

Since ratio k_t intervenes in the relation of the torques, powers and transmission efficiency (see Tables 2 and 3), Case C ($k_t = 0$) is characterized by the following particularities (Figure 9 and Table 5):

- the torque of the rotor $R2$ is equal, in absolute value, to that of the primary rotor $R1$; as a result, the power generated by $R2$ increases with the increase of the k_ω ratio;
- the input powers (P_{R1} and P_{R2}) flow into three branches directly toward the rotor GR and stator GS;
- the transmission efficiency is constant (η = 0.85), regardless of the value of the ratio k_ω;
- the power supply to the stator GS increases with the increase of k_ω: from 12.1% P_G for $k_\omega = 0.5$ to 13.3% P_G for $k_\omega = 1$.

- Case D

Case D (Figure 2d) is derived from Case A by removing rotors $R2$ and $R3$, i.e., $k_\omega = 0$, $k_t = 0$; rotor $R1$ delivers a power whose flow (Figure 10) is similar to the homologous flow from Case C (see Figure 9). The system ensures a power supply of the stator GS of 10% of P_G and a constant efficiency (η = 0.85).

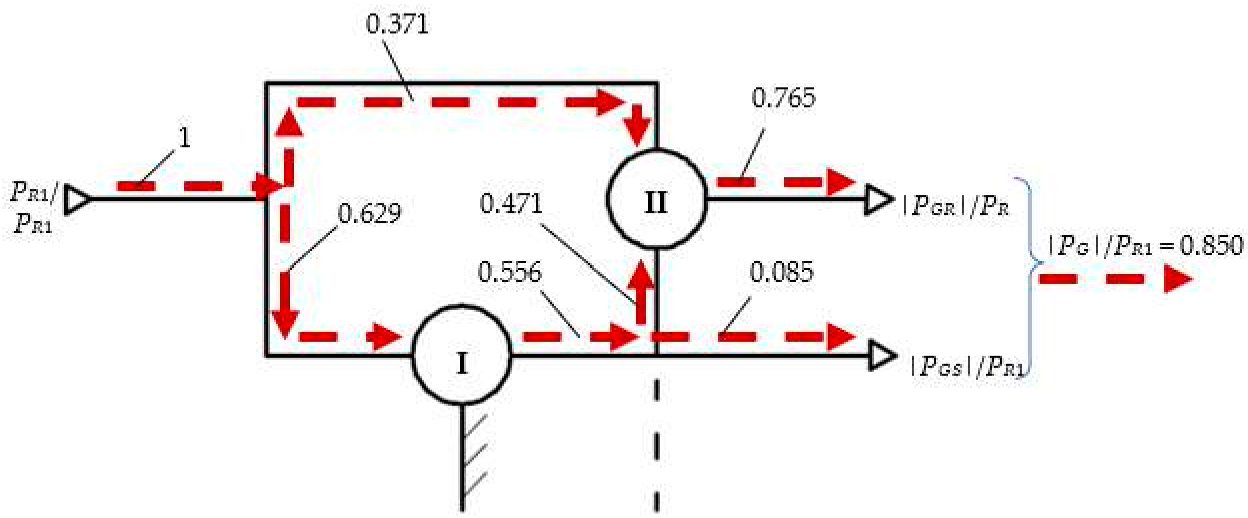

Figure 10. Reduced power flows of the 1-DOF and $L = 3$ system (Case D).

According to Table 5, both the structure's degree of freedom and the number of wind rotors have a major influence on the output power (to the generator) and on the input powers, as well as on the power distribution between secondary rotors $R2$ and $R3$, with a consistent increase for $R3$ in Case A. It should be noted that the 2-DOF transmissions double the speed amplification ratio ($i_a = 30$ for $k_\omega = 1$) compared to the 1-DOF ones ($i_a = 15$ for $k_\omega = 0$); a similar trend has the energy supply brought about by mobile stator GS (see the P_{GS}/P_G ratio in Table 5). Being independent of the ratio k_ω and highly dependent on k_t, the transmission efficiency is higher in Cases A and B ($\eta = 0.917$, $k_t = 1$) vs. Cases C and D ($\eta = 0.850$, $k_t = 0$). The performances of the turbines with two wind rotors and 1-DOF (Case B) or 2-DOF (Case C) speed increasers significantly depend on k_t and k_ω; for the considered data, the 1-DOF transmission (Case B) shows a superior performance when $k_t = 1$ and $k_\omega = 1$.

5. Conclusions

This paper presented a comparative analysis of the performances of four different types of wind turbines with a counter-rotating electric generator. To this end, a differential planetary transmission with a variable structure, derived from an innovative solution proposed by the authors, was firstly proposed. By appropriate combinations of engaging/disengaging of the clutches, the transmission can operate in various structures, of which four cases were selected for analysis: a system with three rotors and a 2-DOF speed increaser (Case A), a 1-DOF system with two counter-rotating wind rotors (Case B), a 2-DOF system with two counter-rotating wind rotors (Case C) and 1-DOF system with a single wind rotor.

Archetype models for speeds, torques, powers and the efficiency of the planetary transmission with a variable structure used as speed increaser in the general case of differential transmission with three inputs (Case A) were developed. The analytical models of the other three cases (B, C and D) were the result of customizing the archetype models based on the correlations specific to each case according to the engaging/disengaging of the component clutches.

The analysis of the numerical results obtained by the simulations of the analytical models of the four *WSCGs*, considering a set of representative values for the simulation ratios k_t and k_ω, allowed drawing the following conclusions:

- the wind turbine with three wind rotors (Case A) allows the increase of the output powers (towards the electric generator) and of the input one compared to those with two counter-rotating wind rotors (Cases B and C); in turn, the systems in Cases B and

C can ensure a better use of the wind potential compared to traditional single-rotor wind turbines (Case D);

- the reduced input powers (corresponding to secondary wind rotors R2 and R3) and the reduced output power, as well as the configuration of the power flows, depend, to a large extent, on the values of ratios k_t and k_ω;
- the transmission efficiency is constant in Cases C and D, because it does not depend on the operating speed nor on the transmitted power; instead, the efficiency in Cases A and B changes with ratio k_t;
- thanks to the property of "summing up" the speeds, the 2-DOF systems (Cases A and C) can offer higher amplification ratios (i_a) than the 1-DOF ones and can implicitly ensure a higher power supply by the stator GS;
- the turbines with two wind rotors (Cases B and C) can have comparable power performances, the 1-DOF system (Case B) being advantaged with superior powers and efficiency in the vicinity of the value $k_t = 1$. The differential system (Case C) achieves higher amplification ratios, accompanied by relatively high powers, as the ratio k_ω increases;
- the maximum input power supply being brought about by rotor R3; the most interesting energy aspects are found in Case A in the vicinity of ratio value $k_t = 1$ for the situation $k_\omega = 0$. Practically, this means a 2-DOF system with two rotors, R1 and R3, were obtained from the case with three wind rotors by removing rotor R2 (i.e., Case B); it is also interesting that, in this system (Figure 1a without rotor R2), planetary gear set I idles (it does not participate in the transmission of the torque and of the power implicitly).

The authors intend to develop this topic more in the future by analyzing the CRWT behavior in dynamic conditions, the transient effects of changing the wind speed, by considering wind turbines and electric generators with known functional characteristics. The experimental validation of these theoretical results is also a future purpose of the authors.

Author Contributions: Conceptualization, M.N., R.S. and C.J.; methodology, M.N., R.S. and O.M.; software, R.S. and N.C.; validation, M.N., R.S., C.J. and O.M.; formal analysis, M.N., R.S., C.J. and O.M.; investigation, M.N., R.S., O.M. and N.C.; writing—original draft preparation, M.N., R.S, C.J. and O.M.; writing—review and editing, M.N., R.S., C.J., O.M. and N.C.; visualization, M.N., R.S., C.J., O.M. and N.C. and supervision, M.N. and C.J. All authors have read and agreed to the published version of the manuscript.

Funding: This research received no external funding.

Institutional Review Board Statement: Not applicable.

Informed Consent Statement: Not applicable.

Data Availability Statement: Not applicable.

Conflicts of Interest: The authors declare no conflict of interest.

Nomenclature

Acronyms	
DOF	Degree of freedom
GR	Generator rotor
GS	Generator stator
WR	Wind rotor
WT	Wind turbine
WSCG	Wind system with counter-rotating generator

Symbols

$C1{,}2{,}3$	Clutch no 1, 2, 3
G	Electric generator
$H_{1,2}$	Satellite carrier no 1, 2
i	Kinematic ratio ($i_{xy} = \omega_x/\omega_y$)
i_0	Interior kinematic ratio
$\overline{i_0}$	Interior static ratio
i_a	Amplification kinematic ratio ($i_a = \omega_G/\omega_{R1}$)
I	Bevel planetary gear set
II	Spur planetary gear set
k_t	Ratio of the input moments ($k_t = -T_{R3}/T_{R1}$)
k_ω	Ratio of the input angular speeds ($k_\omega = -\omega_{R2}/\omega_{R1}$)
L	Total number of external links
P	Power
P_{in}	Sum on the input (positive) powers
$R1{,}2{,}3$	Wind rotor no 1, 2, 3
T	Torque
z	Gear teeth number
η	Mechanical efficiency
η_0	Internal mechanical efficiency
ω	Angular speed

References

1. Oprina, G.; Chihaia, R.A.; El-Leathey, L.A.; Nicolaie, S.; Babutanu, C.A.; Voina, A. A review on counter-rotating wind turbines development. *J. Sustain. Energy* **2016**, *7*, 91–98.
2. Didane, D.H.; Rosly, N.; Zulkafli, M.F.; Shamsudin, S.S. Performance evaluation of a novel vertical axis wind turbine with coaxial contra-rotating concept. *Renew. Energy* **2018**, *115*, 353–361. [CrossRef]
3. Pacholczyk, M.; Karkosinski, D. Parametric Study on a Performance of a Small Counter-Rotating Wind Turbine. *Energies* **2020**, *13*, 3880. [CrossRef]
4. West, R. Wind Turbine System. U.S. Patent 10,316,820 B2, 11 June 2019.
5. Neagoe, M.; Saulescu, R.; Jaliu, C. Design and Simulation of a 1 DOF Planetary Speed Increaser for Counter-Rotating Wind Turbines with Counter-Rotating Electric Generators. *Energies* **2019**, *12*, 1754. [CrossRef]
6. Saulescu, R.; Neagoe, M.; Jaliu, C. Conceptual Synthesis of Speed Increasers for Wind Turbine Conversion Systems. *Energies* **2018**, *11*, 2257. [CrossRef]
7. Mirnikjoo, S.; Abbaszadeh, K.; Abdollahi, S.E. Multi-Objective Design Optimization of a Double-Sided Flux Switching Permanent Magnet Generator for Counter-Rotating Wind Turbine Applications. *IEEE Trans. Ind. Electron.* **2020**, *68*, 6640–6649. [CrossRef]
8. Kutt, F.; Blecharz, K.; Karkosinski, D. Axial-Flux Permanent-Magnet Dual-Rotor Generator for a Counter-Rotating Wind Turbine. *Energies* **2020**, *13*, 2833. [CrossRef]
9. Neagoe, M.; Saulescu, R.; Jaliu, C.; Cretescu, N. Novel Speed increaser used in counter-rotating wind turbines. In *New Advances in Mechanisms, Mechanical Transmissions and Robotics*; Mechanisms and Machine Science Series; Springer: Berlin, Germany, 2017; Volume 46, pp. 143–151. [CrossRef]
10. Giger, U.; Kleinhansl, S.; Schulte, H. Design Study of Multi-Rotor and Multi-Generator Wind Turbine with Lattice Tower—A Mechatronic Approach. *Appl. Sci.* **2021**, *11*, 11043. [CrossRef]
11. Cho, W.; Lee, K.; Choy, I.; Back, J. Development and experimental verification of counter-rotating dual rotor/dual generator wind turbine: Generating, yawing and furling. *Renew. Energy* **2017**, *114*, 644–654. [CrossRef]
12. Jelaska, D.; Podrug, S.; Perkušic, M. A novel hybrid transmission for variable speed wind turbines. *Renew. Energy* **2015**, *83*, 78–84. [CrossRef]
13. Qiu, J.; Liu, B.; Dong, H.; Wang, D. Type Synthesis of Gear-box in Wind Turbine. *Procedia Comput. Sci.* **2017**, *109*, 809–816. [CrossRef]
14. Saulescu, R.; Jaliu, C.; Munteanu, O.; Climescu, O. Planetary Gear for Counter-Rotating Wind Turbines. *Appl. Mech. Mater.* **2014**, *658*, 135–140. [CrossRef]
15. Saulescu, R.; Jaliu, C.; Climescu, O.; Diaconescu, D. On the use of 2 DOF planetary gears as "speed increaser" in small hydros and wind turbines. In Proceedings of the ASME International Design Engineering Technical Conferences & Computers and Information in Engineering Conference IDETC/CIE 2011, Washington, DC, USA, 25–31 August 2011; pp. 601–610. [CrossRef]
16. Vasel-Be-Hagh, A.; Archer, C.L. Wind farms with counter-rotating wind turbines. *Sustain. Energy Technol. Assess.* **2017**, *24*, 19–30. [CrossRef]
17. Blanco, J.; Rodriguez, J.D.; Couce, A.; Lamas, M.I. Proposal of a Nature-Inspired Shape for a Vertical Axis Wind Turbine and Comparison of Its Performance with a Semicircular Blade Profile. *Appl. Sci.* **2021**, *11*, 6198. [CrossRef]
18. Pfaffel, S.; Faulstich, S.; Rohrig, K. Performance and Reliability of Wind Turbines: A Review. *Energies* **2017**, *10*, 1904. [CrossRef]

19. Fan, G.-F.; Qing, S.; Wang, H.; Hong, W.-C.; Li, H.-J. Support Vector Regression Model Based on Empirical Mode Decomposition and Auto Regression for Electric Load Forecasting. *Energies* **2013**, *6*, 1887–1901. [CrossRef]
20. Hong, W.C.; Fan, G.F. Hybrid Empirical Mode Decomposition with Support Vector Regression Model for Short Term Load Forecasting. *Energies* **2019**, *12*, 1093. [CrossRef]
21. Zhiqiang, L.; Yunke, W.; Jie, H.; Zhihong, Z.; Wenqi, C. The study on performance and aerodynamics of micro counter-rotating HAWT. *Energy* **2018**, *161*, 939–954. [CrossRef]
22. Lam, H.F.; Peng, H.Y. Measurements of the wake characteristics of co- and counter-rotating twin H-rotor vertical axis wind turbines. *Energy* **2017**, *131*, 13–26. [CrossRef]
23. Lipian, M.; Dobrev, I.; Massouh, F.; Jozwik, K. Small wind turbine augmentation: Numerical investigations of shrouded- and twin-rotor wind turbines. *Energy* **2020**, *201*, 117588. [CrossRef]
24. Bani-Hani, E.; Sedaghat, A.; Saleh, A.; Ghulom, A.; Al-Rahmani, H.; Al-Zamel, S.; Lopez, J. Evaluating Performance of Horizontal Axis Double Rotor Wind Turbines. *Energy Eng.* **2019**, *116*, 26–40. [CrossRef]
25. Erturk, E.; Sivrioglu, S.; Bolat, F. Analysis Model of a Small Scale Counter-Rotating Dual Rotor Wind Turbine with Double Rotational Generator Armature. *Int. J. Renew. Energy Res.* **2018**, *8*, 1849–1858. [CrossRef]
26. Pamuji, D.; Bramantya, M. Numerical Study on the Performance of 2-Bladed and 3-Bladed Counter Rotating Wind Turbines. *J. Jpn. Soc. Appl. Electromagn. Mech.* **2019**, *27*, 169–174. [CrossRef]
27. Neagoe, M.; Jaliu, C.; Saulescu, R.; Simionescu, P. Steady-State Response of a Dual-Rotor Wind Turbine with Counter-Rotating Electric Generator and Planetary Gear Increaser. In Proceedings of the MSR 2020 USCToMM Symposium on Mechanical Systems and Robotics, Rapid City, SD, USA, 14–16 May 2020; pp. 106–115. [CrossRef]
28. Fan, Z.; Zhu, C.; Li, X.; Liang, C. The transmission characteristic for the improved wind turbine gearbox. *Energy Sci. Eng.* **2019**, *7*, 1368–1378. [CrossRef]
29. Chaichana, T.; Chaitep, S. Performance Evaluation of Co-Axis Counter-Rotation Wind Turbine. *Energy Procedia* **2015**, *79*, 149–156. [CrossRef]
30. Didane, D.H.; Kudam, D.; Zulkafli, M.F.; Mohd, S.; Batcha, M.F.M.; Khalid, A. Development and Performance Investigation of a Unique Dual-rotor Savonius-type Counter-rotating Wind Turbine. *Int. J. Integr. Eng.* **2021**, *13*, 89–98. [CrossRef]
31. Didane, D.H.; Rosly, N.; Zulkafli, M.F.; Shamsudin, S.S. Numerical investigation of a novel contra-rotating vertical axis wind turbine. *Sustain. Energy Technol. Assess.* **2019**, *31*, 43–53. [CrossRef]
32. Cao, Y.; Han, Z.; Zhou, D.; Lei, H. Aerodynamic Performance of Counter-Rotating Vertical Axis Wind Turbine. *J. Shanghai Jiaotong Univ. Sci.* **2021**, *55*, 141–148. [CrossRef]
33. Ilmunandar, A.M.; Bramantya, M.A. Experimental Study of Counter Rotating Wind Turbine (Full Scale, R = 1.5 M) with Single Generator Using Gearbox. *Int. J. Sci. Technol. Res.* **2019**, *8*, 346–351.
34. Koehuan, V.; Sugiyono, S.; Kamal, S. Investigation of Counter-Rotating Wind Turbine Performance using Computational Fluid Dynamics Simulation. *IOP Conf. Ser. Mater. Sci. Eng.* **2017**, *267*, 12034. [CrossRef]
35. Li, Q.; Maeda, T.; Kamada, Y.; Murata, J.; Furukawa, K.; Yamamoto, M. Effect of number of blades on aerodynamic forces on a straight-bladed Vertical Axis Wind Turbine. *Energy* **2015**, *90*, 784–795. [CrossRef]
36. Maleki Dastjerdi, S.; Gharali, K.; Al-Haq, A.; Nathwani, J. Application of Simultaneous Symmetric and Cambered Airfoils in Novel Vertical Axis Wind Turbines. *Appl. Sci.* **2021**, *11*, 8011. [CrossRef]
37. Mirnikjoo, S.; Asadi, F.; Abbasazdeh, K.; Abdollahi, S.E. Effect of Rotor Topology on the Performance of Counter-Rotating Double-Sided Flux Switching Permanent Magnet Generator. *IEEE Trans. Energy Convers.* **2021**, *37*, 65–74. [CrossRef]
38. Jaliu, C.; Diaconescu, D.V.; Neagoe, M.; Saulescu, R. Dynamic features of speed increasers from mechatronic wind and hydro systems. Part I: Structure kinematics. In Proceedings of the EUCOMES 2008—The 2nd European Conference on Mechanism Science, Cassino, Italy, 17–20 September 2008; pp. 351–359. [CrossRef]
39. Saulescu, R.; Neagoe, M.; Munteanu, O.; Cretescu, N. Performance analysis of a novel planetary speed increaser used in single-rotor wind turbines with counter-rotating electric generator. *IOP Conf. Ser. Mater. Sci. Eng.* **2016**, *147*, 012090. [CrossRef]
40. Saulescu, R.; Jaliu, C.; Neagoe, M. Structural and Kinematic Features of a 2 DOF Speed Increaser for Renewable Energy Systems. *Appl. Mech. Mater.* **2016**, *823*, 367–372. [CrossRef]
41. Herzog, R.; Schaffarczyk, A.P.; Wacinski, A.; Zürcher, O. Performance and stability of a counter–rotating windmill using a planetary gearing: Measurements and Simulation. In Proceedings of the European Wind Energy Conference & Exhibition, Warsaw, Poland, 20–23 April 2010; pp. 1–8.
42. Bharani, R.; Sivaprakasam, A. A Review Analysis on Performance and Classification of Wind Turbine Gearbox Technologies. *IETE J. Res.* **2020**, *66*, 1–15. [CrossRef]
43. Nejad, A.R.; Keller, J.; Guo, Y.; Sheng, S.; Polinder, H.; Watson, S.; Dong, J.; Qin, Z.; Ebrahimi, A.; Schelenz, R.; et al. Wind turbine drivetrains: State-of-the-art technologies and future development trends. *Wind. Energy Sci.* **2022**, *7*, 387–411. [CrossRef]
44. Concli, F.; Pierri, L.; Sbarufatti, C. A Model-Based SHM Strategy for Gears—Development of a Hybrid FEM-Analytical Approach to Investigate the Effects of Surface Fatigue on the Vibrational Spectra of a Back-to-Back Test Rig. *Appl. Sci.* **2021**, *11*, 2026. [CrossRef]
45. Concli, F. Tooth Root Bending Strength of Gears: Dimensional Effect for Small Gears Having a Module below 5 mm. *Appl. Sci.* **2021**, *11*, 2416. [CrossRef]

46. Wu, J.; Zhou, Y.; Jiang, W.; Chen, X. Time-Domain Dynamic Modeling and Analysis of Complex Heavy-Duty Gearbox Considering Floating Effect. *Appl. Sci.* **2021**, *11*, 6876. [CrossRef]
47. Lee, G.H.; Park, Y.J.; Nam, J.S.; Oh, J.Y.; Kim, J.G. Design of a Mechanical Power Circulation Test Rig for a Wind Turbine Gearbox. *Appl. Sci.* **2020**, *10*, 3240. [CrossRef]
48. Lin, A.D.; Hung, T.P.; Kuang, J.H.; Tsai, H.A. Power Flow Analysis on the Dual Input Transmission Mechanism of Small Wind Turbine Systems. *Appl. Sci.* **2020**, *10*, 7333. [CrossRef]
49. Climescu, O.; Jaliu, C.; Saulescu, R. Comparative Analysis of Horizontal Small Scale Wind Turbines for a Specific Application. In Proceedings of the 14th IFToMM World Congress, Taipei, Taiwan, 25–30 October 2015; pp. 545–550. [CrossRef]
50. Saulescu, R.; Neagoe, M.; Jaliu, C.; Munteanu, O. Comparative Analysis of Two Wind Turbines with Planetary Speed Increaser in Steady-State. *Appl. Mech. Mater.* **2016**, *823*, 355–360. [CrossRef]
51. Saulescu, R.; Neagoe, M.; Cretescu, N. Comparative analysis of two wind turbines with counter-rotating vs. fixed-stator electric generator. *IOP Conf. Ser. Mater. Sci. Eng.* **2020**, *997*, 012091. [CrossRef]
52. Saulescu, R.; Neagoe, M.; Jaliu, C.; Munteanu, O. A Comparative Performance Analysis of Counter-Rotating Dual-Rotor Wind Turbines with Speed-Adding Increasers. *Energies* **2021**, *14*, 2594. [CrossRef]
53. Farahani, E.; Hosseinzadeh, N.; Ektesabi, M. Comparison of fault-ride-through capability of dual and single-rotor wind turbines. *Renew. Energy* **2012**, *48*, 473–481. [CrossRef]
54. Neagoe, M.; Saulescu, R.; Jaliu, C. Reconfigurable Wind System and Adjustment Method. Patent RO135228 (A0), 30 September 2021. *in press* (In Romanian).
55. Miloiu, G.; Dudita, F.; Diaconescu, D. *Modern Mechanical Transmissions*; "Tehnica" Publishing House: Bucharest, Romania, 1980. (In Romanian)

energies

MDPI

Article

A Generalized Approach to the Steady-State Efficiency Analysis of Torque-Adding Transmissions Used in Renewable Energy Systems

Mircea Neagoe [1], Radu Saulescu [2], Codruta Jaliu [1,*] and Petru A. Simionescu [3]

1 Renewable Energy Systems and Recycling R&D Centre, Transilvania University of Brasov, 500036 Brasov, Romania; mneagoe@unitbv.ro
2 Design of Mechanical Elements and Systems R&D Centre, Transilvania University of Brasov, 500036 Brasov, Romania; rsaulescu@unitbv.ro
3 Department of Engineering, College of Science and Engineering, Texas A & M University Corpus Christi, Corpus Christi, TX 78412, USA; pa.simionescu@tamucc.edu
* Correspondence: cjaliu@unitbv.ro; Tel.: +40-268-413-000

Received: 14 July 2020; Accepted: 31 August 2020; Published: 3 September 2020

check for updates

Abstract: The paper presents a general approach to the steady-state efficiency analysis of one degree of freedom (1-DOF) speed increasers with one or two inputs, and one or two outputs, applicable to wind, hydro and marine-current power generating systems. The mechanical power flow, and the efficiency of this type of complex speed increasers, are important issues in the design and development of new power-generating systems. It is revealed that speed increases, with in-parallel transmission of the mechanical power from the wind or water rotors to the electric generator, have better efficiency than serial transmissions, but their efficiency calculus is still a challenging problem, solved in the paper by applying the decomposition method of complex speed increasers into simpler component planetary gear sets. Therefore, kinematic, steady-state torque and efficiency equations are derived for a generic 1-DOF speed increasers with two inputs and two outputs, obtained by connecting in parallel two gear mechanisms. These equations allow any speed increaser to be analysed with two inputs and one output, with one input and two outputs, and with one input and one output. We discuss a novel design of a patent-pending planetary-gear speed increaser, equipped with a two-way clutch, which can operate (in combination with the pitch adjustment of the rotors blades) in four distinct configurations. It was found that the mechanical efficiency of this speed increaser in the steady-state regime is influenced by the interior kinematic ratios, the input-torque ratio and by the meshing efficiency of its individual gear pairs. The efficiency of counter-rotating dual-rotor systems was found to be the highest, followed by systems with counter-rotating electric generator, and both have higher efficiency than conventional systems with one rotor and one electric generator with fixed-stator.

Keywords: wind energy; marine-current; hydro power; planetary gear; efficiency analysis

1. Introduction

Among the renewable energy technologies, hydro and wind energy conversion systems currently have the largest share of electrical power generation worldwide [1,2]. While, hydro-electric power is a more mature technology, improvements to wind, tidal-stream and marine-current energy conversion systems are reported every year [3,4]. The major research has looked at energy-conversion efficiency for the purpose of maximizing the use of the onsite renewable potential. Moreover, in the case of wind and hydro-power systems of medium and high capacity, power is transmitted from the wind or water turbine to the electric generator via a speed increaser, which amplifies the speed of the turbine shaft approximately three times in case of hydro-electric systems, and by around one hundred in case of wind power systems [5–7]. The best performing speed increasers in use, are one degree of freedom (1-DOF) or two degrees of freedom (2-DOF) planetary transmissions, which achieve higher efficiency, higher transmission ratios and smaller overall sizes than fixed-axis transmissions. However, these benefits come with added complexity, making the respective transmissions more difficult to design and optimize.

Many innovative solutions of wind and tidal turbines have been proposed in recent years (Figure 1), such as counter-rotating rotors [8–19], high-performance mechanical transmissions [3,20] and more compact and efficient electric generators, including the counter-rotating type [21,22]. Shin [8] proposed a large capacity wind turbine that uses multiple, smaller rotors in a spatial arrangement and a high-efficiency planetary speed increaser. Wacinski [11], Brander [12], Climescu et al. [13] and Oprina et al. [16] proposed different solutions of horizontal-axis wind turbines with two coaxial, counter-rotating rotors. Didane et al. [15,19] and West [18] evaluated the performance of new concepts of vertical-axis wind turbines with counter-rotating coaxial rotors. Designers of counter-rotating turbines (CRT) have resorted to a wide variety of innovative solutions of speed increasers, such as variable transmissions [23], differential transmissions with electric motor speed control [24], or novel planetary gears [25–28]. In spite of their larger size and lower efficiency, compared to their planetary counterparts, the most common solution of speed increasers implemented in wind, hydro and marine-current power generating systems, including of the CRT type, are fixed-axis gear mechanisms [29–31].

(**a**)

(**b**)

Figure 1. Dual rotor; (**a**) wind turbine of Kowintech Co. Ltd.; and (**b**) tidal turbine of SIMEC Atlantis Energy (formerly Atlantis Resources Corp.).

Planetary speed increasers are more appropriate for CRT applications because they ensure higher kinematic ratios and reduced overall size, at higher efficiency levels [11,13,25,26,32–41]. Furthermore, CRTs can employ 2-DOF transmissions to sum the input speeds [35,39] or 1-DOF planetary transmissions to sum the input torques of their two rotors [40,41]. The first type of speed increaser has been studied in conjunction with CRT and conventional generator [42–48], or with CRT and counter-rotating electric generator [41]. No generalization has been proposed. Rather, particular designs have been presented and analysed with respect to their performance. The 1-DOF planetary speed increasers with multiple inputs and outputs can operate both, with single or with counter-rotating wind or water rotors, and with conventional (fixed stator) or counter-rotating, (moving stator) electric generator [49–51]. Efficiency analysis of the mechanical transmissions used in wind, tidal-stream and marine-current energy conversion systems is an essential part of their design and development process [52,53].

Based on the literature survey, the authors concluded that a comprehensive analysis of two-input, one degree of freedom planetary transmissions applicable to wind and water turbines is necessary, aiming to model the speed increaser efficiency in steady-state regime.

The paper proposes a generic class of 1-DOF transmissions, with two inputs and two outputs, employing two planetary gear mechanisms connected in parallel. All four possible combinations, i.e., with one or two input rotors, and with one or two generator outputs can be obtained as particular cases. In Section 2, steady-state torque and efficiency equations are derived for this generic speed increaser class with two inputs and two outputs. Three other types of speed increasers, i.e., with two inputs and one output, with one input and two outputs, and with one input and one output are discussed in Section 3 as particular cases. A novel planetary speed increaser with cylindrical gears, which can operate in four variants by means of a two-way clutch [54], is analysed in Section 4 using bivariate three-dimensional (3D) plots. The paper ends with a summary of results and conclusions.

The main contributions of this paper involve the proposed 1-DOF speed increaser class that can operate in four functional cases. To the best of our knowledge, it is the first unifying modeling of transmission performance in different functional cases. The application example is done for a novel design of a patent-pending transmission [54]. The performance study of the transmission is outlined in this paper by using bivariate plots.

2. Problem Formulation

It is known that mechanical transmissions where power is transmitted in parallel, also known as split-power transmissions, have higher efficiency than transmissions formed with mechanisms connected in series [51]. The same applies to speed increasers used in wind, hydro and marine-current power generating systems that integrate two counter-rotating wind or water rotors and/or one counter-rotating electric generator. A 1-DOF transmission consisting of two 1-DOF mechanisms $M1$ and $M2$ is assumed, providing serial (Figure 2a) or in-parallel transmission (Figure 2b,c) of the mechanical power from one rotor (R) or from two counter-rotating rotors ($R1$ and $R2$) to a standard electric generator (G) with a fixed stator, or to a generator with counter-rotating rotor (GR) and moving stator (GS). Mechanisms $M1$ and $M2$ are characterized by their kinematic ratios i_1 and i_2, and efficiencies η_1 and η_2. Each shaft x has an angular velocity ω_x and transmits a torque T_x (where x is either R, $R1$, $R2$, G, GR or GS).

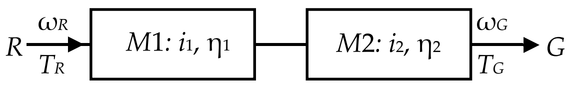

(**a**)

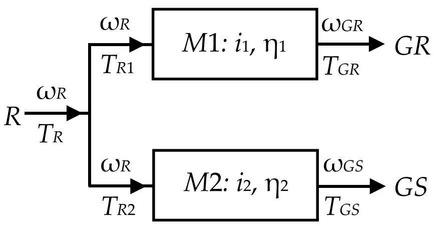

(**b**)

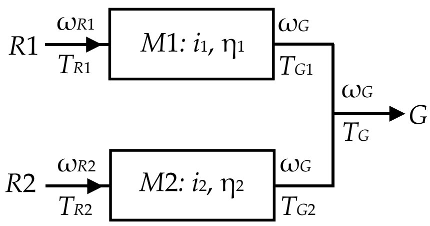

(**c**)

Figure 2. Block diagrams of 1-DOF speed increasers with two 1-DOF mechanisms $M1$ and $M2$, having: (**a**) one rotor and one standard electric generator; (**b**) one rotor and counter-rotating electric generator; (**c**) two counter-rotating input rotors with standard electric generator. R, $R1$ and $R2$ are wind or water rotors, G and GR are the electric-generator rotor; GS is the electric generator stator; T_x is the torque transmitted and ω_x is the angular velocity of shaft x; and i_1 and i_2 are the kinematic ratios and η_1 and η_2 are the efficiencies of constituent mechanisms $M1$ and $M2$.

As explained in references [26,40,51], the efficiencies of the 1-DOF mechanical transmissions have been determined in closed-form, from kinematic, torque equilibrium and energy conservation considerations using Maple computer algebra system.

The efficiencies of the 1-DOF mechanical transmissions in Figure 2 are calculated as follows.

- Case **A** (Figure 2a): speed increaser with one input (R) and one output (G) for which,

$$\omega_G = \frac{\omega_R}{i_1 i_2};\ T_G = -i_1 i_2 \eta_1 \eta_2 T_R \tag{1}$$

the efficiency is:

$$\eta_A = \frac{-P_G}{P_R} = \frac{-T_G \cdot \omega_G}{T_R \cdot \omega_R} = \eta_1 \eta_2 \tag{2}$$

- Case **B** (Figure 2b): speed increaser with one input (R) and two outputs (GR and GS) with:

$$\omega_{GR} = \frac{\omega_R}{i_1};\ \omega_{GS} = \frac{\omega_R}{i_2};\ \omega_G = \omega_{GR} - \omega_{GS} = \frac{i_2 - i_1}{i_1 i_2}\omega_R \tag{3}$$

$$T_{R1} = -\frac{T_{GR}}{i_1 \eta_1};\ T_{R2} = -\frac{T_{GS}}{i_2 \eta_2};\ T_R = T_{R1} + T_{R2} \tag{4}$$

Knowing that the torques transmitted to the rotor and to the moving stator of the electric-generator are equal but of opposite signs (T_{GS} = -T_{GR}), the torque T_G = T_{GR} and mechanical power T_G ω_G delivered to the electric generator are:

$$T_G = T_R \frac{i_1 i_2 \eta_1 \eta_2}{i_1 \eta_1 - i_2 \eta_2} \text{ and } T_G \cdot \omega_G = \eta_1 \eta_2 \frac{i_2 - i_1}{i_1 \eta_1 - i_2 \eta_2} T_R \cdot \omega_R \tag{5}$$

These equations allow the efficiency of the transmission to be calculated as:

$$\eta_B = \frac{-P_G}{P_R} = \frac{-T_G \cdot \omega_G}{T_R \cdot \omega_R} = \eta_1 \eta_2 \frac{i_1 - i_2}{i_1 \eta_1 - i_2 \eta_2} \tag{6}$$

- Case **C** (Figure 2c): speed increaser with two inputs ($R1$ and $R2$) and one output (G).

$$\omega_G = \frac{\omega_{R1}}{i_1} = \frac{\omega_{R2}}{i_2};\ \omega_{R2} = \frac{i_2}{i_1}\omega_{R1} \tag{7}$$

$$T_{G1} = -i_1 \eta_1 T_{R1};\ T_{G2} = -i_2 \eta_2 T_{R2};\ T_G = T_{G1} + T_{G2} \tag{8}$$

$$T_G \cdot \omega_G = -\frac{i_1 \eta_1 T_{R1} + i_2 \eta_2 T_{R2}}{i_1}\omega_{R1} \tag{9}$$

from where the efficiency of the transmission is calculated as:

$$\eta_C = \frac{-P_G}{P_R} = \frac{-T_G \cdot \omega_G}{T_{R1} \cdot \omega_{R1} + T_{R2} \cdot \omega_{R2}} = \frac{i_1 \eta_1 - i_2 \eta_2 k_t}{i_1 - i_2 k_t} \tag{10}$$

where k_t is the input torque ratio:

$$k_t = -\frac{T_{R2}}{T_{R1}} \tag{11}$$

Assuming for convenience that the two component mechanisms M_1 and M_2 have equal efficiencies (η_1 = η_2 = η) Equations (2), (6) and (10) become:

$$\eta_A = \eta^2;\ \eta_B = \eta;\ \eta_C = \eta \tag{12}$$

Equation (12) suggests that if mechanisms M_1 and M_2 have comparable efficiencies, the use of counter-rotating wind or water rotors, or of counter-rotating generator, results in better efficiencies compared to serial arrangements i.e., $\eta_B > \eta_A$ and $\eta_C > \eta_A$. In the next section, a general model for the efficiency analysis of a class of 1-DOF planetary speed increasers with two inputs and two outputs, consisting of two in-parallel planetary gear sets will be presented.

3. Generalized Speed and Steady-State Torque Equations for 1-DOF Speed Increasers with Two Inputs and Two Outputs

Figure 3 shows a general case of a 1-DOF speed increaser with two inputs and two outputs, obtained by connecting in parallel two planetary gear sets *M*1 and *M*2. The main input will be from the primary wind or water-turbine rotor *R*1, while the main output will be the generator rotor *GR*. The two planetary gear sets are connected through two links, one to the frame (i.e., body 0), and the second to both the secondary input-rotor *R2* and to stator *GS* of the electric generator. The other input is connected to the primary rotor *R1*, while the electric generator rotor (*GR*) is connected to the other output.

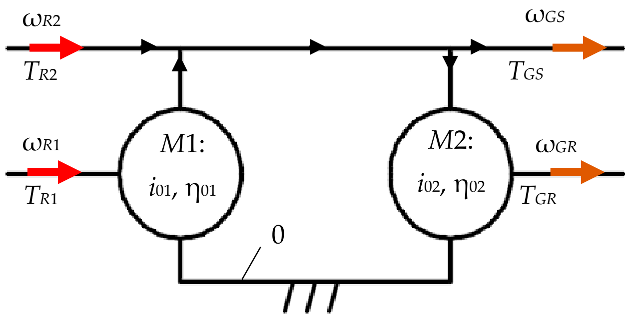

Figure 3. Block diagram of 1-DOF speed increasers with two counter-rotating inputs and two counter-rotating outputs, obtained by connecting in parallel the planetary gear sets *M*1 and *M*2.

With either the sun gear or planet carrier hold fixed to the frame, the two planetary gear sets *M*1 and *M*2 become 1-DOF mechanisms. Due to the constraints introduced by connecting the output of *M*1 to the input of *M*2, the speed increaser with two inputs and two outputs ($L = 4$) will have one degree of freedom.

Four functional variants of the 1-DOF speed increaser in Figure 3 are possible, depending on how the inputs and the outputs of the mechanism are activated:

(1) Variant **V1**: where both inputs *R*1 and *R*2, and both outputs *GR* and *GS* are active ($L = 4$). A system with two counter-rotating rotors and one counter-rotating electric generator is obtained.
(2) Variant **V2**: where both inputs *R*1 and *R*2 and the electric-generator output *GR* are active ($L = 3$). In this case, a system with two counter-rotating rotors and a standard electric generator with $\omega_{GS} = 0$ is obtained.
(3) Variant **V3**: where the main input *R*1 and both outputs are active ($L = 3$), case in which a system with one rotor ($T_{R1} \neq 0$ and $T_{R2} = 0$) and one counter-rotating electric generator is obtained.
(4) Variant **V4**: where only the main input *R*1 and the main output to the generator rotor *GR* are active ($L = 2$). This results in a system with one rotor ($T_{R1} \neq 0$ and $T_{R2} = 0$) and a standard electric generator with $\omega_{GR} \neq 0$ and $\omega_{GS} = 0$.

A 1-DOF mechanism with two inputs and two outputs ($L = 4$) is characterized by the following kinematic and static properties [51]:

(1) It has one independent external angular velocity, with ω_{R1} assumed the independent kinematic parameter;
(2) It has three angular-velocity transmission functions, i.e., three of the external angular velocities depend on the independent velocity i.e., $\omega_{R2} = \omega_{R2}(\omega_{R1})$, $\omega_{RG} = \omega_{RG}(\omega_{R1})$, $\omega_{GS} = \omega_{GS}(\omega_{R1})$;
(3) It has one torque-transmission function $T_{R1} = T_{R1}(T_{R2}, T_{GR}, T_{GS})$ i.e., one dependent external torque (the primary rotor torque T_{R1}) and three independent external torques i.e., T_{R2}, T_{GR} and T_{GS}.

It is also known that these transmission functions are linear, except for non-circular gears. As a result, the transmission functions for angular velocities can be written as,

$$\omega_{GR} = a \cdot \omega_{R1};\ \omega_{R2} = b \cdot \omega_{R1};\ \omega_{GS} = c \cdot \omega_{R1} \tag{13}$$

where coefficients a, b and c are constant, and have meanings of kinematic ratios. The dependent torque T_{R1} can be written as,

$$T_{R1} = A \cdot T_{GR} + B \cdot T_{R2} + C \cdot T_{GS} \tag{14}$$

where coefficients A, B and C are also constant and have meanings of torque ratios.

The counter-rotating electric generator is characterized by the relative angular velocity ω_G between the rotor and the stator, and by the property that the rotor torque T_{GR} and the stator torque T_{GS} are equal and of opposite signs:

$$\omega_G = \omega_{GR} - \omega_{GS} = (a - c)\omega_{R1};\ T_{GS} = -T_{GR} \tag{15}$$

The efficiency η of a 1-DOF speed increaser with two inputs and two outputs is defined as the ratio between the sum of output powers over the sum of input powers. Since efficiency must be positively, and since the output powers of a mechanism are always negative, the efficiency equation writes,

$$\eta = -\frac{\omega_{GR}T_{GR} + \omega_{GS}T_{GS}}{\omega_{R1}T_{R1} + \omega_{R2}T_{R2}} \tag{16}$$

or by using coefficients a, b, c, A, B and C it becomes:

$$\eta = -\frac{a - c}{A - C}\frac{T_{R1} - BT_{R2}}{T_{R1} + bT_{R2}}. \tag{17}$$

The input-torque ratio k_t in Equation (11) varies from zero (i.e., $T_{R2} = 0$) to a maximum value, depending on the geometry of the two rotors $R1$ and $R2$, where the most common method of changing torque T_{R2} is to adjust the pitch angle of the rotor blades. The efficiency of the above four variants **V1** … **V4** can be obtained by considering particular forms of Equations (11) and (17) as follows:

For variant **V1** with two inputs ($R1$, $R2$) and two outputs (GR, GS):

$$\eta_{V1} = -\frac{(a - c)(1 + k_t B)}{(A - C)(1 - k_t b)} \tag{18}$$

For variant **V2** with two inputs ($R1$, $R2$) and one output (GR), i.e., $\omega_{GS} = 0$:

$$\eta_{V2} = -\frac{a(1 + k_t B)}{A(1 - k_t b)}. \tag{19}$$

For variant **V3** with one input ($R1$), i.e., $k_t = 0$, and two outputs (GR, GS):

$$\eta_{V3} = -\frac{a - c}{A - C} \tag{20}$$

For variant **V4** with one input ($R1$), i.e., $k_t = 0$, and one output (GR), i.e., $\omega_{GS} = 0$:

$$\eta_{V4} = -\frac{a}{A} \tag{21}$$

Coefficients a, b, c and A, B, C in Equations (18)–(21) can be determined by applying the principle of superposition. An example on how these coefficients can be determined for the case of a planetary speed increaser with cylindrical gears will be presented next.

4. Case Study Analysis

In this section, a novel cylindrical-gear planetary speed increaser will be considered. Its unique feature is that the input and output motions have opposite directions, provided by planet gear 2 in series with planet gear 3 (see Figure 4a).

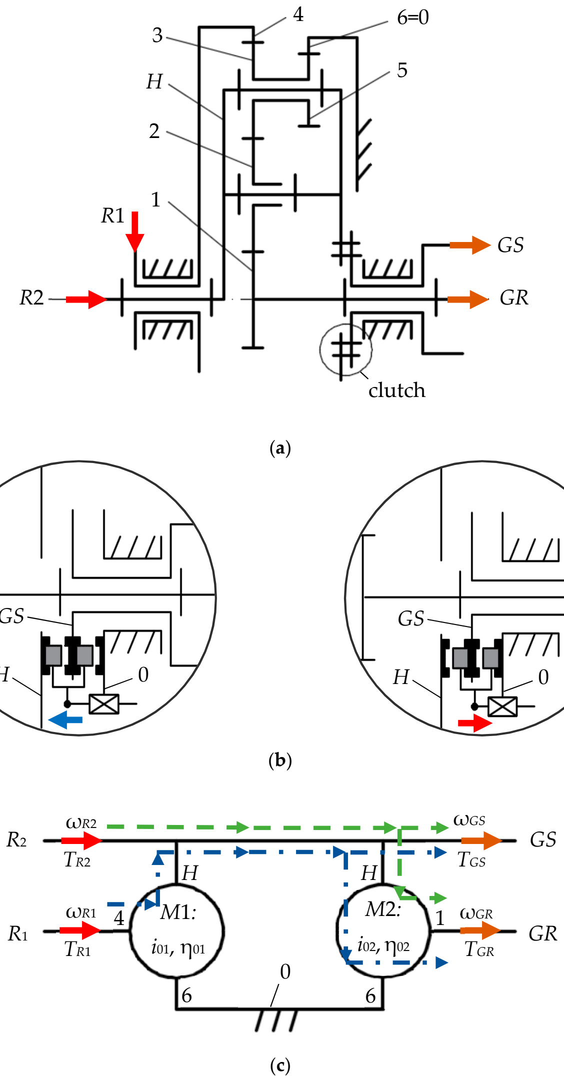

Figure 4. 1-DOF cylindrical-gear speed increaser in a generalized configuration with two inputs and two outputs: (**a**) structural diagram; (**b**) detail of the two-way clutch (left) in the $H \equiv GS$ position and (right) in the $GS \equiv 0$ position; (**c**) block diagram showing the input-output power flow.

Ring gear 4, connected to the primary rotor *R*1 is the main input, and meshes with planet gear 3, while the secondary input is the planet carrier *H*. Ring gear 6 which is fixed, meshes with gear 5 of the compound planet 3–5. Sun gear 1 is connected to the electric-generator rotor (*GR*), while its stator is connected to carrier *H* through a two-way clutch. This clutch allows the transmission of the mechanical power to output shafts *GS* and *GR* (see Figure 4b-left) or, by holding fixed the stator of the electric generator, to output *GR* only (see Figure 4b-right).

According to the block diagram in Figure 4c, the speed increaser consists of planetary gear sets *M*1 and *M*2, of which *M*1 (4-3-5-6-*H*) contains a compound planet with internal - internal gearing, and *M*2 (1-2-3-5-6-*H*) has two planets in series with external-internal gearing. In this configuration, the two component mechanisms share the same moving carrier *H* and the same fixed gear 6.

In its general configuration with two inputs and two outputs, the four operating variants V1 to V4 become (see Figure 5):

(1) Variant V1: a system with two inputs and two outputs (L = 4), in which both input $R1$ and $R2$ and both output GR and GS are active. The input-output torque ratio $k_t > 0$ is controlled by the blade-pitch angle of either or both rotors $R1$ and $R2$, while the clutch is set to connect carrier H to GS (see Figure 4b-left);

(2) Variant V2: a system with two inputs and one output (L = 3), in which the output is connected to the electric-generator rotor GR, and stator GS is fixed by the clutch as shown in Figure 4b-right;

(3) Variant V3: a system with one input and two outputs (L = 3), obtained from V1 by deactivating the secondary rotor $R2$ (k_t = 0);

(4) Variant V4: a system with one input and one output (L = 2), obtained from variant V1 by deactivating the secondary rotor $R2$ (k_t = 0) and by connecting the electric-generator stator to the frame (see Figure 4b-right).

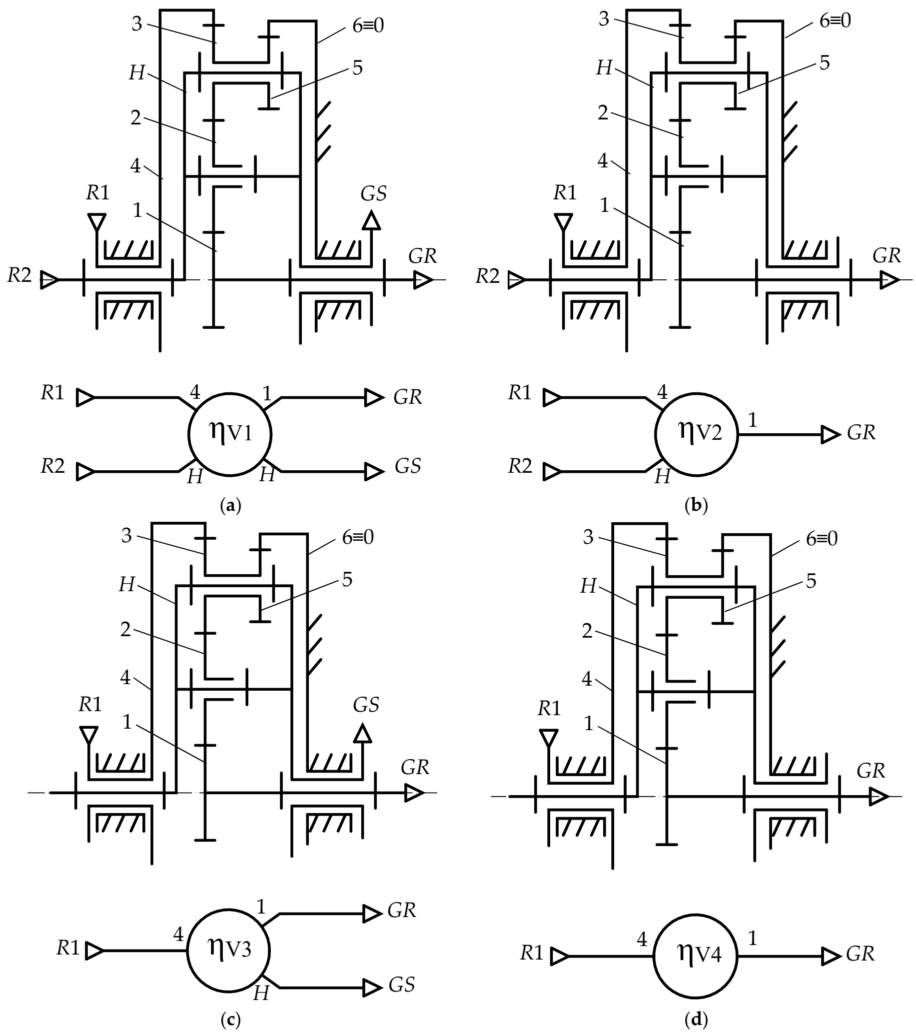

Figure 5. Structural and block diagrams of the 1-DOF speed increaser in Figure 4a with (**a**) two inputs and two outputs (variant **V1**); (**b**) two inputs and one output (variant **V2**); (**c**) one input and two outputs (variant **V3**) and (**d**) one input and one output (variant **V4**).

The two component planetary gear sets $M1$ and $M2$ are characterized by the interior kinematic ratios i_{01} and i_{02},

$$i_{01} = i_{46}^{H} = i_{43}^{H} \cdot i_{56}^{H} = \frac{z_3 z_6}{z_4 z_5} > 0;\ i_{02} = i_{16}^{H} = i_{12}^{H} \cdot i_{23}^{H} \cdot i_{56}^{H} = \frac{z_3 z_6}{z_1 z_5} > 0 \tag{22}$$

where i_{xy}^{z} is the angular speed ratio of body x and body y relative to body z.

For obvious reasons, the number of teeth z_4 of ring gear 4 has to be bigger than the number of teeth z_1 of sun gear 1 (i.e., $z_4 > z_1$), and according to Equation (22), inequality $i_{02} > i_{01}$ should also hold true.

Efficiencies η_{01} and η_{02} are the internal efficiencies of mechanisms $M1$ and $M2$ associated to the respective planetary gear sets, when carrier H is fixed (see Equation (12), where η_0 is the efficiency of one gear pair, and efficiencies η_{xy}^{z} correspond to the power being transmitted from member x to member y when z is held fixed, and where x, y can be either 1, 2, 3, 4, 5 and H, while z can be either 6 and H).

$$\eta_{01} = \eta_{43}^{H} \cdot \eta_{56}^{H} = (\eta_0)^2;\ \eta_{02} = \eta_{12}^{H} \cdot \eta_{23}^{H} \cdot \eta_{56}^{H} = (\eta_0)^3 \tag{23}$$

Coefficients a, b, c defined in Equation (13) can be calculated by applying a motion-inversion relative to planet carrier H [51]:

$$a = i_{14}^{6} = \frac{\omega_{16}}{\omega_{46}} = \frac{1 - i_{02}}{1 - i_{01}};\ b = c = i_{H4}^{6} = \frac{\omega_{H6}}{\omega_{46}} = \frac{1}{1 - i_{01}} \tag{24}$$

In turn, torque-transmission functions are also linear equations according to Equation (25)

$$T_{R1} = T_{R1}^{(GR)} + T_{R1}^{(R2)} + T_{R1}^{(GS)};\ T_{R1}^{(GR)} = A \cdot T_{GR};\quad T_{R1}^{(R2)} = B \cdot T_{R2};\ T_{R1}^{(GS)} = C \cdot T_{GS} \tag{25}$$

where $T_{R1}^{(x)}$ is the torque at the primary rotor shaft $R1$ obtained when all independent external torques are zero, except for T_x, and where coefficients A, B, C defined in Equation (14) are determined by applying the principle of superposition.

For example, torque $T_{R1}^{(GR)}$ is obtained for $T_{GR} \neq 0$ (mechanical power is transmitted only to electric-generator rotor GR) and for $T_{R2} = T_{GS} = 0$ (i.e., the secondary rotor $R2$ and the stator of the electric generator are idling).

Considering only the power flow from $R1$ to GR yields,

$$T_{R1}^{(GR)} \cdot \omega_{46} \cdot \eta_{41}^{6} + T_{GR} \cdot \omega_{16} = 0 => \ T_{R1}^{(GR)} = -T_{GR} \cdot \frac{a}{\eta_{41}^{6}} \tag{26}$$

where,

$$\eta_{41}^{6} = \eta_{4H}^{6} \cdot \eta_{H1}^{6};\ \eta_{4H}^{6} = \frac{1 - \overline{i_{01}}}{1 - i_{01}};\ \eta_{H1}^{6} = \frac{1 - i_{02}}{1 - \overline{i_{02}}} \tag{27}$$

and where $\overline{i_{01}}$ and $\overline{i_{02}}$ are torque ratios [51], defined as:

$$\overline{i_{01}} = i_{01} \cdot \eta_{01}^{x_1};\ x_1 = sign\left(\frac{\omega_{4H}}{\omega_{46}}\right) = sign\left(\frac{i_{01}}{i_{01} - 1}\right) \tag{28}$$

$$\overline{i_{02}} = i_{02} \cdot \eta_{02}^{x_2};\ x_2 = sign\left(-\frac{\omega_{1H}}{\omega_{16}}\right) = sign\left(-\frac{i_{02}}{i_{02} - 1}\right) \tag{29}$$

In the above equations, *sign* represents the sign function, and $x_1 = -1$ for $i_{01} < 1$ and $x_1 = +1$ for $i_{01} > 1$, $x_2 = +1$ for $i_{02} < 1$ and $x_2 = -1$ for $i_{02} > 1$, $i_{01} \neq 1$, $i_{02} \neq 1$. Because in a counter-rotating electric generator, the generator rotor must have a higher angular velocity than the stator i.e., $|\omega_{GR}| > |\omega_{GS}|$, then $|a| > |c|$, and as a result, $i_{02} > 2$ and $x_2 = -1$.

From the condition that rotors $R1$ and $R2$ are counter-rotating, i.e., *sign* (ω_{R1} ω_{R2}) = −1, and since $b < 0$, then $i_{01} > 1$ and $x_1 = +1$ (see Equations (13) and (24)). It also implies that:

$$A = -\frac{a}{\eta_{41}^{6}} = -\frac{1-\overline{i_{02}}}{1-\overline{i_{01}}} = -\frac{1-i_{02}\cdot\eta_{02}^{-1}}{1-i_{01}\cdot\eta_{01}} \tag{30}$$

Coefficients B and C are determined similarly to coefficient A, by considering the power flow from $R1$ to $R2$ and from $R1$ to RS:

$$T_{R1}^{(R2)}\cdot\omega_{46}\cdot\eta_{4H}^{6}+T_{R2}\cdot\omega_{H6}=0 \Rightarrow T_{R1}^{(R2)}=-T_{R2}\cdot\frac{b}{\eta_{4H}^{6}} \tag{31}$$

$$T_{R1}^{(RS)}\cdot\omega_{46}\cdot\eta_{4H}^{6}+T_{RS}\cdot\omega_{H6}=0 \Rightarrow T_{R1}^{(RS)}=-T_{RS}\cdot\frac{c}{\eta_{4H}^{6}} \tag{32}$$

According to Equation (24), $b = c$ which yields:

$$B=C=-\frac{b}{\eta_{4H}^{6}}=-\frac{c}{\eta_{4H}^{6}}=-\frac{1}{1-\overline{\overline{i_{01}}}}=-\frac{1}{1-i_{01}\cdot\eta_{01}} \tag{33}$$

By employing Equations (18)–(21), the efficiencies of the four variants of the 1-DOF planetary speed increaser are obtained.

For variant **V1**: two inputs and two outputs (L = 4):

$$\eta_{V1}=\frac{i_{02}}{\overline{\overline{i_{02}}}}\cdot\frac{1-\overline{i_{01}}-k_t}{1-i_{01}-k_t}=\eta_{02}\cdot\frac{1-i_{01}\eta_{01}-k_t}{1-i_{01}-k_t} \tag{34}$$

For variant **V2**: two inputs and one output (L = 3, $\omega_{GS}=0$):

$$\eta_{V2}=\frac{1-i_{02}}{1-i_{02}\eta_{02}^{-1}}\cdot\frac{1-i_{01}\eta_{01}-k_t}{1-i_{01}-k_t}. \tag{35}$$

For variant **V3**: one input and two outputs (L = 3, $k_t = 0$):

$$\eta_{V3}=\eta_{02}\cdot\frac{1-i_{01}\eta_{01}}{1-i_{01}} \tag{36}$$

For variant **V4**: one input and one output (L = 2, $\omega_{GS}=0$, $k_t = 0$):

$$\eta_{V4}=\frac{1-i_{02}}{1-i_{02}\eta_{02}^{-1}}\cdot\frac{1-i_{01}\eta_{01}}{1-i_{01}} \tag{37}$$

5. Numerical Simulations and Discussions

Four independent parameters, i.e., i_{01}, i_{02}, k_t and η_0 occur in the efficiency Equations (34)–(37) of the planetary speed increaser variants **V1**, **V2**, **V3** and **V4**. The effects of these parameters upon overall efficiency and kinematic ratios of the respective speed increasers have been studied using bivariate plots as explained in [55,56] (see Figures 6–10; note that in some of these plots the z-axis has been reversed for clarity). The value ranges of these four parameters have been considered as follows: the kinematic ratio of the speed increaser $i_{aG} = \omega_G/\omega_{R1} \geq 3$, input torque ratio $k_t < 2$ and efficiency of a typical pair of gears $\eta_0 > 0.94$ [57].

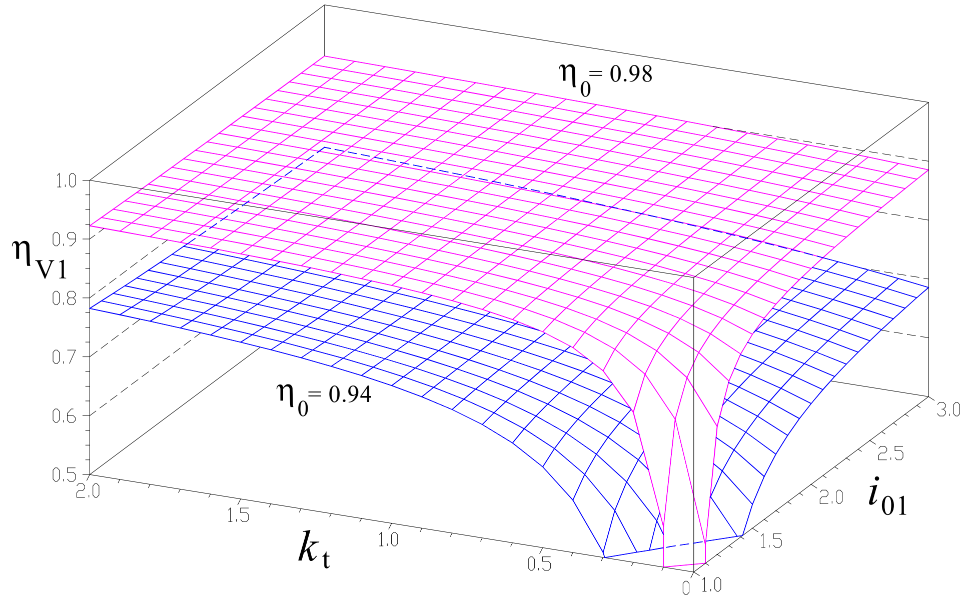

Figure 6. Efficiency of the 1-DOF speed increaser variant **V1** (Figure 5a) as function of the interior kinematic ratio i_{01}, torque ratio k_t, and efficiency of each gear-pair $\eta_0 = 0.98$.

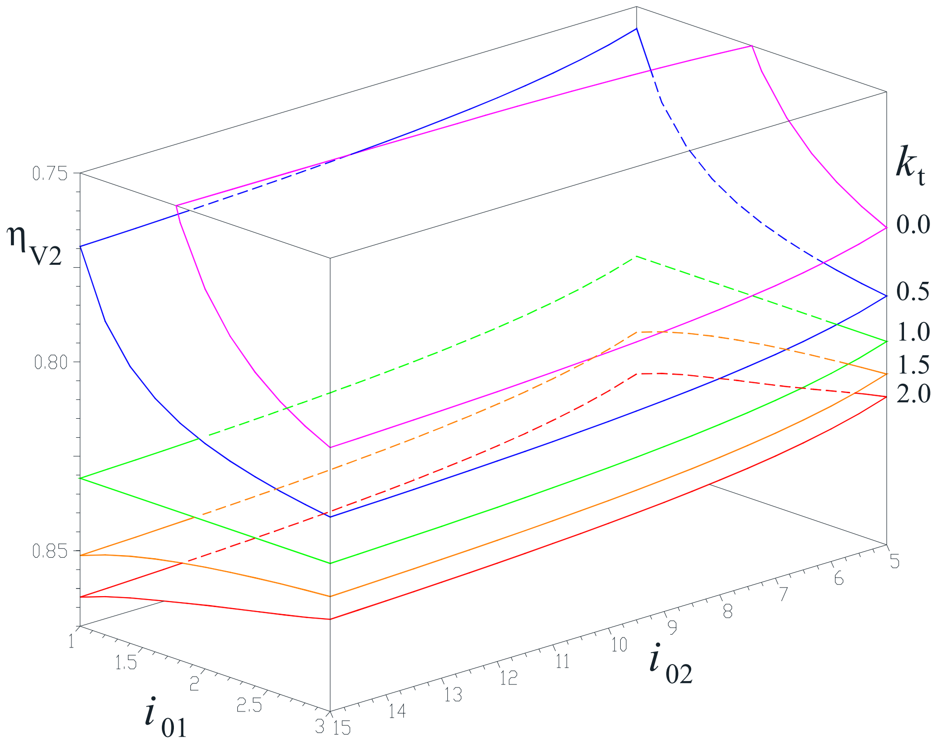

Figure 7. Efficiency of the 1-DOF speed increaser variant **V2** (Figure 5b), as functions of the interior kinematic ratios i_{01} and i_{02}, for torque ratios $k_t = 0$, 0.5, 1.0, 1.5 and 2.0, assuming $\eta_0 = 0.965$.

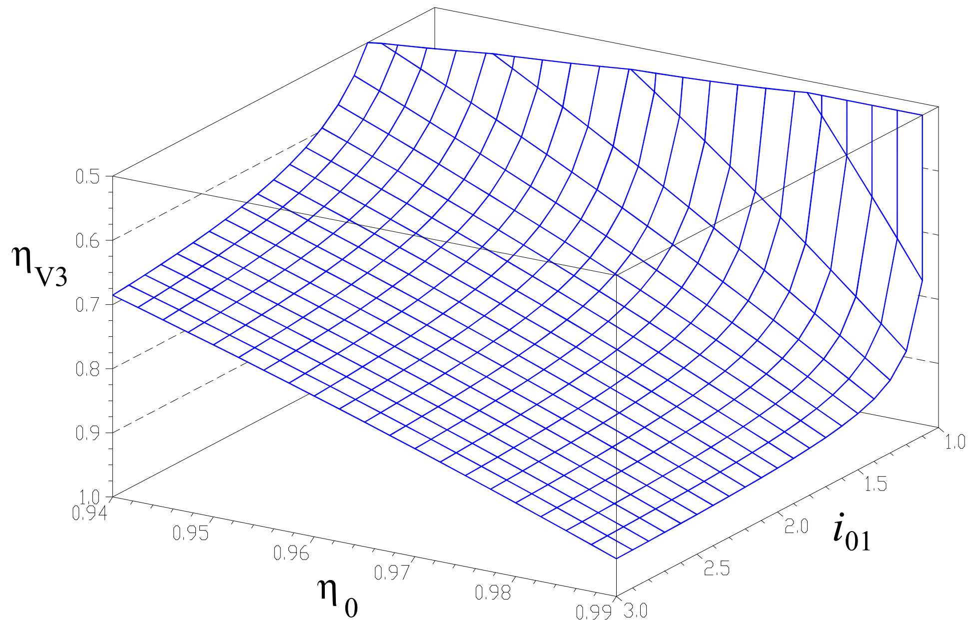

Figure 8. Efficiency of the 1-DOF speed increaser variant **V3** (Figure 5c), as function of the interior kinematic ratio i_{01} and η_0.

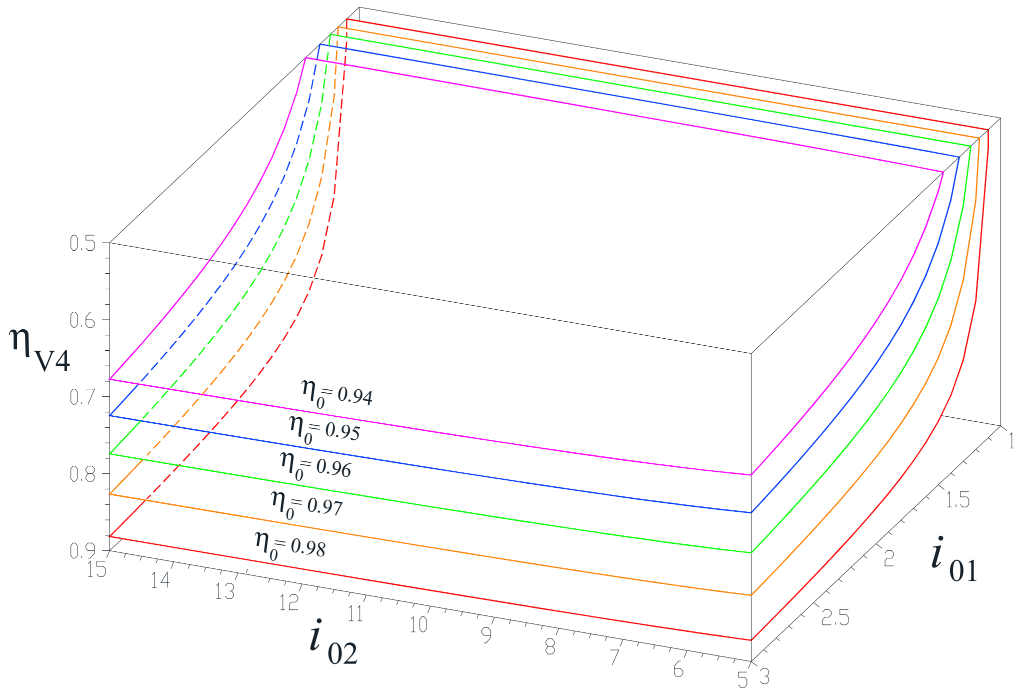

Figure 9. Efficiency of the 1-DOF speed increaser variant **V4** (Figure 5d) as functions of the interior kinematic ratios i_{01} and i_{02}, for various gear-pair efficiencies η_0 = 0.94, 0.95, 0.96, 0.97 and 0.98.

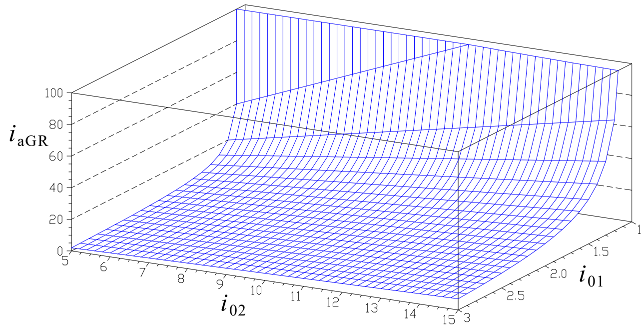

(**a**)

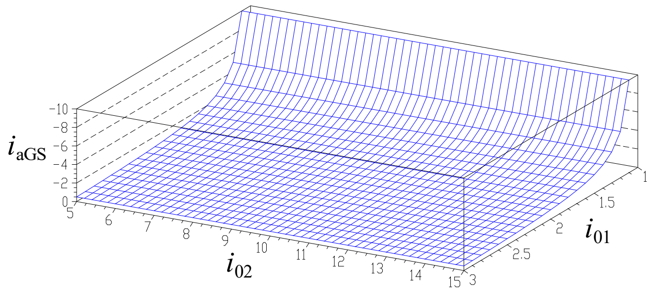

(**b**)

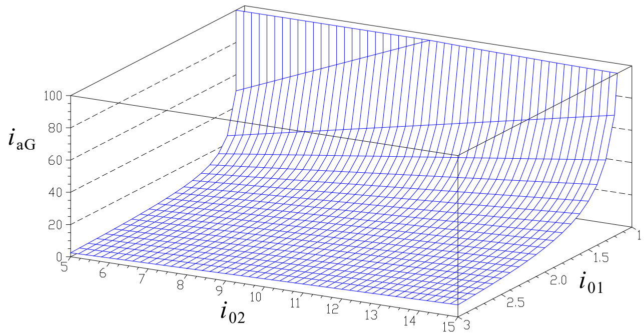

(**c**)

Figure 10. Variations of kinematic ratios (**a**) i_{aGR} (from R1 to GR), (**b**) i_{aGS} (from R1 to GS) and (**c**) i_{aG} (from R1 to G in of counter-rotating electric generator) as functions of the interior kinematic ratios i_{01} and i_{02}.

According to Equation (34), the efficiency of a speed increasers with two counter-rotating wind or water rotors and counter-rotating electric generator (variant **V1**) depends on i_{01}, k_t and η_0, and it is not influenced by the interior kinematic ratio i_{02}. As the plot in Figure 6 shows, the efficiency η_{V1} of the speed increaser is influenced the most by the efficiency η_0 of its constituent gear pairs, resulting in more than 12% increase, for only 4% improvement in η_0 i.e., from 94% to 98%. Consequently, care should be given to the manufacturing quality of the individual gears. Also, what is visible in Figure 7 is a rapid decrease of η_{V1} with a reduction of parameters i_{01} and k_t, most noticeable for $i_{01} < 1.75$ and $k_t < 0.75$. From Figure 10c it additionally becomes apparent that for $1 < i_{01} < 2$, high values of the amplification ratio i_{aG} are obtained. During the operation of a power generating system equipped with such a transmission, torque ratio k_t will be adjusted via the pitch angles of the wind or water rotors. In the design stage, the anticipated range of k_t should be correlated with interior ratio i_{01} and gear-pair efficiency η_0 to achieve best speed increaser efficiency and a high amplification ratio i_{aG}.

In case of variant **V2** of gear increasers (which is the same as variant **V1** but with a locked stator, i.e., $\omega_{GS} = 0$) Equation (35) indicates that the efficiency η_{V2} of the increaser depends on all four parameters i_{01}, i_{02}, k_t and η_0. Assuming that each gear-pair of the transmission has the same efficiency η_0 and equal to 0.965, according to the plot in Figure 7, η_{V2} is influenced manly by the interior kinematic ratio i_{01} and by the torque ratio k_t, and less by the interior ratio i_{02}. As i_{02} increases and for i_{01} and k_t

assumed constant, a slight increase of η_{V2} is observed. Likewise, efficiency η_{V2} increases for $k_t < 1$, and decreases slightly for $k_t > 1$ as i_{01} increases. For $k_t = 1$, efficiency η_{V2} no longer depends on i_{01}, which may be interesting when large kinematic amplification ratios i_{aG} are desired. Same as for variant **V1**, an increase of the torque ratio k_t is accompanied by an increase in efficiency η_{V2}. The increase of η_{V2} with k_t is more significant for small values of i_{01} than is for larger values of i_{01}.

The efficiency of gear transmission variant **V3** with one input *R*1 and two counter-rotating outputs GR and GS, depends only on i_{01} and η_0 (see Equation (36)). The internal gear ratio i_{01} does not affect the efficiency η_{V3} of the increaser and $k_t = 0$. The 3D plot in Figure 8 shows, for i_{01} held constant, a linear correlation of efficiency η_{V3} with η_0. Also apparent is a rapid drop of efficiency η_{V3} with i_{01}, particularly for $i_{01} < 1.75$.

Variant **V4** of gear increaser is characterized by $k_t = 0$ (there is only one input i.e., *R*1) and by $\omega_{GS} = 0$ (the generator has a fixed stator). According to Equation (37) its efficiency η_{V4} depends on parameters i_{01}, i_{02} and η_0. Higher values of the efficiency η_{V4} are obtained for larger values of these three parameters, of which η_0 has the most effect, Figure 9. Internal kinematic ratio i_{02} has a smaller effect, however, a rapid drop in η_{V4} is observed for i_{01} approaching 1.

Based on the same plots in Figures 6–9, the following additional conclusions can be drawn:

- Efficiencies η_{V1} and η_{V2} increase as the input torque ratio k_t increases. This is explicable by the relative increase of the power from the secondary wind or water rotor *R*2. It is worth mentioning that the power flow from R1 passes entirely through mechanism *M*1 and then through part of mechanism *M*2, while the power flow generated by R2 passes only partially through M2 and the rest is transmitted directly to the generator stator GS;
- The interior kinematic ratio i_{01} influences strongly the speed-increaser efficiency in all four variants as k_t approaching 0, particularly if $1 < i_{01} < 1.75$. Furthermore, the mechanism locks (i.e., efficiency becomes negative) for i_{01} approaching 1;
- The interior kinematic ratio i_{02} does not occur in the efficiency Equations (34) and (36) for the speed increaser variants **V1** and **V3** with counter-rotating electric generator. Instead, efficiencies η_{V2} and η_{V4} (the cases with electric generator with a fixed stator) have markedly lower values for small values of parameter i_{02}, but increase with the increase of i_{02};
- The quality of the component gears and therefore the individual gear pair efficiencies η_0, have a major influence upon the efficiency of the speed increaser, regardless of variant V1 to V4. Therefore, it is recommended that good quality gear pairs are used, in order to minimize losses and maximize the efficiency in transmitting mechanical power from wind or water rotors to the electric generator.

As a general conclusion, Figures 6–9 confirm that split-power transmissions have higher efficiencies than serial transmission. Overall, the best efficiencies are provided by variant **V1**, which combines the split input power (Figure 2c) with the split output power (Figure 2b). The second most efficient is variant **V2** with two inputs and one output (Figure 2c), followed by variant **V3** with a single rotor and counter-rotating electric generator (Figure 2b). The least performing variant is **V4** with serial transmission of mechanical power (Figure 2a). Thus, the efficiency of hydro/tidal/wind systems can be increased by adopting either a split-input power transmissions, a split-output power transmissions, or a transmissions with power split both at input and at output.

The interior kinematic ratios i_{01} and i_{02} of the component mechanisms *M*1 and *M*2, directly influence the transmission of input angular speed ω_{R1} to the electric generator, and implicitly, the relative speed ω_G between the generator rotor and stator. The plots in Figure 10, depicted for variant **V1** with two inputs and two outputs, indicate that the amplification ratio $i_{aG} = \omega_G/\omega_{R1}$ increases with the decrease of i_{01} and with the increase of i_{02}. High kinematic ratios i_{aG} can be obtained at reduced internal ratios i_{01} (e.g., $i_{aG} = 50$ for $i_{01} = 1.2$ and $i_{02} = 10$) and/or in combination with high values of internal ratio i_{02} (e.g., $i_{aG} = 30$ for $i_{01} = 1.5$ and $i_{02} = 15$).

6. Conclusions

This paper presented a generalized model of efficiency calculation of 1-DOF speed increasers applicable to hydro and wind energy conversion systems with two gear mechanisms in parallel. Possible operating modes involve one input or two counter-rotating inputs, and with a single or two generator outputs. The inputs are provided by two counter-rotating wind or water rotors, while the outputs are linked to the counter-rotating rotor and the stator of an electric generator.

It was found that the in-parallel or split-power transmissions have higher efficiency compared to the serial transmissions. The in-parallel power transmission can be achieved, either by using two counter-rotating wind or water rotors, or by employing an electric generator with counter-rotating rotor and stator. As a result, counter-rotating systems have higher efficiencies than conventional single input, single output systems.

For the general case of a speed increaser with two inputs and two outputs, an efficiency analysis has been performed where transmissions with only two inputs and one output; one input and two outputs, and with one input and one output result as particular cases. This approach has then been applied to a novel planetary gear speed increaser, which can operate in all four possible combinations using a built-in two-way clutch, and by adjusting the pitch angle of the wind or water rotors.

The results reveal that the speed-increasers with two inputs and two outputs have higher efficiency. The results presented in this paper offer design engineers a useful approach for the analysis and synthesis of high-performance wind/tidal/hydro electrical systems.

Author Contributions: Conceptualization, M.N., R.S. and C.J.; methodology, M.N., R.S., C.J., and P.A.S.; software, M.N., R.S. and P.A.S.; validation, M.N., R.S., C.J. and P.A.S.; formal analysis, M.N., R.S., and P.A.S.; investigation, M.N., R.S., C.J., P.A.S.; resources, M.N., R.S., C.J., and P.A.S.; data curation, M.N., R.S., C.J., and P.A.S.; writing—original draft preparation, M.N., R.S. and C.J.; writing—review and editing, M.N. and P.A.S.; visualization, M.N., R.S., C.J., and P.A.S.; supervision, M.N. All authors contributed equally to editing and revising of this review. All authors have read and agreed to the published version of the manuscript.

Funding: This research received no external funding.

Acknowledgments: The comments, suggestions and recommendations for future research by the anonymous reviewers are gratefully acknowledged.

Conflicts of Interest: The authors declare no conflict of interest.

Nomenclature

CRWT	Counter-Rotating Wind Turbine
SI	Speed increaser
R	Rotor
$R1$	Primary rotor
$R2$	Secondary rotor
P	Power
ω	Angular speed
T	Torque
k_t	Ratio of the input torques
z	Gear teeth number
H	Satellite carrier
a, b, c	Kinematic coefficients
A, B, C	Static coefficients
DOF	Degree of Freedom
$M1, M2$	Mechanism 1 or 2
L	Total number of inputs and outputs
G	Standard electric generator
GR	Electric generator rotor
GS	Electric generator stator
i	Kinematic ratio
$i_{01,2}$	Interior kinematic ratio of the mechanism M1,2
i_a	Amplification kinematic ratio
η	Efficiency of the speed increaser
$\eta_{01,2}$	Interior efficiency of the mechanism M1,2
η_0	Efficiency of a gear pair

References

1. Dincer, I. (Ed.) *Comprehensive Energy Systems*; Elsevier Science & Technology: Amsterdam, The Netherlands, 2018; ISBN 978-0-12-809597-3.
2. World Energy Resources Charting the Upsurge in Hydropower Development. 2015. Available online: www.worldenergy.org/publications/entry/charting-the-upsurge-in-hydropower-development-2015 (accessed on 19 August 2020).
3. Jaliu, C.; Diaconescu, D.V.; Neagoe, M.; Saulescu, R. The eco-impact of small hydro implementation. *Environ. Eng. Manag. J.* **2009**, *8*, 837–841. [CrossRef]
4. Hydro Power. Available online: https://ec.europa.eu/research/energy/index.cfm?pg=area&areaname=renewable_hydro (accessed on 19 August 2020).
5. Visa, I.; Jaliu, C.; Duta, A.; Neagoe, M.; Comsit, M.; Moldovan, M.; Ciobanu, D.; Burduhos, B.; Saulescu, R. *The Role of Mechanisms in Sustainable Energy Systems*; Transilvania University Press: Brasov, Romania, 2015; ISBN 978-606-19-0571-3.
6. Manwell, J.F.; McGowan, J.G.; Rogers, A.L. *Wind Energy Explained: Theory, Design and Application*; Wiley: Hoboken, NJ, USA, 2009.
7. Pelikan, B.; Armand, F.; Schleiss, A.; Bollaert, B.; Manso, P.; Bard, J.; O'Nians, J.; Denis, V.; Corbet, J.-P.; Soderberg, C.; et al. *Guide on How to Develop a Small Hydropower Plant*; European Small Hidro-Power Association (ESHA): Brussels, Belgium, 2004.
8. Shin, C. Multi-Unit Rotor Blade System Integrated Wind Turbine. U.S. Patent No. 5876181, 2 March 1999.
9. Appa, K. *Energy Innovations Small Grant (EISG) Program (Counter Rotating Wind Turbine System)*; EISG Final Report; EISG: Shores, CA, USA, 2002; Available online: https://www.eai.in/ref/invent/upload/00-09%2520FAR%2520Appendix%2520A.pdf (accessed on 19 August 2020).
10. Jung, S.; No, T.; Ryu, K. Aerodynamic performance prediction of a 30 kW counter-rotating wind turbine system. *Renew. Energy* **2005**, *30*, 631–644. [CrossRef]
11. Wacinski, A. Drive Device for a Windmill Provided with Two Counter–Rotative Propellers. U.S. Patent 7,384,239, 10 June 2008.
12. Brander, M. Bi-Directional Wind Turbine. U.S. Patent Application 2008/0197639 A1, 21 August 2008.
13. Climescu, O.; Saulescu, R.; Jaliu, C. Specific features of a counter-rotating transmission for renewable energy systems. *Environ. Eng. Manag. J.* **2011**, *10*, 1105–1113. [CrossRef]
14. Hwang, B.; Lee, S.; Lee, S. Optimization of a counter-rotating wind turbine using the blade element and momentum theory. *J. Renew. Sustain. Energy* **2013**, *5*, 052013. [CrossRef]
15. Didane, D.H.; Rosly, N.; Zulkafli, M.F.; Shamsudin, S.S. Performance evaluation of a novel vertical axis wind turbine with coaxial contra-rotating concept. *Renew. Energy* **2015**, *115*, 353–361. [CrossRef]
16. Oprina, G.; Chihaia, R.A.; El-Leathey, L.A.; Nicolaie, S.; Babutanu, C.A.; Voina, A. A review on counter-rotating wind turbines development. *J. Sustain. Energy* **2016**, *7*, 91–98.
17. Vasel-Be-Hagh, A.; Archer, C. Wind farms with counter-rotating wind turbines. *Sustain. Energy Technol. Assess.* **2017**, *24*, 19–30. [CrossRef]
18. West, R. Wind Turbine System. U.S. Patent 10,316,820B2, 11 June 2019.
19. Didane, D.H.; Rosly, N.; Zulkafli, M.F.; Shamsudin, S.S. Numerical investigation of a novel contra-rotating vertical axis wind turbine. *Sustain. Energy Technol. Assess.* **2019**, *31*, 43–53. [CrossRef]
20. Jaliu, C.; Saulescu, R.; Diaconescu, D.V.; Neagoe, M. Conceptual design of a chain speed increaser for small hydropower stations. In Proceedings of the ASME 2009 International Design Engineering Technical Conferences & Computers and Information in Engineering Conference IDETC/CIE 2009, San Diego, CA, USA, 30 August–2 September 2009; ISBN 978-0-7918-3856-3.
21. Booker, J.D.; Mellor, P.H.; Wrobel, R.; Drury, D. A compact, high efficiency contra-rotating generator suitable for wind turbines in the urban environment. *Renew. Energy* **2010**, *35*, 2027–2033. [CrossRef]
22. Erturk, E.; Sivrioglu, S.; Bolat, F.C. Analysis Model of a Small Scale Counter-Rotating Dual Rotor Wind Turbine with Double Rotational Generator Armature. *Int. J. Renew. Energy Res.* **2018**, *8*, 1849–1858.
23. Hall, J.F.; Mecklenborg, C.A.; Chen, D.; Pratap, S.B. Wind energy conversion with a variable-ratio gearbox: Design and analysis. *Renew. Energy* **2011**, *36*, 1075–1080. [CrossRef]
24. Jelaska, D.; Podrug, S.; Perkusic, M. A novel hybrid transmission for variable speed wind turbines. *Renew. Energy* **2015**, *83*, 78–84. [CrossRef]

25. Saulescu, R.; Neagoe, M.; Munteanu, O.; Cretescu, N. *Performance Analysis of a Novel Planetary Speed Increaser Used in Single-Rotor Wind Turbines with Counter-Rotating Electric Generator*; Materials Science and Engineering—IOP Conference Series: Materials Science and Engineering; IOP Publishing Ltd.: Bristol, UK, 2016. [CrossRef]
26. Neagoe, M.; Saulescu, R.; Jaliu, C.; Cretescu, N. Novel Speed increaser used in counter-rotating wind turbines. In *New Advances in Mechanisms, Mechanical Transmissions and Robotics, Mechanisms and Machine Science 46*; Springer: Berlin, Germany, 2017; pp. 143–151. [CrossRef]
27. Jaliu, C.; Diaconescu, D.V.; Neagoe, M.; Saulescu, R. Dynamic features of speed increasers from mechatronic wind and hydro systems. Part I. Structure Kinematics. In Proceedings of the Second European Conference on Mechanism Science EUCOMES 08, Casino, Italy, 17–20 September 2008; Springer: Dordrecht, The Netherlands, 2008; pp. 355–363, ISBN 987-1-4020-8914-5.
28. Jaliu, C.; Diaconescu, D.V.; Neagoe, M.; Saulescu, R. Dynamic features of speed increasers from mechatronic wind and hydro systems. Part II. Dynamic aspects. In Proceedings of the Second European Conference on Mechanism Science EUCOMES 08, Casino, Italy, 17–20 September 2008; Springer: Dordrecht, The Netherlands, 2008; pp. 365–373, ISBN 987-1-4020-8914-5.
29. Bevington, C.M.; Bywaters, G.L.; Coleman, C.C.; Costin, D.P.; Danforth, W.L.; Lynch, J.A.; Rolland, R.H. Wind Turbine Having a Direct-Drive Drivetrain. U.S. Patent 7431567B1, 7 October 2008.
30. Marjanovic, N.; Isailovic, B.; Marjanovic, V.; Milojevic, Z.; Blagojevic, M.; Bojic, M. A practical approach to the optimization of gear trains with spur gears. *Mech. Mach. Theory* **2012**, *53*, 1–16. [CrossRef]
31. Qiu, J.; Liu, B.; Dong, H.; Wang, D. Type Synthesis of Gear-box in Wind Turbine. *Procedia Comput. Sci. C* **2017**, *109*, 809–816. [CrossRef]
32. Climescu, O.; Jaliu, C.; Saulescu, R. Comparative Analysis of Horizontal Small Scale Wind Turbines for a Specific Application. In Proceedings of the 14th IFToMM World Congress, Taipei, Taiwan, 25–30 October 2015. [CrossRef]
33. Saulescu, R.; Neagoe, M.; Jaliu, C. *Improving the Energy Performance of Wind Turbines Implemented in the Built Environment Using Counter-Rotating Planetary Transmissions*; Materials Science and Engineering—IOP Conference Series: Materials Science and Engineering; IOP Publishing Ltd.: Bristol, UK, 2016. [CrossRef]
34. Saulescu, R.; Jaliu, C.; Neagoe, M. Structural and Kinematic Features of a 2 DOF Speed Increaser for Renewable Energy Systems. *Appl. Mech. Mater.* **2016**, *823*, 367–372. [CrossRef]
35. Saulescu, R.; Neagoe, M.; Jaliu, C.; Munteanu, O. Comparative analysis of two wind turbines with planetary speed increaser in steady-state. *Appl. Mech. Mater.* **2016**, *823*, 355–360. [CrossRef]
36. Saulescu, R.; Jaliu, C.; Munteanu, O.; Climescu, O. Planetary Gear for Counter-rotating Wind Turbines. *Appl. Mech. Mater.* **2014**, *658*, 135–140. [CrossRef]
37. Saulescu, R.; Jaliu, C.; Climescu, O.; Diaconescu, D. On the use of 2 DOF planetary gears as "speed increaser" in small hydros and wind turbines. In Proceedings of the ASME International Design Engineering Technical Conferences & Computers and Information in Engineering Conference IDETC/CIE 2011, Washington, DC, USA, 25–31 August 2011.
38. Herzog, R.; Schaffarczyk, A.P.; Wacinski, A.; Zürcher, O. Performance and stability of a counter–rotating windmill using a planetary gearing: Measurements and Simulation. In Proceedings of the European Wind Energy Conference & Exhibition, Warsaw, Poland, 20–23 April 2010.
39. Neagoe, M.; Saulescu, R.; Jaliu, C. Design and Simulation of a 1 DOF Planetary Speed Increaser for Counter-Rotating Wind Turbines with Counter-Rotating Electric Generators. *Energies* **2019**, *12*, 1754. [CrossRef]
40. Saulescu, R.; Neagoe, M.; Jaliu, C. Conceptual Synthesis of Speed Increasers for Wind Turbine Conversion Systems. *Energies* **2018**, *11*, 2257. [CrossRef]
41. Sapre, R.; Murkute, H.; Agrawal, R. Comparison between single axis wind turbine and counter wind turbine—A case study. *Glob. J. Eng. Appl. Sci.* **2012**, *2*, 144–146.
42. Lee, S.; Kim, H.; Lee, S. Analysis of aerodynamic characteristics on a counter-rotating wind turbine. *Curr. Appl. Phys.* **2010**, *10*, S339–S342. [CrossRef]
43. Lee, S.; Kim, H.; Son, E.; Lee, S. Effects of design parameters on aerodynamic performance of a counter-rotating wind turbine. *Renew. Energy* **2012**, *42*, 140–144. [CrossRef]
44. Farahani, E.M.; Hosseinzadeh, N.; Ektesabi, M. Comparison of fault-ride-through capability of dual and single-rotor wind turbines. *Renew. Energy* **2012**, *48*, 473–481. [CrossRef]

45. No, T.S.; Kim, J.E.; Moon, J.H.; Kim, S.J. Modelling, control, and simulation of dual rotor wind turbine generator system. *Renew. Energy* **2009**, *34*, 2124–2132. [CrossRef]
46. Kubo, K.; Hano, Y.; Mitarai, H.; Hirano, K.; Kanemoto, T.; Galal, A.M. Intelligent wind turbine unit with tandem rotors (discussion of prototype performances in field tests). *Curr. Appl. Phys.* **2010**, *10*, S326–S331. [CrossRef]
47. Chantharasenawong, C.; Suwantragul, B.; Ruangwiset, A. Axial Momentum Theory for Turbines with Co-axial Counter Rotating Rotors. In Proceedings of the Commemorative International Conference of the Occasion of the 4th Cycle Anniversary of KMUTT Sustainable Development to Save the Earth: Technologies and Strategies Vision 2050: (SDSE2008), Bangkok, Thailand, 11–13 December 2008.
48. Zhamalov, A.Z.; Obozov, A.D.; Kunelbaev, M.M.; Baikadamova, L.S. Capacity and Power Characteristics of Disk Generator with Counter-Rotation of Double-Rotor Wind Turbine. *Middle-East J. Sci. Res.* **2013**, *15*, 1655–1662. [CrossRef]
49. Kanemoto, T.; Galal, A.M. Development of intelligent wind turbine generator with tandem wind rotors and double rotational armatures. *JSME Int. J. Ser. B* **2006**, *49*, 450–457. [CrossRef]
50. Caiozza, J. Wind Driven Electric Generator Apparatus. U.S. Patent 7227276 B2, 5 June 2007.
51. Miloiu, G.; Dudita, F.l.; Diaconescu, D. *Modern Mechanical Transmissions*; Tehnica: Bucharest, Romania, 1980. (In Romanian)
52. Santoso, S.; Le, H.T. Fundamental time–domain wind turbine models for wind power studies. *Renew. Energy* **2007**, *32*, 2436–2452. [CrossRef]
53. Hall, J.F.; Chen, D. Dynamic Optimization of Drivetrain Gear Ratio to Maximize Wind Turbine Power Generation—Part 1: System Model and Control Framework. *J. Dyn. Syst. Meas Control* **2012**, *135*, 011016. [CrossRef]
54. Neagoe, M.; Saulescu, R.; Jaliu, C.; Munteanu, O. Reconfigurable Adjustable Planetary Speed Increaser for Wind Turbines and Adjustment Method. Romanian Patent Application No. A/00224, 24 March 2020.
55. Simionescu, P.A.; Smith, M.R. Single-valued function representations in linkage mechanisms design. *Mech. Mach. Theory* **2000**, *35*, 1709–1726. [CrossRef]
56. Simionescu, P.A. Contributions to the Optimum Synthesis of Linkage-Mechanisms with Applications. Ph.D. Thesis, Politehnica University of Bucharest, Bucharest, Romania, 1999. Available online: http://faculty.tamucc.edu/psimionescu/papers.html (accessed on 19 August 2020).
57. Chen, T.H.; Tang, H.C. Meshing Efficiency Analysis of Straight Spur Gear Pair. *Appl. Mech. Mater.* **2015**, *764–765*, 314–318. [CrossRef]

frontiers | Frontiers in Energy Research

TYPE Original Research
PUBLISHED 01 August 2023
DOI 10.3389/fenrg.2023.1215509

Check for updates

OPEN ACCESS

EDITED BY
Juan P. Amezquita-Sanchez,
Autonomous University of Queretaro,
Mexico

REVIEWED BY
Roberto Quintal Palomo,
Universidad Autónoma de Yucatán,
Mexico
Carlos Morales Pérez,
Technological University of Puebla,
Mexico
Arturo G-P,
University of Guanajuato, Mexico
Agnimitra Biswas,
National Institute of Technology, Silchar,
India

*CORRESPONDENCE
Codruta Jaliu,
cjaliu@unitbv.ro
Mircea Neagoe,
mneagoe@unitbv.ro

RECEIVED 02 May 2023
ACCEPTED 10 July 2023
PUBLISHED 01 August 2023

CITATION
Saulescu R, Jaliu C, Neagoe M, Ciobanu D and Cretescu N (2023), Comparative analysis of torque-adding wind energy conversion systems with a counter-rotating vs. conventional electric generator.
Front. Energy Res. 11:1215509.
doi: 10.3389/fenrg.2023.1215509

Comparative analysis of torque-adding wind energy conversion systems with a counter-rotating vs. conventional electric generator

Radu Saulescu[1], Codruta Jaliu[2]*, Mircea Neagoe[2]*, Daniela Ciobanu[2] and Nadia Cretescu[2]

[1]Design of Mechanical Elements and Systems R&D Center, Faculty of Product Design and Environment, Transilvania University of Brasov, Brasov, Romania, [2]Renewable Energy Systems and Recycling R&D Center, Faculty of Product Design and Environment, Transilvania University of Brasov, Brasov, Romania

The paper presents a comparative analysis on the steady-state behavior of two counter-rotating wind turbines with same components, where the generator can operate as a counter-rotating (with both a mobile rotor and stator—*Case a*) vs. conventional (with a fixed stator—*Case b*) electric machine. These wind energy conversion systems (WECSs) also have two coaxial counter-rotating wind rotors and a one-degree-of-freedom (1-DOF) planetary speed increaser with two inputs and one or two outputs for compatibility with the considered generator. The paper aims at highlighting the efficiency and energy performances of WECSs with a counter-rotating vs. conventional generator by investigating three functional scenarios (A, B, and C) of the two WECS cases (*a* and *b*) under the assumption of identical or different counter-rotating wind rotors. A generalized kinetostatic modeling algorithm is first proposed, starting from the general case of WECS with a counter-rotating generator, which allows the establishment of analytical relationships corresponding to speeds and torques at input and output shafts. Numerical simulations of the obtained closed-form model in each scenario highlighted the influence of the constructive parameters on WECS performances, as well as the energetic superiority of WECS, with a counter-rotating generator (*Case a*) vs. conventional generator (*Case b*): higher efficiency by 1.2% and more output power by 1% (Scenario A) to 5.5% (Scenario C).

KEYWORDS

wind turbine, counter-rotating rotors, counter-rotating electric generator, torque-adding speed increaser, modeling, kinematics, statics, operating point

1 Introduction

The European Union (EU) released a revised directive concerning sustainable energy in 2018 (European Union, 2018) which establishes a mandatory objective at the EU level stating that the share of energy from sustainable sources should be at a minimum of 32% until 2030, adding a clause which would allow an ascending revised growth of this percent until 2023 (Windeurope, 2017). Wind energy is the source with the highest percentage of energy production out of the total amount of sustainable energy in EU, and onshore and offshore wind energy is estimated to represent approximately 21% of electric energy production by 2030. When considering the built environment, a main challenge in designing and implementing wind energy conversion systems (WECS) is to get increased efficiency and energy production that can become main arguments toward choosing sustainable energy.

The growth of energetic performance of wind turbines and optimization of wind potential harnessing can be conducted through different technical solutions converging into one main direction—optimization of the conversion of wind energy into electric energy. This issue refers to the design of either the rotor, gearbox, or electric generator. Thus, the use of multi-rotor systems (Kale and Sapali, 2012) and counter-rotating (primary and secondary) rotors vs. single-rotor (conventional) WECS has proved to harvest more wind energy and, consequently, to increase the electricity production by approximately 40% (Li et al., 2013). Counter-rotating WECS contains two coaxial wind rotors rotating in opposite directions, which can be placed on the same side or on both sides of the nacelle. The primary rotor is the upwind rotor, and the secondary one—the downwind rotor. Vasel-Be-Hagh and Archer (2017) stated that using counter-rotating rotors is 22.6% more efficient in power production than using the single-rotor wind farms, while Circiumaru Oprina et al. (2022) established experimentally the efficiency of counter-rotating WECS on the diameters of the two rotors, with an increase in system efficiency of up to 49.14% being achieved for lower ratios between the diameters of front (upwind) and rear (downwind) rotors. Pacholczyk et al. (2017) demonstrated by simulation that a counter-rotating 5 MW wind turbine brings approximately 20% of additional power compared to the conventional type. Other results refer to the performance of counter-rotating WECS at different aerodynamic loads and blade pitch angles (Jung et al., 2005; No et al., 2009; Rosenberg et al., 2014; Blecharz and Pacholczyk, 2018; Wang et al., 2022), for different number of blades (Pamuji and Bramantya, 2019), various rotor axial distances (Irawan and Bramantya, 2016; Koehuan and SugiyonoKamal, 2017; Pacholczyk et al., 2019), or different rotor configurations (Radhakrishnan et al., 2022). Thus, Rosenberg et al. (2014) demonstrated that the power coefficient for counter-rotating rotors is influenced by the distance between the rotors and their diameters, increasing by 8%–9% when the distance equals the rotor radius and by 7% when the diameter of the upwind rotor is a quarter of the downwind rotor diameter. The pitch control strategy for a 1 MW dual-rotor wind turbine and the impact on its performance were established theoretically (No et al., 2009), both in steady-state and transient regimes, and the results concluded that the proposed model has to be refined by testing the turbine in-site. Li et al. (Zhiqiang et al., 2018) analyzed the improvement of the power coefficient of a micro-counter-rotating wind turbine based on the aerodynamics, the diameters, and configuration of the two rotors and proved that the position of the secondary rotor influences the system efficiency. Moreover, Jung et al. (2005) studied a 30 kW counter-rotating WECS and concluded that the best performance can be obtained when the distance between the rotors is half the auxiliary rotor diameter with the power coefficient reaching 0.5. In addition, it was proved experimentally that the power coefficient decreases with the increase in the pitch angle. A 3 kW coaxial, multi-rotor horizontal-axis wind turbine was built and tested by Mitchell's project team, demonstrating that its power output is approximately three times higher at low and medium wind speeds than a single-rotor turbine of the same diameter (Queen, 2007). All research works concluded that the counter-rotating configuration of rotors is preferable for small power applications rather than the single-rotor WECS.

Regarding the electric generators for WECS, Booker et al. (2010) and Habash et al. (2011) proposed the use of counter-rotating electrical generators for wind turbine applications in urban areas, which have a mobile rotor (*GR*) and mobile stator (*GS*) rotating in opposite directions due to their increased energy performance compared to the conventional (with a fixed stator *GS*) generators. The counter-rotating generator was further investigated in terms of performance and rotor topology by Kutt et al. (2020), Egorov et al. (2021), and Mirnikjoo et al. (2021) and in terms of optimized system configuration with counter-rotating rotors (Mirnikjoo et al., 2020; Ullah et al., 2022a; Ullah et al., 2022b). Cho et al. (2017) analyzedthe performance and control of a WECS with counter-rotating rotors and counter-rotating generator and concluded that this configuration can lower the tip speed ratio at which the power curve attains its maximum almost by half in comparison to the single-rotor system. The designers and developers of counter-rotating generators recommend their use mainly in low-power counter-rotating WECS connected directly to the rotors.

In order to achieve the higher speed requirement of the electric generator, the wind turbines need to include a gearbox for increasing the lower speed of wind rotors. Various types of speed increasers are presented and discussed in the literature: fixed-axis type (Jaliu et al., 2008a; Bevington et al., 2008; Marjanovic et al., 2012), planetary transmissions (Shin, 1999; Jaliu et al., 2008b; Jelaska et al., 2015; Saulescu et al., 2016a; Neagoe et al., 2017; Pastor et al., 2021), and variable speed transmissions (Erturk et al., 2018; Bharani and Sivaprakasam, 2020). Due to their advantages, i.e., high kinematic ratio, reduced radial size, and better efficiency, the researchers consider that the planetary speed increasers are suitable for both single-rotor systems, mainly for the high-power WECS, and for the multi-rotor WECS. For instance, Dong et al. (2017) and Vázquez-Hernández et al. (2017) investigated the parameters that affect the design and the conversion efficiency of WECS and concluded that the use of a planetary transmission is the best option for wind turbines.

In addition, in the counter-rotating WECS configurations, the planetary transmissions can operate either as one-degree-of-freedom (1-DOF) or two-DOF speed increasers, improving in both cases the wind turbine performance. The two operation cases were included by Qiu et al. (2017) in a synthesis of planetary transmissions used in WECS as possible gearboxes, while Saulescu et al. (2018) proposed an algorithm for the conceptual design of the planetary 1-DOF and 2-DOF speed increasers for different functioning situations. Various innovative solutions of planetary speed increasers were proposed (Saulescu et al., 2016b; Saulescu et al., 2018; Neagoe et al., 2019) for counter-rotating WECS. The performance in the steady-state regime of the different WECS configurations was investigated comparatively (Saulescu et al., 2016b; Neagoe et al., 2019; Saulescu et al., 2021; Neagoe and Saulescu, 2022), and a generalized approach for the efficiency analysis of 1-DOF speed increasers for counter-rotating WECS was proposed (Neagoe et al., 2020).

Recent research proved that the use of the counter-rotating generators can lead to a higher conversion efficiency of WECS than the conventional system (Saulescu et al., 2016a; Saulescu et al., 2016b; Neagoe et al., 2017; Neagoe et al., 2019; Neagoe et al., 2020; Saulescu et al., 2021; Neagoe and Saulescu, 2022). However, only a few studies analyzed WECS configuration with both counter-rotating rotors and counter-rotating generator and proposed suitable mechanical transmissions (Neagoe et al., 2019; Neagoe et al., 2020; Neagoe and Saulescu, 2022). To the best of our knowledge, a major research gap identified in the literature review was the need for comparative analysis of these types of WECS in different structural–functional scenarios that allow their constructive optimization and highlight their benefits in comparison with WECS with a conventional generator.

The paper proposes two WECS configurations that combine the concepts of counter-rotating wind rotors and counter-rotating or conventional electric generator and integrate a novel 1-DOF planetary speed increaser with two inputs and two outputs. The proposed transmission can accommodate both the conventional generator and the counter-rotating generator. The paper proposes a generalized modeling approach of these two types of counter-rotating systems with a counter-rotating generator (*Case a*) vs. conventional generator (*Case b*) and compares their energy performance simulation results in the steady state by considering three scenarios. The same primary rotor and same electric generator are used for both cases in all scenarios, while the secondary rotor is designed as follows:

- Different in the two applications, being established from the condition of achieving the same ratio of input torques k_t (Scenario A).
- Identical to the primary rotor $R1$ but operating at a torque and angular speed (in absolute value) different from $R1$ (Scenario B).
- Identical to the primary rotor $R1$ and operating at a torque and angular speed (in absolute value) identical to $R1$ (Scenario C).

The remainder of the paper is organized as follows: two WECS configurations (*Case a* and *Case b*), consisting of two counter-rotating rotors—a 1-DOF speed increaser and a counter-rotating or conventional electric generator, are proposed in Section 2. Section 3 presents a generalized analytical kinematic modeling, and the torque and efficiency modeling algorithm is proposed in Section 4, based on the input torque ratio k_t. Section 5 deals with the expression of the k_t ratio and the mechanical characteristics of the rotors and generator, while Section 6 provides the expressions of the operating point for the proposed WECS configurations. Section 7 presents the numerical simulations and discussions for the three scenarios, and Section 8 is devoted to final conclusions.

2 Problem formulation

The two WECSs with counter-rotating rotors ($R1$—primary rotor and $R2$—secondary rotor) considered in this comparative study are schematically illustrated in Figure 1. The analysis is based on the following correlation: the second variant (Figure 1B) can be obtained from the counter-rotating system with two outputs (materialized by the rotor GR and the stator GS of a counter-rotating generator Gc, Figure 1A) by breaking the connection between the speed increaser SI and the stator GS and by fixing the stator (Figure 1B). Therefore, the mathematical models derived in the general case of systems with a counter-rotating generator (*Case a*) allow proving the results obtained for systems with a conventional generator G (*Case b*) by customizing the GS stator state.

The following assumptions are used in the comparative analysis of the two WECSs:

- Both WECSs use the same mechanical transmission SI, for which the following parameters are known: internal kinematic ratio and internal efficiency.
- The same mechanical characteristics are considered for the homologous wind rotors on the one hand and for the electric generators (both conventional and counter-rotating) on the other hand.
- The ratio of the torques of the two wind rotors $k_t = -T_{R2}/T_{R1} > 0$ is introduced; it allows controlling the mechanical characteristic of the rotor $R2$.

The planetary speed increaser (Figure 2) is a complex transmission consisting of two parallel-connected 1-DOF planetary gear sets, 1-2-3-5-6-H (PG I = 01) and 4-3-5-6-H (PG II = 02), which have three sun gears (1, 4, and 6) and a common planet carrier H (Figure 3). The internal kinematic ratios of the two planetary gear sets are denoted by $i_{01} = i_{16}^H = i_{12}^H \cdot i_{23}^H \cdot i_{56}^H = \frac{\omega_1}{\omega_2}\frac{\omega_2}{\omega_3}\frac{\omega_5}{\omega_6} = \left(-\frac{z_2}{z_1}\right)\left(-\frac{z_3}{z_2}\right)\left(+\frac{z_6}{z_5}\right) = +\frac{z_3}{z_1}\frac{z_6}{z_5}$ and $i_{02} = i_{46}^H = i_{43}^H \cdot i_{56}^H = \frac{\omega_4}{\omega_3}\frac{\omega_5}{\omega_6} = \left(+\frac{z_3}{z_4}\right)\left(+\frac{z_6}{z_5}\right) = +\frac{z_3}{z_4}\frac{z_6}{z_5}$, respectively, where z_i is the teeth number of the gear $i = 1 \ldots 6$ and i_{xy}^z is the kinematic

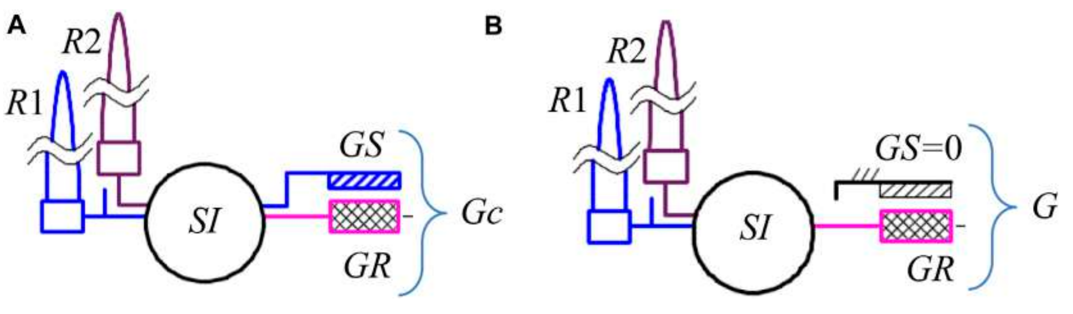

FIGURE 1
Conceptual diagrams of the WECS considered in the comparative analysis: systems with a counter-rotating generator **(A)** and conventional generator **(B)**.

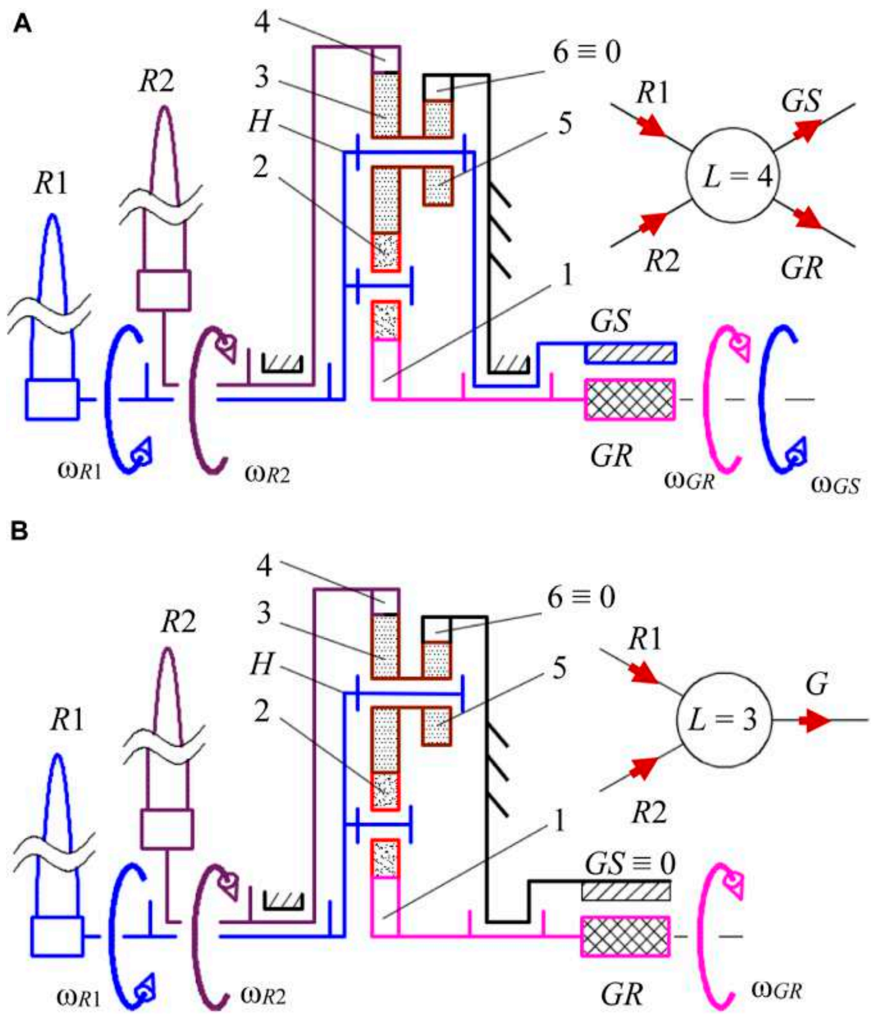

FIGURE 2
Structural schemes and block diagrams of the 1-DOF systems with a counter-rotating generator **(A)** and conventional generator **(B)**.

ratio, where the rotational motion is transmitted from body x to body y and z is considered the reference body.

According to Figure 2A; Figure 3, the WECS with two counter-rotating wind rotors ($R1$ and $R2$), a speed increaser (1-2-3-4-5-6-H), and a counter-rotating electric generator Gc uses a planetary transmission with two inputs ($H \equiv R1$—primary input; $4 \equiv R2$—secondary input) and two outputs ($1 \equiv GR$—primary output; $H \equiv GS$—secondary output). Thus, the 1-DOF planetary speed increaser transmits the mechanical power from the counter-rotating wind rotors to the electric generator whose rotor and stator rotate in opposite directions. This 1-DOF planetary mechanism has the property of a) summing the input torques from the wind rotors (torque-adding) and b) transmission in a determined way of an independent external motion to the other three exterior links. Overall, the planetary transmission (Figure 2A) has four inputs and outputs ($L = 4$): conventionally, the primary input is connected to the wind rotor $R1$, and the secondary input is connected to the wind rotor $R2$; the two outputs are connected to the rotor GR and to the stator GS. According to Figure 2A, the secondary input $R2$ is connected directly to the stator GS. Because the transmission from Figure 2B can be obtained by breaking the connection between the secondary output H and the generator stator and by fastening the stator GS to the base, its kinematic and static model can be derived as a particular case of the mathematical model of the speed increaser from Figure 2A.

The kinematic and static (torque) correlations, which are systematized in relationships (1)–(3), (4), and (5), refer to the systems shown in Figure 2 and allow highlighting their performance by considering the mechanical characteristics of the wind rotors and the generator or the behavior of one wind rotor in relation to the other. The efficiency of the transmission can be determined either based on the torques of the two wind rotors or by using the torque of the primary rotor (T_{R1}) and the input torque ratio k_t.

3 Kinematic modeling

The specific kinematic correlations of the speed increaser and its connections to the external links can be written according to

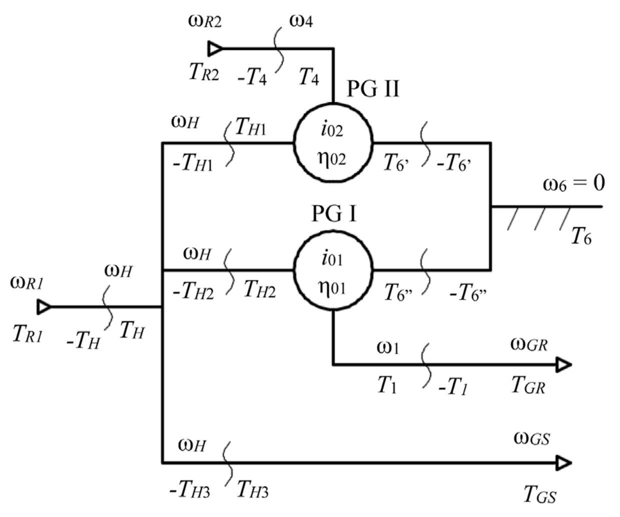

FIGURE 3
Block diagram of the 1-DOF planetary speed increaser with two inputs and two outputs.

Figure 3 starting from the general relationships of a planetary gear set (Neagoe et al., 2020).

Considering the motion of the rotor $R1$ as an independent parameter, Eq. 1 highlights the kinematic correlations specific to the isolated subsystems:

- Input shafts:

$$\omega_{R1} = \omega_H; \quad \omega_{R2} = \omega_4. \tag{1a}$$

- Planetary gear sets:

$$\text{PG I: } \omega_1 - \omega_H(1 - i_{01}) = 0; \quad \text{PG II:} \quad \omega_4 - \omega_H(1 - i_{02}) = 0. \tag{1b}$$

- Transmission connections with the generator stator and rotor:

$$\omega_{GR} = \omega_1; \quad \omega_{GS} = \omega_H. \tag{1c}$$

- The transmission functions of the system:

$$\begin{cases} \omega_{R2} = \omega_{R1}(1 - i_{02}); \\ \omega_{GR} = \omega_{R1}(1 - i_{01}); \\ \omega_{GS} = \omega_{R1}. \end{cases} \tag{1d}$$

Based on the aforementioned equations, the kinematic transmission functions can be obtained as follows:

- 1-DOF speed increaser with two counter-rotating inputs and two counter-rotating outputs, as shown in Figure 2A:

$$\omega_{Gc} = \omega_{GR} - \omega_{GS} = -i_{01}\omega_{R1}. \tag{2}$$

- 1-DOF speed increaser with two counter-rotating inputs and one output, as shown in Figure 2B ($\omega_{GS} = 0$ and $\omega_{GR} = \omega_G$):

$$\omega_G = \omega_{R1}(1 - i_{01}). \tag{3}$$

4 Torques and efficiency modeling

Analogous to the kinematic modeling, the static modeling is performed using the block diagram shown in Figure 3, which allows identifying the static correlations specific to the two planetary gear sets, the equilibrium equations of the links between them and also of the external connections, and the static transmission function. These relationships together with the mechanical characteristics of the wind rotors and the counter-rotating/conventional electric generator can be used for identifying the following: the operating point of the machine of wind rotors—speed increaser—electric generator type; the mechanical power obtained at the input of the electric generator; the power flow through the speed increaser and its efficiency; and the influence of the ratio k_t.

For the 1-DOF speed increaser with two counter-rotating inputs and two counter-rotating outputs, as shown in Figure 2A, the equality $T_{Gc} = T_{GR} = -T_{GS}$ is considered (also valid for the conventional generator) by considering the torque balance for the generator stator and rotor. According to Figure 3, the planetary speed increaser is characterized by the following static correlations starting from its isolated subsystems:

- Input shafts:

$$T_{R1} - T_H = 0; \quad T_{R2} - T_4 = 0. \tag{4a}$$

- Internal shafts:

$$T_H - T_{H_1} - T_{H_2} - T_{H_3} = 0; \quad T_6 - T_{6'} - T_{6''} = 0. \tag{4b}$$

- Planetary gear sets (PG I and PG II):

$$\begin{cases} T_1 + T_{6''} + T_{H_2} = 0; \quad T_4 + T_{6'} + T_{H_1} = 0; \\ T_{6''} = -T_1 \dfrac{i_{01}}{\eta_{01}}; \quad T_{6'} = -T_4 i_{02}\eta_{02}. \end{cases} \tag{4c}$$

- Transmission connections with the generator stator and rotor:

$$T_{GR} - T_1 = 0; \quad T_{GS} + T_{H_3} = 0. \tag{4d}$$

- Transmission functions of the system:

$$T_{GR} = T_{R1} \frac{\eta_{01} - k_t \eta_{01}(1 - i_{02}\eta_{02})}{i_{01}}. \tag{4e}$$

- The mechanical characteristics of the wind rotors and the electric generator:

$$\begin{cases} T_{R1} = -a_{R1}\omega_{R1} + b_{R1}; \\ T_{R2} = -k_t T_{R1} = -a_{R2}\omega_{R2} + b_{R2}; \\ -T_{Gc} = a_G \omega_{Gc} - b_G. \end{cases} \tag{4f}$$

- For the 1-DOF speed increaser with two counter-rotating inputs and one output, as shown in Figure 2B, Eq. 4 is particularized for the fixed stator and $T_{H_3} = 0$:

$$\begin{cases} T_1^* + T_{6''}^* + T_{H_2}^* = 0; \quad T_4^* + T_{6'}^* + T_{H_1}^* = 0 \\ T_{6''}^* = -T_1^* \dfrac{i_{01}}{\eta_{01}}; \quad T_{6'}^* = -T_4^* i_{02}\eta_{02} \\ T_H^* - T_{H_1}^* - T_{H_2}^* = 0; \quad T_6^* - T_{6'}^* - T_{6''}^* = 0; \\ T_{R1} - T_H^* = 0; \quad T_{R2} - T_4^* = 0 \\ T_G - T_1^* = 0 \\ T_G = -T_{R1} \dfrac{\eta_{01} - k_t\eta_{01}(1 - i_{02}\eta_{02})}{\eta_{01} - i_{01}} \\ T_{R1} = -a_{R1}\omega_{R1} + b_{R1}; \quad T_{R2} = -k_t T_{R1} = -a_{R2}\omega_{R2} + b_{R2} \\ -T_G = a_G\omega_G - b_G. \end{cases} \tag{5}$$

In order to avoid possible confusions, the static parameters belonging to the system with a conventional generator, that have different values than those of the first case, are marked with an asterisk.

5 Determination of the k_t ratio

In the general case, the static ratio k_t depends on the input and output mechanical characteristics; a certain value for the k_t ratio can be obtained by modifying appropriately at least one mechanical characteristic. As a result, the analytical expressions of the k_t ratio are further modeled for both systems according to the coefficients of the input and output mechanical characteristics:

- *Case a*, see Figure 2A and Eq. 4:

$$\begin{cases} T_{R2} = -k_t T_{R1}; \\ T_{Gc} = T_{R1} \dfrac{\eta_{01} - k_t\eta_{01}(1 - i_{02}\eta_{02})}{i_{01}}. \end{cases} \tag{6}$$

By replacing the mechanical characteristics presented in Eq. 4 into Eq. 6 and by considering the kinematic correlations from Eqs 1, 2, the following equation system is obtained:

$$\begin{cases} -a_{R2}\omega_{R2} + b_{R2} = a_{R1}k_t\omega_{R1} - b_{R1}k_t; \\ -a_G\omega_{Gc} + b_G = -a_{R1}\dfrac{\eta_{01} - k_t\eta_{01}(1 - i_{02}\eta_{02})}{i_{01}}\omega_{R1} + b_{R1}\dfrac{\eta_{01} - k_t\eta_{01}(1 - i_{02}\eta_{02})}{i_{01}}; \\ \omega_{R2} = \omega_{R1}(1 - i_{02}); \\ \omega_{Gc} = -\omega_{R1} i_{01}. \end{cases} \tag{7}$$

The k_t ratio can be obtained by solving the equation system Eq. 7:

$$k_t = -\frac{a_{R1}b_{R2}\eta_{01} + a_{R2}b_{R1}\eta_{01}(i_{02} - 1) + a_{R2}b_G i_{01}(1 - i_{02}) + a_G b_{R2} i_{01}^2}{a_{R1}[b_{R2}\eta_{01}(i_{02}\eta_{02} - 1) + b_G i_{01}] + b_{R1}[a_{R2}\eta_{01}(i_{02}^2\eta_{02} - i_{02}\eta_{02} - i_{02} + 1) + a_G i_{01}^2]}. \tag{8}$$

By denoting

$$\begin{cases} A = a_{R1}b_{R2}\eta_{01} + a_{R2}b_{R1}\eta_{01}(i_{02} - 1) \\ B = a_{R2}b_G i_{01} \\ C = a_G b_{R2} \\ D = b_{R2}\eta_{01}(i_{02}\eta_{02} - 1) \\ E = a_{R2}\eta_{01}(i_{02}^2\eta_{02} - i_{02}\eta_{02} - i_{02} + 1), \end{cases} \tag{9}$$

it is obtained

$$k_t = -\frac{A + B(1 - i_{02}) + Ci_{01}^2}{a_{R1}[D + b_G i_{01}] + b_{R1}[E + a_G i_{01}^2]}. \tag{10}$$

Case b, see Figure 2B and Eq. 5:

$$\begin{cases} T_{R2} = -k_t T_{R1}; \\ T_G = -T_{R1}\dfrac{\eta_{01} - k_t\eta_{01}(1 - i_{02}\eta_{02})}{\eta_{01} - i_{01}}. \end{cases} \tag{11}$$

Similar to the previous case, by combining Eqs 1, 3, 5 with system (11), it is obtained

$$\begin{cases} -a_{R2}\omega_{R2} + b_{R2} = a_{R1}k_t\omega_{R1} - b_{R1}k_t \\ -a_G\omega_G + b_G = -a_{R1}\dfrac{\eta_{01} - k_t\eta_{01}(1 - i_{02}\eta_{02})}{\eta_{01} - i_{01}}\omega_{R1} + b_{R1}\dfrac{\eta_{01} - k_t\eta_{01}(1 - i_{02}\eta_{02})}{\eta_{01} - i_{01}} \\ \omega_{R2} = \omega_{R1}(1 - i_{02}) \\ \omega_G = \omega_{R1}(1 - i_{01}). \end{cases} \tag{12}$$

The ratio k_t can be determined by solving system (12):

$$k_t = -\frac{A + B(1 - i_{02} - \eta_{01} + \eta_{01}i_{02}) + C(i_{01}^2 + \eta_{01} - i_{01} - i_{01}\eta_{01})}{a_{R1}[D + b_G(i_{01} - \eta_{01})] + b_{R1}[E + a_G(i_{01}^2 - i_{01}\eta_{01} - i_{01} + \eta_{01})]}, \tag{14}$$

where A, B, C, D, and E are defined by Eq. 9.

Taking into account Eqs 2–5, the expressions of the constants a_{R2} and b_{R2} (related to the characteristic of the wind rotor *R2*) are deduced based on the imposed ratio k_t; the following equation can be written from the expression of the k_t ratio:

$$T_{R1}k_t + T_{R2} = 0. \tag{15}$$

An equation of $X\omega_{R1} + Y = 0$ type is obtained from Eq. 15, which leads to

$$[-a_{R1}k_t - a_{R2}(1 - i_{02})]\omega_{R1} + b_{R1}k_t + b_{R2} = 0. \tag{16}$$

As the angular speed ω_{R1} is the independent kinematic parameter, the previous relationship is fulfilled for any value of ω_{R1} only if $X = [-a_{R1}k_t - a_{R2}(1 - i_{02})] = 0$ and $Y = b_{R1}k_t + b_{R2} = 0$; therefore, the coefficients a_{R2} and b_{R2} become

$$\begin{cases} a_{R2} = -\dfrac{a_{R1}k_t}{1 - i_{02}} \\ b_{R2} = -k_t b_{R1}. \end{cases} \tag{17}$$

6 Determination of the operating point

The analytical relationships of the kinematic and static parameters are systematized comparatively in Table 1 for both analyzed WECSs.

The parameters of the operating point (F) reduced on the shaft connected to the generator rotor can be also obtained for the two cases:

- *Case a*, Figure 2A (see Eqs 2, 4):

TABLE 1 Analytical expressions of the kinematic and static parameters.

Parameter		η_{01}	η_{02}	k_t	i_a		η_a	
Relationship					*Case a*	*Case b*	*Case a*	*Case b*
		η_g^3	η_g^2	$-\frac{T_{R2}}{T_{R1}}$	$-i_{01}$	$1-i_{01}$	$\eta_{01}\frac{1-k_t(1-i_{02}\eta_{02})}{1-k_t(1-i_{02})}$	$\frac{\eta_{01}(1-i_{01})}{\eta_{01}-i_{01}}\frac{1-k_t(1-i_{02}\eta_{02})}{1-k_t(1-i_{02})}$
Case a	Parameter	ω_{Gc}			T_{Gc}		P_{Gc}	
	Relationship	$-\omega_{R1}i_{01}$			$T_{R1}\frac{\eta_{01}}{i_{01}}[1-k_t(1-i_{02}\eta_{02})]$		$-\omega_{R1}T_{R1}\eta_{01}[1-k_t(1-i_{02}\eta_{02})]$	
Case b	Parameter	ω_G			T_G		P_G	
	Relationship	$\omega_{R1}(1-i_{01})$			$-T_{R1}\frac{\eta_{01}[1-k_t(1-i_{02}\eta_{02})]}{\eta_{01}-i_{01}}$		$-\omega_{R1}T_{R1}\frac{\eta_{01}(1-i_{01})[1-k_t(1-i_{02}\eta_{02})]}{\eta_{01}-i_{01}}$	

TABLE 2 Values of the parameters related to the steady-state operating point for Scenario (A).

Parameter		ω [s^{-1}]	T [kNm]	P [kW]	ω_{Gc}; ω_G [s^{-1}]	T_{Gc}; T_G [kNm]	P_{Gc}; P_G [kW]	η_a [%]
Case a	*R*1	14.97	113.25	1,696.13	−149.76	10.27	−1,538.71	0.795
	*R*2	−2.99	−79.27	237.45				
Case b	*R*1	16.57	102.87	1,704.95	−149.16	10.20	−1,522.59	0.783
	*R*2	−3.31	−72.01	238.69				
a_{R1} = 6.5 kNms; b_{R1} = 210.6 kNm;								
a_{R2} = 22.75 kNms; b_{R2} = −147.42 kNm;								
a_G = 0.11 kNms; b_G = −6.2 kNm.								
i_{01} = 10, i_{02} = 1.2, η_{01} = 0.857, η_{02} = 0.9025, and k_t = 0.7.								

$$\begin{cases} \omega_F = \dfrac{b_G - \frac{b_{R1}\eta_{01}[1-k_t(1-i_{02}\eta_{02})]}{i_{01}}}{a_G + \frac{a_{R1}\eta_{01}[1-k_t(1-i_{02}\eta_{02})]}{i_{01}^2}}; \\ T_F = -a_G\omega_F + b_G; \quad P_F = \omega_F T_F. \end{cases} \tag{18}$$

- *Case b*, Figure 2B (see Eqs 3, 5):

$$\begin{cases} \omega_F^* = \dfrac{b_G + \frac{b_{R1}\eta_{01}[1-k_t(1-i_{02}\eta_{02})]}{\eta_{01}-i_{01}}}{a_G + \frac{a_{R1}\eta_{01}[1-k_t(1-i_{02}\eta_{02})]}{(\eta_{01}-i_{01})(1-i_{01})}}; \\ T_F^* = -a_G\omega_F^* + b_G; \quad P_F^* = \omega_F^* T_F^*. \end{cases} \tag{19}$$

7 Numerical results and discussion

For the purpose of comparative analysis, numerical simulations are further performed by considering that each of the two WECSs is characterized by the internal kinematic ratios $i_{01} = 10$ and $i_{02} = 1.2$ and the internal efficiency $\eta_{01} = \eta_g^3 = 0.95^3 = 0.857$ and $\eta_{02} = \eta_g^2 = 0.95^2 = 0.9025$ for all three scenarios, under following general assumptions:

- The primary rotors *R*1 have the same mechanical characteristic (i.e., same values of a_{R1} and b_{R1}, respectively, see Table 2).
- The electric generators have the same mechanical characteristic in both cases (i.e., same values of a_G and b_G, respectively, see Table 2).

The behavior of the two WECSs is analyzed in three different scenarios, in which the secondary wind rotor and the speed increaser are modified according to the following assumptions:

Scenario (A): the static ratio in both cases is $k_t = 0.7$, achieved by the appropriate selection of the mechanical characteristic of the rotor *R*2.

Scenario (B): the rotors *R*2 of the two WECSs are identical with the rotors *R*1, but different values of k_t are registered for the two cases.

Scenario (C): the rotors *R*2 are identical with the rotors *R*1 in both cases, and the same value of k_t ($k_t = 1$) is obtained for the two WECSs by changing $i_{02} = 2$. In this particular case, the wind rotors *R*1 and *R*2 rotate with equal speeds in opposite directions.

The values of the coefficients $a_{R1,2}$ and $b_{R1,2}$ from the mechanical characteristics of the wind rotors *R*1 and *R*2, which are dependent on the blade aerodynamic behavior, were obtained by applying the algorithm presented in Neagoe and Saulescu (2022). The behavior of the two types of WECSs is further presented comparatively based on the values of the kinematic and static parameters in the operating point, also following the influence of the mechanical characteristics on the system behavior and energy performance.

7.1 Comparative analysis in Scenario A

The coefficients of the mechanical characteristics describing the behavior of the rotors *R*2 are determined based on the previous data, by means of Eq. 17 and imposing $k_t = 0.7$; then, the parameters of the operating points of the two systems are determined based on Eqs 18, 19. The obtained values related to the steady-state operating points are centralized in Table 2 and illustrated in Figures 4–6. The mechanical characteristics of the two wind rotors (Figure 4) are

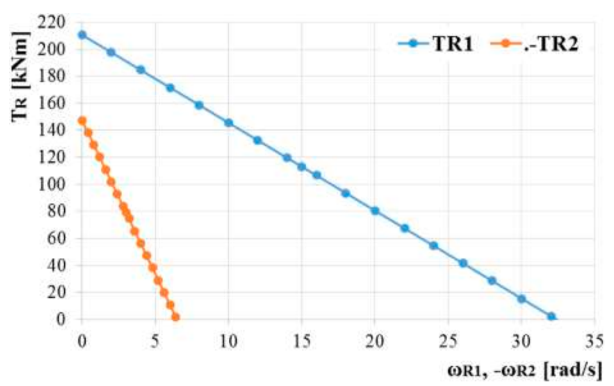

FIGURE 4
Mechanical characteristics of the wind rotors *R1* and *R2* in Scenario A.

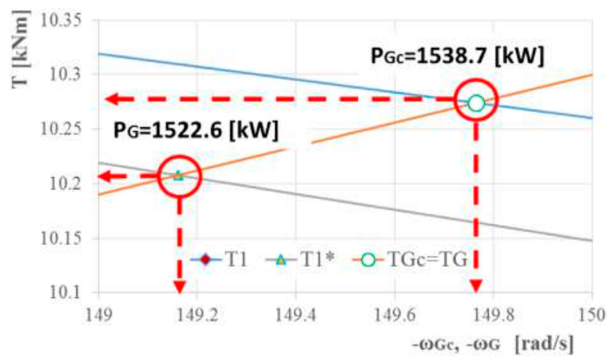

FIGURE 6
Operating points in Scenario A reduced on the generator shafts with the specification of the afferent mechanical power.

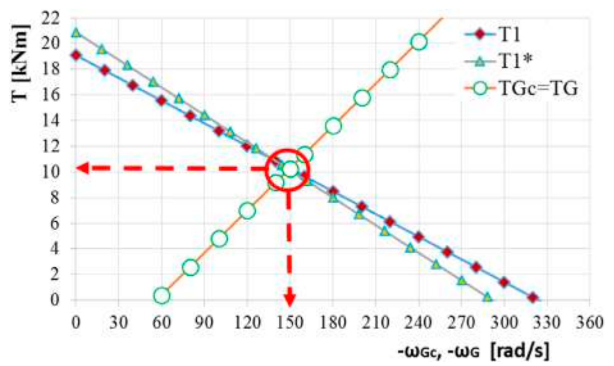

FIGURE 5
Operating points in Scenario A reduced on the shaft of the counter-rotating generator $T_1 = T_{Gc} = T_{Gc}(\omega_{Gc})$ and on the shaft of the conventional generator $T_1^* = T_G = T_G(\omega_G)$.

TABLE 3 Values of the parameters related to the steady-state operating point for Scenario (B).

Parameter	*Case a* (Figure 2A)	*Case b* (Figure 2B)
ω_{R1} [s^{-1}]	15.45	17.14
T_{R1} [kNm]	110.15	99.19
P_{R1} [kW]	1,702.24	1,700.12
ω_{R2} [s^{-1}]	−3.09	−3.43
T_{R2} [kNm]	−190.51	−188.32
P_{R2} [kW]	588.83	645.53
ω_{Gc}; ω_G [s^{-1}]	−154.54	−154.25
T_{Gc}; T_G [kNm]	10.80	10.77
P_{Gc}; P_G [kW]	−1,668.97	−1,661.01
η_a [%]	0.728	0.708
k_t	1.729	1.898
$i_a = \omega_{Gc(G)}/\omega_{R1}$	−10	−9
$a_{R1} = a_{R2} = 6.5$ kNms; $b_{R1} = -b_{R2} = 210.6$ kNm;		
$a_G = 0.11$ kNms; $b_G = -6.2$ kNm.		
$i_{01} = 10$, $i_{02} = 1.2$, $\eta_{01} = 0.857$, and $\eta_{02} = 0.9025$.		

reduced on the *SI* outputs, and thus the operating points in both cases are obtained, as depicted in Figures 5, 6.

Figure 6 details Figure 5 and presents comparatively the two operating points reduced on the transmission output shaft and the afferent mechanical powers. It shows that the output power in *Case a* is higher by ~1% than that in *Case b*, due to the generator benefits of a higher torque and a higher angular speed, implicitly.

From the results systematized in Table 2, it appears that the efficiency of the system with a counter-rotating generator is higher than that of the system with a conventional generator; this aspect is due to the branched transmission of the mechanical power at the output of the speed increaser, in which case the power transmitted to the stator of the electric generator is without friction losses (Figure 3). In the case of the system with a conventional generator, the entire mechanical power is transmitted through the speed increaser only to the rotor of the electric generator, and implicitly, the frictional losses are higher. Therefore, considering a theoretical case of 1 kW cumulative input power generated by the two wind rotors, the 1-DOF transmission with two inputs and two outputs delivers to the generator a power of 795 W, while the system with two inputs and one output delivers a power of 783 W for the same static ratio $k_t = 0.7$.

Due to the higher efficiency in *Case a* compared to *Case b*, an output power $P_{Gc} > P_G$ is obtained despite the lower powers of the rotors *R1* and *R2*, where both rotors operate at lower speeds and higher torques. This phenomenon can be an advantage, especially at lower wind speeds.

7.2 Comparative analysis in Scenario B

The values obtained in this scenario are given in Table 3, by considering identical wind rotors in both cases. Similar to Scenario

TABLE 4 Values of the parameters related to the steady-state operating point for Scenario (C).

Parameter	*Case a* (Figure 2A)	*Case b* (Figure 2B)
ω_{R1} [s^{-1}]	18.42	20.02
T_{R1} [kNm]	90.87	80.45
P_{R1} [kW]	1,673.81	1,610.98
ω_{R2} [s^{-1}]	−18.42	−20.02
T_{R2} [kNm]	−90.87	−80.45
P_{R2} [kW]	1,673.81	1,610.98
ω_{Gc}; ω_G [s^{-1}]	−184.20	−180.18
T_{Gc}; T_G [kNm]	14.06	13.62
P_{Gc}; P_G [kW]	−2,590.33	−2,454.19
η_a [%]	0.773	0.761
k_t	1	1
$i_a = \omega_{Gc(G)}/\omega_{R1}$	−10	−9
$a_{R1} = a_{R2} = 6.5$ kNms; $b_{R1} = -b_{R2} = 210.6$ kNm;		
$a_G = 0.11$ kNms; $b_G = -6.2$ kNm.		
$i_{01} = 10$, $i_{02} = 2$, $\eta_{01} = 0.857$, and $\eta_{02} = 0.9025$.		

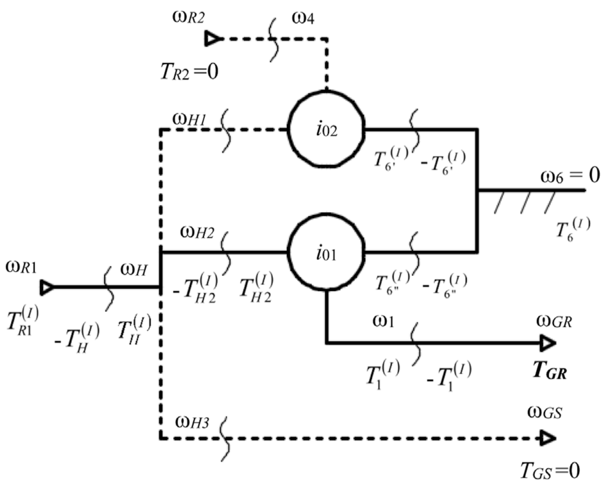

FIGURE 7
Block diagram of the planetary speed increaser from Figure 3 in the functional case of $T_{GR} \neq 0$, $T_{GS} = 0$, and $T_{R2} = 0$.

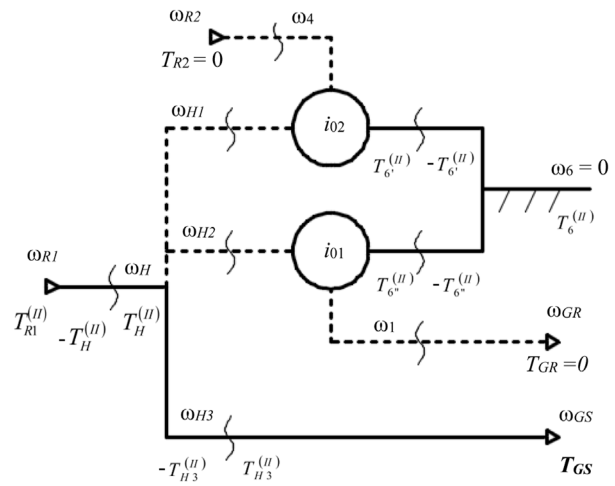

FIGURE 8
Block diagram of the planetary speed increaser from Figure 3 in the functional case of $T_{GR} = 0$, $T_{GS} \neq 0$, and $T_{R2} = 0$.

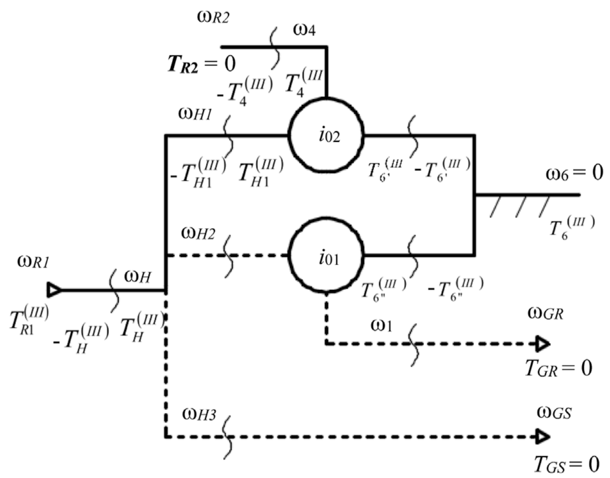

FIGURE 9
Block diagram of the planetary speed increaser from Figure 3, for which the independent torque T_{R2} is considered to be non-zero, i.e., $T_{GR} = 0$, $T_{GS} = 0$, and $T_{R2} \neq 0$.

A, the counter-rotating generator system (*Case a*) achieves a slightly higher power output (by ~0.5%) than *Case b*, as the mechanical power is flowing at a higher efficiency (0.728 vs. 0.708) due to the branched transmission of the output power. Implicitly, the counter-rotating generator operates at higher torque and rotational speed than the conventional generator.

In *Case a*, the rotor *R*2 extracts a lower power from wind and the rotor *R*1 extracts a higher power than *Case b*. The ratio $k_t > 1$ in both cases (i.e., 1.729 vs. 1.898), that is, the rotor *R*2 operates at a higher torque and lower rotational speed than the rotor *R*1.

7.3 Comparative analysis in Scenario C

In order to meet the premise of $k_t = 1$ in both cases, the value of kinematic ratio i_{02} is determined by imposing $\omega_{R2}/\omega_{R1} = -1$ in Eq. 1d:

$$i_{02} = 1 - \frac{\omega_{R2}}{\omega_{R1}} = 2. \tag{20}$$

Table 4 shows the values of the operating points in *Case a* and *Case b* for Scenario C. By imposing the two rotors which rotate in opposite directions with the same speed, an increase in the power supply brought by the rotor *R*2 and a better efficiency are obtained compared with Scenario B. The kinematic and static relative behavior of the two cases is similar to the previous

10.3389/fenrg.2023.1215509

TABLE 5 Expressions of the torques and speeds for the speed increaser with two inputs and two outputs (*Case a*, Figure 3).

	$T_j^{(I)}$ (Figure 7)	$T_j^{(II)}$ (Figure 8)	$T_j^{(III)}$ (Figure 9)	$T_j = T_j^{(I)} + T_j^{(II)} + T_j^{(III)}$
T_{H1}	0	0	$k_t T_{R1}(1 - i_{02}\eta_{02}^w)$	$k_t T_{R1}(1 - i_{02}\eta_{02}^w)$
T_{H2}	$-T_{R1}\frac{(1-i_{01}\eta_{01}^x)[1-k_t(1-i_{02}\eta_{o2}^w)]}{i_{01}\eta_{01}^x}$	0	0	$-T_{R1}\frac{(1-i_{01}\eta_{01}^x)[1-k_t(1-i_{02}\eta_{o2}^w)]}{i_{01}\eta_{01}^x}$
T_{H3}	0	$T_{R1}\frac{[1-k_t(1-i_{02}\eta_{o2}^w)]}{i_{01}\eta_{01}^x}$	0	$T_{R1}\frac{[1-k_t(1-i_{02}\eta_{o2}^w)]}{i_{01}\eta_{01}^x}$
T_H	$-T_{R1}\frac{(1-i_{01}\eta_{01}^x)[1-k_t(1-i_{02}\eta_{o2}^w)]}{i_{01}\eta_{01}^x}$	$T_{R1}\frac{[1-k_t(1-i_{02}\eta_{o2}^w)]}{i_{01}\eta_{01}^x}$	$k_t T_{R1}(1 - i_{02}\eta_{02}^w)$	T_{R1}
ω_H	ω_{R1}			
T_4	0	0	$-k_t T_{R1}$	$-k_t T_{R1}$
ω_4	$\omega_{R1}(1 - i_{02})$			
T_1	$T_{R1}\frac{[1-k_t(1-i_{02}\eta_{o2}^w)]}{i_{01}\eta_{01}^x}$	0	0	$T_{R1}\frac{[1-k_t(1-i_{02}\eta_{o2}^w)]}{i_{01}\eta_{01}^x}$
ω_1	$\omega_{R1}(1 - i_{01})$			
$T_{6'}$	0	0	$k_t T_{R1} i_{02}\eta_{02}^w$	$k_t T_{R1} i_{02}\eta_{02}^w$
$T_{6''}$	$-T_{R1}[1 - k_t(1 - i_{02}\eta_{o2}^w)]$	0	0	$-T_{R1}[1 - k_t(1 - i_{02}\eta_{o2}^w)]$
T_6	$-T_{R1}[1 - k_t(1 - i_{02}\eta_{o2}^w)]$	0	$k_t T_{R1} i_{02}\eta_{02}^w$	$-T_{R1}(1 - k_t)$
ω_6	0			
where $j = H, H1, H2, H3, 1, 4, 6', 6'', 6$, $x = -1$, and $w = +1$.				

scenarios, with the efficiency of the speed increaser with two outputs bringing an improvement of ~1.5%. In this scenario, both rotors $R1$ and $R2$ registered in *Case a* have higher power and torque, accompanied by smaller rotational speed, than those in *Case b*.

7.4 Power flow

Analytically, the static transmission functions can be determined either by solving the system of equations formed by the static relationships from Eq. 4 or using the "effects overlapping" method; according to this method, initially abstracting from the wind rotors and the electric generator, the static analysis of the considered 1-DOF mechanism with $L = 4$ can be reduced (due to its linear-type functions) to the analysis of $L = 3$ simpler 1-DOF mechanisms ($L = 2$); they are obtained from the initially considered mechanism (Figures 2A, 3), leaving non-null in turn for each of the three independent torques: T_{GR}, T_{GS}, and T_{R2}. It is obtained as follows: the mechanism with the block diagram from Figure 7 (with $T_{GR} \neq 0$, $T_{GS} = 0$, and $T_{R2} = 0$), the mechanism from Figure 8 (with $T_{GR} = 0$, $T_{GS} \neq 0$, and $T_{R2} = 0$), and the mechanism from Figure 9, respectively (with $T_{GR} = 0$, $T_{GS} = 0$, and $T_{R2} \neq 0$).

By "overlapping the static effects" of the mechanisms from Figures 7–9, the expressions of the static transmission functions of the initial mechanism (Figure 3) and the torque of the electric generator are obtained. Similarly, the other torques are determined (see Table 5) while being required in the organologic calculations.

As explained in the problem formulation, the 1-DOF speed increaser with two inputs and one output (Figure 2B) was obtained from the speed increaser with two inputs and two outputs (Figure 3) by breaking the stator connection and by fixing it (i.e., $\omega_{GS} = 0$). This speed increaser with one output is a particular case of the one from Figure 3. Its internal torques and speeds are presented in Table 6 by processing the relationships (3) and (5).

TABLE 6 Expressions of the torques and speeds for the speed increaser with two inputs and one output (*Case b*).

T_{H1}^*	$k_t T_{R1}(1 - i_{02}\eta_{02}^w)$
T_{H2}^*	$T_{R1}[1 - k_t(1 - i_{02}\eta_{o2}^w)]$
T_{H3}^*	0
T_H^*	T_{R1}
ω_H	ω_{R1}
T_4^*	$-k_t T_{R1}$
ω_4	$\omega_{R1}(1 - i_{02})$
T_1^*	$-T_{R1}\frac{[1-k_t(1-i_{02}\eta_{o2}^w)]}{1-i_{01}\eta_{01}^x}$
ω_1	$\omega_{R1}(1 - i_{01})$
$T_{6'}^*$	$k_t T_{R1} i_{02}\eta_{02}^w$
$T_{6''}^*$	$T_{R1}\frac{[1-k_t(1-i_{02}\eta_{o2}^w)]i_{01}\eta_{01}^x}{1-i_{01}\eta_{01}^x}$
T_6^*	$T_{R1}\left\{k_t i_{02}\eta_{02}^w + \frac{[1-k_t(1-i_{02}\eta_{o2}^w)]i_{01}\eta_{01}^x}{1-i_{01}\eta_{01}^x}\right\}$
ω_6	0
where $x = -1$ and $w = +1$.	

A modeling of the power flow from inputs to outputs in both cases is further developed by considering the input power of the primary rotor (P_{R1}) as an independent variable and known values for the input parameters $k_t = 0.7$, $i_{01} = 10$, $i_{02} = 1.2$, and $\eta_g = 0.95$, as used in Scenario A. The correlations corresponding to the speeds and torques for highlighting the power flow in *Case a* (Figure 10) and *Case b* (Figure 11) are obtained by processing Eqs 2, 4, according to Figures 3, 7–9 (see Table 5).

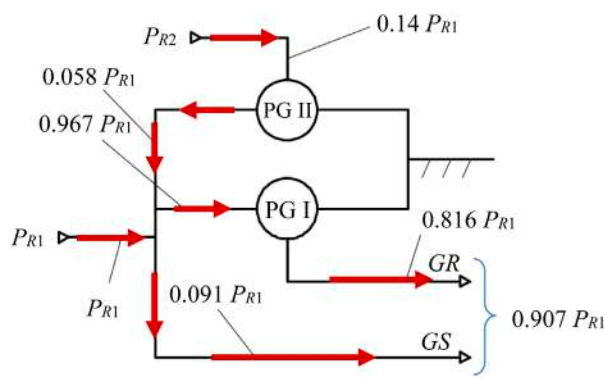

FIGURE 10
Power flow for the 1-DOF speed increaser with two inputs and two outputs (*Case a*).

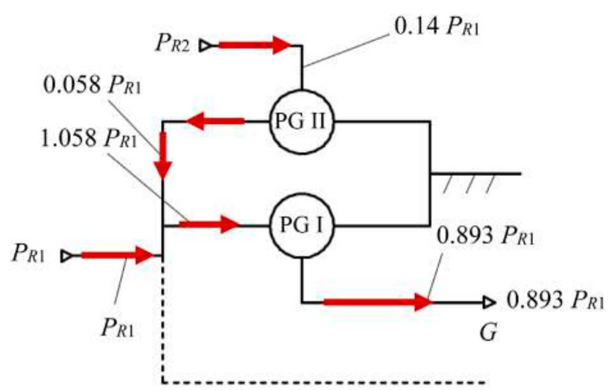

FIGURE 11
Power flow for the 1-DOF speed increaser with two inputs and one output (*Case b*).

In both cases, the rotor *R*2 generates lower mechanical power than the primary rotor (0.14 P_{R1}), which is then directed through the planetary gear set PG II and subsequently connected with power P_{R1}. This cumulative power flows on two branches in *Case a* toward the generator rotor and stator (Figure 10) and is completely directed to the generator rotor in *Case b*, crossing the PG I. Due to the direct transmission of a significant power share to the *GS* (0.091 P_{R1}, Figure 10), the output power in *Case a* is higher than in *Case b* (0.907 P_{R1} vs. 0.893 P_{R1}).

8 Conclusion

The generalized algorithm presented in the paper refers to a 1-DOF planetary transmission with two inputs and two outputs ($L = 4$), used as a torque-adding speed increaser in WECS with two counter-rotating rotors and generator with a mobile stator.

The conclusions drawn from the comparative analysis of the obtained results under the considered premises show the following:

- A WECS with a 1-DOF speed increaser with two counter-rotating outputs achieves a higher efficiency than the WECS with a single output; considering the initial characteristics and a cumulative power of 1 kW at the input, the speed increaser with two counter-rotating outputs brings power gain of 1.2% compared to the case with one output.
- The mechanical characteristics can significantly influence the functionality of a system; for example, the WECS with the set of coefficients defined in Table 2 (Scenario A) achieves a higher efficiency than the homologous WECS with the set of coefficients from Table 3 (Scenario B): by 6.7% more in *Case a* and by 7.7% more in *Case b*.
- The correlation between the speeds of the wind rotors influences decisively their behavior, including static ratio k_t; the increase in the ratio of the wind rotor speeds is accompanied by the increase in the static ratio k_t, as well as input power and output power delivered to the generator, whilst the mechanical efficiency decreases (Table 3 vs. Table 4).

The considered planetary transmission reverses the direction of rotation with respect to the wind rotor *R*1, sums up the input torques, and increases the input speed $i_a = -i_{01}$ times (compared to the motion of the wind rotor R1) while reducing the torque T_{GR}/T_{R1} times.

The efficiency of the 1-DOF transmission with two counter-rotating inputs and two counter-rotating outputs does not depend on the internal kinematic ratio i_{01} (Table 1) and thus on the amplification ratio.

Depending on the power required by the generator and the torque ratio, the proposed algorithm allows determining the mechanical power parameters on each branch, corresponding to the transmission outputs (rotor and stator of the electric generator).

The results of this work are limited to the steady-state behavior of WECS, where constant wind speed is considered and the inertial effects are null, implicitly. The authors intend in the future to address the problem of dynamic modeling and simulation of these WECS types by considering their body moments of inertia and their impact under transitory conditions at variable wind speeds and starting or stopping regimes. It is also intended to experimentally validate the numerical results by developing a specific stand for WECS small-scale prototypes.

Data availability statement

The original contributions presented in the study are included in the article/Supplementary Material; further inquiries can be directed to the corresponding authors.

Author contributions

Conceptualization, RS, CJ, MN, DC, and NC; methodology, RS, CJ, MN, DC, and NC; software, RS, DC, and NC; validation, RS, CJ, MN, DC, and NC; investigation, RS, CJ, MN, DC, and NC; interpretation, RS, CJ, MN, DC, and NC; writing—original draft preparation, RS, CJ, MN, DC, and NC; writing—review and editing, CJ and MN; supervision, MN and CJ. All authors contributed to the article and approved the submitted version.

Conflict of interest

The authors declare that the research was conducted in the absence of any commercial or financial relationships that could be construed as a potential conflict of interest.

Publisher's note

All claims expressed in this article are solely those of the authors and do not necessarily represent those of their affiliated organizations, or those of the publisher, the editors, and the reviewers. Any product that may be evaluated in this article, or claim that may be made by its manufacturer, is not guaranteed or endorsed by the publisher.

References

Bevington, C. M., Bywaters, G. L., Coleman, C. C., Costin, D. P., Danforth, W. L., Lynch, J. A., et al. (2008). *Wind turbine having a direct-drive drivetrain*. U.S. Patent 7,431,567 B1.

Bharani, R., and Sivaprakasam, A. (2020). A review analysis on performance and classification of wind turbine gearbox technologies. *IETE J. Res.* 68, 3341–3355. doi:10.1080/03772063.2020.1756936

Blecharz, K., and Pacholczyk, M. (2018). Rotor blade performance analysis for small counter rotating wind turbine. *Zesz. Nauk. Wydz. Elektrotechniki i Autom. Politech. Gdańskiej* 61. doi:10.32016/1.61.13

Booker, J. D., Mellor, P. H., Wrobel, R., and Drury, D. (2010). A compact, high efficiency contra-rotating generator suitable for wind turbines in the urban environment. *Renew. Energy* 35, 2027–2033. doi:10.1016/j.renene.2010.02.003

Cho, W., Lee, K., Choy, I., and Back, J. (2017). Development and experimental verification of counter-rotating dual rotor/dual generator wind turbine: Generating, yawing and furling. *Renew. Energy* 114, 644–654. doi:10.1016/j.renene.2017.06.083

Circiumaru Oprina, G., Chihaia, R., Tanase, N., El-Leathey, A., and Voina, A. (2022). Increasing energy efficiency of counter-rotating wind turbines by experimental modelling. *IOP Conf. Ser. Mater. Sci. Eng.* 1235, 012064. doi:10.1088/1757-899X/1235/1/012064

Dong, H., Zhang, C., Wang, D., Xu, S., and Qiu, J. (2017). Dynamic characteristics of gear box with PGT for wind turbine. *Procedia Comput. Sci.* 109, 801–808. doi:10.1016/j.procs.2017.05.331

Egorov, A., Kaizer, Y., Lysyannikov, A., Kuznetsov, A., Shram, V., Pavlov, A., et al. (2021). Counter-rotating electric generator for wind power plants with liquid metal energy transfer. *J. Phys. Conf. Ser.* 2094, 052018. doi:10.1088/1742-6596/2094/5/052018

Erturk, E., Sivrioglu, S., and Bolat, F. C. (2018). Analysis model of a small scale counter-rotating dual rotor wind turbine with double rotational generator armature. *Int. J. Renew. Energy Res.* 8, 1849–1858. doi:10.20508/ijrer.v8i4.8235.g7549

European Union (2018). Directive (EU) 2018/2001 of the European Parliament and of the Council of 11 December 2018 on the promotion of the use of energy from renewable sources. https://eur-lex.europa.eu/legal-content/EN/TXT/?uri=uriserv:OJ.L_.2018.328.01.0082.01.ENG&toc=OJ:L:2018:328:TOC.

Habash, R. W. Y., Groza, V., Yang, Y., Blouin, Ch., and Guillemette, P. (2011). Performance of a contrarotating small wind energy converter. *Int. Sch. Res. Netw. ISRN Mech. Eng.* 2011, 1–10. doi:10.5402/2011/828739

Irawan, Y., and Bramantya, A. "Numerical simulation of the effect of axial distance between two rotors in counter-rotating wind turbines," in Proceedings of the 2016 2nd International Conference on Science and Technology-Computer (ICST), Yogyakarta, Indonesia, October 2016, 1–5. doi:10.1109/ICSTC.2016.7877338

Jaliu, C., Diaconescu, D. V., Neagoe, M., and Saulescu, R. "Dynamic features of speed increasers from mechatronic wind and hydrosystems. Part II. Dynamic aspects," in Proceedings of the Second European Conference on Mechanism Science EUCOMES 08, Casino, Italy, September 2008.

Jaliu, C., Diaconescu, D. V., Neagoe, M., and Saulescu, R. "Dynamic features of speed increasers from mechatronic wind and hydrosystems. Part I. Structure Kinematics," in Proceedings of the Second European Conference on Mechanism Science EUCOMES 08, Casino, Italy, September 2008.

Jelaska, D., Podrug, S., and Perkušic, M. (2015). A novel hybrid transmission for variable speed wind turbines. *Renew. Energy* 83, 78–84. doi:10.1016/j.renene.2015.04.021

Jung, S. N., No, T.-S., and Ryu, K.-W. (2005). Aerodynamic performance prediction of a 30kW counter-rotating wind turbine system. *Renew. Energy* 30 (5), 631–644. doi:10.1016/j.renene.2004.07.005

Kale, Sandip A., and Sapali, S. N. (2012). Comprehensive evaluation of innovative multi rotor wind turbine designs. *Int. J. Mech. Eng. Technol. (IJMET)* 3 (2), 730–739.

Koehuan, V., and SugiyonoKamal, S. (2017). Investigation of counter-rotating wind turbine performance using computational fluid dynamics simulation. *IOP Conf. Ser. Mater. Sci. Eng.* 267, 012034. doi:10.1088/1757-899X/267/1/012034

Kutt, F., Blecharz, K., and Karkosinski, D. (2020). Axial-Flux permanent-magnet dual-rotor generator for a counter-rotating wind turbine. *Energies* 13, 2833. doi:10.3390/en13112833

Li, Z., Wang, Y., and Xiao, H. "Experimental study on structures of counter-rotating wind turbines," in Proceedings of the ICMREE 2013 - Proceedings: 2013 International Conference on Materials for Renewable Energy and Environment, Chengdu, China, August 2013. doi:10.1109/ICMREE.2013.6893685

Marjanovic, N., Isailovic, B., Marjanovic, V., Milojevic, Z., Blagojevic, M., and Bojic, M. (2012). A practical approach to the optimization ofgear trains with spur gears. *Mech. Mach. Theory* 53, 1–16. doi:10.1016/j.mechmachtheory.2012.02.004

Mirnikjoo, S., Abbaszadeh, K., and Abdollahi, E. (2020). Multi-objective design optimization of a double-sided flux switching permanent magnet generator for counter-rotating wind turbine applications. *IEEE Trans. Industrial Electron.* 68, 6640–6649. doi:10.1109/TIE.2020.3005106

Mirnikjoo, S., Asadi, F., Abbasazdeh, K., and Abdollahi, E. (2021). Effect of rotor topology on the performance of counter-rotating double-sided flux switching permanent magnet generator. *IEEE Trans. Energy Convers.* 37, 65–74. doi:10.1109/TEC.2021.3103555

Neagoe, M., and Saulescu, R. (2022). Comparative energy performance analysis of four wind turbines with counter-rotating rotors in steady-state regime. *Energy Rep.* 8, 1154–1169. doi:10.1016/j.egyr.2022.07.092

Neagoe, M., Saulescu, R., Jaliu, C., and Cretescu, N. (2017). "Novel Speed increaser used in counter-rotating wind turbines," in *New advances in mechanisms, mechanical transmissions and robotics, mechanisms and machine science* (Berlin, Germany: Springer), 143–151.

Neagoe, M., Saulescu, R., and Jaliu, C. (2019). Design and simulation of a 1 DOF planetary speed increaser for counter-rotating wind turbines with counter-rotating electric generators. *Energies* 12, 1754. doi:10.3390/en12091754

Neagoe, M., Saulescu, R., Jaliu, C., and Simionescu, P. A. (2020). A generalized approach to the steady-state efficiency analysis of torque-adding transmissions used in renewable energy systems. *Energies* 13, 4568. doi:10.3390/en13174568

No, T. S., Kim, J.-E., Moon, J. H., and Kim, S. J. (2009). Modeling, control, and simulation of dual rotor wind turbine generator system. *Renew. Energy* 34 (10), 2124–2132. doi:10.1016/j.renene.2009.01.019

Pacholczyk, M., Blecharz, K., and Karkosinski, D. (2017). Modelling of the counter rotating wind turbine. *Proc. XXVII Seminar Organ. by Pol. Soc. Theor. Appl. Electr. Eng. PTETiS, Gdańsk Sect.* 57, 81–84.

Pacholczyk, M., Blecharz, K., and Karkosinski, D. (2019). Numerical investigation on the performance of a small counter-rotating wind turbine. *Energy Mater. Sci. Eng. Energy Syst.* 116, 00055. doi:10.1051/e3sconf/201911600055

Pamuji, D., and Bramantya, A. (2019). Numerical study on the performance of 2-bladed and 3-bladed counter rotating wind turbines. *J. Jpn. Soc. Appl. Electromagn. Mech.* 27, 169–174. doi:10.14243/jsaem.27.169

Pastor, D. G. S. B., Nalianda, D., Sethi, V., Midgley, R., Rolt, A., and Novelo, D. A. B. (2021). Preliminary design framework for the power gearbox in a contra-rotating open rotor. *J. Eng. Gas. Turbines Power* 143, 041022. doi:10.1115/1.4049411

Qiu, J., Liu, B., Dong, H., and Wang, D. (2017). Type synthesis of gearbox in wind turbine. *Procedia Comput. Sci.* 109, 809–816. doi:10.1016/j.procs.2017.05.333

Queen, R. (2007). *Build and test a 3 kilowatt prototype of a coaxial multi-rotor wind turbine*. San Diego, CA, USA: California Energy Commission.

Radhakrishnan, J., Zuber, M., Sridhar, S., Ng, E., and Shenoy, S. "Comparative analysis of counter rotating and conventional vertical axis wind turbine," in Proceedings of the 2022 4th International Conference on Energy, Power and Environment (ICEPE), Shillong, India, April 2022, 1–6. doi:10.1109/ICEPE55035.2022.9798188

Rosenberg, A., Selvaraj, S., and Sharma, A. (2014). A novel dual-rotor turbine for increased wind energy capture. *J. Phys. Conf. Ser.* 524 (1), 012078. doi:10.1088/1742-6596/524/1/012078

Saulescu, R., Neagoe, M., and Jaliu, C. (2018). Conceptual synthesis of speed increasers for wind turbine conversion systems. *Energies* 11, 2257. doi:10.3390/en11092257

Saulescu, R., Neagoe, M., Jaliu, C., and Munteanu, O. (2021). A comparative performance analysis of counter-rotating dual-rotor wind turbines with speed-adding increasers. *Energies* 14, 2594. doi:10.3390/en14092594

Saulescu, R., Neagoe, M., Jaliu, C., and Munteanu, O. (2016b). Comparative analysis of two wind turbines with planetary speed increaser in steady-state. *Appl. Mech. Mater.* 823, 355–360. doi:10.4028/www.scientific.net/AMM.823.355

Saulescu, R., Neagoe, M., Munteanu, O., and Cretescu, N. (2016a). Performance analysis of a novel planetary speed increaser used in single-rotor wind turbines with counter-rotating electric generator. *Mater. Sci. Eng. – IOP Conf. Ser. Mater. Sci. Eng.* 147 (1), 012090. doi:10.1088/1757-899X/147/1/012090

Shin, C. (1999). *Multi-unit rotor blade system integrated wind turbine*. U.S. Patent 5,876,181.

Ullah, W., Khan, F., and Hussain, S. (2022a). A comparative study of dual stator with novel dual rotor permanent magnet flux switching generator for counter rotating wind turbine applications. *IEEE Access* 10, 8243–8261. doi:10.1109/ACCESS.2022.3143166

Ullah, W., Khan, F., and Hussain, S. (2022b). Dual mechanical port power distribution in dual rotor permanent magnet flux switching generator for counter-rotating wind turbine applications. *IET Renew. Power Gener.* 16, 1267–1277. doi:10.1049/rpg2.12450

Vasel-Be-Hagh, A., and Archer, C. (2017). Wind farms with counter-rotating wind turbines. *Sustain. Energy Technol. Assessments* 24, 19–30. doi:10.1016/j.seta.2016.10.004

Vázquez-Hernández, C., Serrano-González, J., and Centeno, G. (2017). A market-based analysis on the main characteristics of gearboxes used in onshore wind turbines. *Energies* 10, 1686. doi:10.3390/en10111686

Wang, K., Liu, T., Wan, Y., Ong, M. C., and Wu, T. (2022). Numerical investigation on aerodynamic characteristics of dual-rotor wind turbines. *J. Mar. Sci. Eng.* 10, 1887. doi:10.3390/jmse10121887

Windeurope, (2017). Wind energy in europe: Scenarios for 2030. https://windeurope.org/wp-content/uploads/files/about-wind/reports/Wind-energy-in-Europe-Scenarios-for-2030.pdf.

Zhiqiang, L., Yunke, W., Jie, H., Zhihong, Z., and Wenqi, C. (2018). The study on performance and aerodynamics of micro counter-rotating HAWT. *Energy* 161, 939–954. doi:10.1016/j.energy.2018.07.049

Nomenclature

a_G	speed coefficient in the generator mechanical characteristic
a_R	speed coefficient in the wind rotor mechanical characteristic
b_G	torque term in the generator mechanical characteristic
b_R	torque term in the wind rotor mechanical characteristic
DOF	degree of freedom
F	operating point
G	conventional electric generator
Gc	counter-rotating electric generator
GR	generator rotor
GS	generator stator
H	satellite carrier
i_0	internal kinematic ratio
i_a	speed amplification ratio
i_{xy}^z	kinematic ratio where the rotational motion is transmitted from body *x* to body *y* and *z* is considered as the reference body
k_t	ratio of the input torques
L	total number of inputs and outputs
P	power
P^*	power for the system with a conventional electric generator
PG	planetary gear set
R1/R2	primary/secondary wind rotor
T	torque
T^*	torque for the system with a conventional electric generator
η	efficiency
η_0	internal efficiency
η_a	WECS overall efficiency
η_g	efficiency of a gear pair
ω	angular speed
ω^*	angular speed in the case of the system with a conventional electric generator
SI	speed increaser
WECS	wind energy conversion system
z_i	number of teeth of gear *i*

energies

Article

A Comparative Performance Analysis of Counter-Rotating Dual-Rotor Wind Turbines with Speed-Adding Increasers

Radu Saulescu [1], Mircea Neagoe [2,*], Codruta Jaliu [2] and Olimpiu Munteanu [2]

1 Design of Mechanical Elements and Systems R&D Centre, Transilvania University of Brasov, 500036 Brasov, Romania; rsaulescu@unitbv.ro
2 Renewable Energy Systems and Recycling R&D Centre, Transilvania University of Brasov, 500036 Brasov, Romania; cjaliu@unitbv.ro (C.J.); omunt@unitbv.ro (O.M.)
* Correspondence: mneagoe@unitbv.ro; Tel.: +40-268-413-000

Abstract: Increasing the efficiency of wind power conversion into electricity poses major challenges to researchers and developers of wind turbines, who are striving for new solutions that can ensure better use of local wind potential in terms of both feasibility and affordability. The paper proposes a novel concept of wind systems with counter-rotating wind rotors that can integrate either conventional or counter-rotating electric generators, by means of the same differential planetary speed increaser, aiming at providing a comparative analysis of the energy performance of counter-rotating wind turbines with counter-rotating vs. conventional electric generators. To this end, a generalized analytical model for angular speeds and torques has been developed, which can be customized for both system configurations. Three numerical simulation scenarios have been contrasted: (a) a scenario with identical wind rotors in both systems, (b) a scenario with the secondary wind rotors being identical in the two applications, but different from the primary rotors, and (c) a scenario with different secondary rotors in the two wind turbines. The results have shown that the wind systems with counter-rotating generator are more efficient and have a higher amplification ratio, compared to systems with conventional generators. In addition, the analyzed wind system with a counter-rotating generator displays better energy performance with low values for output power and ratio of input speeds, whereas the wind turbine with a conventional generator proves to be more efficient in the high-value range of the above-mentioned parameters.

Keywords: wind turbine; counter-rotating wind rotors; counter-rotating electric generator; planetary speed increaser; speed-adding increaser; modeling; operational point

check for updates

Citation: Saulescu, R.; Neagoe, M.; Jaliu, C.; Munteanu, O. A Comparative Performance Analysis of Counter-Rotating Dual-Rotor Wind Turbines with Speed-Adding Increasers. *Energies* **2021**, *14*, 2594. https://doi.org/10.3390/en14092594

Academic Editor: Andrzej Bielecki

Received: 29 March 2021
Accepted: 28 April 2021
Published: 1 May 2021

1. Introduction

Wind energy has become increasingly popular among renewable energy sources worldwide, representing a valuable alternative to fossil fuels and other polluting sources of energy production. Most of the wind turbines that are currently in operation both onshore and offshore have a conventional structure, consisting of a single wind rotor, a speed increaser and a conventional generator. However, as the use of wind energy is gathering pace, there is a constant need for either improving the existing wind turbines or developing innovative higher performance models. Thus, a better use of wind potential and a more efficient energy conversion, leading to a boost in electricity production, are major milestones that researchers, designers and developers in the field are constantly striving to reach.

In recent years, several innovative wind turbine solutions have been developed with improvements regarding the wind rotor, the speed increaser or the electric generator. For instance, a number of studies have been conducted on various issues, such as:

- the development of innovative concepts of wind turbines (with horizontal axis and counter-rotating rotors [1–4], or with multiple and smaller rotors in a spatial arrangement [5]). An example of comprehensive, but not exhaustive overview of research achievements in counter-rotating wind turbine systems development, characterization and use can be found in [4];

- the influence of rotor pitch on the output power of a conventional wind turbine [6] and of a counter-rotating wind turbine [7];
- the effect of the number of blades of counter-rotating wind turbines on the system performance [8];
- the performance of new types of counter-rotating wind turbine with vertical axis [9,10], etc.

Several studies have offered a contrastive approach to single-rotor vs. counter-rotating wind turbines, proving that the latter can increase the power conversion efficiency by 40% as against the former [7,11]. When using the two types of rotor in wind farms, Vasel-Be-Hagh et al. concluded that the use of a counter-rotating configuration leads to 22.6% more power than in the case of single-rotor wind turbines [11].

Wind turbines usually include a speed increaser, whose function is to transmit mechanical energy, as well as to boost the lower speed of wind rotors so that the electric generator's speed requirement be met. Research on speed increasers has covered various topics, such as: the fixed-axis gearbox type [12–14], planetary transmissions [5,15–19] or variable transmissions [20–22], analyzed as part of single-rotor wind turbines or counter-rotating systems, by e.g., the structure of an improved wind turbine gearbox is presented for meeting the operation of the optimized wind turbine power-wind speed curve [22].

The planetary speed increaser type is mainly used in high-power conventional wind systems and in counter-rotating turbines, due to their advantages: high amplification ratios, reduced radial sizes and better efficiency [1,3,16,17,23–32]. With dual-rotor systems, the speed increaser, operating as a 2-*DOF* transmission, sums up the rotors' input speeds [26,30], while operating as a 1-*DOF* planetary transmission, it sums up the rotors' input torques [31–33]. Qiu et al. proposed in [23] a synthesis of planetary speed increasers mainly for high-power wind turbines, considering both 1-*DOF* and 2-*DOF* types.

A dynamic response of a wind turbine gearbox under different excitation conditions is reported in [34] by Zhao and Ji, while Dong et al. used a similar approach and investigated the dynamics of a planetary transmission for wind turbines that influences the conversion efficiency and proves that the use of a planetary gear train is the best option for wind turbines [35]. Vázquez-Hernández C. et al. analyzed in [36] different gearbox arrangements for onshore wind turbines, as well as the factors that affect their design, proving that the current trend in the market is to use planetary transmissions rather than gearless wind turbines. Farahani et al. [37] evaluated and compared the transient performance of the single-rotor and the counter-rotating wind turbines, concluding that performance would be enhanced by using the second type.

Recently, new developments in electric generators for wind turbines have been presented in the specialist literature, many of which are in the prototype phase. For example, an axial-flux generator with a counter-rotating field and armature for counter-rotating wind turbines is proposed and analyzed by Kutt et al. in [38], but the solution has proven to have low efficiency; a permanent magnet synchronous generator with mobile armatures (both stator and rotor) is put forth in various studies [32,39–42], the innovative design being proposed for low-power applications. Still, research in this area has shown that the use of counter-rotating (with mobile stator)—instead of conventional (with fixed stator)—electric generators can provide additional energy gain.

Combining the previous concepts, Pacholczyk et al. [43] proposed a small counter-rotating wind turbine consisting of two counter-rotating rotors, a 1-*DOF* planetary gearbox and a counter-rotating generator. The authors investigated its performance and operational point as functions of axial distance and tip speed ratio of each rotor. Another study on the comparative behavior of a single-rotor wind turbine with 1-*DOF* planetary speed increaser and counter-rotating vs. conventional electric generator was reported by Saulescu et al. in [44]. The operating point was derived by reducing the mechanical characteristic of the wind rotor at the shaft of the electric generator rotor. Numerical simulations highlighted higher efficiency for systems with parallel flow of mechanical power. However, in both studies, authors presented a particular configuration of wind turbine—the model not being generalized. Other approaches can be find in [45] and [46], where Fan et al. and Hong and Fan, respectively, utilise the empirical mode decomposition method and the particle swarm optimization algorithm, who have been successfully hybridized with the support vector regression to produce satisfactory forecasting performance. A review of the performance and reliability of wind turbines is done by Pfaffel et al. in [47].

The foregoing brief survey of specialist literature reveals that a relatively small number of studies have contrasted only particular configurations of counter-rotating wind turbines. However, they do not report generalized analytical models that can be customized to different operational cases of wind turbines. This paper aims to bridge the gap and proposes a novel concept of a counter-rotating wind system that can integrate one of the two types of electric generator and uses the same 2-*DOF* planetary speed increaser. The goal is to compare the energy performance of counter-rotating wind turbines with a counter-rotating vs. conventional electric generator. To this end, a generalized analytical model for angular speeds and torques is developed, which can be customized for both system configurations and which allows to obtain the operational point of the two types of wind turbine. Three numerical simulation scenarios will be considered: (a) a scenario with identical wind rotors in both systems, (b) a scenario with the secondary wind rotors being identical in the two applications, but different from the primary rotors, and (c) a scenario with different secondary rotors in the two wind turbines—where the mechanical characteristics are obtained from the condition of achieving the same ratio between the input angular speeds of both wind systems. Thus, the influence of mechanical characteristics on the behavior of the considered wind systems can be identified. The results of this comparative study will confirm the acknowledged conclusion that the counter-rotating type is more efficient, and they will also allow to define the extent to which performance of wind systems with a counter-rotating generator exceeds that of conventional generator applications.

Subsequent to these introductory, general considerations, the paper has the following structure: Section 2, in which two configurations are proposed of counter-rotating wind turbines consisting of two counter-rotating rotors, a speed increaser that can function as a 2 in-1 out or 2 in-2 out transmission, and either a conventional or counter-rotating electric generator; Section 3, in which a generalized analytical model is presented for angular speeds, torques, efficiency and operational point with both configurations; Section 4, in which numerical simulations and analyses are performed for the three scenarios; and Section 5, which provides final conclusions.

The main contributions of this paper to the scientific endeavor in the field are: a novel concept of a counter-rotating wind system using the same differential planetary speed increaser and either counter-rotating or conventional electric generator; a generalized close-form model of 2-*DOF* wind systems which can be used, by customization, for performance investigation of both types of wind turbine (with a counter rotating vs. conventional electric generator); three numerical simulation scenarios performed and analyzed comparatively, aiming to identify performance of each type of wind turbine in relation to relevant input parameters.

2. Problem Formulation

The in-parallel transmission of mechanical power from inputs to outputs can be achieved by power split at input, output or both, which ensures a higher efficiency compared to transmissions obtained by serial connection of the same component mechanisms [48]. A new approach to the development of modern wind turbines is the use of two counter-rotating coaxial rotors and the integration of a counter-rotating electric generator, which requires a mechanical transmission with power split at both input and output.

In order to identify the energy gain brought by a counter-rotating electric generator as against a conventional, fixed-stator generator, the paper presents a comparative study of two wind turbines having the same components (wind rotors, speed increaser and electric generator), so that the reference wind system (with a conventional generator) is derived from the wind system with two inputs and two outputs as a particular case, by releasing the stator of the electric generator and fixing it to the frame. Thus, the general case is considered of a wind turbine with two counter-rotating rotors *R*1 and *R*2, a 2-*DOF* speed increaser (*SI*), and an electric generator consisting of either a mobile rotor *GR* and a mobile stator *GS* (in the case of a counter-rotating generator, the 2 in-2 out wind system type shown in Figure 1a) or a fixed stator (conventional generator $GS \equiv 0$, the 2 in-1 out wind system type shown in Figure 1b). In order to ensure equivalence of the two wind systems under comparative analysis, the following hypotheses are considered:

- The same set of rotors *R*1 and *R*2 is used in both wind systems and the same set of mechanical characteristics is considered in modeling these systems, implicitly. Conventionally, *R*1 is the primary wind rotor and *R*2—the secondary rotor. The mechanical characteristics of wind turbines can be considered as linear functions with constant coefficients in operation at a constant wind speed. However, the values of these coefficients depend on both the value of wind speed and the characteristics of wind rotor, e.g., the pitch angle of blades.
- In both cases, the speed increaser *SI* has the same structure and the same values for internal kinematic ratio i_0 and internal efficiency η_0 [49]. The mechanical transmission is a differential mechanism (2-*DOF*) with two inputs that are connected to wind rotors *R*1 and *R*2, and one or two outputs, through which the mechanical power is transmitted either to rotor *GR* of the conventional generator or to rotor *GR* and stator *GS* of the counter-rotating generator.
- The counter-rotating electric generator is obtained from the conventional one, by setting the stator *GS* to rotate in opposite direction to the rotor *GR*; the two generators have the same mechanical characteristics with respect to the relative speed of rotor *GR* and stator *GS*, i.e., $\omega_G = \omega_{GR} - \omega_{GS}$. For the sake of simplicity, the case of direct current (*DC*) generators is further considered, which are characterized by linear mechanical characteristics with constant coefficients, is further considered.
- The ratio of angular speeds of wind rotors is denoted by $k_\omega = -\omega_{R2}/\omega_{R1} > 0$. The ratio k_ω can be adjusted during wind turbine operation by changing the pitch angle of the two rotors *R*1 and *R*2, which also changes their mechanical characteristics.

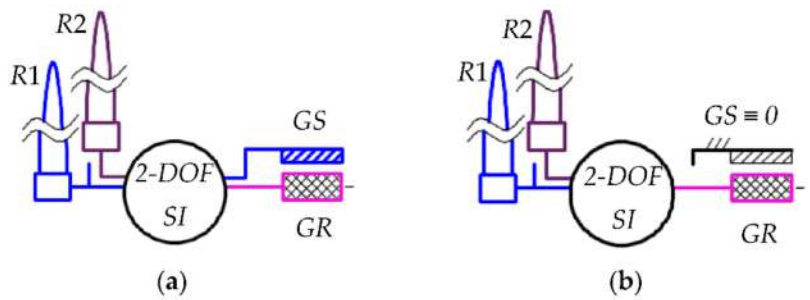

Figure 1. Block diagrams of the differential counter-rotating wind systems that are considered in the comparative analysis: (**a**) with counter-rotating generator; (**b**) with conventional generator.

The proposed mathematical model of a wind system with a counter-rotating generator, under the above-mentioned hypotheses, also allows for the description of the system with a conventional electric generator by customizing the state of stator *GS*: the stator is fixed to the frame after disconnecting it from the speed increaser (see Figure 1).

The case of a planetary speed increaser with cylindrical gears and single serial satellite gears—illustrated in Figure 2 below only through its upper half—is further used to exemplify the mathematical modeling and to identify the relevant properties by numerical simulation of the two wind systems. This transmission consists of two sun gears 1 and 4, meshing with two or more sets of serial satellites 2–3 that are articulated through revolute joints to a satellite carrier *H*. The speed increaser has two inputs, carrier *H* and gear 4, which are connected to primary wind rotor *R*1 and secondary wind rotor *R*2, respectively, and which can operate with either two outputs (1 and *H*, Figure 2a) or a single output (1, Figure 2b). The main output is through gear 1, which is connected to rotor *GR*, while, in the case of the counter-rotating generator, the secondary output *H* is held fixed to stator *GS*. As a result, the analyzed planetary transmission has either $L = 4$ (Figure 2a) or $L = 3$ (Figure 2b) external connections, two degrees of freedom ($M = 2$) and, therefore, two independent external speeds (ω_H and ω_4), as sun gear 1, ring gear 4 and carrier *H* are mobile bodies.

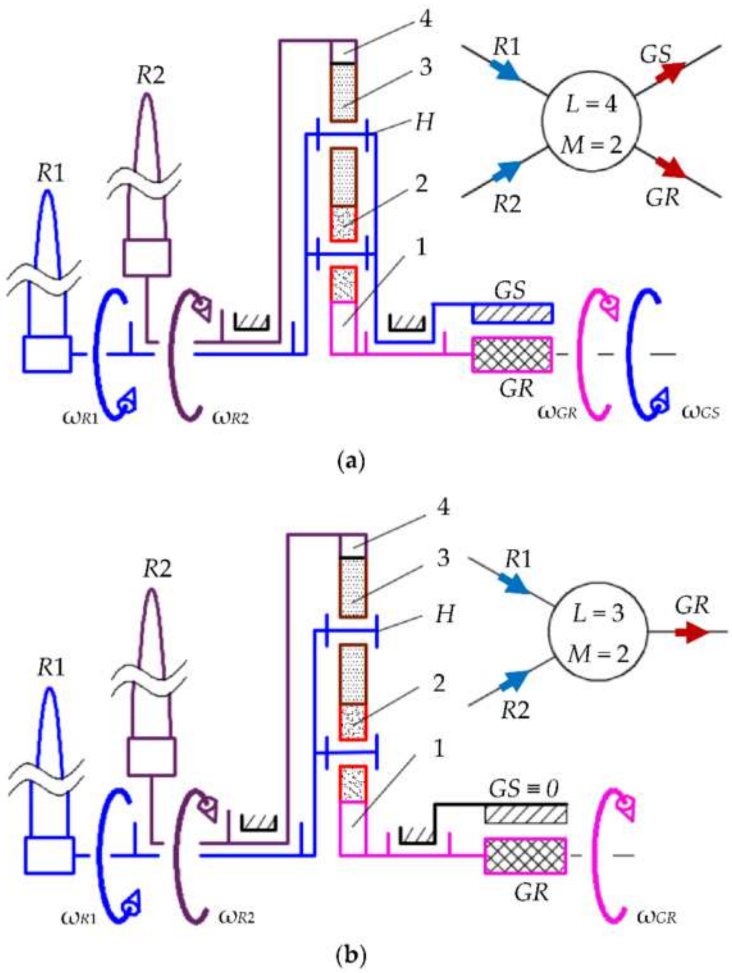

Figure 2. Structural and block diagrams for wind systems with two counter-rotating inputs, a differential planetary speed increaser and: (**a**) counter-rotating generator; (**b**) conventional generator.

Wind rotors *R*1 and *R*2 have angular speeds ω_{R1} and ω_{R2} in opposite directions—a property ensured by setting opposite inclinations of the two rotors' blades. The two outputs of the speed increaser, by 1 and *H*, are also counter-rotating due to the kinematic property given by the planetary transmission structure, as highlighted in the next section. Being a differential mechanism, the speed increaser sums up the two input angular speeds ω_{R1} and ω_{R2} in an output angular speed ω_{GR}. Angular speed ω_{GS} of stator *GS* is identical to the input speed of primary rotor *R*1 (Figure 2a), as a result of the direct connections *GS*-*H*-*R*1.

The analytic modeling of angular speed, torque, power and efficiency of the two wind systems starts from the general case of a wind turbine with a counter-rotating generator and then customized for the particular case of a system with a conventional generator. To this purpose, the kinematic and static correlations of the planetary speed increaser are established on the basis of the block diagrams shown in Figure 3 below and detailed in [33], as well as on the mechanical characteristics of the wind rotors and electric generator, considering the influence of the ratio of input speeds $k_\omega = -\omega_{R2}/\omega_{R1}$ on the behavior and performance of the two wind systems. Notations in Figure 3 are: T_x and ω_x for torque and angular speed of kinematic body x; i_0 and η_0 for internal kinematic ratio and internal efficiency of the speed increaser—all of which representing the intrinsic parameters of the planetary transmission [33]. In particular, carrier H is connected to primary rotor $R1$ by HR shaft and to the generator stator GS by HS shaft (see Figure 3a).

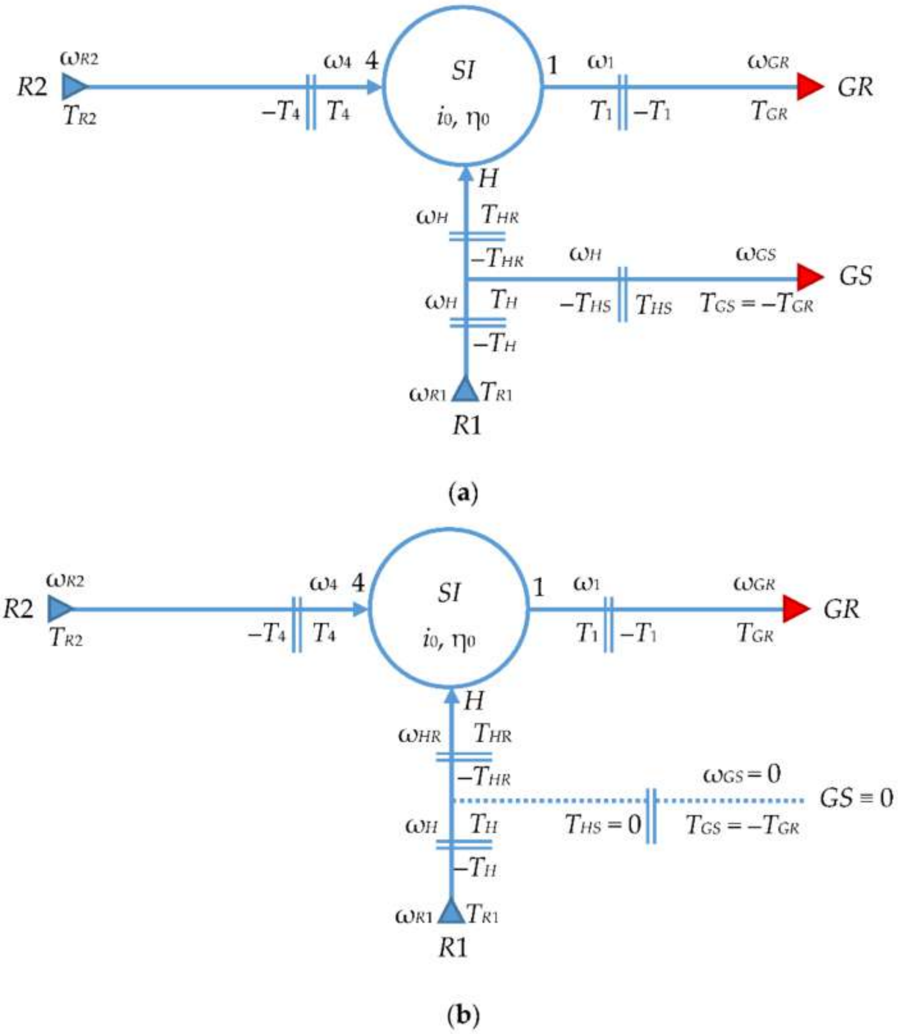

Figure 3. Block diagram of the differential wind system with two inputs and: (**a**) two outputs; (**b**) one output.

The system with conventional generator, Figure 3b, can be illustrated and analyzed as a particular case of the system with counter-rotating generator, Figure 3a, by disconnecting the shaft HS from the carrier H (i.e., $T_{HS} = 0$) and by fixing the stator GS to the frame (i.e., $\omega_{GS} = 0$).

3. Analytic Modeling of Wind Systems

The mathematical modeling of the generalized counter-rotating wind turbine system (with a counter-rotating generator) is performed by applying the method of isolating the components, which involves breaking their connections and replacing them with the appropriate parameters of mechanical power transmitted through these connections. The steps of the applied algorithm for the analytical modeling of the considered wind systems (Figure 2), according to the block diagram and notations in Figure 3, are presented in the flowchart depicted in Figure 4.

Decomposition of the wind system into components, Figure 3

C1: 2-DOF planetary speed increaser *SI* (i_0, η_0);
C2: primary wind rotor R1 ; C3: secondary wind rotor R2;
C4: electric generator rotor *GR*; C5: electric generator stator *GS*;
C6: intermediate shaft between *R*1, *GS* and carrier *H*.

↓

Kinematic modeling, Equation (1)

K1: angular speed transmitting function of the planetary speed increaser;
K2: kinematic equations of the connections between components;
K3: kinematic ratio of the input angular speeds, k_ω , Equation (3);
Input parameters: ω_{R1} *and* k_ω.
Output parameters: ω_{R2}, ω_{GR}, ω_{GS}, ω_H, ω_1, ω_4, $\omega_G = \omega_{GR} - \omega_{GS}$.
Remark: in the particular case of the 2in-1out system, $\omega_{GS} = 0$.

↓

Static modeling, Equations (7)

S1: torque transmitting functions of the planetary speed increaser;
S2: static equilibrium equations of the components C2...C6;
S3: static equilibrium equation of the electric generator, $T_{GR} + T_{GS} = 0$;
Input parameters: T_{R1} *and* (i_0, η_0).
Output parameters: T_{R2}, T_{GR}, T_{GS}, T_G, T_H, T_{HR}, T_{HS}, T_1, T_4.
Remark: in the particular case of the 2in-1out system, $T_{HS} = 0$ instead of $T_{HS} + T_{GS} = 0$.

↓

Power modeling, Table 1

Input parameters: $P_{R1} = T_{R1}\omega_{R1}$, k_ω *and* (i_0, η_0).
Output parameters: P_{R2}, P_{GR}, P_{GS}, P_G, P_H, P_{HR}, P_{HS}, P_1, P_4.

↓

Efficiency modeling, Equations (10) and (11)

Input parameters: k_ω *and* (i_0, η_0).
Output parameter: η.

↓

Steady-state operational point modeling, Equations (14) and (15)

M1: mechanical characteristic of the primary wind rotor *R*1, Equation (12);
M2: mechanical characteristic of the secondary wind rotor *R*2, Equation (12);
M3: mechanical characteristic of the electric generator *G*, Equation (13);
Inputs: kinematic and static transmitting functions of the mechanism, Equations (1) and (7), and the mechanical caracteristics M1...M3.
Output parameters: operational point at the generator level (ω_F, T_F);
kinematic ratio k_ω, *Equations (18) and (21).*

Figure 4. Algorithm for analytical modeling of the generalized 2-*DOF* dual-rotor counter-rotating wind systems.

3.1. Kinematic Modeling

This modeling aims at establishing the relationships between the dependent angular speeds and the two independent external angular speeds of the speed increaser (ω_H and ω_4). For this purpose, the speed increaser is characterized by a function of transmitting angular speeds, while each connection (represented by a double line in Figure 3) between the components of the wind system is described through a distinct kinematic equation. Thus, the following system of equations can be written [33]:

$$\begin{cases} \omega_1 = \omega_H(1 - i_0) + \omega_4 i_0; \\ \omega_{R1} = \omega_H;\ \omega_{R2} = \omega_4; \\ \omega_{GR} = \omega_1;\ \omega_{GS} = \omega_H. \end{cases} \tag{1}$$

where the internal kinematic ratio i_0 can be calculated from the particular case when H is assumed to be fix, given by relation (2):

$$i_0 = i_{14}^H = \omega_{1H}/\omega_{4H} = z_4/z_1, \tag{2}$$

where i_{14}^H—angular speed transmission ratio from gear 1 to gear 4 when carrier H is considered fixed (or reference body), ω_{xy}—angular speed of body x relative to body y, z_j—the number of teeth of gear j; i_0 is defined as the kinematic ratio of the fixed axes mechanism that is associated to the planetary gear train, being obtained by reversing the motion relative to the carrier H [49].

Based on the relation between the input angular speeds, as defined by ratio k_ω:

$$\omega_{R2} = -k_\omega \omega_{R1}, \tag{3}$$

the relative angular speed between rotor GR and stator GS of the electric generator, ω_G, can be obtained:

$$\omega_G = \omega_{GR} - \omega_{GS} = -\omega_{R1} i_0 (1 + k_\omega). \tag{4}$$

The system of Equation (1) is equally valid for the wind turbine with one output (Figure 2b), except that the last equation has to be replaced by Equation (5):

$$\omega_{GS} = 0 \tag{5}$$

that characterizes the stator GS, which is fixed to the frame after disconnecting it from wind rotor $R1$. Therefore, the relative angular speed of the electric generator becomes:

$$\omega_G = \omega_{GR} = \omega_{R1}[1 - i_0(1 + k_\omega)]. \tag{6}$$

3.2. Torque Correlation and Efficiency Modeling

According to the diagram in Figure 3, the wind system with counter-rotating generator is modeled by a set of 9 static equilibrium equations consisting of:

- two torque transmitting functions that are obtained from the static modeling of the differential planetary speed increaser; the number of functions is equal to the mechanism degree of freedom (M = 2). Additionally, the condition of static equilibrium of the planetary transmission can be added as dependent equation for verification purposes;
- a static equilibrium equation for each of the other five components of the wind system, which are obtained after breaking the connections;
- the static equilibrium equation of the electric generator, described from the condition that the torque values at rotor GR and stator GS are equal and in opposite direction.

As a result, the set of equations for the differential wind system in Figure 2a—with two counter-rotating inputs and two counter-rotating outputs—can be written as follows:

$$\begin{cases} T_{HR} = -T_1(1 - i_0\eta_0^{-1});\ T_4 = -T_1 i_0 \eta_0^{-1};\ \ T_1 + T_4 + T_{HR} = 0; \\ T_{R1} - T_H = 0;\ T_{R2} - T_4 = 0;\ \ T_{GR} - T_1 = 0;\ \ T_{GS} + T_{HS} = 0;\ T_H - T_{HR} - T_{HS} = 0; \\ T_G = T_{GR} = -T_{GS}; \end{cases} \tag{7}$$

where the internal efficiency of the planetary transmission is:

$$\eta_0 = \eta_{14}^H = \eta_{12}^H \cdot \eta_{23}^H \cdot \eta_{34}^H = \eta_g^3, \tag{8}$$

where η_{xy}^H is the efficiency of the fixed-axis gear mechanism consisting of gears x and y (considering $H \equiv 0$), while η_g is the efficiency of a component gear pair; in this case, the three cylindrical fixed-axis gear pairs (1-2, 2-3, and 3-4) are considered to have identical efficiency values.

With a differential wind system having two counter-rotating inputs and a conventional generator, Figure 2b, the equation $T_{GS} + T_{HS} = 0$ in system (7) has to be replaced by $T_{HS} = 0$, as the connection of stator GS to wind rotor $R1$ is broken and then fixed to the frame ($\omega_{GS} = 0$).

In the general case 2 in-2 out, the efficiency of speed increaser can be obtained starting from its definition:

$$\eta = -\frac{\omega_{GR} T_{GR} + \omega_{GS} T_{GS}}{\omega_{R1} T_{R1} + \omega_{R2} T_{R2}}, \tag{9}$$

from which—after some algebraic processing of the systems of Equations (1) and (7)—the efficiency for wind turbines with two counter-rotating rotors and counter-rotating generator can be expressed by:

$$\eta = \eta_0, \tag{10}$$

as well as for wind turbines with conventional generator:

$$\eta = \eta_0 \frac{1 - i_0(1 + k_\omega)}{\eta_0 - i_0(1 + k_\omega)}. \tag{11}$$

3.3. Steady-State Operational Point

The operational point of a motor-mechanism-effector type machine is the set of values of the external parameters (kinematic and static) of the mechanism at which the machine operates in steady-state mode. The operational point is obtained by solving the system of equations consisting of the kinematic and static transmitting functions of the speed increaser, Equations (1) and (7), and:

- the mechanical characteristics of the two wind rotors $R1$ and $R2$, described as linear functions with constant coefficients under stationary conditions (constant wind speed, same values of pitch angles):

$$\begin{cases} T_{R1} = -a_{R1}\omega_{R1} + b_{R1}; \\ T_{R2} = -a_{R2}\omega_{R2} + b_{R2}; \end{cases} \tag{12}$$

- the mechanical characteristic of DC generator, represented by a linear function with constant coefficients, describing generator's torque T_G in relation to angular speed ω_G. By convention, the torque of the generator is $T_G = T_{GR}$:

$$-T_G = a_G\omega_G - b_G. \tag{13}$$

Usually, the values of the power parameters on a shaft are first obtained by reducing the mechanical characteristics to that shaft and solving analytically or grapho-analytically the point of intersection between the reduced mechanical characteristics.

Further on, the operational point (F) at the level of the electric generator is analytically determined, by considering the operating angular speed $\omega_F = \omega_G$ and the torque $T_F = T_G$. Thus, for the two analyzed wind systems, the following expressions of parameters ω_F, T_F and power P_F are obtained:

- for the wind system with counter-rotating generator, Figure 2a:

$$\begin{cases} \omega_F = \dfrac{b_G - \frac{b_{R1}\eta_0}{i_0}}{a_G + \frac{a_{R1}\eta_0}{i_0^2(1+k_\omega)}}; \\ T_F = -a_G\omega_F + b_G; \quad P_F = \omega_F T_F. \end{cases} \tag{14}$$

- for the wind system with conventional generator, Figure 2b:

$$\begin{cases} \omega_F = \dfrac{b_G - \frac{b_{R1}\eta_0}{i_0-\eta_0}}{a_G - \frac{a_{R1}\eta_0}{(i_0-\eta_0)[1-i_0(1+k_\omega)]}}; \\ T_F = -a_G\omega_F + b_G; \quad P_F = \omega_F T_F. \end{cases} \tag{15}$$

3.4. Input Angular Speeds Ratio k_ω

Generally, the input speeds ratio k_ω depends on the mechanical characteristics of the motor and effector sub-systems and on the intrinsic parameters of the speed increaser (i.e., i_0 and η_0); in practical applications, ratio k_ω can be adjusted to a given value by modifying appropriately at least one mechanical characteristic through different approaches, e.g., by changing the pitch angle of the blades, or controlling the electric generator.

The analytical expressions of ratio k_ω for the two wind systems considered in this comparative analysis can be obtained by processing Equations (1), (3), (4), (6), (7), (12) and (13). Thus, in the case of a system with counter-rotating generator (Figure 2a), it can be concluded from Equation (7) that:

$$\begin{cases} T_1 = T_H\frac{\eta_0}{i_0} = -T_4\frac{\eta_0}{i_0} \Rightarrow T_H = -T_4 \Rightarrow T_{R2} = -T_{R1}; \\ T_4 = -T_1\frac{i_0}{\eta_0} \Rightarrow T_1 = T_G \Rightarrow T_{R2} = -T_G\frac{i_0}{\eta_0}. \end{cases} \tag{16}$$

By replacing the mechanical characteristics of the wind rotors and electric generator from Equations (12) and (13) in Equation (16), and corroborating with Equations (3) and (4), we get:

$$\begin{cases} -a_{R2}\omega_{R2} + b_{R2} = a_{R1}\omega_{R1} - b_{R1}; \\ -a_{R2}\omega_{R2} + b_{R2} = a_G\omega_{ge}\frac{i_0}{\eta_0} - b_G\frac{i_0}{\eta_0}; \\ \omega_{R2} = -k_\omega\omega_{R1}; \\ \omega_G = -\omega_{R1}i_0(1+k_\omega), \end{cases} \tag{17}$$

which allows one to obtain the expression of k_ω:

$$k_\omega = -\frac{a_{R1}b_G i_0 + a_{R1}b_{R2}\eta_0 + a_G b_{R1}i_0^2 + a_G b_{R2}i_0^2}{a_{R2}b_{R1}\eta_0 + a_G b_{R1}i_0^2 + a_G b_{R2}i_0^2 - a_{R2}b_G i_0}. \tag{18}$$

Similarly, the following correlations can be written for the system with conventional generator (Figure 2b):

$$\begin{cases} T_1 = -T_H\frac{\eta_0}{\eta_0-i_0} = -T_4\frac{\eta_0}{i_0} \Rightarrow T_4 = T_H\frac{i_0}{\eta_0-i_0} \Rightarrow T_{R2} = T_{R1}\frac{i_0}{\eta_0-i_0}; \\ T_4 = -T_1\frac{i_0}{\eta_0} \Rightarrow T_1 = T_G \Rightarrow T_{R2} = -T_G\frac{i_0}{\eta_0}, \end{cases} \tag{19}$$

and by combining them with Equations (3), (6), (7), (12) and (13), we get:

$$\begin{cases} -a_{R2}\omega_{R2} + b_{R2} = a_{R1}\frac{i_0}{\eta_0 - i_0}\omega_{R1} - b_{R1}\frac{i_0}{\eta_0 - i_0}; \\ -a_{R2}\omega_{R2} + b_{R2} = a_G\omega_G\frac{i_0}{\eta_0} - b_G\frac{i_0}{\eta_0}; \\ \omega_{R2} = -k_\omega\omega_{R1}; \\ \omega_G = \omega_{R1}[1 - i_0(1 + k_\omega)]. \end{cases} \tag{20}$$

The k_ω expression is the result of solving the system of Equation (20):

$$k_\omega = -\frac{a_{R1}b_G i_0 + a_{R1}b_{R2}\eta_0 + a_G b_{R2}(\eta_0 - i_0) - a_G b_{R2} i_0(\eta_0 - i_0) - a_G b_{R1} i_0(1 - i_0)}{a_{R2}b_G(\eta_0 - i_0) + a_{R2}b_{R1}\eta_0 + a_G b_{R1} i_0^2 - a_G b_{R2} i_0(\eta_0 - i_0)}. \tag{21}$$

The influence of ratio k_ω on the behavior of the two wind turbines is herein considered by adjusting only the mechanical characteristic of the secondary wind rotor $R2$ and keeping unchanged the mechanical characteristics of wind rotor $R1$ and the electric generator. Under these assumptions, coefficients a_{R2} and b_{R2} become variables which are dependent on both ratio k_ω and the constant coefficients of the mechanical characteristic of primary rotor $R1$.

Thus, the following equation is obtained for the wind system with counter-rotating generator (Figure 2a), by considering the equality $T_{R2} = -T_{R1}$ from Equation (16):

$$-\omega_{R1}(a_{R1} + a_{R2}k_\omega) + b_{R1} + b_{R2} = 0, \tag{22}$$

where ω_{R1} is the independent parameter; this equality is mathematically satisfied only if the following two conditions are met simultaneously:

$$\begin{cases} a_{R1} + a_{R2}k_\omega = 0; \\ b_{R1} + b_{R2} = 0, \end{cases} \tag{23}$$

which leads to the solution:

$$\begin{cases} a_{R2} = a_{R1}/k_\omega; \\ b_{R2} = -b_{R1}\,. \end{cases} \tag{24}$$

Similarly, for the wind turbine system with conventional generator (Figure 2b), the starting point is established from the equality deduced in Equation (19):

$$T_{R2} = T_{R1}\frac{i_0}{\eta_0 - i_0}\,, \tag{25}$$

from which Equation (26) is obtained as function of ω_{R1}:

$$\omega_{R1}[a_{R1}i_0 + a_{R2}(\eta_0 - i_0)k_\omega] - b_{R1}i_0 + b_{R2}(\eta_0 - i_0) = 0, \tag{26}$$

as well as the expressions of coefficients a_{R2} and b_{R2} are determined:

$$\begin{cases} a_{R2} = -a_{R1}i_0/[(\eta_0 - i_0)k_\omega]; \\ b_{R2} = b_{R1}i_0/(\eta_0 - i_0)\,. \end{cases} \tag{27}$$

For comparison, the relations for the kinematic and static parameters of the two wind systems are tabulated below (see Table 1); the relations are established as functions of the parameters of primary wind rotor $R1$ in the analytical modeling presented above.

Table 1. The analytical expressions of the kinematic and static parameters of the wind systems.

Parameter	Symbol	Wind System 2 in-2 out, Figure 2a	Wind System 2 in-1 out, Figure 2b
Amplification kinematic ratio	$i_a = \frac{\omega_G}{\omega_{R1}}$	$-i_0(1+k_\omega)$	$1 - i_0(1+k_\omega)$
Efficiency	η	η_0	$\eta_0 \frac{1-i_0(1+k_\omega)}{\eta_0 - i_0(1+k_\omega)}$
Angular speed of the generator	$\omega_G = \omega_{GR} - \omega_{GS}$	$-\omega_{R1} i_0 (1+k_\omega)$	$\omega_{R1}[1 - i_0(1+k_\omega)]$
Generator torque	$T_G = T_{GR}$	$-T_{R1}\frac{\eta_0}{\eta_0 - i_0}$	$-T_{R1}\frac{\eta_0}{\eta_0 - i_0}$
Generator power	$P_G = T_G\, \omega_G$	$T_{R1}\omega_{R1}\eta_0 \frac{i_0(1+k_\omega)}{\eta_0 - i_0}$	$-T_{R1}\omega_{R1}\eta_0 \frac{1-i_0(1+k_\omega)}{\eta_0 - i_0}$
Angular speed of the generator rotor	ω_{GR}	$\omega_{R1}[1 - i_0(1+k_\omega)]$	$\omega_{R1}[1 - i_0(1+k_\omega)]$
Generator rotor torque	T_{GR}	$T_{R1}\frac{\eta_0}{i_0}$	$T_{R1}\frac{\eta_0}{i_0}$
Generator rotor power	P_{GR}	$T_{R1}\omega_{R1}\frac{\eta_0[1-i_0(k_\omega+1)]}{i_0}$	$T_{R1}\omega_{R1}\frac{\eta_0[1-i_0(k_\omega+1)]}{i_0}$
Angular speed of the generator stator	ω_{GS}	ω_{R1}	0
Generator stator torque	T_{GS}	$-T_{R1}\frac{\eta_0}{i_0}$	$-T_{R1}\frac{\eta_0}{i_0}$
Generator stator power	P_{GS}	$-T_{R1}\omega_{R1}\frac{\eta_0}{i_0}$	0
Angular speed of the carrier *H*	ω_H	ω_{R1}	ω_{R1}
H carrier torque	T_H	T_{R1}	T_{R1}
H carrier power	P_H	$T_{R1}\omega_{R1}$	$T_{R1}\omega_{R1}$
Angular speed of the shaft *HR*	ω_{HR}	ω_{R1}	ω_{R1}
HR shaft torque	T_{HR}	$T_{R1}\frac{i_0 - \eta_0}{i_0}$	T_{R1}
HR shaft power	P_{HR}	$T_{R1}\omega_{R1}\frac{i_0 - \eta_0}{i_0}$	$T_{R1}\omega_{R1}$
Angular speed of shaft *HS*	ω_{HS}	ω_{R1}	0
HS shaft torque	T_{HS}	$T_{R1}\frac{\eta_0}{i_0}$	$T_{R1}\frac{\eta_0}{i_0}$
HS shaft power	P_{HS}	$T_{R1}\omega_{R1}\frac{\eta_0}{i_0}$	0
Angular speed of gear 4	ω_4	$-k_\omega \omega_{R1}$	$-k_\omega \omega_{R1}$
Torque on gear 4	T_4	$-T_{R1}$	$-T_{R1}\frac{i_0}{i_0 - \eta_0}$
Power of gear 4	P_4	$k_\omega T_{R1}\omega_{R1}$	$\omega_{R1} T_{R1}\frac{k_\omega i_0}{i_0 - \eta_0}$

The analytical relations for the wind system with conventional electric generator (2 in-1 out, last column of Table 1) were obtained by the appropriate customization of the general model described for the case of the system with counter-rotating generator, i.e., breaking the connection between H and SG (i.e., T_{HS} = 0) and fixing the stator SG to the frame (i.e., ω_{SG} = 0). The analysis of the relations from Table 1 can highlight the following properties of wind systems of 2 in-2 out type compared to 2 in-1 out type systems:

- achieve a kinematic amplification ratio, in absolute value, higher than 1 (as both the ratios i_0 and k_ω have positive values);
- have a higher efficiency, which does not depend on the kinematic configuration of the speed increaser and which is equal to the internal efficiency η_0;
- ensure the operation with higher angular speeds ω_G and powers P_G of the electric generator, for the same power of the primary wind rotor $P_{R1} = T_{R1}\ \omega_{R1}$;
- the wind rotor $R2$ operates at lower torques and powers.

4. Numerical Simulations and Discussions

The comparative analysis of the performance of the two wind systems presented above, which integrate the same planetary speed increaser (i.e., the same values of the intrinsic parameters i_0 and η_0), is performed under equivalence conditions, by considering the following three numerical simulation scenarios:

Scenario A: the two wind turbines use the same wind rotors *R*1 and *R*2, as well as the same electric generator—used as a counter-rotating generator with the 2 in-2 out wind system (Figure 2a) and as a conventional generator with the 2 in-1 out wind system (Figure 2b). In this scenario, rotors *R*1 and *R*2 are identical and, therefore, have identical mechanical characteristics with the same constant coefficients.

Scenario B: very similar to *Scenario A*, except that rotors *R*1 and *R*2 are different and, as a result, they have mechanical characteristics with different constant coefficients.

Scenario C: derived from *Scenario B*, with the difference that secondary wind rotors *R*2 are adjusted differently in the two wind turbines (coefficients of mechanical characteristics for rotors *R*2 are different), with a view to providing the same value of ratio k_ω.

These scenarios aim at determining the operational points of the two wind turbines, i.e., the values of angular speed and torque for the external connections of the mechanism, which allow the calculation of the efficiency and output power. Therefore, Equations (14) and (15) are used to obtain the operational point of the rotor *GR* shaft, which allows the identification of the operational point of the primary wind rotor *R*1 and then all the other parameters, based on the relations in Table 1.

The intrinsic parameters of the planetary speed increaser remain constant in all scenarios, the following values being considered in the simulations: i_0 = 10 and$\eta_0 = \eta_g^3 = 0.95^3 = 0.857$.

4.1. Scenario A

In this scenario, the two wind turbines are characterized by the following features, see Rel. (7):

- wind rotors *R*1 and *R*2 are identical, since they have the same mechanical characteristics: $T_{R1} = -a_{R1}\omega_{R1} + b_{R1} = -18.763\ \omega_{R1} - 204.81$ and $T_{R2} = -a_{R2}\omega_{R2} + b_{R2} = -18.763\ \omega_{R2} + 204.81$;
- electric generators have the same mechanical characteristic $-T_G = -a_G\omega_{R1} - b_G = -;0.4\omega_G - 35$.

The results of the numerical simulations for the operational points of the two wind turbines are tabulated below (see Table 2).

Table 2. The values of the parameters related to the steady-state operational point for *Scenario A*.

Parameter	Wind System 2 in-2 out, Figure 2a	Wind System 2 in-1 out, Figure 2b
ω_{R1}[s^{-1}]	−5.470	−5.989
T_{R1}[kNm]	−102.176	−92.438
P_{R1}[kW]	558.905	553.613
ω_{R2}[s^{-1}]	5.470	5.527
T_{R2}[kNm]	102.176	101.106
P_{R2}[kW]	558.905	558.818
ω_G[s^{-1}]	109.401	109.171
T_G[kNm]	−8.760	−8.669
P_G[kW]	−958.382	−946.366
η	0.8573	0.8507
k_ω	1.000	0.923
$i_a = \omega_G/\omega_{R1}$	−20.000	−17.209

$a_{R1} = a_{R2}$ = 18.763 [kNms]; $b_{R1} = b_{R2} = -204.81$ [kNm]; a_G = 0.4 [kNms]; b_G = 35 [kNm]; i_0 = 10; η_0 = 0.857.

From these numerical results, the following conclusions can be drawn: compared to the 2 in-1 out wind system, the wind turbine with counter-rotating generator (2 in-2 out) operates at a higher efficiency (85.73% vs. 85.07%), ensures a higher amplification ratio in absolute value (20.00 vs. 17.21) and has a higher power by approx. 1.3% (958.38 vs. 946.37). Both wind rotors have similar lower angular speeds and higher torques, which leads to close input powers. As a result, when using identical wind rotors $R1$ and $R2$ in both systems and constant intrinsic parameters of the speed increaser and the considered mechanical characteristics, the wind turbine with a counter-rotating generator ensures slightly higher performance than the wind turbine with a conventional generator. Although preferred in terms of performance, the 2 in-2 out wind turbine can be surpassed by the 2 in-1 out turbine due to an increased complexity of the counter-rotating electric generator—if an economically-grounded multicriteria analysis might be performed.

4.2. Scenario B

The facts and figures in *Scenario A* change significantly by using secondary wind rotors which are different from the primary ones. Therefore, the *Scenario B* aims at identifying the operational point of the two wind turbines by considering, for both types of wind system:

- the same wind rotor $R1$, with the mechanical characteristic $T_{R1} = -a_{R1}\omega_{R1} + b_{R1} = -18.763\ \omega_{R1} - 204.81$
- the same wind rotor $R2$, with the mechanical characteristic $T_{R2} = -a_{R2}\omega_{R2} + b_{R2} = -18.763\ \omega_{R2} + 204.81$; established from the condition that the two wind turbines generate equal power;
- the same electric generator, with the mechanical characteristic $T_G = -a_G\omega_{R1} - b_G = -0.4\omega_G - 35$.

Under these conditions, the two wind turbines are stabilized in steady-state at the operational point values listed in Table 3 below.

Table 3. The values of the parameters related to the steady-state operational point for *Scenario B*.

Parameter	Wind System 2 in-2 out, Figure 2a	Wind System 2 in-1 out, Figure 2b
$\omega_{R1}[\mathrm{s}^{-1}]$	−4.754	−5.283
T_{R1}[kNm]	−115.604	−105.693
P_{R1}[kW]	549.622	558.332
$\omega_{R2}[\mathrm{s}^{-1}]$	6.474	6.474
T_{R2}[kNm]	115.604	115.604
P_{R2}[kW]	748.372	748.372
$\omega_G[\mathrm{s}^{-1}]$	112.279	112.279
T_G[kNm]	−9.912	−9.912
P_G[kW]	−1112.868	−1112.868
η	0.8574	0.8516
k_ω	1.362	1.225
$i_a = \omega_G/\omega_{R1}$	−23.616	−21.255

a_{R1} = 18.763 [kNms];]; b_{R1}−204.81 [kNm]; a_{R2} = 13.780 [kNms]; b_{R2} = 204.81 [kNm]; a_G = 0.4 [kNms]; b_G = 35 [kNm]; i_0 = 10; η_0 = 0.857.

Under the condition of equal output power, used for driving the electric generator, it is found that wind rotor $R2$ extracts the same power from the wind in both systems, while primary wind rotor $R1$ operates at higher parameters with 2 in-1 out wind turbine. Instead, the wind system with a counter-rotating generator has slightly better efficiency (85.74% vs. 85.16%), which provides the energy compensation required to obtain a power output equal to that of the system with a conventional generator. Choosing the secondary wind rotor (by setting the coefficient a_{R2}) is a challenging task for designers, which can lead to changing the option for one or the other type of wind turbine. Parameters marked by asterisk (*) in the following diagrams, Figure 5, refer to the wind turbine with a conventional generator.

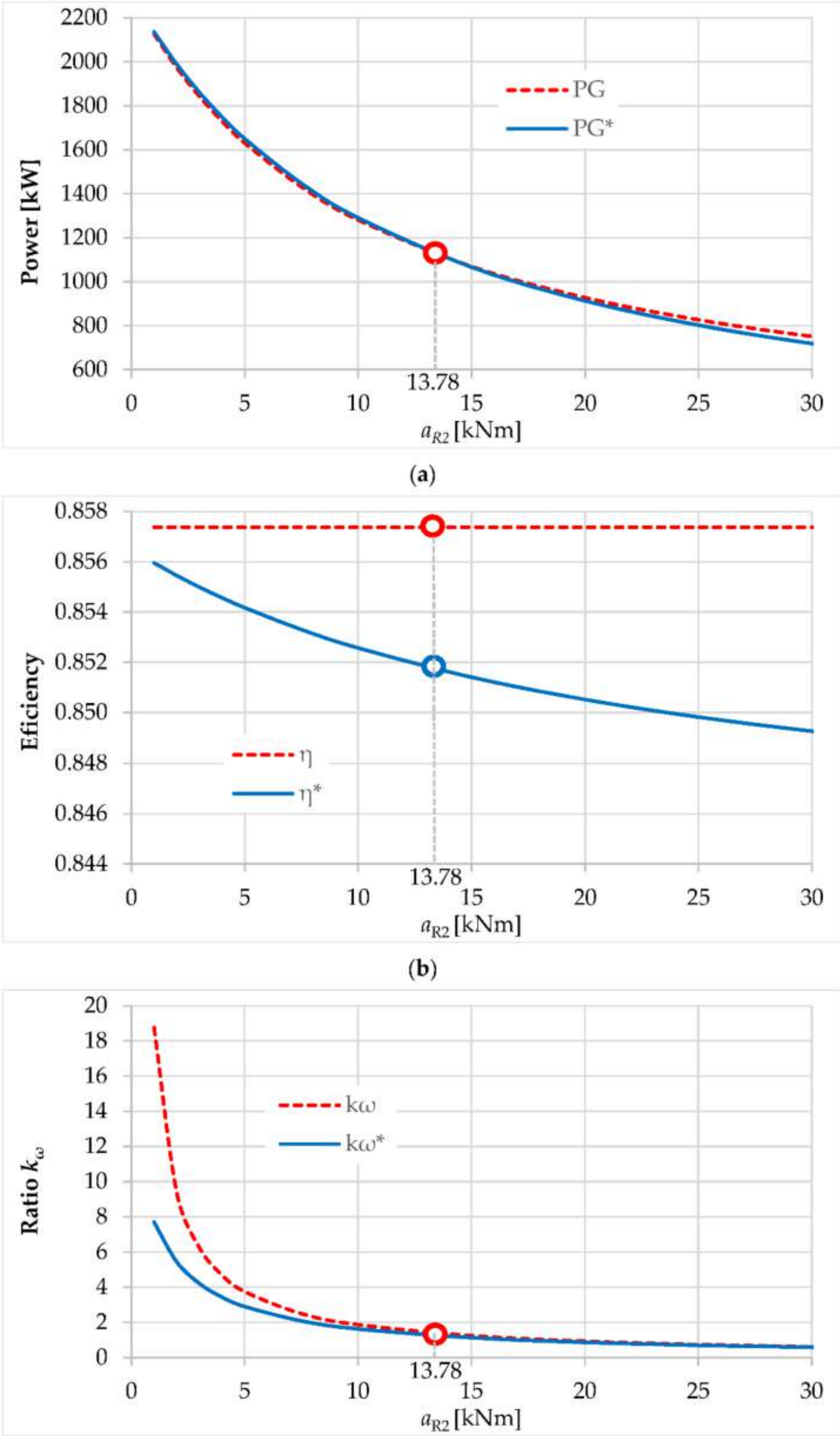

(**a**) (**b**) (**c**)

Figure 5. Variation with respect to a_{R2} coefficient of: (**a**) output power, (**b**) efficiency and (**c**) ratio k_ω, in both wind systems.

According to Figure 5a, the wind turbine with a conventional generator ensures an output power (*PG** curve) higher than that of the 2 in-2 out turbine, for values of coefficient $a_{R2} < 13.78$, and generates power values significantly close to those of the turbine with a counter-rotating generator (*PG* curve), for values of coefficient $a_{R2} > 13.78$. The efficiency of the conventional turbine decreases with the increase of values for a_{R2} (see Figure 5b). In all instances, the wind turbine with a counter-rotating generator is stabilized at higher values of ratio k_ω, i.e., a greater difference between input speeds, but with less significant differences for $a_{R2} > 13.78$ (see Figure 5c).

Thus, it should be emphasized that the performance of the two wind systems is significantly influenced by the external mechanical characteristics, modified in this study by changing the coefficient values $a_{R1} = a_{R2}$.

4.3. Scenario C

The *Scenario C* is an extension of the *Scenario B*, by ensuring the additional condition of obtaining the same ratio k_ω for both wind turbines. Under the conditions of maintaining the same primary wind rotor *R*1 and the same electric generator as in *Scenarios A* and *B*, this goal can only be achieved if the secondary wind rotors *R*2 are different, i.e., $a_{R2} \neq a^*_{R2}$ and $b_{R2} \neq b^*_{R2}$. As a case study, the target value of ratio $k_\omega = 2.5$ is further considered and, therefore, the coefficients of the mechanical characteristics of rotors *R*2 can be calculated, by means of Equations (24) and (27). The values of the steady-state operational points for the two wind turbines are displayed in Table 4 below. As in *Scenario B*, the parameters marked by * refer to the wind system with a conventional generator.

Table 4. The values of the parameters related to the steady-state operational point for *Scenario C*.

Parameter	Wind System 2 in-2 out, Figure 2a	Wind System 2 in-1 out, Figure 2b
$\omega_{R1}[\mathrm{s}^{-1}]$	−3.367	−3.529
T_{R1}[kNm]	−141.630	−138.592
P_{R1}[kW]	476.908	489.117
$\omega_{R2}[\mathrm{s}^{-1}]$	8.418	8.823
T_{R2}[kNm]	141.630	151.589
P_{R2}[kW]	1192.301	1337.455
$\omega_G[\mathrm{s}^{-1}]$	117.857	119.992
T_G[kNm]	−12.143	−12.997
P_G[kW]	−1431.138	−1559.516
η	0.8574	0.8538
$i_a = \omega_G/\omega_{R1}$	−35.000	−34.000

a_{R1} = 18.763 [kNms];]; b_{R1} −204.81 [kNm]; a_{R2} = 7.505 [kNms]; b_{R2} = 204.81 [kNm]; k_ω = 2.5; a^*_{R2} = 8.209 [kNms]; b^*_{R2} = 224.016 [kNm]; a_G = 0.4 [kNms]; b_G - 35 [kNm]; i_0 = 10; η_0 = 0.857.

According to the results in Tables 2–4 and Figure 6a, it can be concluded that the efficiency of the speed increaser is higher with systems having a counter-rotating generator, as a result of in-parallel transmission of the output mechanical power, compared to wind systems with a conventional generator. The efficiency dependence on ratio k_ω—described by Equations (10) and (11) and illustrated in Figure 6a—highlights the fact that efficiency of a 2 in-2 out wind system is constant and always higher than that achieved by a 2 in-1 out system, whose values tend to infinity toward this constant value. Thus, the efficiency of the two wind systems can have close values only for very high values of k_ω, which is not justified in the operation of a wind system with counter-rotating rotors.

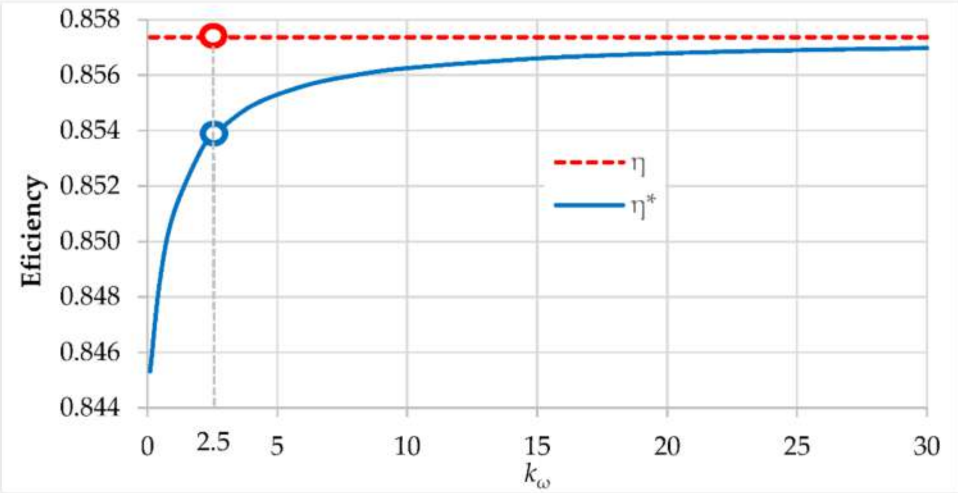

(a)

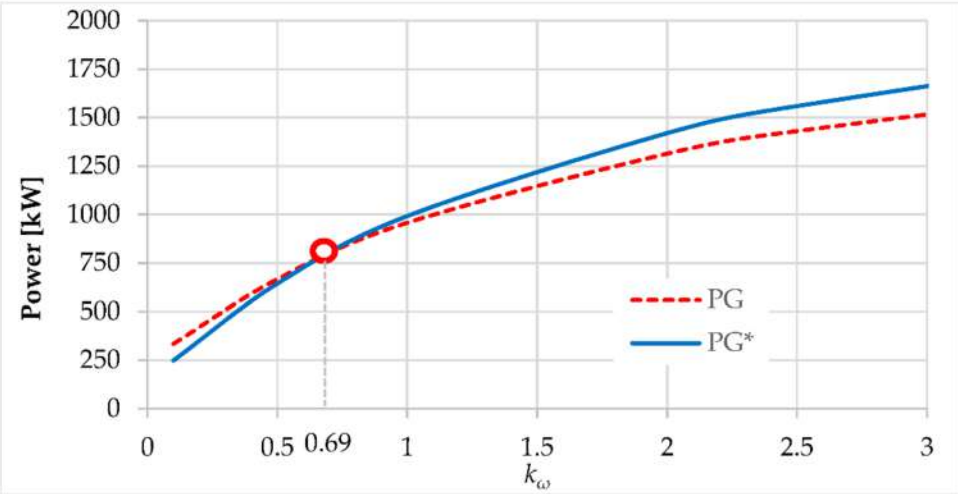

(b)

Figure 6. Variation with respect to ratio k_ω of: (**a**) efficiency and (**b**) output power, in both wind systems.

As in *Scenario B*, the wind turbine with a counter-rotating generator has higher energy performance for low values of ratio k_ω and output power, implicitly (Figure 6b). Instead, the wind turbine with a conventional generator proves to be more efficient for higher values of ratio k_ω and output power.

To conclude the discussions for the three numerical simulation scenarios, the power flows for both wind systems with counter-rotating electric generator (Figure 7a) vs. conventional generator (Figure 7b) are comparatively represented in Figure 7. It is noticeable for both systems the increase of the output power from *Scenario A* to *Scenario C*, as well as the effectiveness of the 2 in-2 out system at lower powers and, respectively, of the 2 in-1 out system at higher powers.

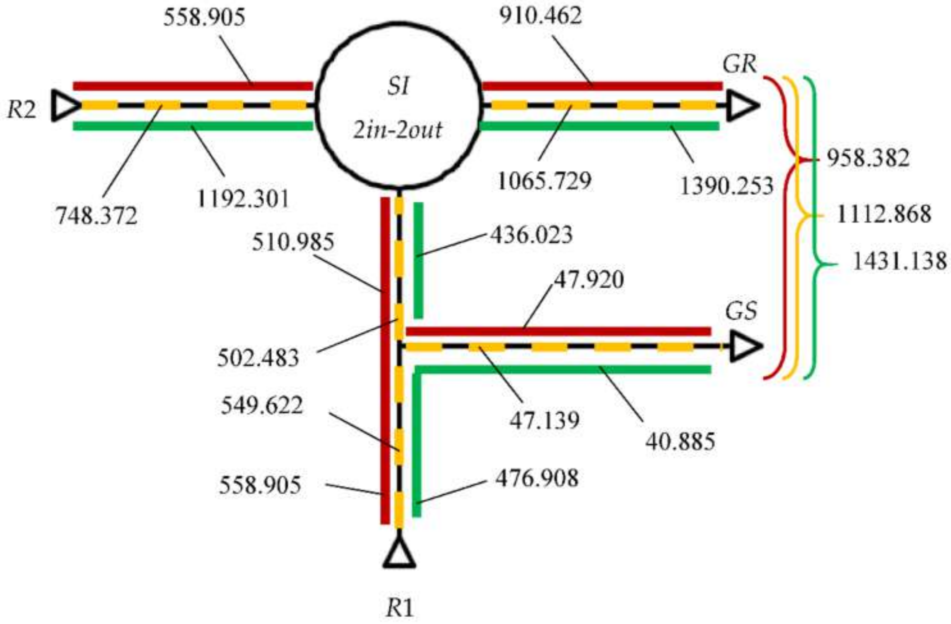

(a)

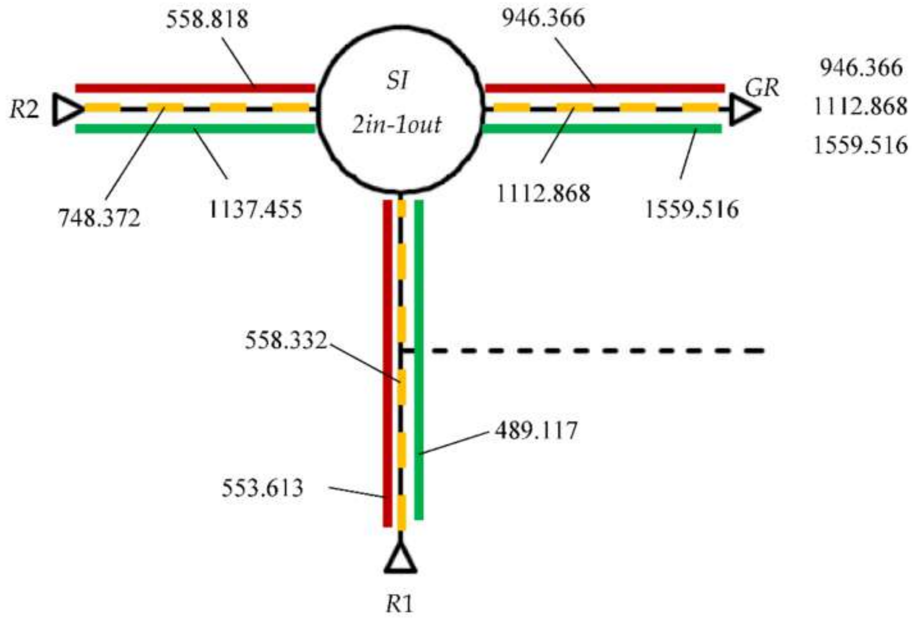

(b)

Figure 7. Power flow in the *Scenarios A* (continuous red line), *B* (yellow dashed line) and *C* (continuous green line) through: (**a**) 2 in-2 out wind system; (**b**) 2 in-1 out wind system.

5. Conclusions

The paper presented a comparative study of the energy performance of wind turbines with two counter-rotating rotors ($R1$ and $R2$) and differential speed increaser, in the functional configurations with counter-rotating vs. conventional generator. To this end, the analytical modeling of the operational point of the two types of wind system has been presented and numerically analyzed in three scenarios, with distinct situations regarding the way the secondary wind rotor $R2$ characteristic is chosen: $R2$ identical to the primary wind rotor $R1$ (*Scenario A*); $R2$ different from $R1$, and $R2$ identical in both applications (*Scenario B*); and $R2$ different from $R1$, and $R2$ different in the two applications (*Scenario C*).

According to the analyzed scenarios, the comparative study of the numerical results allows drawing the following final conclusions:

- The differential wind system with a counter-rotating electric generator, which is characterized by in-parallel transmission of power at both input and output, always ensures better efficiency of mechanical power transmission from inputs to outputs, compared to the wind system with a conventional generator. In the case of counter-rotating outputs, the efficiency of the wind system is equal to the internal efficiency η_0 of the planetary transmission; instead, the efficiency of the wind turbine with a conventional generator is significantly influenced by system parameters (i.e., ratio k_ω, coefficients of mechanical characteristics, kinematic ratio i_0), the value η_0 being the upper limit of efficiency variation for this type of wind turbine.
- The energy response of the two types of wind system depends significantly on the characteristics of the selected wind rotors and electric generator. Thus, the advantage of better mechanical efficiency of wind turbines with a counter-rotating generator is accompanied by higher energy performance only in certain system configurations—generally, in the range of lower power. Considering the higher complexity of counter-rotating electric generators, due to their mobile stator, the designers' decision to choose a type of counter-rotating wind turbine seems to be a compromise between technical, energy and economic performance.

The proposed models are useful in the synthesis of differential speed increasers with counter-rotating inputs and outputs, which ensure higher output speed by speed-adding, in conditions of higher efficiency. Considering these facts, the findings emerged from this contrastive approach might prove particularly useful to wind system designers in selecting the most adequate technical solution, depending on the amount of power needed and the wind potential in the area of implementation.

In the future, the authors intend to generalize the modeling of the behavior of counter-rotating wind turbines with counter-rotating electric generator vs. conventional generator in both cases of operation, as a 2-*DOF* (speed-adding) and a 1-*DOF* (torque-adding) system, followed by experimental validation of analytical results by developing and using an versatile rig to test these types of counter-rotating wind turbines.

Author Contributions: Conceptualization, R.S. and M.N.; Data curation, R.S., M.N. and C.J.; Formal analysis, R.S, M.N. and C.J.; Investigation, R.S., M.N. and C.J.; Methodology, R.S., M.N., C.J. and O.M.; Software, R.S. and M.N.; Supervision, M.N., C.J. and O.M.; Validation, M.N. and C.J.; Visualization, R.S., M.N., C.J. and O.M.; Writing—original draft, R.S. and M.N.; Writing—review & editing, C.J. and O.M. All authors have read and agreed to the published version of the manuscript.

Funding: This research received no external funding.

Acknowledgments: The comments, suggestions and recommendations for future research by the anonymous reviewers are gratefully acknowledged.

Conflicts of Interest: The authors declare no conflict of interest.

Nomenclature

SI	Speed increaser	DOF	Degree of freedom
$R1$	Primary wind rotor	M	Mechanism mobility
$R2$	Secondary wind rotor	L	Total number of inputs and outputs
P	Power	G	Electric generator
ω	Angular speed	GR	Electric generator rotor
T	Torque	GS	Electric generator stator
k_ω	Ratio of the input angular speeds	i	Kinematic ratio
z	Number of gear teeth	i_0	Internal kinematic ratio
H	Satellite carrier	i_a	Amplification kinematic ratio
F	Operational point	η	Efficiency of the speed increaser
a	Angular speed coefficient	η_0	Internal efficiency
b	Torque coefficient	η_g	Efficiency of a gear pair

References

1. Wacinski, A.; Sàrl, E. Drive Device for a Windmill Provided with Two Counter–Rotative Propellers. U.S. Patent 7,384,239, 6 September 2008.
2. Brander, M. Bi-Directional Wind Turbine. U.S. Patent 0,197,639 A1, 21 August 2008.
3. Jaliu, C.; Climescu, O.; Saulescu, R. Speci fic features of a counter-rotating transmission for renewable energy systems. *Environ. Eng. Manag. J.* **2011**, *10*, 1105–1113. [CrossRef]
4. Oprina, G.; Chihaia, R.A.; El-Leathey, L.A.; Nicolaie, S.; Babutanu, C.A.; Voina, A. A review on counter-rotating wind tur-bines development. *J. Sustain. Energy* **2016**, *7*, 91–98.
5. Shin, C. Multi-Unit Rotor Blade System Integrated Wind Turbine. U.S. Patent 5,876,181, 2 March 1999.
6. Muhtadi, R.Z.; Bramantya, M.A. Experimental study of local pitch variations on electric power generated by counter rotating wind turbine with single generator without gearbox. *IOP Conf. Ser. Mater. Sci. Eng.* **2018**, *434*, 012176. [CrossRef]
7. Li, Z.; Wang, Y.; Xiao, H. Experimental study on structures of counter-rotating wind turbines. In Proceedings of the 2013 International Conference on Materials for Renewable Energy and Environment, Chengdu, China, 19–21 August 2013; Volume 1, pp. 368–372. [CrossRef]
8. Pamuji, D.; Bramantya, M. Numerical Study on the Performance Of 2-Bladed and 3-Bladed Counter Rotating Wind Turbines. *J. Jpn. Soc. Appl. Electromagn. Mech.* **2019**, *27*, 169–174. [CrossRef]
9. Didane, D.H.; Rosly, N.; Zulkafli, M.F.; Shamsudin, S.S. Performance evaluation of a novel vertical axis wind turbine with coaxial contra-rotating concept. *Renew. Energy* **2018**, *115*, 353–361. [CrossRef]
10. West, R. Wind Turbine System. U.S. Patent 10,316,820 B2, 11 June 2019.
11. Vasel-Be-Hagh, A.; Archer, C.L. Wind farms with counter-rotating wind turbines. *Sustain. Energy Technol. Assess.* **2017**, *24*, 19–30. [CrossRef]
12. Jaliu, C.; Diaconescu, D.V.; Neagoe, M.; Saulescu, R. Dynamic features of speed increasers from mechatronic wind and hydro systems. Part II. Dynamic aspects. In Proceedings of the Second European Conference on Mechanism Science EUCOMES 08, Casino, Italy, 17–20 September 2008; Springer: Dordrecht, The Netherlands, 2008; pp. 365–373, ISBN 987-1-4020-8914-5.
13. Bevington, C.M.; Bywaters, G.L.; Coleman, C.C.; Costin, D.P.; Danforth, W.L.; Lynch, J.A.; Rolland, R.H. Wind Turbine Having a Direct-Drive Drivetrain. U.S. Patent 7,431,567 B1, 7 October 2008.
14. Marjanovic, N.; Isailovic, B.; Marjanovic, V.; Milojevic, Z.; Blagojevic, M.; Bojic, M. A practical approach to the optimization of gear trains with spur gears. *Mech. Mach. Theory* **2012**, *53*, 1–16. [CrossRef]
15. Pastor, D.G.S.B.; Nalianda, D.; Sethi, V.; Midgley, R.; Rolt, A.; Novelo, D.A.B. Preliminary Design Framework for the Power Gearbox in a Contra-Rotating Open Rotor. *J. Eng. Gas Turbines Power* **2021**, *143*, 041022. [CrossRef]
16. Jelaska, D.; Podrug, S.; Perkušić, M. A novel hybrid transmission for variable speed wind turbines. *Renew. Energy* **2015**, *83*, 78–84. [CrossRef]
17. Saulescu, R.; Neagoe, M.; Munteanu, O.; Cretescu, N. Performance analysis of a novel planetary speed increaser used in single-rotor wind turbines with counter-rotating electric generator. *IOP Conf. Ser. Mater. Sci. Eng.* **2016**, *147*, 012090. [CrossRef]
18. Neagoe, M.; Saulescu, R.; Jaliu, C.; Cretescu, N. Novel Speed increaser used in counter-rotating wind turbines. In *New Advances in Mechanisms, Mechanical Transmissions and Robotics, Mechanisms and Machine Science 46*; Springer: Berlin, Germany, 2017; pp. 143–151. [CrossRef]
19. Jaliu, C.; Diaconescu, D.V.; Neagoe, M.; Saulescu, R. Dynamic features of speed increasers from mechatronic wind and hydro systems. Part I. Structure Kinematics. In Proceedings of the Second European Conference on Mechanism Science EUCOMES 08, Casino, Italy, 17–20 September 2008; Springer: Dordrecht, The Netherlands, 2008; pp. 355–363, ISBN 987-1-4020-8914-5.
20. Erturk, E.; Sivrioglu, S.; Bolat, F.C. Analysis Model of a Small Scale Counter-Rotating Dual Rotor Wind Turbine with Double Rotational Generator Armature. *Int. J. Renew. Energy Res.* **2018**, *8*, 1849–1858.
21. Bharani, R.; Sivaprakasam, A. A Review Analysis on Performance and Classification of Wind Turbine Gearbox Technologies. *IETE J. Res.* **2020**, 1–15. [CrossRef]

22. Fan, Z.; Zhu, C.; Li, X.; Liang, C. The transmission characteristic for the improved wind turbine gearbox. *Energy Sci. Eng.* **2019**, *7*, 1368–1378. [CrossRef]
23. Qiu, J.; Liu, B.; Dong, H.; Wang, D. Type Synthesis of Gear-box in Wind Turbine. *Procedia Comput. Sci.* **2017**, *109*, 809–816. [CrossRef]
24. Climescu, O.; Jaliu, C.; Saulescu, R. Comparative Analysis of Horizontal Small Scale Wind Turbines for a Specific Applica-tion. In Proceedings of the 14th IFToMM World Congress, Taipei, Taiwan, 25–30 October 2015. [CrossRef]
25. Saulescu, R.; Neagoe, M.; Jaliu, C. Improving the Energy Performance of Wind Turbines Implemented in the Built Environment Using Counter-Rotating Planetary Transmissions. *IOP Conf. Ser. Mater. Sci. Eng.* **2016**, *147*, 012089. [CrossRef]
26. Saulescu, R.; Jaliu, C.; Neagoe, M. Structural and Kinematic Features of a 2 DOF Speed Increaser for Renewable Energy Systems. *Appl. Mech. Mater.* **2016**, *823*, 367–372. [CrossRef]
27. Saulescu, R.; Neagoe, M.; Jaliu, C.; Munteanu, O. Comparative Analysis of Two Wind Turbines with Planetary Speed Increaser in Steady-State. *Appl. Mech. Mater.* **2016**, *823*, 355–360. [CrossRef]
28. Saulescu, R.; Jaliu, C.; Munteanu, O.; Climescu, O. Planetary Gear for Counter-Rotating Wind Turbines. *Appl. Mech. Mater.* **2014**, *658*, 135–140. [CrossRef]
29. Saulescu, R.; Jaliu, C.; Climescu, O.; Diaconescu, D. On the use of 2 DOF planetary gears as "speed increaser" in small hydros and wind turbines. In Proceedings of the ASME International Design Engineering Technical Conferences & Computers and Information in Engineering Conference IDETC/CIE 2011, Washington, DC, USA, 25–31 August 2011.
30. Herzog, R.; Schaffarczyk, A.P.; Wacinski, A.; Zürcher, O. Performance and stability of a counter–rotating windmill using a planetary gearing: Measurements and Simulation. In Proceedings of the European Wind Energy Conference & Exhibition, Warsaw, Poland, 20–23 April 2010.
31. Neagoe, M.; Saulescu, R.; Jaliu, C. Design and Simulation of a 1 DOF Planetary Speed Increaser for Counter-Rotating Wind Turbines with Counter-Rotating Electric Generators. *Energies* **2019**, *12*, 1754. [CrossRef]
32. Saulescu, R.; Neagoe, M.; Jaliu, C. Conceptual Synthesis of Speed Increasers for Wind Turbine Conversion Systems. *Energies* **2018**, *11*, 2257. [CrossRef]
33. Neagoe, M.; Jaliu, C.; Saulescu, R.; Simionescu, P. Steady-State Response of a Dual-Rotor Wind Turbine with Counter-Rotating Electric Generator and Planetary Gear Increaser. In Proceedings of the USCToMM MSR 2020, Rapid City, SD, USA, 14–16 May 2020; pp. 106–115. [CrossRef]
34. Zhao, M.; Ji, J. Dynamic Analysis of Wind Turbine Gearbox Components. *Energies* **2016**, *9*, 110. [CrossRef]
35. Dong, H.; Zhang, C.; Wang, D.; Xu, S.; Qiu, J. Dynamic characteristics of gear box with PGT for wind turbine. *Procedia Comput. Sci.* **2017**, *109*, 801–808. [CrossRef]
36. Vázquez-Hernández, C.; Serrano-González, J.; Centeno, G. A Market-Based Analysis on the Main Characteristics of Gearboxes Used in Onshore Wind Turbines. *Energies* **2017**, *10*, 1686. [CrossRef]
37. Farahani, E.; Hosseinzadeh, N.; Ektesabi, M. Comparison of fault-ride-through capability of dual and single-rotor wind turbines. *Renew. Energy* **2012**, *48*, 473–481. [CrossRef]
38. Kutt, F.; Blecharz, K.; Karkosiński, D. Axial-Flux Permanent-Magnet Dual-Rotor Generator for a Counter-Rotating Wind Turbine. *Energies* **2020**, *13*, 2833. [CrossRef]
39. Mirnikjoo, S.; Abbaszadeh, K.; Abdollahi, S.E. Multi-Objective Design Optimization of a Double-Sided Flux Switching Permanent Magnet Generator for Counter-Rotating Wind Turbine Applications. *IEEE Trans. Ind. Electron.* **2020**, 1. [CrossRef]
40. Zhamalov, A.Z.; Obozov, A.D.; Kunelbaev, M.M.; Baikadamova, L.S. Capacity and Power Characteristics of Disk Generator with Counter-Rotation of Double-Rotor Wind Turbine. *Middle-East J. Sci. Res.* **2013**, *15*, 1655–1662. [CrossRef]
41. Kanemoto, T.; Galal, A.M. Development of Intelligent Wind Turbine Generator with Tandem Wind Rotors and Double Rotational Armatures. *JSME Int. J. Ser. B* **2006**, *49*, 450–457. [CrossRef]
42. Caiozza, J. Wind Driven Electric Generator Apparatus. U.S. Patent 7,227,276 B2, 5 June 2007.
43. Pacholczyk, M.; Karkosiński, D. Parametric Study on a Performance of a Small Counter-Rotating Wind Turbine. *Energies* **2020**, *13*, 3880. [CrossRef]
44. Saulescu, R.; Neagoe, M.; Cretescu, N. Comparative analysis of two wind turbines with counter-rotating vs. fixed-stator electric generator. *IOP Conf. Ser. Mater. Sci. Eng.* **2020**, *997*, 012091. [CrossRef]
45. Fan, G.-F.; Qing, S.; Wang, H.; Hong, W.-C.; Li, H.-J. Support Vector Regression Model Based on Empirical Mode Decomposition and Auto Regression for Electric Load Forecasting. *Energies* **2013**, *6*, 1887–1901. [CrossRef]
46. Hong, W.-C.; Fan, G.-F. Hybrid Empirical Mode Decomposition with Support Vector Regression Model for Short Term Load Forecasting. *Energies* **2019**, *12*, 1093. [CrossRef]
47. Pfaffel, S.; Faulstich, S.; Rohrig, K. Performance and Reliability of Wind Turbines: A Review. *Energies* **2017**, *10*, 1904. [CrossRef]
48. Neagoe, M.; Saulescu, R.; Jaliu, C.; Simionescu, P.A. A Generalized Approach to the Steady-State Efficiency Analysis of Torque-Adding Transmissions Used in Renewable Energy Systems. *Energies* **2020**, *13*, 4568. [CrossRef]
49. Miloiu, G.; Dudita, F.; Diaconescu, D. *Modern Mechanical Transmissions*; Tehnica: Bucharest, Romania, 1980. (In Romanian)

(19) OFICIUL DE STAT PENTRU INVENŢII ŞI MĂRCI
București

ROMÂNIA

(11) **RO 134401 B1**

(51) **Int.Cl.**
F03D 15/10 (2016.01);
F03D 1/02 (2006.01);
F16H 37/08 (2006.01)

(12) **BREVET DE INVENŢIE**

(21) Nr. cerere: **a 2020 00224**

(22) Data de depozit: **27/04/2020**

(45) Data publicării menţiunii acordării brevetului: **28/02/2025** BOPI nr. **2/2025**

(41) Data publicării cererii:
28/08/2020 BOPI nr. **8/2020**

(73) Titular:
• **UNIVERSITATEA "TRANSILVANIA" DIN BRAŞOV**, *BD.EROILOR NR.29, BRAŞOV, BV, RO*

(72) Inventatori:
• **NEAGOE MIRCEA**, *STR.MOLIDULUI NR.103, SĂCELE, BV, RO;*
• **SĂULESCU RADU-GABRIEL**, *STR.PANSELUŢEI NR.10, BL.3, SC.A, ET.4, AP.17, CODLEA, BV, RO;*
• **JALIU CODRUŢA ILEANA**, *BD.VICTORIEI NR.10, BL.43, BRAŞOV, BV, RO;*
• **MUNTEANU OLIMPIU**, *STR. COL. BUZOIANU NR. 51, AP. 3, BRAŞOV, BV, RO*

(56) Documente din stadiul tehnicii:
CN 210371010 U; FR 2944845 A1

(54) **AMPLIFICATOR DE TURAŢIE PLANETAR REGLABIL RECONFIGURABIL PENTRU TURBINE EOLIENE ŞI METODĂ DE REGLARE A ACESTUIA**

RO 134401 B1

Examinator: **ing. CRISTEA DELIA-FLORENTINA**

Invenţia se referă la un amplificator de turaţie planetar cu structură adaptabilă la configuraţii de tip mecanism monomobil şi mecanism bimobil, cu una sau două intrări şi cu una sau două ieşiri coaxiale, precum şi la o metodă de reglare a acestuia, destinat integrării în turbine eoliene, exploatate în condiţiile unui domeniu larg de variaţie sezonieră a vitezei vântului, şi în standuri de testare, în condiţii reale sau de laborator, a turbinelor eoliene cu unul sau două rotoare eoliene şi un generator electric contrarotativ (cu rotor şi stator rotative în sensuri contrare) sau generator electric clasic (cu stator fix), cu scopul de a identifica comportamentul şi optimiza performanţele energetice ale acestor turbine eoliene.

Se cunoaşte din documentul **CN 210371010 U** un sistem de transmisie a mişcării pentru o turbină eoliană. Turbina cuprinde un rotor având un diametru mic şi al cărui arbore intră într-un arbore tubular al unui rotor cu diametru mai mare, cele două rotoare se rotesc în direcţii opuse. Capătul de ieşire al arborelui tubular este conenctat cu o roată centrală cu dantură interioară dispusă concentric cu arborele rotorului mic şi o roată centrală cu dantură exterioară. Două roţi satelit sunt dispuse simetric între roata centrală cu dantură interioară şi roata centrală cu dantură exterioară, de asemenea între cele două roţi satelit şi roata centrală cu dantură exterioară sunt dispuse alte roţi dinţate care schimbă sensul de rotaţie al rotorului mic. Cele două roţi satelit sunt conectate la capetele de intrare ale unui element port-sateliţi, iar capătul de ieşire al acestui element este legat de un generator electric printr-un ax şi o cutie de viteze.

Mai este cunoscut din documentul **FR 2944845 A1** o transmisie variabilă pentru o instalaţie de generare a energiei electrice, bazată pe un angrenaj epiciclic controlat electronic care face posibilă garantarea unei viteze constante sau variabile după cum este necesar la ieşire, indiferent de viteza la intrare. Sistemul deviază o mică parte din energia transferată (mai puţin de 15%) pentru a controla viteza de rotaţie a elementului port-sateliţi al angrenajului epiciclic folosind o unitate de control. Transmisia cuprinde o coroana dinţată conectată la un arbore de intrare, o roată centrală cu dantură exterioară conectată la un arbore de ieşire, un element port-sateliţi ce cuprinde două roţi satelit conectate la unitatea de control.

Este cunoscut din documentul **US 5876181 A** un sistem eolian cu două rotoare eoliene, în care amplificatorul de turaţie integrează angrenaje conice cu axe fixe şi o unitate planetară cilindrică bimobilă cu două intrări şi o ieşire, care însumează mişcările de intrare, având dezavantajul unui mecanism complex cu gabarit mărit.

Mai este cunoscut din documentul **US 4291233 A** un amplificator de turaţie cu roţi dinţate din componenţa unei turbine cu un rotor eolian şi un generator electric contrarotativ, format din două angrenaje conice cu axe fixe care acţionează o unitate planetară cilindrică bimobilă cu sateliţi simpli. Soluţia menţionată prezintă dezavantajul utilizării unui singur rotor eolian, care dezvoltă puteri nominale mai reduse comparativ cu turbinele eoliene contrarotative, a unei complexităţi constructive ridicate, determinată de roata conică de pe arborele de intrare care formează, cu celelalte două roţi conice coaxiale, două angrenaje cu unghiuri diferite între axele de rotaţie, şi a unui randament redus.

Problema tehnică pe care o rezolvă invenţia constă în creşterea turaţiei generatorului electric şi a puterii mecanice de acţionare a generatorului electric.

Amplificatorul de turaţie planetar reglabil propus soluţionează problema tehnică prin aceea că este alcătuit dintr-un stator fix sau mobil şi un rotor, constituit dintr-un element port-sateliţi şi o roată centrală cu dantură interioară, care pun în mişcare două sau mai multe roţi satelit dispuse echiunghiular, unde cel puţin o roată satelit cu dantură exterioară angrenează cu roata centrală cu dantură interioară şi cu o altă roată satelit cu dantură exterioară ce angrenează cu o roată centrală cu dantură exterioară şi care asigură sensuri de rotaţie contrare pentru cele două ieşiri materializate prin elementul port-sateliţi şi roata centrală cu dantură interioară, unde fiecare roată satelit cu dantură exterioară este solidarizată cu câte o altă roată satelit cu dantură exterioară care angrenează cu câte o roată centrală cu dantură interioară, de asemenea amplificatorul mai cuprinde patru cuplaje intermitente comandate, respectiv un cuplaj dublu ce permite cuplarea primului rotor atât cu elementul port-sateliţi cât şi cu o bază fixă, al doilea cuplaj dublu permite cuplarea celui de-al doilea rotor atât cu roata centrală cu dantură interioară, cât şi cu o bază fixă, al treilea cuplaj dublu permite cuplarea statorului generatorului atât cu elementul port-sateliţi, cât şi cu baza fixă, iar cuplajul simplu permite cuplarea roţii centrale cu dantură interioară cu baza fixă sau lasă liberă mişcarea acestei roţi.

Amplificatorul de turaţie planetar reglabil pentru turbine eoliene, conform invenţiei, prezintă următoarele avantaje comparativ cu soluţiile cunoscute:

a) Poate fi utilizat în construcţia turbinelor eoliene cu unu sau două rotoare eoliene contrarotative şi generator electric clasic sau contrarotativ, permiţând adaptarea în exploatare pentru creşterea producţiei de energie electrică în condiţii de variaţii sezoniere mari ale vitezei vântului;

b) Poate fi integrat în standuri de testare a turbinelor eoliene în aer liber sau în condiţii de laborator;

c) Se reconfigurează uşor şi simplu pentru diverse situaţii funcţionale corespunzătoare tipurilor de turbine eoliene (cu unul sau două rotoare, cu generator electric clasic sau contrarotativ, cu însumarea ponderată a vitezelor de intrare sau a momentelor de intrare);

d) Poate fi reglat şi în timpul funcţionării, prin utilizarea cuplajelor intermitente comandate;

e) Permite blocarea rotoarelor eoliene în situaţii speciale, precum viteza vântului mai mare decât cea admisă în funcţionare, intervenţii pentru întreţinere sau reparaţii etc.;

f) Realizează randamente superioare soluţiilor clasice similare cu o intrare şi o ieşire, în aceleaşi condiţii de calitate şi precizie a roţilor dinţate componente;

g) Asigură o turaţie mai ridicată a generatorului electric (turaţia relativă dintre rotorul şi statorul acestuia), obţinută atât prin însumarea ponderată a vitezelor celor două rotoare eoliene, în cazul transmisiei bimobile, cât şi prin însumarea vitezelor de ieşire datorată mişcărilor contrarotative ale statorului şi rotorului generatorului electric, în cazul utilizării unui generator electric contrarotativ;

h) Asigură un moment mai mare de acţionare a generatorului electric prin însumarea ponderată a momentelor de intrare, în cazul transmisiei monomobile;

i) Are o complexitate structural-constructivă mai scăzută;

j) Are o construcţie robustă şi nu necesită tehnologii de fabricaţie pretenţioase;

k) Poate fi realizat pentru o gamă largă de puteri ale turbinelor eoliene, cu ax vertical sau orizontal.

Se prezintă în continuare un exemplu de realizare a invenţiei, în legătură cu fig. 1...17:

- fig. 1, schema conceptuală a unui amplificator planetar de turaţie reglabil, în cazul general al unei turbine eoliene cu două rotoare contrarotative şi un generator electric contrarotativ;
- fig. 2, detaliul cuplajului C dublu în configuraţia de cuplare a rotorului A eolian cu baza 8;
- fig. 3, detaliul cuplajului C dublu în configuraţia de cuplare a rotorului A eolian cu elementul 1 port-sateliţi;

- fig. 4, detaliul cuplajului D dublu în configuraţia de cuplare a rotorului B eolian cu baza 8;
- fig. 5, detaliul cuplajului D dublu în configuraţia de cuplare a rotorului B eolian cu roata 2;
- fig. 6, detaliul cuplajului E dublu în configuraţia de cuplare a statorului G al generatorului electric cu baza 8;
- fig. 7, detaliul cuplajului E dublu în configuraţia de cuplare a statorului G al generatorului electric cu elementul 1 port-sateliţi;
- fig. 8, detaliul cuplajului F în configuraţia de cuplare a roţii 7 cu baza 8;
- fig. 9, detaliul cuplajului F în configuraţia de decuplare a roţii 7 de la baza 8 (rotaţie liberă);
- fig. 10, exemplu de configurare a amplificatorului de turaţie pentru o turbină diferenţială cu două rotoare eoliene şi generator electric contrarotativ (C cuplat conform fig. 3, D cuplat conform fig. 5, E cuplat conform fig. 7, F decuplat conform fig. 9);
- fig. 11, exemplu de configurare a amplificatorului de turaţie pentru o turbină diferenţială cu două rotoare eoliene şi generator electric clasic (C cuplat conform fig. 3, D cuplat conform fig. 5, E cuplat conform fig. 6, F decuplat conform fig. 9);
- fig. 12, exemplu de configurare a amplificatorului de turaţie pentru o turbină monomobilă cu două rotoare eoliene şi generator electric contrarotativ (C cuplat conform fig. 3, D cuplat conform fig. 5, E cuplat conform fig. 7, F cuplat conform fig. 8);
- fig. 13, exemplu de configurare a amplificatorului de turaţie pentru o turbină monomobilă cu două rotoare eoliene şi generator electric clasic (C cuplat conform fig. 3, D cuplat conform fig. 5, E cuplat conform fig. 6, F cuplat conform fig. 8);
- fig. 14, exemplu de configurare a amplificatorului de turaţie pentru o turbină monomobilă cu un rotor eolian A şi generator electric contrarotativ (C cuplat conform fig. 3, D cuplat conform fig. 4, E cuplat conform fig. 7, F cuplat conform fig. 8);
- fig. 15, exemplu de configurare a amplificatorului de turaţie pentru o turbină monomobilă cu un rotor eolian A şi generator electric generator electric clasic (C cuplat conform fig. 3, D cuplat conform fig. 4, E cuplat conform fig. 6, F cuplat conform fig. 8);
- fig. 16, exemplu de configurare a amplificatorului de turaţie pentru o turbină monomobilă cu un rotor eolian B şi generator electric contrarotativ (C cuplat conform fig. 2, D cuplat conform fig. 5, E cuplat conform fig. 7, F cuplat conform fig. 8);
- fig. 17, exemplu de configurare a amplificatorului de turaţie pentru o turbină monomobilă cu un rotor eolian B şi generator electric generator electric clasic (C cuplat conform fig. 2, D cuplat conform fig. 5, E cuplat conform fig. 6, F cuplat conform fig. 8).

Amplificator de turaţie planetar reglabil, conform invenţiei, în legătură cu fig. 1...9, destinat implementării în sisteme cu un rotor **A** eolian sau cu un rotor **B** eolian, precum şi în sisteme cu două rotoare **A** şi **B** eoliene contrarotative (cu sensuri de rotaţie contrare). Rotoarele **A** şi **B** eoliene pot avea două sau mai multe pale dispuse echiunghiular. Rotoarele **A** şi **B** eoliene pot fi cuplate la intrările transmisiei sau la un element fix (bază) prin intermediul a două cuplaje **C** şi **D** duble. Amplificatorul de turaţie poate avea o ieşire sau două ieşiri prin comanda unui cuplaj **E** dublu şi poate funcţiona ca mecanism monomobil sau diferenţial prin comanda unui cuplaj **F**. Cuplajul **E** dublu permite cuplarea ieşirilor amplificatorului de turaţie la un stator **G** şi la un rotor **H** al unui generator electric contrarotativ (statorul **G** şi rotorul **H** se rotesc în sensuri contrare) sau la un rotor **H** al unui generator electric clasic în cazul unei singure ieşiri. Cuplajele **C**, **D**, **E** şi **F** sunt cuplaje intermitente comandate şi pot fi realizate în diverse variante constructive, precum cuplaje cu fricţiune cu suprafeţe plane sau conice, cuplaje cu dinţi frontali etc.

Amplificatorul de turaţie planetar reglabil conţine două intrări materializate printr-un element **1** port-sateliţi şi o roată **2** dinţată centrală cu dantură interioară, care transmit simultan mişcările de intrare către două sau mai multe roţi **3** satelit, uzual dispuse echiunghiular şi aflate în angrenare cu două sau mai multe roţi **4** satelit intermediare, de asemenea dispuse echiunghiular. Roţile **4** angrenează la rândul lor cu o roată **5** centrală şi asigură sensuri de rotaţie contrare pentru cele două ieşiri materializate prin elementul **1** şi roata **5**. Roţile **3**, **4** şi **5** sunt roţi cu dantură exterioară. Fiecare roată **3** satelit este solidarizată cu câte o roată **6** satelit cu dantură exterioară, care angrenează cu o roată **7** centrală cu dantură interioară.

Rotorul **A** eolian poate fi cuplat cu elementul **1** port-sateliţi de intrare sau poate fi solidarizat cu o bază **8** fixă prin comanda adecvată a cuplajului **C** dublu. Rotorul **B** eolian poate fi cuplat la cealaltă intrare, roata **2**, sau poate fi menţinut fix prin solidarizare cu baza **8** prin intermediul cuplajului **D** dublu. Roata **5** centrală este permanent cuplată cu rotorul **H** mobil al generatorului electric. Statorul **G** al generatorului electric poate fi conectat la cealaltă ieşire, elementul **1** port-sateliţi, sau poate fi fixat la baza **8**, în funcţie de comanda cuplajului **E**. Cuplajul **E** permite funcţionarea generatorului electric cu statorul **G** mobil, când acesta este comandat pentru a solidariza elementul **1** cu statorul **G** (fig. 7), respectiv funcţionarea cu statorul **G** fix prin solidarizarea acestuia cu baza **8** (fig. 6). Roata **7** se poate roti liber sau poate fi solidarizată cu baza **8** prin comanda adecvată a cuplajului **F**, permiţând astfel însumarea ponderată a celor două mişcări de intrare (fig. 9) sau a momentelor de intrare (fig. 8). Intrările şi ieşirile amplificatorului de turaţie sunt coaxiale.

Cuplajele **C**, **D**, **E** şi **F** conţin un element **9** intermediar de cuplare având o mişcare comandată de translaţie relativă faţă de rotorul **A**, rotorul **B**, statorul **G** şi respectiv roata **7**. Pentru reducerea efectelor inerţiale în regim variabil de funcţionare, rotorul **H** al generatorului electric se roteşte cu o turaţie mai mare în valoare absolută decât cea a statorului **G**. Energia produsă de un generator electric este direct dependentă de turaţia relativă a rotorului **H** faţă de statorul **G**. Amplificatorul planetar poate avea două sau mai multe roţi **3-6** satelit şi un număr egal de roţi **4** satelit intermediare, montate în paralel pentru transmiterea ramificată a puterii în interiorul amplificatorului de turaţie şi auto-echilibrarea dinamică a sateliţilor.

Amplificatorul de turaţie planetar reglabil, conform invenţiei, în legătură cu fig. 10-17, poate fi configurat pentru opt situaţii funcţionale în care puterea mecanică se transmise între intrări şi ieşiri:

a) Mecanism diferenţial cu două intrări şi două ieşiri (fig. 10): rotorul **A** eolian este conectat la elementul **1** (cuplaj **C** cuplat conform fig. 3), rotorul **B** eolian este conectat la roata **2** (cuplaj **D** cuplat conform fig. 5), cuplajul **E** solidarizează statorul **G** cu elementul **1** (fig. 7), cuplajul **F** lasă liberă mişcarea roţii **7** (fig. 9). Mecanismul însumează ponderat vitezele de intrare şi realizează mişcări de ieşire contrarotative;

b) Mecanism diferenţial cu două intrări şi o ieşire (fig. 11): rotorul **A** eolian este conectat la elementul **1** (cuplaj **C** cuplat conform fig. 3), rotorul **B** eolian este conectat la roata **2** (cuplaj **D** cuplat conform fig. 5), cuplajul **E** solidarizează statorul **G** cu baza **8** (fig. 6), cuplajul **F** lasă liberă mişcarea roţii **7** (fig. 9). Mecanismul însumează ponderat vitezele de intrare;

c) Mecanism monomobil cu două intrări şi două ieşiri (fig.12): rotorul **A** eolian este conectat la elementul **1** (cuplaj **C** cuplat conform fig. 3), rotorul **B** eolian este conectat la roata **2** (cuplaj **D** cuplat conform fig. 5), cuplajul **E** conectează statorul **G** cu elementul **1** (fig. 7), cuplajul **F** solidarizează roata **7** cu baza **8** (fig. 8). Mecanismul însumează ponderat momentele de intrare şi realizează mişcări de ieşire contrarotative;

d) mecanism monomobil cu două intrări şi o ieşire (fig.13): rotorul **A** eolian este conectat la elementul **1** (cuplaj **C** cuplat conform fig. 3), rotorul **B** eolian este conectat la roata **2** (cuplaj D cuplat conform fig. 5), cuplajul **E** solidarizează statorul **G** cu baza **8** (fig. 6), cuplajul **F** solidarizează roata **7** cu baza **8** (fig. 8). Mecanismul însumează ponderat momentele de intrare;

e) Mecanism monomobil cu o intrare şi două ieşiri (fig. 14): rotorul A eolian este conectat la elementul 1 (cuplajul C cuplat conform fig. 3, cuplajul D cuplat conform fig. 4), cuplajul E conectează statorul G cu elementul 1 (fig. 7), cuplajul F solidarizează roata 7 cu baza 8 (fig. 8). Mecanismul transmite determinat mişcarea de intrare către cele două ieşiri contrarotative;

f) Mecanism monomobil cu o intrare şi o ieşire (fig. 15): rotorul **A** eolian este conectat la elementul **1** (cuplajul **C** cuplat conform fig. 3, cuplajul **D** cuplat conform fig. 4), cuplajul **E** solidarizează statorul **G** cu baza **8** (fig. 6), cuplajul **F** solidarizează roata **7** cu baza **8** (fig. 8). Mecanismul transmite determinat mişcarea de intrare către rotorul **H**.

g) Mecanism monomobil cu o intrare şi două ieşiri (fig. 16): rotorul **B** eolian este conectat la roata **2** (cuplajul **C** cuplat conform fig. 2, cuplajul **D** cuplat conform fig. 5), cuplajul **E** conectează statorul **G** cu elementul **1** (fig. 7), cuplajul **F** solidarizează roata **7** cu baza **8** (fig. 8). Mecanismul transmite determinat mişcarea de intrare către cele două ieşiri contrarotative;

f) Mecanism monomobil cu o intrare şi o ieşire (fig. 17): rotorul **B** eolian este conectat la roata **2** (cuplajul **C** cuplat conform fig. 2, cuplajul **D** cuplat conform fig. 5), cuplajul **E** solidarizează statorul **G** cu baza **8** (fig. 6), cuplajul **F** solidarizează roata **7** cu baza **8** (fig. 8). Mecanismul transmite determinat mişcarea de intrare către rotorul **H**.

Amplificatorul de turaţie planetar reglabil, conform invenţiei, utilizează o transmisie planetară cu două intrări (**1** şi **2**) şi două ieşiri (**1** şi **5**), având următoarele proprietăţi:

- în cazul transmisiei diferenţiale: are la intrare două mişcări exterioare independente, pe care le însumează ponderat;
- în cazul transmisiei monomobile: are la intrare două mişcări exterioare dependente şi însumează ponderat momentele de intrare;
- cele două ieşiri au mişcări contrarotative şi astfel se asigură creşterea turaţiei generatorului electric contrarotativ, obţinută prin însumarea turaţiilor rotorului **H** şi statorului **G**;
- turaţia rotorului **H** este amplificată în raport cu turaţiile de intrare;
- mişcările de rotaţie ale celor două intrări sunt de sens contrar, proprietate asigurată prin sensurile de înclinare opuse ale palelor celor două rotoare **A** şi **B** eoliene, în cazul transmisiei bimobile, şi de configuraţia cinematică a mecanismului pentru transmisia monomobilă ($z_3 \cdot z_7 < z_2 \cdot z_6$, în care z_i reprezintă numărul de dinţi ai roţii **A**).

Roţile **2**, **3**, **4**, **5**, **6** şi **7** pot fi roţi dinţate sau, în cazul unor sisteme de mică putere, roţi de fricţiune. La modificarea vitezei vântului, o turbină eoliană contrarotativă care integrează un amplificatorul de turaţie planetar reglabil, conform invenţiei, poate asigura o creştere a producţiei electrice faţă de cazul unei turbine eoliene clasice prin comutarea amplificatorului de turaţie într-o situaţie funcţională optimală, în funcţie de tipul turbinei eoliene (cu rotoare eoliene contrarotative şi/sau cu generator electric contrarotativ).

Metoda de reglare a amplificatorului de turaţie planetar reglabil, conform invenţiei, constă în următoarele etape, respectiv reglajele comandate ale cuplajelor **C**, **D**, **E** şi **F**, care permit - prin combinaţii compatibile ale acestor reglaje - obţinerea situaţiilor funcţionale precizate anterior:

1) Cuplajul **C** comandat pentru a solidariza rotorul **A** cu baza 8 (fig. 2): intrarea prin elementul 1 este anulată;

2) Cuplajul **C** comandat pentru a conecta rotorul **A** cu elementul **1** (fig. 3): se obţine o transmisie cu intrare prin elementul **1**;

3) Cuplajul **D** comandat pentru a solidariza rotorul **B** cu baza **8** (fig. 4): intrarea prin roata **2** este anulată (roata **2** se roteşte liber);

4) Cuplajul **D** comandat pentru a conecta rotorul **B** cu roata **2** (fig. 5): se obţine o transmisie cu intrare prin roata **2**;

5) Cuplajul **E** comandat pentru a solidariza statorul **G** cu baza **8** (fig. 6): se obţine o transmisie cu o singură ieşire;

6) Cuplajul **E** comandat pentru a conecta statorul **G** cu elementul **1** (fig. 7): se obţine o transmisie cu două ieşiri contrarotative;

7) Cuplajul **F** comandat pentru a solidariza roata **7** cu baza **8** (fig. 8): se obţine o transmisie monomobilă;

8) Cuplajul **F** comandat pentru a lasă roata **7** în rotaţie liberă (tară moment), fig. 9: se obţine o transmisie bimobilă. In acest caz, pentru a obţine o situaţie funcţională care să permită transmiterea puterii mecanice (momente şi viteze unghiulare) de la intrări la ieşiri, este necesară activarea ambelor intrări prin comanda cuplajului **C** pentru a conecta rotorul **A** cu elementul 1 (fig. 3) şi a cuplajul **D** pentru a conecta rotorul **B** cu roata **2** (fig. 5).

9) Combinaţia de comenzi de anulare simultană a celor două intrări, prin reglarea cuplajului **C** pentru a solidariza rotorul **A** cu baza **8** (fig. 2) şi a cuplajului **D** pentru a solidariza rotorul **B** cu baza **8** (fig. 4), conduce la blocarea celor două rotoare **A** şi **B** eoliene, acţiune necesară pentru protecţia turbinei eoliene când viteza vântului are valori peste cele admisibile, pentru întreţinerea sau reparaţia acesteia etc.

Revendicări

1. Amplificator de turaţie planetar reglabil destinat turbinelor eoliene cu unul sau două rotoare (**A**, **B**) eoliene contrarotative şi generator electric alcătuit dintr-un stator (**G**) fix sau mobil şi un rotor (**H**), constituit dintr-un element (**1**) port-sateliţi şi o roată (**2**) centrală cu dantură interioară, care pun în mişcare două sau mai multe roţi satelit dispuse echiunghiular, unde cel puţin o roată (**3**) satelit cu dantură exterioară angrenează cu roata (**2**) centrală cu dantură interioară şi cu o altă roată (**4**) satelit cu dantură exterioară ce angrenează cu o roată (**5**) centrală cu dantură exterioară şi care asigură sensuri de rotaţie contrare pentru cele două ieşiri materializate prin elementul (**1**) port-sateliţi şi roata (**5**) centrală cu dantură interioară, **caracterizat prin aceea că** fiecare roată (**3**) satelit cu dantură exterioară este solidarizată cu câte o altă roată (**6**) satelit cu dantură exterioară care angrenează cu câte o roată (**7**) centrală cu dantură interioară, de asemenea amplificatorul mai cuprinde patru cuplaje intermitente comandate, respectiv un cuplaj (**C**) dublu ce permite cuplarea primului rotor (**A**) atât cu elementul (**1**) port-sateliţi cât şi cu o bază (**8**) fixă, al doilea cuplaj (**D**) dublu permite cuplarea celui de-al doilea rotor (**B**) atât cu roata (**2**) centrală cu dantură interioară, cât şi cu o bază (**8**) fixă, al treilea cuplaj (**E**) dublu permite cuplarea statorului (**G**) generatorului atât cu elementul (**1**) port-sateliţi, cât şi cu baza (**8**) fixă, iar cuplajul (**F**) simplu permite cuplarea roţii (**7**) centrale cu dantură interioară cu baza fixă (**8**) sau lasă liberă mişcarea acestei roţi (**7**).

2. Amplificator de turaţie planetar reglabil, conform revendicării 1, **caracterizat prin aceea că în** cazul turbinelor eoliene de putere medie-mare cele patru cuplaje (**C**, **D**, **E**, **F**) sunt de tipul cuplajelor cu dinţi frontali, iar pentru turbinele eoliene de putere mică-medie cele patru cuplaje (**C**, **D**, **E**, **F**) sunt cuplaje cu fricţiune cu suprafeţe plane sau conice, caz în care roţile transmisiei sunt roţi de fricţiune.

3. Amplificator de turaţie planetar reglabil, conform revendicării 1, **caracterizat prin aceea că** două dintre cuplajele (**C**, **D**) duble sunt cuplaje permanente cu arborii de intrare, caz în care rotoarele (**A**, **B**) eoliene permit reglarea unghiului axial al palelor pentru anularea momentului generat de vânt.

4. Amplificator de turaţie planetar reglabil, conform revendicării 1, **caracterizat prin aceea că** în funcţie de modul în care sunt comandate cele patru cuplaje (**C**, **D**, **E**, **F**), amplificatorul este constituit ca un mecanism monomobil sau bimobil având una sau două intrări şi una sau două ieşiri coaxiale, pentru adaptarea turbinei la variaţiile sezoniere ale vitezei vântului în vederea creşterii producţiei electrice.

5. Metodă de reglare a amplificatorului de turaţie planetar reglabil reconfigurabil **caracterizată prin aceea că** se realizează în următoarea succesiune de etape:

- se reglează primul cuplaj (**C**) dublu prin comanda de solidarizare a primului rotor (**A**) eolian cu baza (**8**) fixă, pentru a anula intrarea prin elementul (**1**) port-sateliţi, respectiv prin comanda de conectare a primului rotor (**A**) eolian cu elementul (**1**) port-sateliţi pentru obţinerea unei transmisii cu intrare prin elementul (**1**) port-sateliţi;
- se reglează al doilea cuplaj (**D**) dublu prin comanda de solidarizare a celui de-al doilea rotor (**B**) eolian cu baza (**8**) fixă pentru a anula intrarea în roata (**2**) centrală cu dantură interioară, respectiv pentru comanda de conectare a rotorului (**B**) eolian cu roata (**2**) centrală cu dantură interioară, pentru a se obţine o transmisie cu intrare prin roata (**2**) centrală;
- se reglează al treilea cuplaj (**E**) dublu prin comanda de solidarizare a statorului (**G**) generatorului cu baza (**8**) fixă pentru a se obţine o transmisie cu o singură ieşire prin rotorul (**H**) generatorului electric, respectiv prin comanda de conectare a statorului cu elementul (**1**) port-sateliţi pentru a se obţine o transmisie cu două ieşiri contrarotative;

- se reglează cuplajul (**F**) simplu prin comanda de solidarizare a roţii (**7**) centrale cu dantură interioară cu baza (**8**) fixă pentru a se obţine o transmisie monomobilă, respectiv roata (**7**) centrală cu dantură interioară se roteşte liber pentru a se obţine o transmisie bimobilă care funcţionează numai cu cele două rotoare (**A**,**B**) eoliene activate simultan, respectiv se conectează primul rotor (**A**) eolian cu elementul (**1**) port-sateliţi, prin comanda primului cuplaj (**C**) dublu, iar al doilea rotor (**B**) eolian se conectează cu roata (**2**) centrală cu dantură interioară, prin comanda celui de-al doilea cuplaj (**D**) dublu;
- se reglează simultan primul cuplaj (**C**) dublu pentru a solidariza primul rotor (**A**) eolian cu baza (**8**) fixă şi al doilea cuplaj (**D**) dublu pentru a solidariza al doilea rotor (**B**) eolian cu baza (**8**) fixă, atunci când este necesară deblocarea celor două rotoare (**A**, **B**) eoliene.

(51) Int.Cl.
F03D 15/10 (2016.01);
F03D 1/02 (2006.01);
F16H 37/08 (2006.01)

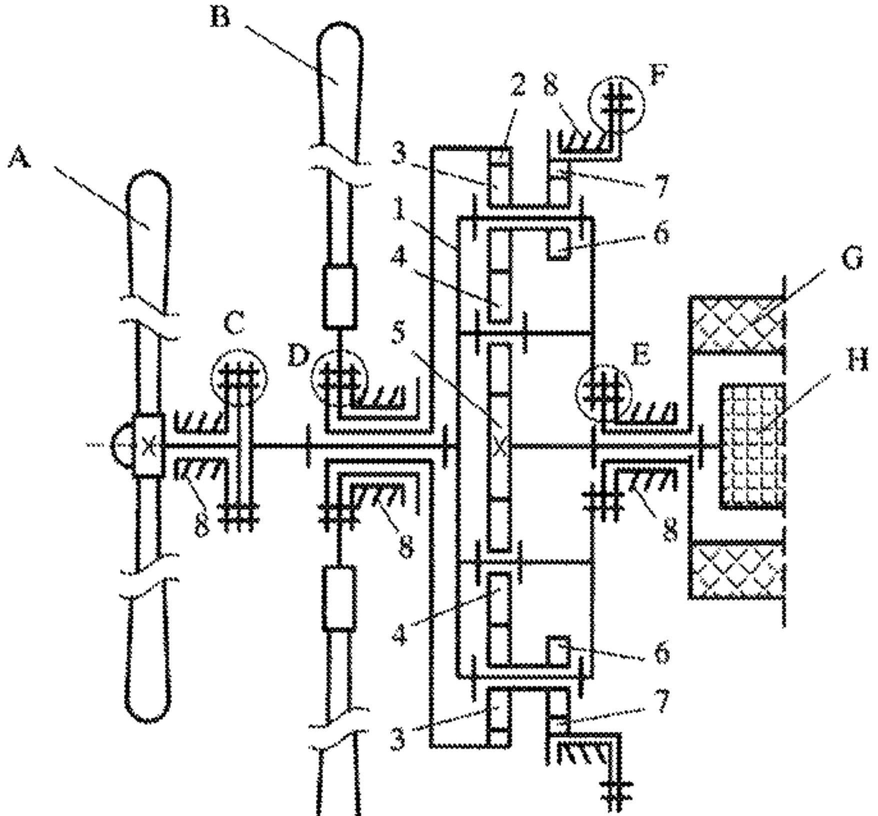

Fig. 1

(51) Int.Cl.
F03D 15/10 (2016.01);
F03D 1/02 (2006.01);
F16H 37/08 (2006.01)

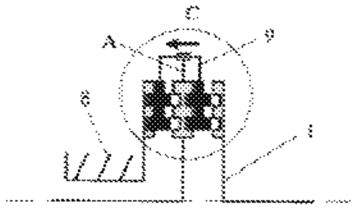

Fig. 2

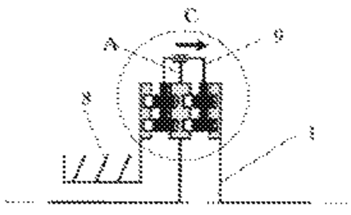

Fig. 3

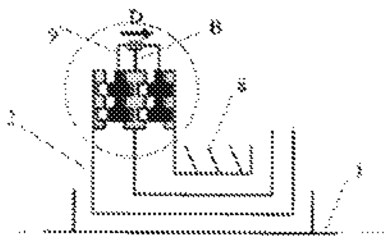

Fig. 4

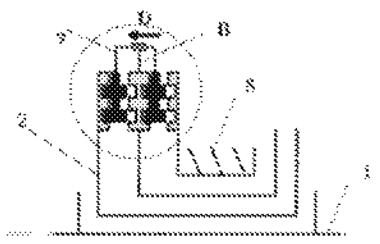

Fig. 5

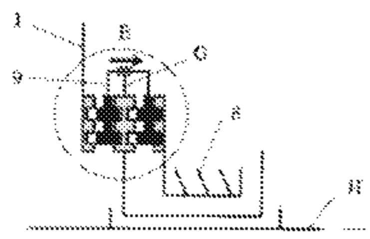

Fig. 6

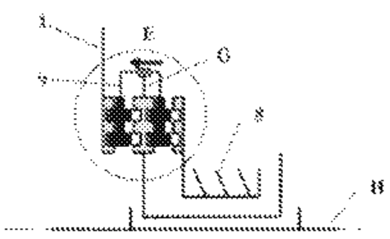

Fig. 7

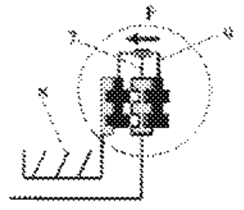

Fig. 8

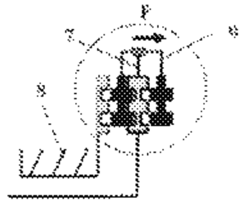

Fig. 9

(51) Int.Cl.
F03D 15/10 (2016.01);
F03D 1/02 (2006.01);
F16H 37/08 (2006.01)

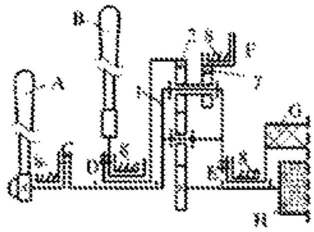

Fig. 10

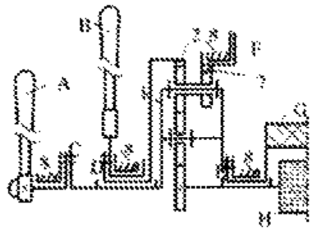

Fig. 11

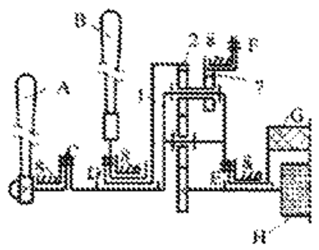

Fig. 12

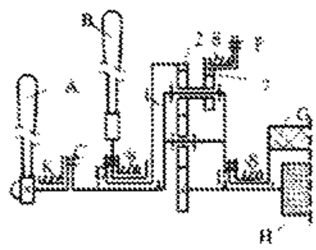

Fig. 13

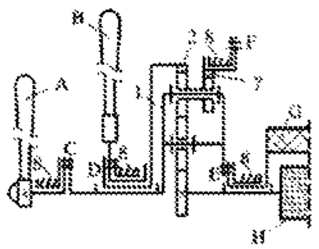

Fig. 14

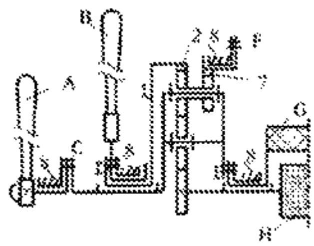

Fig. 15

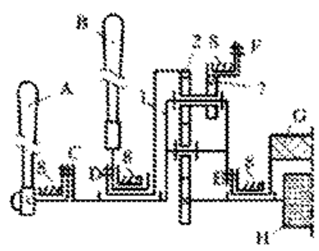

Fig. 16

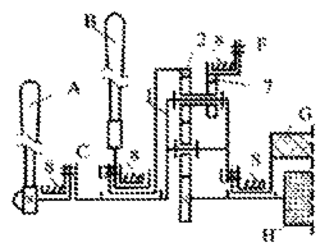

Fig. 17

Editare şi tehnoredactare computerizată - OSIM
Tipărit la Oficiul de Stat pentru Invenţii şi Mărci
sub comanda nr. 55/2025